CERTIFICATO DI FIRMA DIGITALE

Si certifica che questo documento informatico

PhD_unisi_107368.pdf

composto da n°180 pagine

È stato firmato digitalmente in data odierna con Firma Elettronica Qualificata (FEQ), avente l'efficacia e gli effetti giuridici equivalenti a quelli di una firma autografa, ai sensi dell'art. 2702 del Codice Civile e dell'art. 25 del Regolamento UE n. 910/2014 eIDAS (electronic IDentification Authentication and Signature).

PROCESSI INFORMATICI COMPLETATI

- **Apposizione di Firma Elettronica Qualificata Remota** emessa da Intesi Group S.p.A. in qualità di prestatore di servizi fiduciari qualificati autorizzato da AgID, per garantire con certezza l'autenticità, l'integrità, il non ripudio e l'immodificabilità del documento informatico e la sua riconducibilità in maniera manifesta e inequivoca all'autore, ai sensi dell'art. 20 comma 2 del CAD - D.lgs 82/2005.
- **Apposizione di Marca Temporale Qualificata** emessa da Intesi Group S.p.A. in qualità di prestatore di servizi fiduciari qualificati autorizzato da AgID, per attribuire una data e un orario opponibile a terzi, ai sensi dell'art. 20 comma 3 del CAD - D.lgs 82/2005 e per far sì che la Firma Elettronica Qualificata apposta su questo documento informatico, risulti comunque valida per i prossimi 20 anni a partire dalla data odierna, anche nel caso in cui il relativo certificato risultasse scaduto, sospeso o revocato.
- **Apposizione di Contrassegno Elettronico**, l'unica soluzione tecnologica che permette di prorogare la validità giuridica di un documento informatico sottoscritto con firma digitale e/o marcato temporalmente, rendendolo inalterabile, certo e non falsificabile, una volta stampato su supporto cartaceo, ai sensi dell'art. 23 del CAD - D.lgs 82/2005.

  Per risalire all'originale informatico è necessario scansionare il Contrassegno Elettronico, utilizzando l'applicazione HONOS, disponibile per dispositivi Android e iOS.

UNIVERSITY OF SIENA

Department of Biotechnology, Chemistry and Pharmacy

PHD SCHOOL IN BIOCHEMISTRY AND MOLECULAR BIOLOGY - BIBIM 2.0, XXXVI CYCLE

PhD coordinator: Prof.ssa Lorenza Trabalzini

"Identification of human monoclonal antibodies from single cells: two different approaches in the context of infectious diseases"

S.S.D: BIO/10-BIO/11

Tutor:

Dr. Cristina Tinti

Dr. Piero Pileri

Prof. Ottavia Spiga

PhD student:

Veronica Strazza

Academic year: 2022/2023

Acknowledgements

First, I would like to thank my supervisors Dr. Cristina Tinti, Dr. Piero Pileri, Prof. Simon Draper and Dr. Kirsty McHugh. Thank you for your guidance, supervision, enthusiasm and full support for these projects. I have been immensely fortunate to have spent time in each of your lab groups.

Cristina, the motivation and management I have received from you has been unwavering. Piero, the teaching and stimuli you gave me were inestimable. I am constantly impressed by your scientific rigour and quality and I am grateful to have had you both as tutors. I am so proud of the work we have done together and what we have built in the lab during these three years.

Simon and Kirsty, I feel greatly privileged to have been able to spend time with you and your group, it was a great and positive period for me. The model you provide of collaboration, conversation, good research and humour is one to which I can only aspire.

I feel greatly blessed to have been able to spend time with you, you bring out the best in the people you mentor with your commitment, enthusiasm and positivity.

I would like to thank the scientists from the Toscana Life Sciences HARD Lab group: Andrea, Marco,Vittoria, Martina, Sara, Chiara, Silvia and also my dear friend Ilaria.

From the Draper Lab I would like to thank the scientists Barney, Fran, Martino, Mimi, Dimitra, Doris, Cassie, Lloyd and the friends I found during this period Wendy, Laty and Jonas. But also, let me thank Giacomo, Patries and Lana.

A special thank go to my friends, old and new ones they have been a very important part of my life and of the PhD period. I had a great time with them and they have never made me feel alone. Thanks to Camilla, Leonardo, Niccolò, Guillaume and Sofia who also decided to come and visit me in England, while I was away for a part of this research.

I am thankful to my housemate Antonia, without her it wouldn't have been the same, we know.

My sincere thanks to another part of my heart Caterina, Aunt Paola, Ada, Olimpia, Michela and Andrea, it is impossible to describe their support and love.

Thanks to who is no more with me, but who is always with me…

Thanks to my family, they are always by my side even when they probably don't understand what is passing through my mind, it is always time to say that everything will be all right.

The love and support I have always had from my Mum, Dad and Giacomo means everything to me. Without you, I would not be where I am today. Thank you always.

INDEX:

List of Figures:

List of Tables:

Abstract

In the age of personalised medicine, creating and producing molecules with strong affinity and specificity, like monoclonal Antibodies (mAbs), presents a great research opportunity. Various techniques exist for large-scale mAb production, making them one of the most powerful tools both for research and therapy. However, the identification of monoclonal antibodies with the desired characteristics of affinity, functional activity and developability still remains a challenging task for scientists. In this context, single B cell isolation methods have become a crucial research technique to interrogate the immune repertoire in humans.

This thesis aimed to investigate the feasibility, efficiency and efficacy of two distinct methods to generate monoclonal antibodies from single B cells in the context of infectious diseases.

Study A was carried out at Toscana Life Sciences (TLS) in the HARD Lab group, with the support of the University of Siena while, Study B was carried out at the Department of Biochemistry of Oxford University, in the Draper Lab group.

The objective of study A was to establish a rapid and efficient workflow for the generation of human recombinant monoclonal antibodies using an innovative Fluorescence Activated Cell Sorting (FACS)-free technology based on Ferrofluid particles. Starting from single Antibody Secreting Cells (ASCs), enriched for the marker CD138 by magnetic cell sorting, cells were selected for their antigen-specificity by Enzyme-Linked ImmunoSorbent Assay (ELISA) of their cell culture supernatants. These cells were then used to generate recombinant mAbs by direct transfection of PCR fragments called “minigenes”, containing variable regions of the mAbs, which were validated by ELISA for specificity to the antigen of interest. In the context of the pandemic situation, the SARS-CoV-2 infection was considered a good opportunity to test the feasibility of generating mAbs using this platform, starting from the peripheral blood of convalescent COVID-19 donors who had recovered from the disease. In this proof-of-concept study, we aimed to develop a method and demonstrate the feasibility of this in less than 10 days, while pooling a panel of SARS-CoV-2 Spike-specific mAbs for further characterisation of functional activity by neutralisation assays.

The aim of study B was to isolate antimalarial human mAbs against the *Plasmodium falciparum* Reticulocyte-binding protein Homolog 5 (RH5) antigen. RH5 is currently a leading blood-stage malaria vaccine target and clinical trials of vaccines containing this antigen are ongoing. It plays an essential role in parasite invasion of erythrocytes as part of the PCRCR invasion complex and, through its interaction with basigin, it is a major target

of growth inhibitory antibodies. Immunity directed against the blood-stage is unique because it would allow for the development of naturally-acquired immunity and reduce morbidity and mortality. However, antibody-mediated immunity against the blood stage requires high levels of antibodies, which has been difficult to achieve thus far. Starting with PBMCs samples from RH5-vaccinated volunteers, antigen-specific memory B cells were single-cell sorted by FACS using fluorescently-labelled RH5 antigen probes.

While a large number of RH5-specific antibodies have been generated previously by the Draper group, the focus of this part of the thesis was to isolate human mAbs that bind to uncharacterised regions on RH5, potentially identifying new sites of vulnerability on RH5 or "inert" sites that could be excluded from RH5 in next-generation vaccine designs to improve the response. Here we have developed a repertoire of mAbs from the peripheral blood of UK adults vaccinated with *Pf*RH5 (VAC063 trial), a vaccine reported to be safe and immunogenic in phase I/IIa (*Pf*RH5 in adjuvant VAC063 clinical trial, NCT02927145). We generated two new panels of mAbs: one against the full-length RH5 protein (RH5.1) and one against the N-terminus portion of the protein (RH5-NT). The mAbs in the second panel will also be used to investigate the biological role of the N-terminus, which is still unclear. Both panels of mAbs were characterised by ELISA and an *in vitro* parasite Growth Inhibition Assay (GIA).

Although both projects have common aspects, the first study is more focused on establishing a methodology to develop mAbs in a rapid and reliable way, while the second study uses an established antibody discovery pipeline and aims to develop and characterise two panels of mAbs and provide more information in the context of vaccine design.

1. GENERAL INTRODUCTION

1.1. The immune response and monoclonal antibodies

The immune system, a complex system of organs, white blood cells, proteins and chemicals, works together through biological processes to protect our bodies from foreign invaders such as bacteria, viruses, parasites and fungi that are responsible for infections and diseases.
The immune system can be divided into two branches: the innate immune response and the adaptive immune response.
The innate immune response is the body's first line of defence against invading pathogens; it is an immediate and non-specific defence mechanism that is present from birth and does not require prior exposure to the pathogen. In contrast, the adaptive immune response is highly specific to each invader and destroys invading pathogens through humoral and cell-mediated immunity. Antibodies, also known as immunoglobulins (Igs), are key players in humoral immunity. They are soluble proteins that can specifically bind to antigens, foreign substances such as glycoproteins, polysaccharides or proteins [1]. These molecules were first described in 1890 by Emil von Behring and Kitasato Shibasaburō as antitoxins that could protect animals exposed to diphtheria or tetanus toxins [2].
We will focus on monoclonal Antibodies (mAbs), immunoglobulins produced by a single lymphoid B cell clone with affinity for a unique antigenic determinant, as opposed to polyclonal Antibodies (pAbs), Igs secreted by different plasma cell clones that can recognise and bind multiple epitopes, or antigenic determinants, of the same antigen.
Antibodies are molecules composed of a pair of 50kDa Heavy Chains (HCs) and a pair of 25kDa Light Chains (LCs). These four chains are held together in a Y-shaped quaternary structure by hydrophobic interactions and disulfide bonds (**Figure 1.1.1**).
According to the chemical structure, the heavy chains, which determine the class or isotype of an immunoglobulin, are divided into five varieties (IgG, IgA, IgM, IgD, and IgE), while the light chains are divided into two varieties (Igκ and Igλ). Immunoglobulin G (IgG) makes up the majority of serum antibodies; IgGs are further divided into four subclasses (IgG1, IgG2, IgG3, IgG4) and are the only class of antibodies used as therapeutics [3].

Each HC is made up of a variable domain (V_H), which is unique to each mAb, and three constant domains (C_H1, C_H2 and C_H3), while the two LCs are made up of a variable domain (V_L) and a constant domain (C_L), which varies between IgGs, and determines the two isotypes, kappa and lambda.

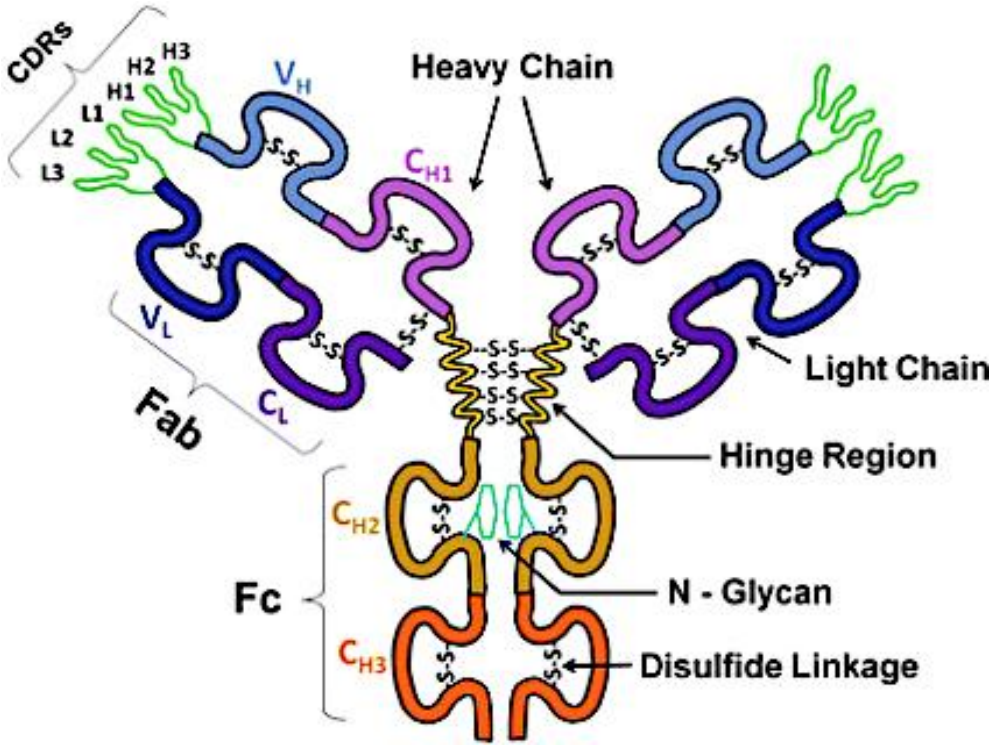

Figure 1.1. *Schematic representation of a monoclonal antibody.*

Image adapted from Moorthy, B.S. et al. [4].

In general, the V region consists of two fragment antigen-binding (Fab) domains that contain the Complementary-Determining Regions (CDRs) that play an essential role in determining the specificity and affinity with which antibodies bind target antigens. Instead, the C region consists of the fragment crystallisable region (Fc) domain, which binds receptors (Fc receptors) on immune cells to mediate effector function [5].

The mechanisms by which immunoglobulins help the immune system are diverse and specific:

- Opsonisation: once the antibodies have recognised the pathogenic antigen, they are able to recruit immune cells such as neutrophils and macrophages to phagocytose the pathogens;

- Neutralisation of toxins or pathogens by binding directly to them or by capturing and agglutinating them in an immune complex;

- Complement lysis of the pathogen, following the classical pathway, by binding C1q via Fc, thus triggering the enzymatic cascade leading to the Membrane Attack Complex (MAC);

- Recruitment of Natural Killer (NK) cells to degranulate and kill the infected cells.

The strength of the humoral immune system is undoubtedly the diversity of epitopes that antibodies can potentially bind.

How B cells can generate antibody diversity was explained in the late 1970s and early 1980s by Susumu Tonegawa, who was awarded the Nobel Prize in Physiology or Medicine in 1987 [6,7]. Antibodies achieve this successful strategy of recognising and killing many different microbes through two distinct diversification processes: V(D)J (Variable, Diverse, and Joining regions) recombination and somatic hypermutation [8]. The heavy and light chains of antibodies are encoded by different multigene families that undergo a process of genetic rearrangement to generate diversity and the final genetic organisation. The V_L and V_H domains are in contact with the antigen and are responsible for antigen binding. The diversity present in the sequence of the variable regions is mainly due to four major diversity processes, three in the early development of a B cell and one in activated B cells.

In early naïve B cells, a V_H transcript is assembled from one of 65 heavy variable exons (V_H), one of 27 diversity exons (D) and one of 6 joining heavy exons (J_H), similarly, the V_L transcript is assembled from one of 70 light variable exons (V_L) and one of 9 joining light exons (J_L), this is called "combinatorial diversity" [9]. Then, further "junctional diversity" can be added at the junction between any two variable exons containing recombination signal sequences, up to 20 P and N nucleotides can be added by the enzymes RAG-1/2 and TdT [10]. The third type of diversity, which occurs during early B cell development is generated by the pairing of HC and LC and gives rise to many additional binding sites. The preimmune repertoire of human B cells is estimated to be over 100 billion [11,12].

Somatic HyperMutation (SHM) is the major source of sequence diversity in antibody paratopes, the antigen binding sites. This process occurs after the B cell has been activated by an antigen and is therefore seen as a way of increasing pre-existing affinity for a target.

SHM takes place in activated B cells at lymphoid sites called germinal centres, where the genes encoding the heavy and light chain variable domains undergo a high rate of point mutations due to the action of the enzyme Activation Induced cytidine Deaminase (AID) and an error-prone process of base pair excision and DNA polymerase repair process. Somatic hypermutation results in approximately one nucleotide change per variable gene per

cell division. As a result, each daughter B cell will have slight amino acid differences in the variable domains, increasing the diversity of the antibody pool. However, the mutations are non-specific and most result in non-productive mutations or no increase in affinity, but the B cells that gain increased affinity for the target are positively selected by clonal expansion. Thus, somatic hypermutation can strongly influence the antigen-specific affinity [13].

1.2. Application of monoclonal antibodies

Monoclonal antibodies, first produced in 1975 by George Köhler and Cesar Milstein using an innovative experimental technique called "hybridoma technology", have had a major impact and soon became an important tool for basic biochemical and biological research as well as for medical and clinical applications.

Both the old and new techniques for developing mAbs are characterised by the identification and conservation of the genetic information of the individual antibody, thus generating mAbs with high specificity. The ability to produce large quantities of highly specific mAbs has made these molecules increasingly interesting for a variety of applications, including research, diagnostics and therapeutic tools.

Because of their high degree of specificity, mAbs can be engineered to recognise and bind to specific antigens, such as proteins or molecules on the surface of pathogens, allowing, for example, the precise identification and study of an infectious agent.

Monoclonal antibodies can also be used to identify key antigens that can be targeted by vaccines and to improve the quality of the immune response, making them a fundamental tool in drug discovery and development.

As diagnostic tools in research and laboratories, mAbs can be used in various applications such as Enzyme-Linked ImmunoSorbent Assay (ELISA), RadioImmunoAssay (RIA), flow cytometry, immunohistochemistry, fluorescence microscopy, electron microscopy, confocal microscopy, ELISPOT, proteome microarray, immunoprecipitation, immunoblot and Western blot [14-20].

Monoclonal antibodies have great diagnostic applications, particularly for tests that detect such molecules in body fluids. For example, some tests can detect pregnancy by identifying human chorionic gonadotrophin, a hormone found in urine that is secreted by the placenta.

Another important role for diagnostic mAbs is in cancer diagnosis, where the broad spectrum of mAbs able to detect immune cell antigens has improved the diagnosis of leukaemia and lymphoma, but mAbs are also important in the diagnosis of solid tumours such as colon, rectal, lung and breast cancer.

An important area is the identification of Cluster Differentiation (CD) markers; for example, mAbs developed to detect CD4 can be used to detect Th cells, which can be used to diagnose and stage Acquired ImmunoDeficiency Syndrome (AIDS) when the number of CD4 cells is reduced. Recently, mAbs have also been used to identify some sexually transmitted diseases such as gonorrhoea and chlamydia infection [21,22].

Several mAbs have been developed as therapeutic tools in clinical medicine. Chimeric and humanised antibodies have been developed to overcome the problem of immunogenicity of murine antibodies and Human Anti-Mouse Antibodies (HAMA).

The former is produced by combining genetic components from a non-human animal (usually a mouse) and a human. Chimeric mAbs, identified by the suffix -ximab, have a prolonged serum half-life and consist of approximately 65% human genetic material.

In humanised antibodies, which instead end with the suffix -zumab, the murine hypervariable regions are grafted onto amino acids to produce humanised antibodies, making these mAbs almost 95% human in origin [23]. Due to the wide range of applications, more than one hundred therapeutic mAbs are currently in late-stage clinical trials and 126 antibody drugs have been approved by the US Food and Drug Administration (FDA) and the EU's European Medicines Agency (EMA), some examples of which are shown in **Figure 1.2.1** [24,25].

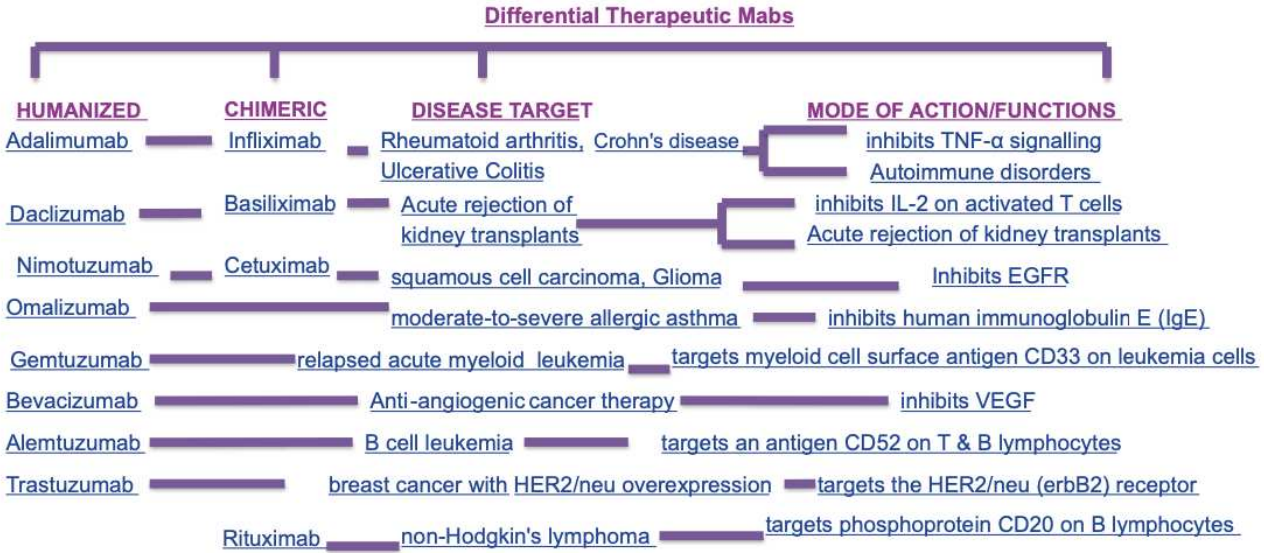

Figure 1.2. *Chimeric and humanised therapeutic monoclonal antibodies applied to different disease targets and with different functions.*

Image adapted from Ansar, W. et al. [26].

1.3. Techniques for monoclonal antibodies development

There are currently, several different approaches to mAb development, each with its own advantages and disadvantages, but none of them is considered the gold standard. Some of the main techniques are described below.

Hybridoma technology

This technique was first developed in 1976, as mentioned above, and aims to obtain specialised cells for the production of mAbs, hybridomas.

As shown in **Figure 1.3.1**, the basic strategy is divided into six main steps.

First, the desired antigen is identified, purified in a sufficient quantity and characterised in order to proceed with the immunisation of animals (1). The antigen is administered by intraperitoneal or subcutaneous injection, as an immunogen in the form of a protein or short peptide coupled to a carrier protein. Mice are usually chosen because of their ability to produce plasma cell tumours that are used as fusion partners, but other animal models such as rats or rabbits are also used [27-29].

Once the animal with the appropriate immune repertoire has been identified (2), B cells from lymphoid tissues (spleen, bone marrow and lymph nodes) are fused (3) with histocompatible myeloma cells that are unable to synthesise the enzyme Hypoxanthine Guanine PhosphoRibosyl Transferase (HGPRT), which is required to rescue the nucleic acid pathway.

The hybridomas are then grown in Hypoxanthine Aminopterin Thymidine (HAT) selective medium and only fused cells grow (4). This is because aminopterin is a folic acid analogue that inhibits a key enzyme in the *de novo* pathway for purine biosynthesis, Dihydrofolate Reductase (DHFR). Therefore, only B-myeloma fused cells are able to survive in such a medium, thanks to the enzyme provided by the splenic B cells.

The consolidated hybridomas, which are monitored for 20-30 days after fusion, are then propagated in multi-well plates. Once these hybrid clones have been produced, the secreted antibodies are tested for their ability to bind to the antigens using immunoassays. Once the single positive hybridoma has been identified, it is recovered and expanded in tissue culture flasks (5). At this point, the mAbs produced by the selected hybridoma are characterised for isotype, reactivity and specificity (6) [30].

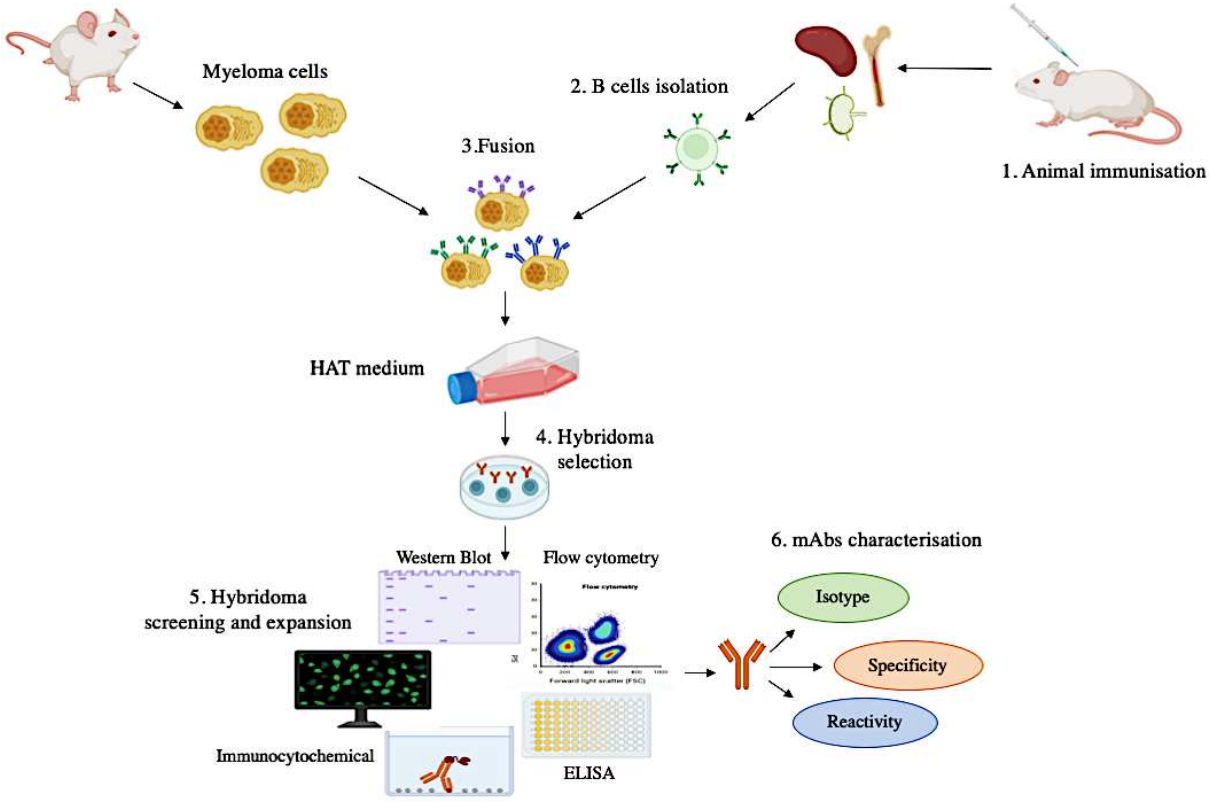

Figure 1.3. *Schematic representation of the hybridoma technology.*

Here are shown the main steps of this technology.

Although hybridoma technology is an important and well-established method of producing monoclonal antibodies, it has some drawbacks and limitations.

The method is based on the fusion of myeloma cells with antibody-secreting B cells, so success depends on the conditions of the myeloma, which means that the cells must be kept under optimal conditions, routinely monitored, passaged and, of course, free of mycoplasma contamination.

Due to the complexity of the technology, the yield of the hybrid is low (~0.43% of all B cells) [31].

Another problem for the development of human hybridoma mAbs is the need for a suitable cell line for B cell fusion, although some investigators have reported that stable hybridomas can be obtained by fusing human B cells with non-secreting mouse heteromyelomas [32].

In addition, hybridomas have been shown to synthesise additional H and L chains of immunoglobulins in ~32% of cases, meaning that these antibodies are not monospecific [33].

Display methods

Since the concept of peptide phage display was first described by G.P. Smith in 1985, display methods have been considered desirable tools for the generation of highly specific monoclonal antibodies [34].

In vitro display technologies are mainly used to isolate peptides and antibody fragments in SFv, single domain antibody (sdAb) or Fab fragment formats. This technology mimics the *in vivo* process of antibody generation and is characterised by cycles of selection and amplification on combinatorial antibody libraries to isolate the ligand of interest [35].

This technology is particularly advantageous due to its ability to generate antibodies against multiple targets by constructing a naive or synthetic antibody repertoire that is not dependent on an *in vivo* immune response; thus, it is possible to generate antibody libraries against toxic, non-immunogenic antigens or self-antigens [36].

The libraries that can be generated are different:

- **Naïve libraries**: are generated from cDNA of the variable regions on the immunoglobulin genes, obtained by Reverse Transcription-PCR (RT-PCR) from mRNA of a natural source, such as B cells from healthy donors. To increase the diversity of the library, only the heavy chain-related mRNA of the IgM isotype is amplified. These libraries are used to isolate antibodies capable of recognising a wide range of antigens due to the high level of unbiased sequence diversity [37,38];

- I**mmune libraries:** are generated from the B cell antibody repertoire of an infected or vaccinated donor. In contrast to naive libraries, they are smaller in size and aim to generate a limited panel of immunogens. Due to the high transcription rate of variable region chain genes, these libraries are well representative of antibody-secreting B lymphocytes and thus provide a rich source of high-affinity antibodies [39,40];

- **Synthetic libraries:** are based on the artificial design and synthesis of different parts of antibody domains or peptide variants. Some controlled sequence degeneration is introduced into the CDR loops to mimic somatic hypermutation and natural immune maturation [41]. The advantage of these libraries is that they offer greater control and flexibility in designing molecules, especially when diversity and specific modifications cannot be achieved with other systems;

- **Semi-synthetic libraries**: are a subset of synthetic libraries and combine synthetic and natural elements to create a diverse pool of peptides or antibody variants. They typically consist of CDRs isolated from natural elements and inserted *in silico* into a sequence encoding the antibody backbone. These libraries offer a compromise between fully synthetic and fully natural libraries, with a greater range of sequence diversity due to the maturation process of antibodies *in vivo* [42].

At this point, antibody libraries need to be incorporated into a vector system to generate a display unit that can then be used to scan and select the hmAbs that can bind the antigen of interest.

Some of the major display technologies are: phage display, yeast display, bacterial display, ribosome display, mammalian cell display and cell-free display [37,43-46].

These units, which "display" a single member of the corresponding antibody library of origin, are then screened against the antigen of interest to detect the antibodies with higher affinity.

The displaying units are recovered and the cDNAs encoding the hmAbs are amplified; once the antigen-specific hmAbs are identified the corresponding cDNA is subcloned into a mammalian expression vector for mass production.

Phage display technology

Phage display technology (**Figure 1.3.2)** is a widely used method for the development of human mAbs and was the first display technology developed by presenting exogenous peptides or proteins on the surface of bacteriophages, which are viruses that infect bacteria [34].

In general, phage DNA is engineered to produce a fusion protein or peptide (mAbs) to one of the phage coat proteins, allowing exposure of the protein/antibody fragment on the capsid surface. The most commonly used bacteriophages are members of the Ff family, such as M13, Fd or f1, but enterobacterial phage λ and Escherichia viruses T4 and T7 can also be used [47-50].

Antibodies are usually fused to the N-terminus of the minor coat protein III (pIII) of M13 [51]. The gene of interest is cloned into the gene 3 protein (g3p) of phage DNA in a plasmid containing an antibiotic marker for selection and an M13 phage origin of replication for rolling circle amplification. The polypeptide fusion protein is expressed on the phage surface by infection of the phagemid-holding bacteria with helper phage containing the complete M13 genome to produce functional phage display units, or without the helper phage by bacterial packaging technology [52].

Other display systems use proteins such as the major coat protein VIII (pVIII) of M13 and the minor coat protein IX (pIX) [53].

Once the first step of library construction is complete, the preferred mAb-pIII fusion protein is selected by *in vitro* panning.

The library is exposed to a target molecule (e.g., proteins, cell surface glycans, and receptors) [54] that has been previously immobilised on a solid surface such as immunoplates, nitrocellulose, magnetic tubes or polystyrene immunotubes. After incubation, phage particles carrying binding molecules that interact with the target with good affinity are retained, while non-binding phages are washed away.

After this passage, the bound phage particles are eluted to recover the positive clones, often determined by ELISA [55].

The eluted positive candidates are then amplified by infection with *E. coli* with or without the helper phage, in selective plates for three to five repeated cycles to yield the desired high affinity mAbs [56].

Additional site-directed mutagenesis or depletion approaches can be used to improve the desired antibody characteristics. These selected phages are characterised to confirm specificity and affinity of binding to the target molecule.

Finally, the genes encoding the selected mAbs can be cloned into an IgG expression vector and then transfected into mammalian cells to produce fully human mAbs that can be used for various applications such as diagnostics, therapeutics or research tools.

Phage display technology is a powerful and versatile technique for mAb development due to its high diversity and rapid selection and screening process, which is highly adaptable to different targets.

Despite these advantages, there are some limitations and drawbacks to be aware of.

These methods may have some limitations in terms of complexity, as they rely on the random combination of Abs variable region genes during library preparation, thus reducing diversity due to the loss of natural cognate heavy and light chain pairing, usually developed in an *in vivo* immune response [57].

In addition, phage display panning requires a target antigen to be purified and immobilised on solid surfaces, which makes this step particularly suitable for linear epitopes but may have some limitations for mAbs that recognise conformational epitopes or some proteins (e.g., structurally complex transmembrane proteins or glycosylated proteins).

This technique is also labour intensive and good technical expertise is required to set up a working phage display experiment.

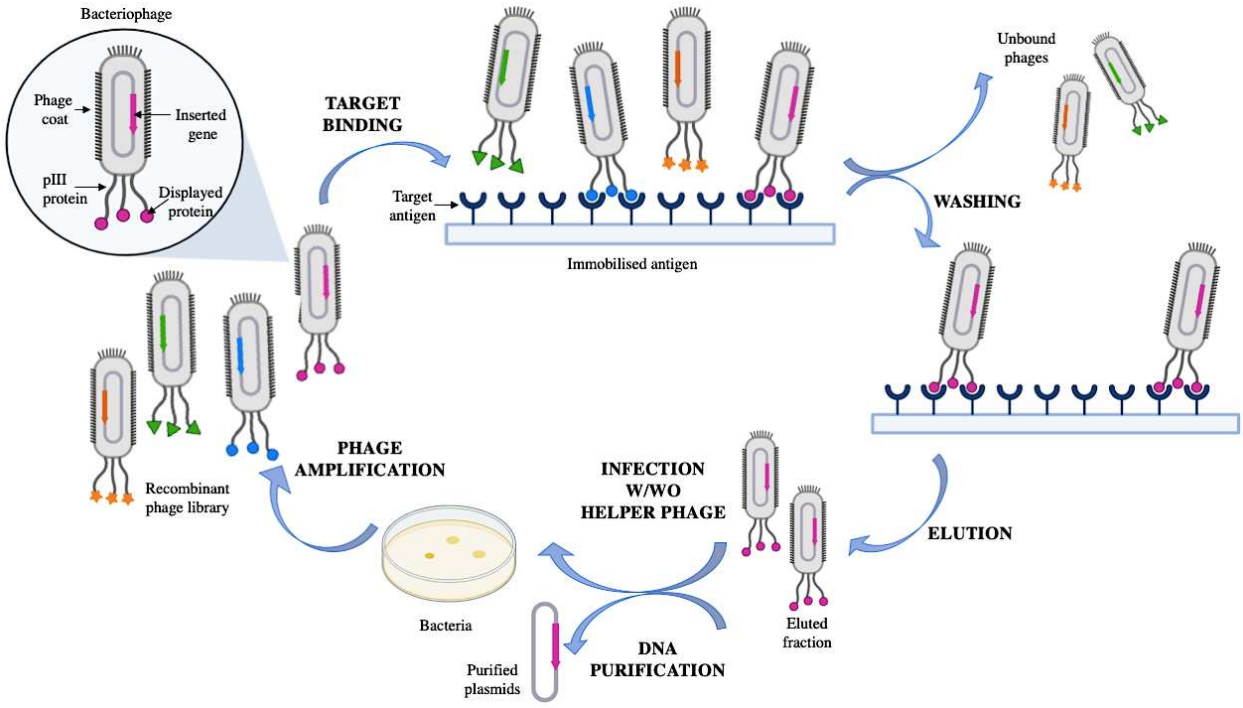

Figure 1.4. *Schematic representation of phage display technology.*

Main stages are: Target binding, Washing, Elution, Infection with or without helper phage, DNA purification and phage amplification.

Transgenic mice

One of the main difficulties in generating antibodies for some applications, such as therapeutics, is the immunogenicity of animal-derived mAbs in human patients, which mainly leads to reduced efficacy and rapid clearance [58,59].

Human sequence mAbs could provide a potential solution to this challenge, therefore an alternative strategy such as transgenic mice could help to generate immunotherapeutic mAbs or drugs with low immunogenicity.

Transgenic mice are created by silencing the mouse Ig variable region genes and introducing the human antibody-producing genes into the mouse genome at the germline level. The engineered mouse genome can then be productively rearranged in the B cell population to generate mouse B lymphocytes expressing human Ig chains.

The introduction of large parts of the human germline repertoire has been facilitated by microcell-mediated chromosome transfer, a technique in which a human fibroblast-derived microcell is fused with a mouse Embryonic Stem (ES) cell to produce a pluripotent cell line with a single chromosome or fragment thereof.

One research group has generated ES cell lines and chimeric mice containing fragments of human chromosomes 2 and 14, which contain the κ light and heavy chains, and the intact chromosome 22, which contains the λ light chain [60].

To obtain an antigen-specific response, traditional immunisation protocols can be used and then single antigen-specific B cells can be recovered and used to generate mAbs by fusing activated B cells with mouse myeloma cells to create hybridomas.

This technology is a source of diverse, high-affinity and highly specific mAbs [61].

With several transgenic mice currently on the market, this method will likely be extended to rat and bovine systems in the future [62,63].

The transgenic mouse approach exploits the natural immune selection of organisms allowing the generation of high-affinity mAbs without further in vitro engineering. To date this approach has led to the invention of 19 FDA-approved fully human antibodies [64,65].

The transgenic mouse platform has several advantages and, although larger studies are required, a lack of immunogenicity has been observed, so it appears that this system has indeed solved the problem for which it was generated [61].

However, this technology has several limitations. The human transgenic mouse model generates a limited repertoire, although these mice are engineered to express human antibody genes, they retain their genetic immune background, particularly in terms of T cell antigen processing and B cell regulation. In addition, mAbs have mouse-specific glycosylation,

which limits the immunotherapeutic applications due to the recognition by anti-Gal1α 1-3Gal antibodies present in human serum [66].

There are also some ethical limitations. The generation of transgenic mice is subject to regulatory restrictions and often is not available to the scientific community due to the industrial nature of biotechnology.

1.4. Single B cell technologies

Among the various approaches to antibody discovery, single B cell screening is a powerful and efficient strategy for monoclonal antibody research and development. The advantages of these technologies are short production time, high throughput, high specificity, rich genetic diversity, natural pairing of V_H and V_L chains and the need for relatively few cells.

These single B cell screening technologies have evolved tremendously in recent years, with the first efficient method for mAb production based on single B cell sorting described in 1996 [67].

This overall method for generating mAbs from single cells is summarised in three main steps: isolation of single B cells, amplification, sequencing and cloning, and final antibody screening and validation (**Figure 1.4.1**).

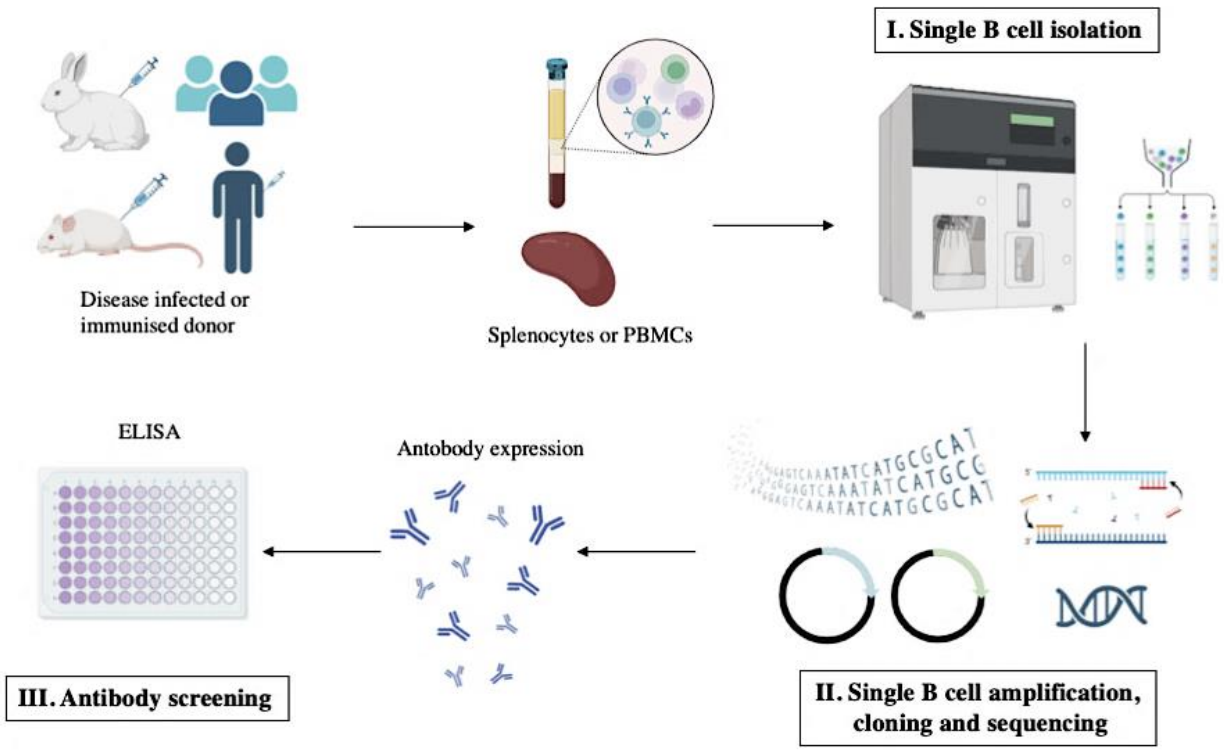

Figure 1.5. *Generation of single B cell cloning antibodies.*

Here it is shown the general method with the three main steps.

In the first step of cell isolation, cells are isolated from lymphoid tissues or peripheral blood using various techniques such as laser capture microdissection, micromanipulation [68,69] or in an antigen-selective manner using antigen-coated magnetic beads, the fluorescent foci method or more advanced platforms such as fluorescence-activated cell sorting (FACS) and beacon technology [70-73]. Both FACS and beacon technologies have a short turnaround time, high throughput and are able to bind rare binders but are very expensive.

In the second step, the mRNA of the isolated B cells is reverse transcribed to cDNA and the IgH and IgL genes are amplified by two cycles of nested or semi-nested PCR. During the second round of PCR, primer mixes are used to increase specificity. At this point, restriction sites for subsequent cloning steps or linear expression cassettes, for direct transfection into mammalian cells for in vitro expression of mAbs can be incorporated into the amplicons [74]. After amplification, the IgH and IgL chain genes can be sequenced to provide further data on antibody specificity, mutations and alterations induced by somatic hypermutation of the V,D, J fragments [75,76]. The final step is the screening and evaluation of mAbs. Larger scale production of mAbs is usually required for more detailed analysis. Typically, mAbs are expressed in bacterial systems (e.g., *E. coli*) as antigen-binding fragments (Fabs) or in mammalian cell systems such as HEK 293 or CHO cells as complete IgGs.

STUDY A

1.A. Introduction

1.A.1. Humoral immunity: from B cells to antibody-secreting cells

Humoral adaptive immunity is a type of immunity mediated by B lymphocytes and effector B cells, plasma cells, which produce antibodies against foreign antigens, as explained earlier. The name "humoral" comes from the mechanism by which it works, through substances found in body fluids, "humour". It is also called "antibody-mediated immunity" because antibodies are one of the protagonists in the development of this immunity, and the following section will explain the process of activation of this system.

When an unprocessed antigen is encountered by specific cells of the immune system, a signalling cascade is initiated. Antibody responses to different antigens follow two different pathways: T-dependent or T-independent pathways, depending on whether the help of T cells is required or not [77] (**Figure 1.A.1.1**).

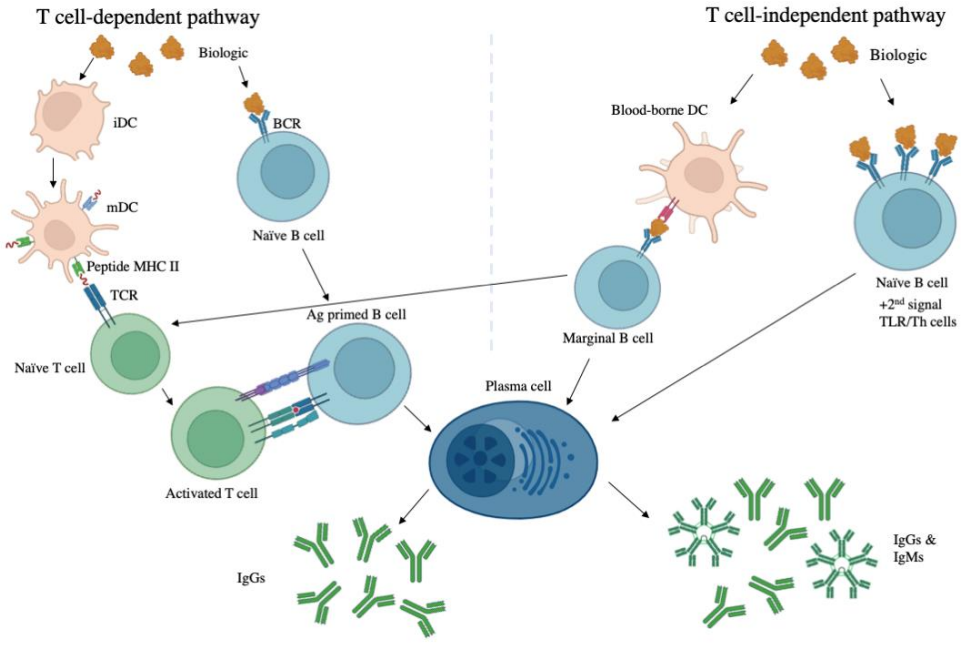

Figure 1.A.1.1. *T cell-dependent and independent pathway in an immunogenic response.*

The T-cell dependent pathway involves the uptake of protein antigens by antigen-presenting cells like immature Dendritic Cells (iDCs) and B cells [78,79] .

To initiate the response, Dendritic Cells (DC) internalise and process the biologic, generate a peptide (T-epitope) presentable on Major Histocompatibility Complex Class II (MHC II), mature and migrate to the T-cell zone of the draining lymph nodes, where they present the antigenic peptides to naive T-cells expressing antigen-specific T-cell receptors [80]. In this way, T-cells are activated and proliferate. B cells can also take up biologics through their B Cell Receptor (BCR), process them and present them to T cells. This action results in activated T cells that stimulate B cells to produce antigen-specific antibody-secreting plasma cells. The T cell-independent pathway involves direct stimulation of B cells by polysaccharides, nucleic acids, lipids and other multivalent antigens. In this pathway, marginal zone B cells are stimulated by blood-borne peripheral dendritic cells that have already been exposed to the biologics. This results in the generation of short-lived plasma cells that secrete mainly low affinity IgM antibodies [81].

1.A.2. Plasma cell differentiation

Antibody-Secreting Cells (ASCs) are the terminally differentiated cells of the humoral immune response committed to the mass production of antibodies.

One of the key aspects of the adaptive immune response is the high and rapid rate of antibody production (between 10-1,000 Ab molecules per cell per second, compatible with about 0.2-22pg per cell per day), starting from naïve or memory B cells after antigen-induced activation, proliferation and differentiation[82-84].

ASCs undergo several morphological and homeostatic changes during terminal differentiation. In terms of cellular rearrangement, ASCs increase their cytoplasm, Endoplasmic Reticulum (ER) and Golgi apparatus to increase the amount of protein they are programmed to produce [85]. As ASCs mature, they change their protein surface phenotype, loosing their surface in favour of other markers such as CD19, CD27, CD38 and CD138, also known as syndecan-1, which is considered a good plasma cell biomarker [86-89] .

ASCs differentiate from B cells in the draining lymph nodes or within the Germinal Centres (GCs), or outside as an extrafollicular reaction [90,91].

Most blood circulating ASCs undergo apoptosis, some of them survive and migrate to the Bone Marrow (BM) or other tissues where they can eventually mature into Long-Lived Plasma Cells (LLPCs). These cells are quiescent, terminally differentiated, non-dividing cells capable of producing specific Abs for years after an initial infection [92].

There is evidence that ASCs derived from GC responses have the potential to form LLPCs, rather than those derived from extrafollicular spaces [93-95].

ASCs and LLPCs are controlled by both intrinsic mechanisms such as autophagy, anti-apoptosis and cell metabolism and other extrinsic factors such as cytokines, chemokines and BM stromal cells [96-98].

Different metabolic pathways in ASCs are regulated by different gene expression programmes, all aimed at promoting differentiation, survival and large production of Abs.

Transcription factors that maintain the B cell programme include PAX5, Bach2 and BCL6, which is expressed primarily in GC B cells to promote survival and cell proliferation [85,99,100]. Transcription factors, uniquely upregulated in the plasma transcriptome [101,102] , include Blimp1 and XMP1, which are essential for differentiation, homeostasis and Ab secretion, and IRF4, which is required for survival (**Figure 1.A.2.1**) [103–105].

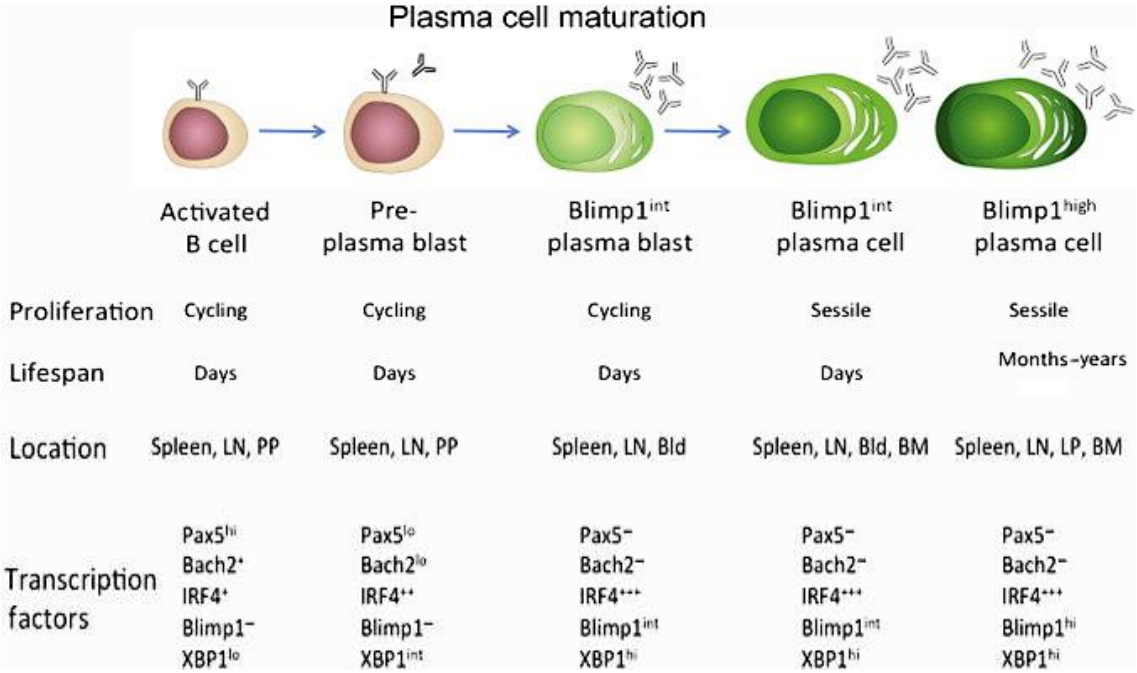

Figure 1.A.2.1. *Plasma cell maturation.*

This image was adapted from Yoshida T et al. [106].

Antibody-secreting cells adapt their metabolism to produce Abs in an attempt to maintain homeostasis and optimise the energy required for survival. When nutrients are limited these cells recycle their protein aggregates and organelles through autophagy, which is regulated in ASCs by proteins such as *Atg5*, *Atg9* and *Atg13* [102,107]. Extrinsic factors that control the maintenance and maturation of ASCs include cells homing to the bone marrow microenvironment. Mesenchymal Stromal/Stem Cells (MSCs) secrete chemokines such as CXCL12, which interact with CXCR4 on ASCs [108–110], and IL-6, which is critical for ASCs differentiation and long-term survival [111]. Cells such as neutrophils, eosinophils, megakaryocytes, osteoclasts as well as BM MSCs secrete APRIL, another important ASC

survival factor [112]. ASCs are rare cells, representing no more than ~0.01-1% of total cellularity in the circulation and lymphoid tissues, but are fundamental to the functionality of the immune system. After infection or vaccination, ASCs circulate in the blood for days, accounting for the first pick of the serum Ab titer and then disappear; upon re-encounter with the antigen, a new pick is detected, due to long-lived PCs[113].

1.A.3. Emerging and re-emerging Viral diseases: Sars-CoV-2

Infectious diseases are a constant challenge to medical science. Despite significant advances in medical research, novel viruses are still considered a major and uncontrollable problem for human health [114,115] .

The emergence of novel human pathogens or the re-emergence of some diseases are strongly influenced by human, ecological, environmental and viral factors, as well as human association with reservoir hosts and changes in vector populations [116,117].

Viruses such as avian influenza A (H7N9), Ebola and coronaviruses are emerging viruses that have evolved over different periods [118].

Examples of coronaviruses that are considered serious infectious agents include Severe Acute Respiratory Syndrome Coronavirus (SARS-CoV), which caused an outbreak in 2003, Middle East Respiratory Syndrome Coronavirus (MERS-CoV), which caused a dangerous disease in 2012, and Severe Acute Respiratory Syndrome Coronavirus-2 (SARS-CoV-2), which caused the last pandemic [119,120].

SARS-CoV-2 is a recently emerged beta coronavirus belonging to the family Coronaviridae designated by the WHO as COVID-19 [121] . By causing severe respiratory infections in humans, COVID-19 has become a global health problem [122]. Coronaviruses are enveloped, positive-sense, single-stranded RNA viruses with external Spike proteins. These molecules protrude from the viral envelope like the spikes of a crown giving the coronavirus its name (**Figure 1.A.3.1.**) [123].

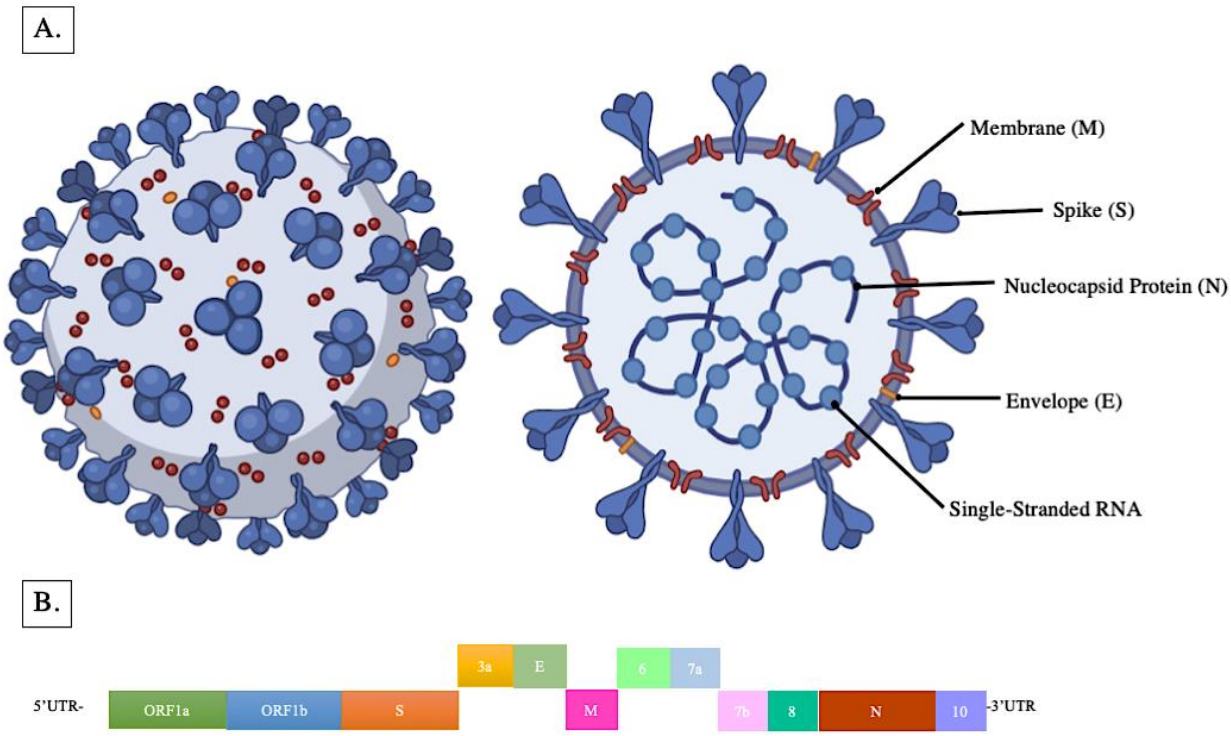

Figure 1.A.3.1. *SARS-CoV-2 structure and genome.*

A*. Here are represented the structural proteins of the Sars-CoV-2 virus such as the Spike (S), Envelope (E), Membrane (M), and Nucleocapsid proteins (N), and the internal Single-Stranded RNA.* ***B****. In the lower part, it is shown the Genomic sequence of Sars-CoV-2. UTR-Untranslated region, ORF-Open reading Frame, S-Spike protein, E-Envelope protein, M-Membrane protein, N-Nucleocapsid protein.*

The SARS-CoV-2 genome consists of 10 Open Reading Frames (ORFs). The first ORF /ORF1a/b, which represents two-thirds of the viral RNA, encodes 16 non-structural proteins and polyprotein1a and polyprotein1b. The other ORFs encode structural proteins: Spike (S), Envelope (E), Membrane (M), Nucleocapsid (N) and accessory proteins [124,125].

The Spike glycoprotein is responsible for the recognition of the host receptor, human Angiotensin Converting Enzyme 2 (hACE2), its binding and fusion with the membrane. The S protein also promotes the adhesion of infected cells to neighbouring cells, thereby enhancing the spread of the virus. The S protein is approximately 141kDa and consists of an ectodomain, a transmembrane region and a short intracellular C fragment. The ectodomain consists of two subunits, the S1, which is required for receptor binding and the S2, which assists in membrane fusion. The Spikes adopt a trimeric form at the cell surface as shown in **Figure 1.A.3.2**. [126,127].

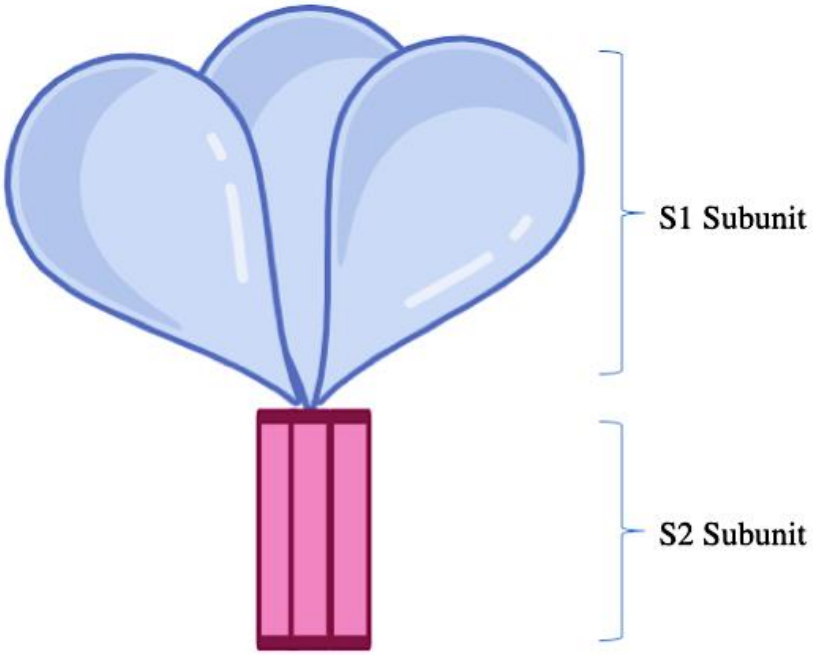

Figure 1.A.3.2. *Spike structure.*

Schematic Illustration of the Structure of Spike Protein composed of Subunit 1 and Subunit 2.

The trimeric Spike is able to bind the host cell receptor ACE2 thanks to the open conformation of the Receptor Binding Domain (RBD) present in the S1 subunit. This binding results in the transition of neighbouring RBDs to the open conformation, facilitating the binding of additional molecules. This interaction also induces conformational changes that destabilise the S1 and S2 interactions. Each S1 can be divided into an N-Terminal Domain (NTD) and an RBD. Cleavage by the type II Transmembrane Serine Protease (TMPRSS2), co-expressed with hACE2 in type II pneumocytes, leads to membrane fusion and viral entry and spread to neighbouring cells [128,129].

The N protein is the most abundant viral protein; it binds and protects RNA and forms the core of a ribonucleoprotein that facilitates host cell entry and interaction with cellular processes after virus fusion. In addition, the N protein has other activities that are essential for the proliferation and functioning of the virus, making it another key component along with the S protein [130].

The E protein is a small integral membrane protein of 8-12KDa, a viral translocation channel that is a critical component in the assembly, release and virulence phases of the viral life cycle [131,132].

The M protein is thought to be the primary driver of viral assembly, although its precise role in this process and membrane budding is unknown. In addition, recent data suggest that the SARS-CoV-2 M protein also functions as a viroporin [133].

Transmission of SARS-CoV-2 can occur through direct, indirect or close contact with infected persons, mainly by secretions, respiratory droplets, airborne and, to a lesser extent, fomites and faecal-oral transmission [134]. Once inside the body the virus binds to the cellular receptor ACE2, which is highly expressed in oral epithelial cells, and the infection process begins. The human body's response to this foreign invasion is characterised by an initial asymptomatic phase, an upper respiratory tract infection that spreads to the lower respiratory tract, viral transmission and clinical manifestations [135]. People with COVID-19 have a wide range of symptoms, from mild to severe illness. Symptoms may include fever and chills, cough, shortness of breath, sore throat, loss of smell or taste, fatigue, nausea and diarrhoea. In certain situations, Sars-CoV-2 can worsen, leading to respiratory failure, multiple organ failure and even death [136,137]. Due to the high infectivity, human-to-human transmission and pathogenicity of the virus the World Health Organization (WHO) declared the novel coronavirus outbreak (COVID-19) a global pandemic on 11 March 2020 [138]. The emergence of novel pandemic viruses is a concern for human health and is considered a global issue, therefore knowledge and awareness of the main risk factors contributing to the development of these diseases could be of great importance.

Here we review some of the factors that contribute to the emergence of viral infectious diseases. A major source of transmission is the close interaction between humans and animals. The majority of all human infectious diseases and pandemics have originated through the cross-species transmission of microorganisms. In the case of Coronavirus, it has been established that transmission occurs from bats, although further studies are required to elucidate the molecular mechanisms, as intermediate hosts may play a crucial role [139].

While in previous studies bats have been identified as the natural reservoir for Sars-CoV-2 viruses, there is no evidence of human contact with bats infected with Sars-CoV-2 so far. The Sars-CoV-2 outbreak has been linked to the Wuhan Seafood Market in China, where several rodents, birds and rabbits were sold. Even if other HCoVs have been transmitted to intermediate hosts in the same market before spreading to humans [140–142] and COVID-19 is undoubtedly a zoonotic disease, it has not been proven that the virus has come from an infected snake, civet cat or other animals such as pangolins, one of the most illegally traded mammals in the world [143].

International travel is also a potent force in the emergence of diseases. COVID-19, for example, originated in China and spread very quickly in other countries through travellers.
On this evidence, to prevent the spread of emerging diseases is crucial to implement programmes at global levels for surveillance, early detection and rapid response [144].
In the same way, high population density due to intensive urbanisation and mass gathering, is also responsible for rapid spread of viruses and pose a major public health risk [145].
Other important factors contributing to the re-emergence of infectious diseases are virus-related. For example, rapidly mutating viruses are more often recognised as emerging pathogens [146].
RNA viruses have error-prone polymerases, allowing this class of viruses to mutate or evolve more rapidly.
Genomic mutation and adaptation of Coronaviruses are the basis of their evolution over the years, as demonstrated by the onset of Sars-CoV in 2003, MERS-CoV in 2012 and the current pandemic we are focusing on, COVID-19 [115,147].
Although the medical field is making great strides, the emergence or re-emergence of novel pandemic pathogens is a global burden that needs to be addressed.

1.A.4. Isolation of rare cells

In the era of personalised medicine, where the patient's treatment is often tailored to the individual's molecular phenotype, the isolation and analysis of cells from patients is of paramount importance.
One of the main challenges is finding cells of interest among a large heterogeneous population. It is often necessary to isolate cells that are very uncommon or not easily detectable.
Although there is no official definition, a cell can be considered "rare" if it represents a subpopulation of less than 0.01% of the total population [148].
Examples of such cells include Circulating Tumour Cells (CTCs), Peripheral Haematopoietic Stem cells (HSTs), fetal cells in maternal blood and antigen-specific lymphocytes [149–151].
In the immune system, single cell analysis is fundamental to the study of the immune response during infection and disease progression. After receiving external stimuli, for example from a pathogen such as a virus, B cells proliferate rapidly and differentiate into ASCs as previously described.

There are several methods to isolate individual cells, such as Fluorescence-Activated Cell Sorting (FACS), microfluidic systems or magnetic cell separation technologies (MACS). While microfluidic systems provide basic separation approaches, FACS and magnetic cell sorting rely on the interaction between cell surface antigens and antibodies conjugated to fluorochromes rather than magnetic particles and are therefore very specific and sensitive techniques [152].

Magnetic sorting methods can be used for macro- to micro-separation, depending on the magnetic field, particle size and gradient. MACS allows miniaturisation of assays and simplification of cell sorting mechanics by providing sensing and actuation capabilities [153].

In 2011, CellSearch™ patented a method for capturing and detecting rare Circulating Plasma Cells (CPC) and abnormal plasma cells or Multiple Myeloma Cells (CMMC) using an anti-CD138 FerroFluid conjugated antibody to detect, monitor and characterise CMMC diseases, including Monoclonal Gammopathy of Undetermined Significance (MGUS) and Smoldering Multiple Myeloma (SMM) [154,155].

The possibility of having a quick and easy way to isolate rare cells from biological samples can allow the study of important immunological molecules, with valuable applications for countering new emerging infectious diseases such as COVID-19.

In this study we used the FerroFluid technology in an innovative way to enrich and subsequently isolate single and rare ASCs from human peripheral blood samples.

2.A. Outline and aim of STUDY A

In an immune response, memory B cells do not directly produce the antibodies that are shed into the bloodstream. Instead, these antibodies are released by specialised antibody-secreting cells. Therefore, studying the repertoire of antigen-specific plasma cells can provide valuable information about the true nature of the immune response.

Several technologies for single B cell analysis have been developed to efficiently sample the B cell repertoire. However, most of these methods have limitations in screening antigen-specific plasma cells and other immunoglobulin-secreting B cell subsets. This challenge is mainly due to the lack of surface immunoglobulins and the difficulty of culturing these particular cells.

Therefore, given the importance of monoclonal antibodies in the immune response, Study A of my PhD project aimed to develop a reliable, rapid and efficient method for screening, studying and producing human recombinant monoclonal antibodies as tool for application in the context of infectious diseases.

To set the study, the starting point was to test an innovative methodology based on the FerroFluid™ technology, previously used to detect rare cells in the context of circulating tumour cells. Since CD-138 is considered one of the reference markers for the detection of human plasma cells, we took advantage of the availability of anti-CD138 antibody conjugated to FerroFluid™[156].

The overall aim of the project was to develop a rapid method for the detection and screening of human monoclonal antibodies. This goal could be achieved through several steps:

ASCs isolation using FerroFluid™ technology, identification and isolation of antigen-specific ASCs, recovery of monoclonal antibody coding sequences and subsequent production, purification and characterisation or recombinant mAbs.

In the context of a global pandemic, Sars-CoV-2 provided a good infectious disease model for the development of this method due to the immunogenicity of this virus.

3.A. Material and Methods

3.A.1. Recruitment of SARS-CoV-2 donors and Peripheral Blood Mononuclear Cells (PBMCs) isolation from peripheral blood

Samples from SARS-CoV-2 convalescent donors of both sexes, who gave written consent, were provided by the Azienda Ospedaliero Universitaria Pisana - UO Malattie Infettive.
The study was approved by the local ethics committee (Ethics Committee CE AVNO - Regione Toscana; Authorization #17761) and was conducted in accordance with good clinical practice as defined by the Declaration of Helsinki (European Council 2001, US Code of Federal Regulations, ICH 1997).
Blood samples (~40mL) were collected from convalescent adult blood donors 15-44 days after the onset of SARS-CoV-2 infection. The eligibility criteria used to choose convalescent patients for the study was to have 2 consecutive nasopharyngeal swabs tests negative for SARS-CoV-2.
PBMCs were then purified from human blood using a Ficoll-Paque PLUS density gradient centrifugation medium. Whole blood was diluted with an equal volume of Dulbecco's Phosphate-Buffered Saline (DPBS) (*Gibco*), layered on a volume of Ficoll-Paque PLUS (*Cytiva*), and then centrifuged at 600g for 30min at RT. PBMCs were collected from the Ficoll-Paque Plus-plasma interface in a 15mL Falcon and washed with DPBS (800g, 10min, 4°C).

3.A.2. Cell cultures

- Expi293F™ Cells (*Gibco*) were cultured in Expi293™ Expression Medium (*Gibco*). This suspension cell line was maintained in Nalgene™ Single-Use PETG Erlenmeyer Flask at 125rpm (*Thermo Scientific*), or in Deepwell Plate 96/2mL (*Eppendorf*) at 1,000rpm with MixMate™ Shaker (*Eppendorf*), at 37°C in a shaker with a humidified atmosphere of 8% CO_2;

- ExpiCHO-S™ Cells (*Gibco*) were cultured in ExpiCHO™ Expression Medium (*Gibco*). This suspension cell line was maintained in Nalgene™ Single-Use PETG Erlenmeyer Flask at 37°C in a shaker with a humidified atmosphere of 8% CO_2 at 125rpm.

All the cell lines were tested for mycoplasma contamination through PCR analysis before any use [157].

3.A.3. SARS-CoV-2 Spike protein cloning, expression and purification

The Spike protein of SARS-CoV-2 is a trimeric class I fusion protein that exists in a metastable prefusion conformation that undergoes a substantial structural rearrangement to fuse the viral membrane with the host cell membrane. A human codon-optimized nucleotide sequence coding for a soluble version of the S protein (amino acids 1-1208; GenBank: MN994467) including the T4 fold on trimerization domain, a histidine tag, and a strep-tag, was commercially synthesized (*GeneArt*) and cloned into the mammalian expression vector pcDNA^{TM} 3.4 TOPO^{TM}. The protein sequence was modified to remove the polybasic cleavage site (RRAR to GSAS), and two stabilizing mutations were also introduced (K986P and V987P).

The recombinant protein was produced by transient transfecting of ExpiCHO-S^{TM} cells using ExpiCHO Expression System Kit (*Gibco*) in 250mL non-baffled flasks (*Corning*), according to the manufacturer's protocol. Transfected cells supernatant was harvested at 8-days post-transfection (dpt) and the recombinant protein was purified using His Trap HP Ni Sepharose High-Performance nickel-charged IMAC resin (*Cytiva*). The appropriate fractions containing recombinant protein were dialyzed against Phosphate Buffered Saline (PBS) pH 7.4 using Slide-A-Lyzer MINI Dialysis Device, 20K MWCO (*Thermo Scientific*) in agitation at 4°C. The exact concentration of the protein was determined by measuring the colorimetric response at 562nm using the Pierce BCA protein assay kit (*Thermo Scientific*), following the manufacturer's instructions.

3.A.4. Spike-specific ELISA for serum titration

In order to titrate the serum of patients a Spike-specific ELISA was performed. A volume of 10µL per well of SARS-CoV-2 Spike glycoprotein was used to coat SpectraPlate-384 High Binding plates (*Perkin Elmer*), which have a high binding capacity, and then incubated overnight at 4°C. The following day, plates were washed three times with 100µL/well of Washing Buffer (PBS + 0.05% Tween-20 (*Sigma-Aldrich*)) and saturated with 35µL/well of Blocking Buffer (PBS + 1% Bovine Serum Albumin BSA (*Fisher Scientific*) + 1% Fetal Bovine Serum FBS) for 1h at 37°C. After three washes, 12µL of serum at different dilutions was added to the plate.

After incubation for 1h at 37°C, the plates were washed four times and incubated again for 1h at 37°C with 20µL of goat anti-human IgG (H+L) HRP conjugate antibody (*Invitrogen*, #A18805) diluted 1:3,500 in Blocking Buffer. Subsequently, the plates were washed six

times, and 20µL of 1-Step™ Ultra TMB (3,3′,5,5′-tetramethylbenzidine)-ELISA Substrate Solution (*Thermo Scientific*) was added and incubated for 20min at RT in the dark, followed by the addition of 20µL of 0.5M HCl. Absorbance was then measured at 450nm using a Spectramax M2 Microplates Reader. The threshold for sample positivity was set at twice the Optical Density (OD) of the blank.

3.A.5. Enrichment of ASCs from PBMCs

Enriched $CD138^+$ plasma cell preparations were obtained from PBMCs using the reagents provided with the CellSearch CMMC enumeration system (*Menarini Silicon Biosystems*) with some modifications.

In detail, 4×10^7 PBMCs were diluted in 2mL DPBS plus 2mL Dilution Buffer with 150µL capture enhancement reagent and anti-human CD138 conjugated to ferrofluid particles.

The enrichment was realized through three steps of incubation of 10min, plus 10min and another 20min in a quadrupole magnetic separation system (QMS17, *Immunicon Corp*). Each step was interspersed with gentle agitation of the cells and reagents present in the tube. At the end of the incubations, $CD138^+$ cells were attached to the tube wall, while unbound cells were removed with a Pasteur pipette without touching the tube wall in contact with the magnet. A wash step was then executed by adding 3mL of wash buffer (DPBS plus Binding Buffer) to the tube, followed by incubation in the magnetic separation system for 10min. The tube was then removed from the magnet to rescue the positively selected cells, which were then resuspended in 224µL of a mixture of equal volumes of DPBS and dilution buffer. Cell-bound ferrofluid particles were removed by a final incubation with biotin-containing buffer (included in the Menarini Silicon Biosystems kit) for 20min at RT in the dark, then it was washed with DPBS to finally obtain a cell population highly enriched for $CD138^+$ cells.

3.A.6. Selection of antigen-specific plasma cells

The enriched CD138$^+$ cells were counted and plated at 50 cells per well in low volume 384-well tissue culture treated microplates (*Corning*) in Antibody Expression Medium composed of RPMI 1640 (*Sigma-Aldrich*) + 10% FBS (*Gibco*), supplemented with 1× NeAA, 10ng/mL of recombinant human IL-6 and filtered supernatant of M2-10B4 feeder cells (ATCC CRL-1972).

After approximately 20h of incubation at 37°C with a humified atmosphere of 5% CO_2, the supernatant of each well was tested for antigen specificity using a Spike-specific ELISA assay, using Spectra Plate-384 High Binding plates previously coated with recombinant Spike protein at 10µg/mL (as previously described in section 3.A.4). For this analysis, it was prepared a negative control, only Antibody Expression Medium, and a positive control, using patient 5 serum dilutions. The wells that resulted positive for our antigen of interest were replated in the same condition by limiting dilution (0.7 cells per well in accordance with the Poisson Distribution rule) to have one cell per well. The following day, the ELISA assay was repeated to identify cells secreting Spike-specific immunoglobulins. These positive plasma cells were washed with 1× DPBS and preserved in 4µL of a specific lysis buffer composed of UltraPure^{TM} DNAse/RNAse-Free Distilled H_2O (*Invitrogen*), 10× sterile PBS, 0.1M DTT (*Promega*) and 40U/µL RNasin^{TM} Plus RNase Inhibitor (*Promega*). This step was performed in sterile conditions and these samples are then used for the Reverse-Transcriptase Chain Reaction (RT-PCR), or cryopreserved at -80°C.

3.A.7. Recovery of V_H and V_L coding sequences from single antigen-specific ASCs and "minigenes" assembly

The Spike-specific single CD138$^+$ plasma cell lysates were reverse transcribed to cDNA, using volume using Superscript IV reverse transcriptase (*Invitrogen*). The reaction volume for the RT was of 20µL, Oligo(dT)$_{12-18}$ Primer (*Invitrogen*) and Custom LNA Oligonucleotide Template-Switching Oligos-TSO (*Qiagen*) [AAGCAGTGGTATCAACGCAGAGTACATrGrG+G] were used for this reaction [158].

For this amplification step, Eppendorf^{TM} ep Dualfilter T.I.P.S^{TM} (*Eppendorf*) PCR clean and sterile were used, and all subsequent mixes were prepared in a DNA/RNA-free hood.

Single CD138$^+$ plasma cell lysates were thawed on ice for 5min and centrifugated at 400g for 30sec at 4°C. To each sample was then added 4µL of RT-PCR Mix I (Table **3.A.7.1**) in a circular motion along the edges of the tube:

Table 3.A.7.1. *RT-PCR Mix I.*

RT-PCR Mix I	**1×**	**Final concentration**
UltraPure™ DNase/RNase-Free Distilled H_2O (*Invitrogen*)	3µL	
25mM each dNTPs Mix (*Thermo Scientific*)	0.8µL	1mM each
100µM Oligo(dT)$_{12-18}$ Primer (*Invitrogen*)	0.2µL	1µM
Final volume/sample	4µL	

Subsequently, they were centrifuged at 400g for 1min at 4°C and incubated for 3min at 72°C in pre-heated MiniAmp™ Plus Thermal Cycler. After the incubation, samples were placed on ice for 1-5min, during which time the RT-PCR Mix II was prepared as shown below (**Table 3.A.7.*2***).

Table 3.A.7.2. *RT-PCR Mix II.*

RT-PCR Mix II	**1×**	**Final concentration**
5× SSIV Buffer(*Invitrogen*)	4µL	1×
50mM Betaine (*Merck*)	2.9µL	7.25mM
50mM $MgCl_2$ (*Invitrogen*)	2.4µL	6mM
100µM DL-DTT (*Promega*)	1µL	5µM
100µM Custom LNA Oligonucleotide TSO (*Qiagen*)	0.2µL	1µM
40U/µL RNasin™ Plus RNase Inhibitor (*Promega*)	0.5µL	1U/µL
200U/µL SuperScript™ IV Reverse Trascriptase (*Invitrogen*)	1µL	10U/µL
Final volume/sample	12µL	

12µL of RT-PCR Mix II were added to each sample, then they were centrifugated at 400g for 1min at 4°C and incubated in a MiniAmp™ Plus Thermal Cycler with the following amplification profile (**Table 3.A.7.3**):

Table 3.A.7.3. *Amplification profile of RT-PCR.*

Temperature	**Time**
42°C	10min
25°C	10min
50°C	1h
94°C	5min
4°C	∞

The cDNA obtained was pre-amplified with Terra^{TM} PCR Direct Polymerase (*Takara Bio*), in order to increase the total amount of genetic material while maintaining reduced amplification bias, and IS-PCR primers [AAGCAGTGGTATCAACGCAGAGT] (*Eurofins Genomics*) [159].

In order to do this, 10µL of each cDNA sample diluted 1:2 in UltraPure^{TM} DNase/RNase-Free Distilled H_2O were added to 15µL of preAmp-PCR Mix (as in the table below).

Table 3.A.7.4. *PreAmp-PCR Mix.*

preAmp-PCR Mix	**1×**	**Final concentration**
UltraPure^{TM} DNase/RNase-Free Distilled H_2O (*Invitrogen*)	1.95µL	
2× Terra PCR Direct Buffer (*Takara Bio*)	12.5µL	1×
10µM IS-PCR primers (*Eurofins Genomics*)	0.05µL	20nM
1.25U/µL Terra PCR Direct Polymerase Mix (*Takara Bio*)	0.5µL	0.025U/µL
Final volume/sample	15µL	

cDNA pre-amplification was conducted using a MiniAmp^{TM} Plus Thermal Cycler, with the following amplification profile (**Table 3.A.7.*5***):

Table 3.A.7.5. *Amplification profile used for cDNA pre-amplification.*

Step	Temperature	Time	Cycle
Initial denaturation	98°C	3min	1
Denaturation	98°C	15sec	18
Annealing	65°C	30sec	
Extension	68°C	4min	
Final extension	72°C	10min	1
Maintenance	4°C	∞	-

Primers adapted from Tiller T. et al. [160], were used to amplify immunoglobulin heavy (IgH) and light chains (Igκ and Igλ) by two nested PCR reactions, using KOD DNA Polymerase and Taq DNA Polymerase. That means that the template for the I PCR was the cDNA and the pre-amplified DNA, while the template for the II PCR was the cDNA and the pre-amplified DNA resulting from the first PCR. A third PCR was then carried out to produce the transcriptionally active PCR (TAP) linear DNA fragments for both the heavy and light chains, which included the variable regions, a constant region fragment (containing a poly-A signal sequence), and a promoter region useful for direct transfection in mammalian cells. As templates to obtain pCMV and C_H/Cκ/Cλ-polyA constant region fragments, it was used AbVec2.0-IGHG1 (Addgene plasmid #80795; AbVec2.0-IGHG1), AbVec1.1-IGKC (Addgene plasmid #80796; AbVec1.1-IGKC) and AbVec1.1-IGLC2-XhoI (Addgene plasmid #99575; AbVec1.1-IGλC), three recombinant plasmids encoding respectively immunoglobulin heavy and light chains with constant region (IgG1 and kappa or lambda isotype) of a human antibody [161].

In this minigenes assembly or TAP PCR to 22μL of V_H/V_L PCR Mix was added 1μL of AbVec2.0-IGHG1/AbVec1.1-IGKC/ AbVec1.1-IGLC2-XhoI plasmids, previously diluted with UltraPure™ DNase/RNase-Free Distilled H_2O to a final concentration of 10ng/μL, and 2μL of the insert deriving from II PCR proportionally diluted.

Primers used in each amplification step were resuspended with UltraPure™ DNase/RNase-Free Distilled H_2O at 100pmol/μL and the mixed together, **Table 3.A.7.6.** shows primers used. Subsequently, 0.1μL of each primer mix was added to the corresponding PCR mix.

Primers used for the TAP step were CMV-WA-F (CGCCCGACATTGATTATTGACTAG) and SV40epA2-R (GATCCAGACATGATAAGATACATTG).

Table 3.A.7.6. *Primer sequences.*

Forward primer	Primer name	Sequence 5'-3'
VH1F	hIGHV-1/7-066-F	ACAGGTGCCCACTCCCAGGTGCAG
VH1F	hIGHV-3-066-F	AAGGTGTCCAGTGTGARGTGCAG
VH1F	hIGHV-4/6-066-F	CCCAGATGGGTCCTGTCCCAGGTGCAG
VH1F	hIGHV-5-066-F	CAAGGAGTCTGTTCCGAGGTGCAG
VH1F	hIGHV-1/7-017-F	ATGGACTGGACCTGGAG
VH1F	hIGHV-1/7-041-F	TCCTCTTTGTGGTGGCAGCAGC
VH1F	hIGHV-2-035-F	TCCACGCTCCTGCTRCTGAC
VH1F	hIGHV-3-057-F	TAAAAGGTGTCCAGTGT
VH1F	hIGHV-4-022-F	ATGAAACACCTGTGGTTCTTCC
Vκ1F	hIGKV-1-060-F	ATGAGGSTCCCYGCTCAGCTGCTGG
Vκ1F	hIGKV-3-049-F	CTCTTCCTCCTGCTACTCTGGCTCCCAG
Vκ1F	hIGKV-4-049-F	ATTTCTCTGTTGCTCTGGATCTCTG
Vλ1F	hIGLV-1-068-F	GGTCCTGGGCCCAGTCTGTGCTG
Vλ1F	hIGLV-2-068-F	GGTCCTGGGCCCAGTCTGCCCTG
Vλ1F	hIGLV-3-068-F	GCTCTGTGACCTCCTATGAGCTG
Vλ1F	hIGLV-4/5-068-F	GGTCTCTCTCSCAGCYTGTGCTG
Vλ1F	hIGLV-6-068-F	GTTCTTGGGCCAATTTTATGCTG
Vλ1F	hIGLV-7-068-F	GGTCCAATTCYCAGGCTGTGGTG
Vλ1F	hIGLV-8-083-F	GAGTGGATTCTCAGACTGTGGTG
VH3F	AgeI VH1	CTGCAACCGGTGTACATTCCCAGGTGCAGCTGGTGCAG
VH3F	AgeI VH1-18	CTGCAACCGGTGTACATTCCCAGGTTCAGCTGGTGCAG
VH3F	AgeI VH1-24	CTGCAACCGGTGTACATTCCCAGGTCCAGCTGGTACAG
VH3F	AgeI VH1/5	CTGCAACCGGTGTACATTCCGAGGTGCAGCTGGTGCAG
VH3F	AgeI VH3	CTGCAACCGGTGTACATTCTGAGGTGCAGCTGGTGGAG
VH3F	AgeI VH3-9	CTGCAACCGGTGTACATTCTGAAGTGCAGCTGGTGGAG
VH3F	AgeI VH3-23	CTGCAACCGGTGTACATTCTGAGGTGCAGCTGTTGGAG
VH3F	AgeI VH3-33	CTGCAACCGGTGTACATTCTCAGGTGCAGCTGGTGGAG
VH3F	AgeI VH4	CTGCAACCGGTGTACATTCCCAGGTGCAGCTGCAGGAG
VH3F	AgeI VH4-34	CTGCAACCGGTGTACATTCCCAGGTGCAGCTACAGCAGTG
VH3F	AgeI VH4-39	CTGCAACCGGTGTACATTCCCAGCTGCAGCTGCAGGAG
VH3F	AgeI VH6-1	CTGCAACCGGTGTACATTCCCAGGTACAGCTGCAGCAG
VH3F	AgeI VH7	CTGCAACCGGTGTACATTCTCAGGTGCAGCTGGTGCAATCTGG
Vκ3F	AgeI VK1-5-F	CTGCAACCGGTGTACATTCTGACATCCAGATGACCCAGTC
Vκ3F	AgeI VK1-5b-F	CTGCAACCGGTGTACATTCAGACATCCAGTTGACCCAGTCT
Vκ3F	AgeI VK1-6-F	CTGCAACCGGTGTACATTCTGCCATCCAGATGACCCAGTC
Vκ3F	AgeI VK1-13-F	CTGCAACCGGTGTACATTCTGCCATCCAGTTGACCCAGTC

Vκ3F	AgeI VK1D-43-F	CTGCAACCGGTGTACATTGTGCCATCCGGATGACCCAGTC
Vκ3F	AgeI VK2-24-F	CTGCAACCGGTGTACATGGGGATATTGTGATGACCCAGAC
Vκ3F	AgeI VK2-28-F	CTGCAACCGGTGTACATGGGGATATTGTGATGACTCAGTC
Vκ3F	AgeI VK2-30-F	CTGCAACCGGTGTACATGGGGATGTTGTGATGACTCAGTC
Vκ3F	AgeI VK3-11-F	CTGCAACCGGTGTACATTCAGAAATTGTGTTGACACAGTC
Vκ3F	AgeI VK3-15-F	CTGCAACCGGTGTACATTCAGAAATAGTGATGACGCAGTC
Vκ3F	AgeI VK3-20-F	CTGCAACCGGTGTACATTCAGAAATTGTGTTGACGCAGTCT
Vκ3F	AgeI VK4-1-F	CTGCAACCGGTGTACATTCGGACATCGTGATGACCCAGTC
Vλ3F	AgeI VL1-F	CTGCTACCGGTTCCTGGGCCCAGTCTGTGCTGACKCAG
Vλ3F	AgeI VL2-F	CTGCTACCGGTTCCTGGGCCCAGTCTGCCCTGACTCAG
Vλ3F	AgeI VL3-F	CTGCTACCGGTTCTGTGACCTCCTATGAGCTGACWCAG
Vλ3F	AgeI VL4/5-F	CTGCTACCGGTTCTCTCTCSCAGCYTGTGCTGACTCA
Vλ3F	AgeI VL6-F	CTGCTACCGGTTCTTGGGCCAATTTTATGCTGACTCAG
Vλ3F	AgeI VL7/8-F	CTGCTACCGGTTCCAATTCYCAGRCTGTGGTGACYCAG
Reverse primer	**Primer name**	**Sequence 5'-3'**
VH1R	hIGHG-137-R	GGAAGGTGTGCACGCCGCTGGTC
VH1R	hIGHA-111-R	GTCCGCTTTCGCTCCAGGTCACACT
VH1R	hIGHM-082-R	GGAAGGAAGTCCTGTGCGAGGC
Vκ1R	hIGKC-172-R	GTTTCTCGTAGTCTGCTTTGCTCA
Vλ1R	hIGLC-057-R	CACCAGTGTGGCCTTGTTGGCTTG
VH3R	Hu-VH-PP-R	CTTGGAGGAGGGTGCCAGGGGGAAGACcga
Vκ3R	C080-VKsh-R	GATTTCAACTGCTCATCAGATGGCGGGAAG
Vλ3R	Hu-VL-PP-R	GTTGGCTTGAAGCTCCTCAGAGGAG

3.A.8. Recombinant antibody produced by the transient expression of TAP in the Deepwell plates Expi 293 system

The minigenes obtained through the TAP PCR were used to transiently transfect Expi293F™ cells by using the ExpiFectamine™ 293 Transfection Kit (*Gibco*), adapting manufacturer's instructions to a smaller scale transfection, Deepwell Plates 96/2mL.

The day before the transfection, Expi293F™ cells were grown at a density of 1-2×10^6 viable cells/mL in 125mL shaker flasks (*Corning*) and maintained Over Night (O/N) at 37°C, 8% CO_2, shaking at 125rpm.

On the day of transfection 7×10^7 viable cells were recovered and diluted in 49mL of fresh, pre-warmed Expi293F™ Expression Medium, in order to have approximatively a final density of 1.4×10^6 viable cells per mL. Subsequently, 700µL of cells were aliquoted into the 60 internal wells of the 96-deepwell plate, reaching a concentration of 1×10^6 cells per well, while the external 36 wells were filled with distilled water in order to prevent evaporation.

Paired Transcriptionally Active heavy and light chain PCR fragments (TAP) or plasmid DNA encoding cloned antibodies at a 1:2 ratio. The TAP DNA for each well was diluted in OptiMEM™ I Reduced Serum Medium to a final volume of 35µL. In the meantime, 1.08µL of Expifectamine™ 293 reagent, necessary for the process of transfection, instead, was diluted to a final volume of 35µL in OptiMEM™I Reduced Serum Medium and incubated for 5min at RT.

At this point, the DNA dilutions were mixed with the diluted mix of ExpiFectamine to have a final volume of 70µL, incubated for 20min at RT and then added drop by drop to each well containing the Expi293F™ cells. The deepwell was then incubated at 37°C, in an environment with a humified atmosphere of 8% CO_2, at 1,000rpm with MixMate™ Shaker.

ExpiFectamine™ 293 Transfection Enhancers 1 (2µL/well) and 2 (20µL/well) were added 18-22 hours post-transfection (hpt) into each well, based on the manufacturer's protocol to enhance both transfection and protein expression.

The supernatants from the cell culture were collected at 3 and 6 dpt. Next, the cells were centrifuged at 400g for 5min. The collected supernatants were further analysed, at a single point and dilution curve, through a qualitative ELISA to validate the binding activity against the Spike protein (see section 3.A.4) and a quantitative ELISA to determine the Igs concentrations.

3.A.9. Quantitative ELISA assay for the detection of Immunoglobulins produced by a single ASC/ TAP products

The secretion of human IgGs by individual ASCs or recombinant monoclonal antibodies present in transiently transfected Expi293F™ cell supernatant was quantified using an ELISA assay.

Recombinant Cetuximab (*Merck*) was used as the standard or positive control. Spectra Plate 384 High-Binding Plates were coated with 10µL/well of unconjugated goat anti-human IgG Fc (*Invitrogen*) at a concentration of 1µg/mL. Plates were incubated at 4°C overnight. After this step, the plates were washed three times with a Washing Buffer containing phosphate-buffered saline and Tween-20 (0.05%). Thirty-five microliters of blocking buffer containing 1% BSA, 1% FBS, and phosphate-buffered saline were added to each well.

The plate was incubated at 37°C for 1h. Following three washes, single-concentration/serially diluted supernatants or the diluted standard were added. The blank was prepared with the blocking buffer. After incubating for 1h at 37°C, the plates were washed four times. Then, 20µL of the diluted secondary antibody solution, containing goat anti-human IgG H+L HRP conjugate and blocking buffer in the ratio of 1:3,500, was added. The plates were then incubated for an additional hour at 37°C and washed six more times. Then, 20µL of the 1-Step™ Ultra TMB ELISA Substrate Solution was added to the mixture, which was subsequently incubated for 20min in a dark room at room temperature. Finally, 20µL of 0.5M HCl was added. The level of absorbance was quantified at a wavelength of 450nm. The concentration of immunoglobulin in the supernatant was determined by extrapolating the sample values using the standard curve as a reference.

3.A.10. V_H and V_L sequences cloning into expression vectors

Once assessed the effective Spike specificity, the best mAbs were selected and prepared for the generation of stably coding plasmids, useful for both sequencing and functional analyses. The coding sequences of the corresponding heavy and light variable regions genes were inserted into AbVec2.0-IGHG1 and AbVec1.1-IGKC and AbVec1.1-IGLC2-XhoI recombinant plasmids, which will act as expression systems for their large-scale production. First of all recombinant plasmids were enzymatically cleaved using the restriction enzymes EcoRI HF and Hind III HF, opening in this way the plasmid backbone.

Then the V_H/V_L TAP products were amplified using specific primers (**Table 3.A.10.1**), gel purified by using QIAquick Gel Extraction Kit, and then cleaved using the same restriction enzymes EcoRI HF and Hind III HF, to obtain the variable linear fragment of DNA.

Table 3.A.10.1. *Primer sequences.*

These two primers were used for cloning, H-IgClo-F as a forward primer and H-IgClo-R as a reverse primer.

Primer name	**Sequence 5'-3'**
H-IgClo-F	ACTGCACCTCGGTTCTATCG
H-IgClo-R	ACAAGTTGGGCCATGGCG

The vector and the insert were then ligated in a 20µL reaction (1:10 molar ratio) by using the T4 enzyme (*Invitrogen*).

All plasmids were transformed in *Escherichia coli* DH5α competent cells (*Life Technologies-Invitrogen*), following the manufacturer's instructions.

Briefly, an aliquot of 50µL of chemically competent cells for each transformation was carefully thawed on ice and added to 1:10 of ligase reaction, previously placed into a 1.5mL microcentrifuge tube. Cells with DNA were incubated on ice for 30min and then heat-shocked for 20sec at 42°C in the water bath. After an incubation of 2min on ice, 1mL of pre-warmed sterilized LB medium (Miller LB broth- *Sigma-Aldrich*) was added to each tube and incubated at 37°C for 1h at 225rpm, using Minitron Incubator Shaker (*Infors HT*). Then transformed cells were spread on pre-warmed selective plates for bacterial culture and incubated at 37°C O/N. These plates were previously prepared with Lennox LB broth with agar (*Sigma-Aldrich*) plus 100µg/mL Ampicillin (*Millipore*).

The following day, colonies present on the plates were expanded in 100µL of LB + 100µg/mL ampicillin medium for 3h at 37°C in the incubator shaker for bacterial cultures at

250rpm, and screened through colony PCR with specific primers to evaluate the effective presence of the insert of interest in the plasmid. Only 1µL of the bacterial culture was used for the PCR reaction, better detailed in **Table 3.A.10.2.**

Table 3.A.10.2. *Colony PCR Mix.*

Colony PCR Mix	**1×**	**Final concentration**
UltraPure™ DNase/RNase-Free Distilled H_2O (*Invitrogen*)	5.6µL	
10× Taq DNA Polymerase PCR Buffer (*Invitrogen*)	1µL	1×
2.5mM each dNTP Mix (*Invitrogen*)	1µL	0.25mM each
50mM $MgCl_2$ (*Invitrogen*)	1µL	5mM
100µM Primer Forward (*Eurofins Genomics*)	0.1µL	1µM
100µM Primer Reverse (*Eurofins Genomics*)	0.1µL	1µM
5U/µL Taq DNA Polymerase, recombinant (*Invitrogen*)	0.2µL	0.1U/µL
Final volume/sample	9µL	

Then the quality of the amplified products was evaluated by run on an electrophoresis 1% agarose gel with 1× TAE Buffer, using 1 Kb DNA Ladder for DNA sizing.

Only if positive, colonies were expanded into 5mL LB + 100µg/mL ampicillin medium, to amplify and purify plasmids using QIAprep Spin Miniprep Kit, (*Qiagen*), as per manufacturers' instructions.

Briefly, the bacterial cultures were centrifuged at 4,000rpm for 10min, then the pellets were resuspended in 250µL of Resuspension Buffer P1. The bacterial cells were at this point lysed by adding 250µL of Lysis Buffer P2, mixed by inversion of the tube, and incubated for a maximum of 5min at RT. After that, 350µL of Neutralization/Binding Buffer N3 was added to stop the cell lysis: this determined the formation of precipitates with a gelatinous consistency that contains both cellular debris and genomic DNA.

The suspensions obtained were centrifuged at 13,000rpm for 10min. The supernatants, containing the DNA of interest, were transferred into a QIAprep spin column and centrifuged at 8,000rpm for 1min, in order to retain the plasmid DNA in the silica membrane. The columns were washed by first adding 500µL of Wash Buffer PB and then 750µL of Wash Buffer PE, a centrifugation step was performed each time at 13,000rpm for 1min. To remove any residual ethanol traces of Wash Buffer PE from the silica membranes, an additional centrifuge step of 2min at 13,000rpm was done.

The plasmids were, in the end, eluted in 50µL of Elution Buffer EB and recovered by centrifugation at 13,000rpm for 2min.

Quantification of DNA and purity was determined by measuring the absorbance at 260nm and 280nm with NanoVue^{TM} 4282 V1.7 Spectrophotometer (*GE Healthcare*).

Only plasmids with a A_{260}/A_{280} ratio between 1.75 and 2.00 were kept and used for the subsequent transfection and sequencing steps.

3.A.11. SARS-CoV-2 virus neutralization assay

The neutralization assay for SARS-CoV-2 virus was conducted on Vero E6 cells (ATCC CRL-1586) in a 96-well microplate. Two-fold serial dilutions (1:4 to 1:1024) of mAbs, each at 25µL, were combined with an equivalent volume of SARS-CoV-2 WT strain (SARS-CoV-2/human/ITA/Siena-1/2020; GenBank: MT531537.2), Delta (B.1617.2) (SARS-CoV-2/human/ITA/TUS-Siena-40/2021; GenBank: OM736177.1), or Omicron (BA.1) (SARS-CoV-2/human/ITA/TUS-Siena5324294/2022; GenBank: OM956353.1), each containing 100 $TCID_{50}$. This was followed by incubating the mixture at 37°C for 90min. A final addition of 50µL of Vero E6 cell suspension (2×10^5 cells/mL) prepared in complete DMEM (*Lonza*) was made to each well. The cultures were incubated at 37°C and examined daily under an Olympus IX51 microscope to identify the presence of CytoPathic Effects (CPE). The Reed-Muench method [26] was used to calculate the 50% endpoint titer, and the assay included positive and negative control serum. The Geometric Mean Titers (GMTs) for the neutralization assays were calculated.

3.A.12. *In silico* study of mAbVE-12, binding interactions with NTD and RBD regions of the Spike glycoprotein

The possible binding modes between the RBD of the Spike and mAbVE-12, as well as, between the N-terminal domain and mAbVE-12 were studied using antibody homology modelling and the crystal structures of NTD and RBD of the Spike. The homology modelling of the Variable Regions of the mAb has been attempted with ABodyBuilder-ML web server [162]. The Antibody CDRs were defined using the IMGT (ImMunoGeneTics database), numbering scheme [163]. The missing residues of the RBD and the NTD of the Spike structure were modelled using the method available in the web server Swiss-Model [164] using as a starting structure the coordinate set identified by the Protein Data Bank (PDB) code 6VXX. This structure was selected on a set of criteria including the experimental method used, the resolution, if applicable, and the coverage, calculated as the percentage of solved residues over the total number of amino acids of the protein (UniProt numbering). Delta and Omicron Variants of Spike NTD and RBD and antibody complexes have been modelled by *in silico* mutagenesis using the *ad hoc* tools in PyMOL [165]. Docking experiments were performed with ClusPro [166]. Protein-protein interaction energy was predicted with the method implemented in PRODIGY [167] using the default parameters (temperature 25°C). The interactions taking place at the interface of the predicted complexes were identified with the RING 2.0 web server [168]. Protein structural analysis and visualization have been carried out with PyMOL.

3.A.13. Monoclonal antibody repertoire analyses

V_H and V_L sequence reads of monoclonal antibodies were manually curated and retrieved using CLC Main Workbench (*Qiagen*). The analyzed reads were saved in FASTA format, and the repertoire analyses were performed using standalone IgBlast [169]. Comparison analysis was performed in Python using NumPy (https://numpy.org/) and Pandas (https://pandas.pydata.org/), while figures were produced using the Matplotlib tool (https://matplotlib.org/) and Seaborn (https://seaborn.pydata.org/).

4.A. Results

4.A.1. Antibody immune response to the Spike protein in subjects.

The study began with the systematic evaluation of serum from subjects whose peripheral blood had been collected for the isolation of PBMCs, the source cells for the development of the method.

The samples were obtained from five convalescent donors recovering from SARS-CoV-2 infection, provided by the Azienda Ospedaliero Universitaria Pisana - UO Malattie Infettive. The blood was collected after viral clearance, confirmed by two negative PCR tests.

As shown in **Table 4.A.1.1**, the age of the five patients ranged from 44 to 78 years, and the blood was donated between 2 and 6 weeks after illness onset.

As a first step at the start of the study, patients were characterised on the basis of their antibody titres in the ELISA, using an antigen-specific ELISA test with the Spike protein (**Figure 4.A.1.1**).

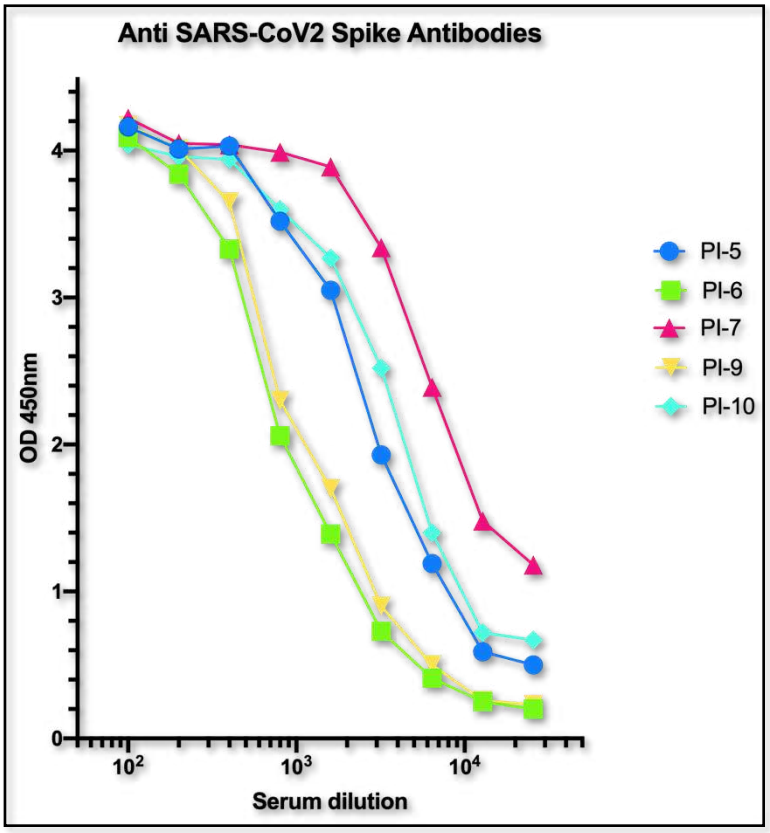

Figure 4.A.1.1. *Antibody immune response to the Spike protein in study subjects.*

The legend on the right side shows the different samples tested (PI-5, PI-6, PI-7, PI-9, PI-10), on the X-axis we can find the serum dilution and on the Y-axis the OD value.

The half-maximal Effective Concentration (EC50), which is the concentration of serum antibody that induces a biological response midway between the baseline and the maximum after the specified exposure time, is shown on the right-hand side of **Table 4.A.1.1**.

Table 4.A.1.1. *Summary table of study subjects.*

For each patient, it is indicated the age, days from recovery and the EC50 titers in ELISA.

Patient code	**Age**	**Days after onset**	**ELISA titers EC50**
PI-005	44	20	3062
PI-006	62	15	677
PI-007	72	44	9780
PI-009	53	24	872
PI-010	78	22	4588

According to the EC50 data, patients 7, 10, and 5 showed a very strong serum titration, whereas patients 6 and 9 had slightly lower titers. In general, the serum titration was very good, which led us to select these samples for the subsequent steps.

4.A.2. Isolation of plasma cells using FerroFluid™ technology

The aim of this study was to develop a simple, rapid and reproducible method for the generation and screening of mAbs starting from the peripheral blood of convalescent patients.

This section describes the methodology developed to isolate plasma cells using the FerroFluid™ (FF) technology, adapting and refining the guidelines provided by Menarini.

The method for ASC isolation is shown in **Figure 4.A.2.1** and described below.

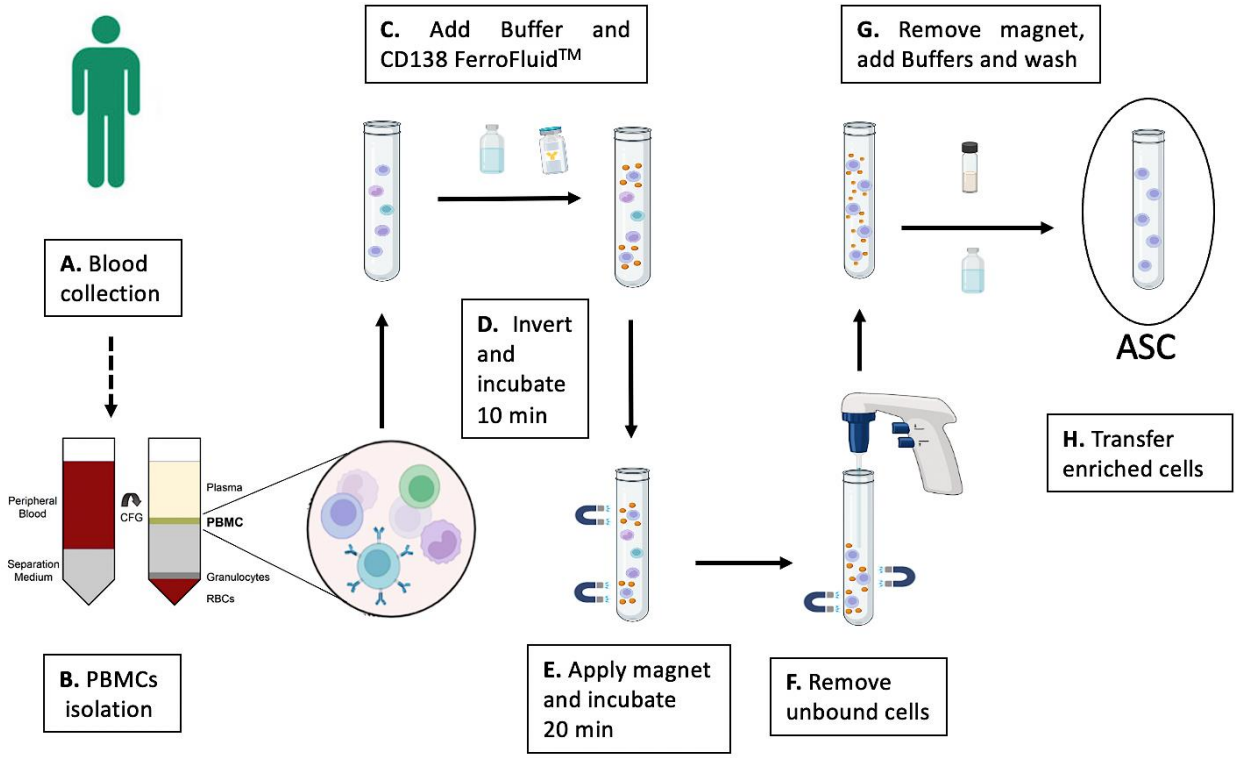

Figure 4.A.2.1. *Overview of ASCs isolation using FerroFluid™ technology.*

Schematic illustration of the key steps in the enrichment of the blood ASC population using CD138-coupled magnetic nanoparticle technology.

Approximately 40mL of blood was collected from patients (A) and PBMCs were purified using Ficoll (B) as described in the Materials and Methods section.

The recovered PBMCs were diluted with both Dilution Buffer and PBS and then the FF-CD138 mAb diluted in Capture Enhancement Buffer was added (C).

The tube containing the sample and reagents was well mixed and incubated for 10min (D).

After further mixing by inversion, the tube was placed in the magnet and incubated for 20min (E). At this point, the $CD138^{+}$ cells conjugated to the FF particles are bound to the tube wall by the magnetic field.

Unbound cells are now removed with a Pasteur pipette (F) without touching the wall.
The tube containing the cells of interest is removed from the magnet and, after a further incubation in the dark, is eluted with diluted biotin buffer (G).
The ASCs are then collected, centrifuged and diluted in an appropriate volume of medium (H). The process of enrichment and isolation of ASCs from peripheral blood takes approximately 2 hours.
As shown in **Table 4.A.2.1,** the starting material of PBMCs was variable between samples, ranging from 42 to 117×10^6 cells. The recovered $CD138^+$ cells ranged from 0.6 to 5.9‰ of the total PBMCs, with a mean detection of these rare cells of approximately 3.7‰ of the total.
Overall, the number of ASCs per µL of blood is variable, patient 9 has a lower number but according to these data it is possible to say that the blood contains on average 5.7 ASCs per microlitre.
These data are calculated using our $CD138^+$ cell isolation system in a proof-of-concept study, so further data may be needed to implement and confirm these figures.

Table 4.A.2.1. *Summary table: yields of ASC-enriched PBMCs.*

This table shows for each sample the amount of blood used (mL), the number of PBMCs isolated, the number of CD138-positive antibody-secreting cells recovered, the number of ASCs per microlitre of blood and the percentage of ASCs per PBMC.

Source ID	**Blood obtained (mL)**	**Recovered PBMCs ($\times10^6$)**	**Recovered $CD138^+$ ASCs ($\times10^3$)**	**ASC/uL blood**	**‰ ASC in PBMCs**
PI-005	44	117	136	6.2	2.3
PI-006	40	42	167	4.2	4.0
PI-007	40	62	280	7.0	4.5
PI-009	40	90	25	1.3	0.6
PI-010	40	68	400	10.0	5.9

To understand whether the recovered CD138-enriched cells could be used to screen for antigen-specific monoclonal antibodies, their ability to secrete antibodies was tested in a functional assay *in vitro* by establishing single cell cultures and testing the supernatants in a quantitative ELISA. After 16 hours of culture, 4% of the culture supernatants contained detectable amounts of human IgGs above the 200ng/mL sensitivity of our assay, as shown in **Figure 4.A.2.2**, demonstrating the feasibility of our approach.

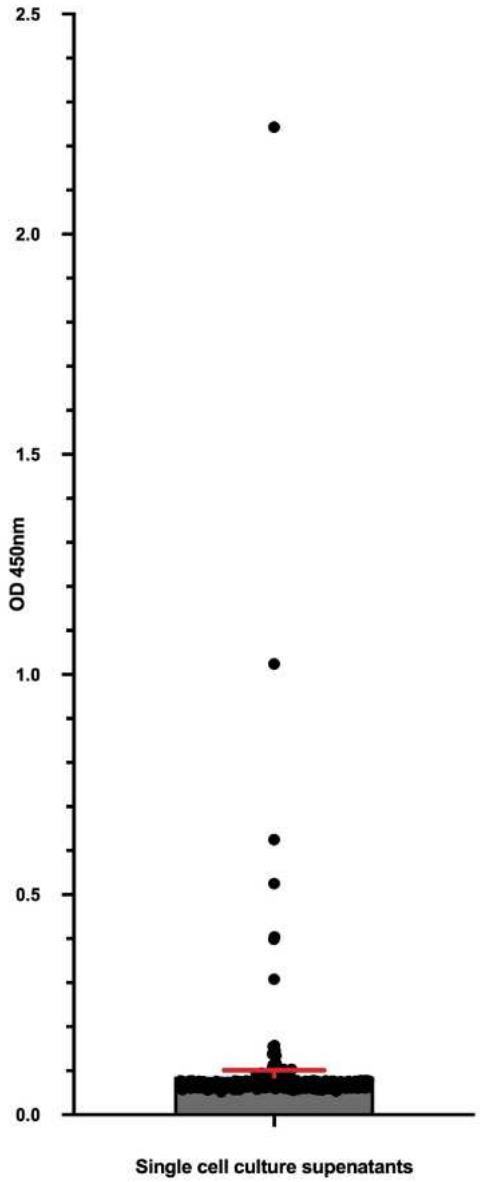

Figure 4.A.2.2. *Evaluation of IgG secretion in ASC-enriched cultures.*

The quantitative ELISA graph shows the amount of IgGs produced by a single cell after 16 hours of culture, with each point representing a single result. The assay threshold is set at 200ng/mL. Human IgG concentrations exceeding 200ng/mL were detected in more than 4% of the culture supernatants.

4.A.3. Isolation of Spike-specific PCs

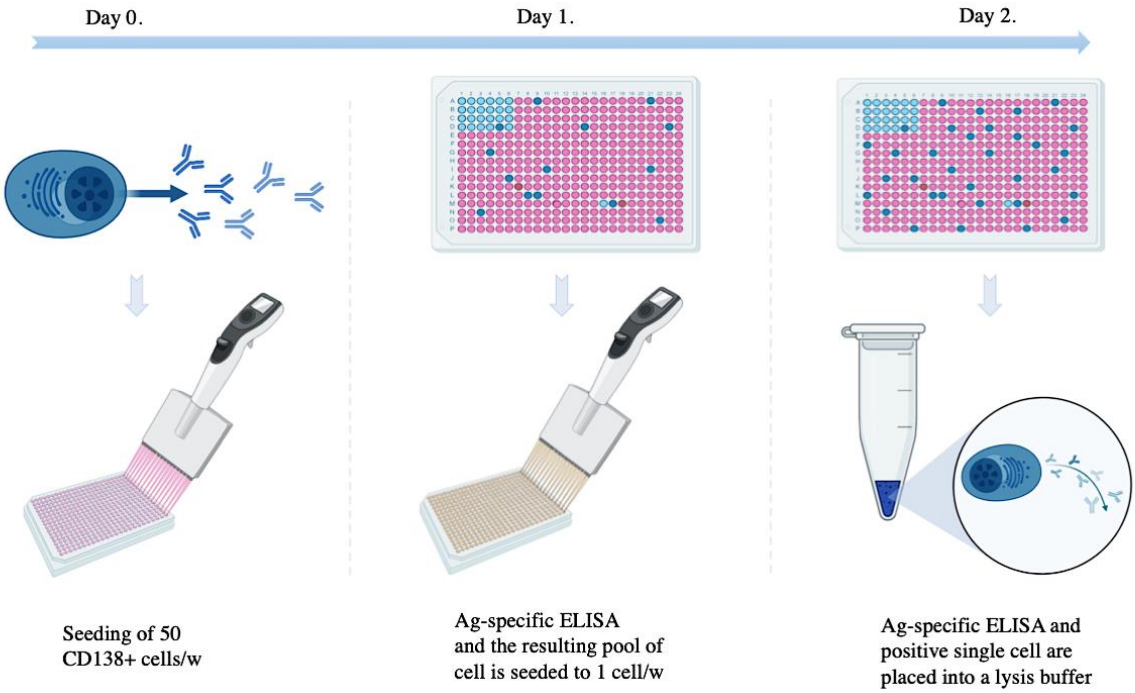

Figure 4.A.3.1. *Schematic of the method used to isolate single Spike specific CD138$^+$ plasma cells.*

Day 0. On the day of enrichment, CD138$^+$ cells are plated in a 384-well plate with the nutrient medium at a concentration of 50 cells/well. Day 1. After a Spike-specific ELISA with the supernatant of the cells plated the day before, it is determined which pool of cells (coloured wells) is positive and therefore needs to be replated again with fresh medium, but at a density of 1 cell per well. Day 2. Another Spike-specific ELISA is performed to determine which wells, i.e. individual cells, have antigen-specific mAbs, indicating which cells need to be harvested and frozen for the subsequent steps.

The second step of this method involves the isolation of single antigen-specific ASCs, the process shown in **Figure 4.A.3.1**.

For this, on the day of the enrichment, the CD138$^+$ samples were seeded in a pool of 50 cells per well in 384 microplates with the medium, IL-6 and a precise amount of secretome, conditions essential for cell survival and capable of stimulating antibody secretion, as observed after several tests to determine the best culture conditions, and kept in the incubator at 37°C overnight. The next day, the supernatant from each well was tested in a Spike-specific ELISA to determine which well contained a pool of antigen-specific ASCs.

The results were analysed and those wells with OD values greater than three times the background value were considered as positive wells, which were then replated, under the same culture conditions by limiting dilution to have 0.7 cells per well according to the Poisson distribution.

After overnight, the supernatant of each individual cell was tested in a second screening round to identify each Spike-specific ASC. These cells were then added to a small volume of lysis buffer to allow for subsequent amplification steps.

Using this approach, it was possible to identify and isolate over one hundred single Spike-specific antibody-secreting plasma cells from the peripheral blood of the five donors (**Table 4.A.3.1**).

Table 4.A.3.1. *Summary of antigen-specific single ASCs recovered from the CD138$^+$ enriched plasma cells.*

The starting number of ASCs used for each donor, the number of Spike-specific single cells recovered and the percentage of antigen-specific ASCs compared to the total are reported here.

Source ID	**ASCs input (×10^3)**	**Single Antigen-specific ASCs**	**‰ of Ag-specific ASCs**
PI-005	50	6	0.12
PI-006	105	17	0.16
PI-007	20	1	0.05
PI-009	25	28	1.12
PI-010	240	80	0.33
Total	440	132	0.3

4.A.4. Recovery of V_H and V_L genes of immunoglobulins from single antigen-specific ASCs and "minigenes" assembly

The Spike-specific single CD138$^+$ plasma cell lysates were reverse transcribed into cDNA and pre-amplified to obtain abundant starting material. This cDNA was subjected to a two-step PCR to amplify the cognate V_H and V_L genes of the antibodies, and then a third PCR was used to insert them into a fragment encoding the constant region together with a strong promoter and polyadenylation signal, creating Transcriptionally Active PCR (TAP) fragments called "minigenes".

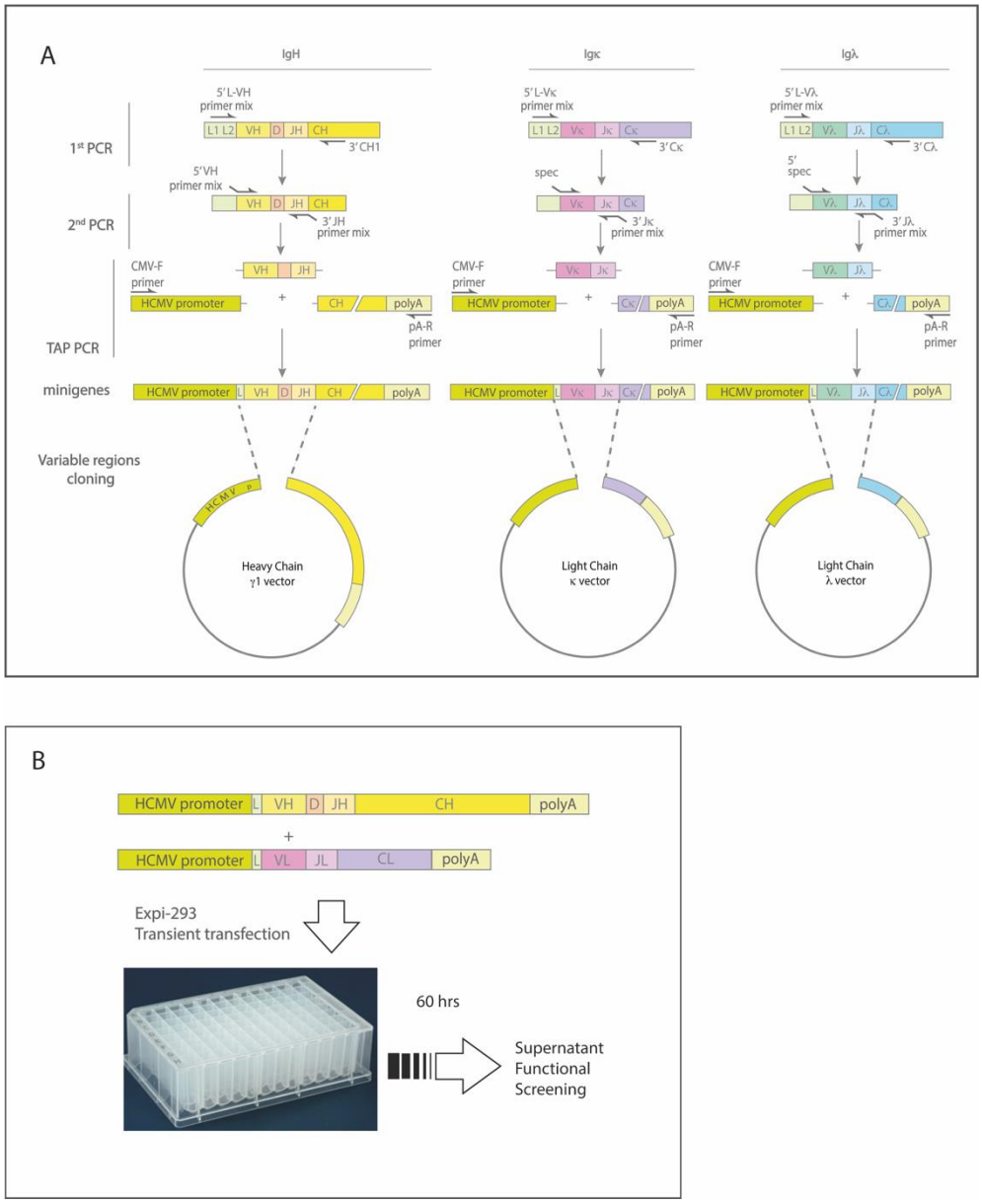

Figure 4.A.4.1. *PCR strategy used.*

A. *Schematic of 1st, 2nd and TAP PCR.* ***B.*** *Strategy for minigene assembly and expression of human mAbs in mammalian cells.*

Figure 4.A.4.1.A shows the I, II and III PCRs for the heavy and light (k and lambda) chains. In the first PCR, a specific mix of primers is used to amplify the heavy and light variable region sequences by annealing to the 5' end of the leader sequence, upstream of the FrameWork 1 Region (FWR1) of the mature V_H and V_L sequences, and to the 3' end of the corresponding C_H1 (heavy) and Cκ or Cλ (light) regions. In the second nested PCR, the primers anneal with FWR1 at the 5' end and the J regions at the 3' end, adding the specific isotype for the heavy variable regions. These oligonucleotides add a few base pairs (approximately 20-15bps) and this is essential for the generation of overlapping regions at the end of the 1st PCR products, which are required for the assembly of the TAP products (3rd PCR). On the right, **Figure 4.A.4.1.B**, it is shown that these linear minigenes contain a human CMV promoter and a human heavy and light chain constant region fused to a polyadenylation (poly A) signal at the 5' and 3' ends of the V_H and V_L regions, respectively. These regulatory regions were previously amplified from AbVec2.0-IGHG1 and AbVec1.1-IGKC and AbVec1.1-IGLC2 plasmids.

At this point, the TAP linear products are obtained (**Figure 4.A.4.2)** and are ready for direct transfection into mammalian cells to generate human recombinant monoclonal antibodies directly from the paired H and L chain PCR products without further cloning or purification steps.

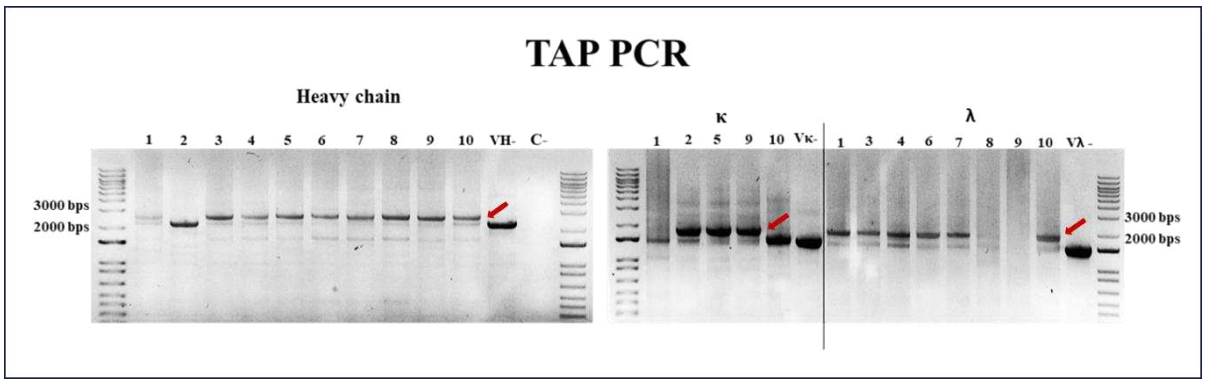

Figure 4.A.4.2. *Transcriptionally active PCR (TAP) products.*

Minigenes are assembled by Polymerase Chain Reaction (PCR).

Figure 4.A.4.3 shows the amplified products of the second PCR for the HC, the expected band of about 480bps and KC, of about 370bps and λC, similar to the previous one of about 390bps. On the left side is the amplification obtained directly from the cDNA, while on the right side of the figure, the same PCR was performed starting from the pre-amplified products; this additional data is also important to confirm that our amplification product is

indeed what we expect. Usually, for a sample it is possible to see the amplification of the variable heavy chain and one of the two variable light chains or $V_L\kappa$ or $V_L\lambda$.

We also wanted to compare two different batches of samples, fresh and frozen, isolated from the same patient, in order to reduce the variability of the results observed. Interestingly, with our RT-PCR protocol and subsequently with the nested PCR steps, it appears that the amplification products are quite similar in quantity and quality for both samples, which is an important factor considering that it is likely that the thawing process could degrade the fragile materials (**Figure 4.A.4.3).**

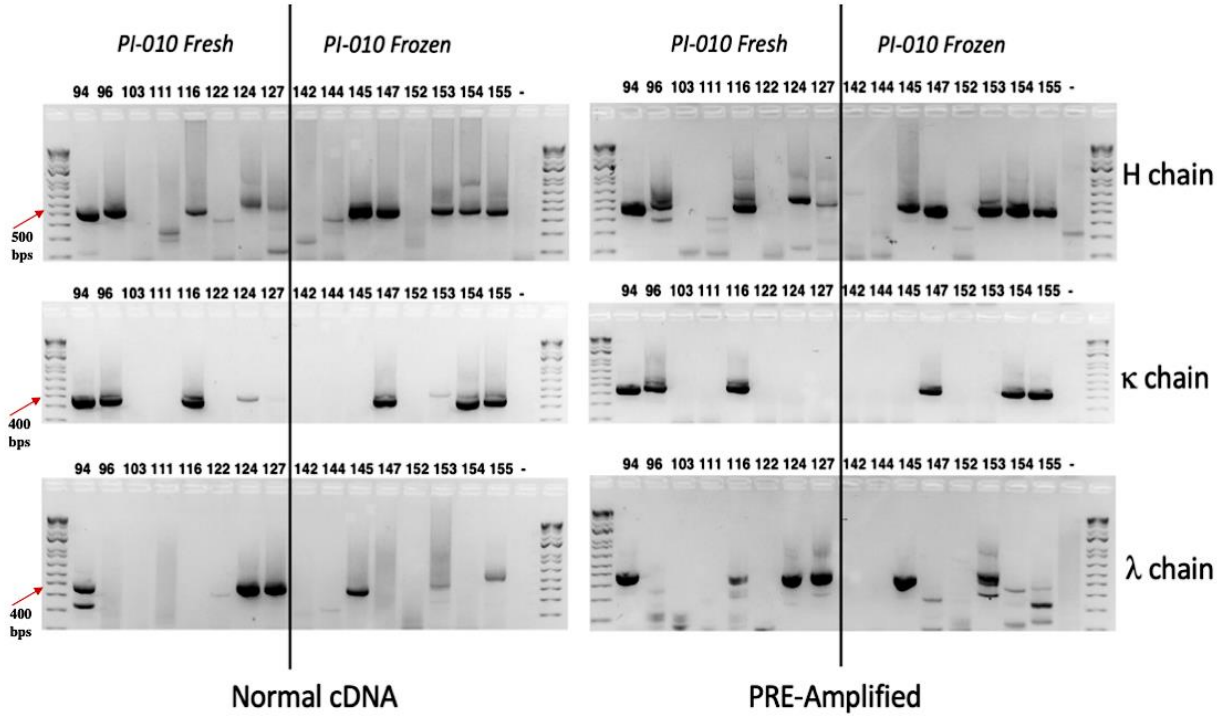

Figure 4.A.4.3. *Amplification of Variable Heavy (V_H) and light ($V_L\kappa$ or $V_L\lambda$) chain PCR products.*

Comparison of recovery of immunoglobulin heavy and light chain variable regions from single antigen-specific plasmablasts in fresh (shown on the left) and frozen (shown on the right) PBMCs from the same individual. On the left panel the input material was the cDNA, on the right instead was the amplified DNA.

A complete summary of single ASCs obtained from each donor, relative amplification samples used, paired chains obtained and mAbs transfected is present in **Table 4.A.4.1**.

Table 4.A.4.1. *Paired minigene yields from individual antigen-specific ASCs.*

(*) Due to the exploratory nature of the study, only a subset of the enriched ASCs was used to isolate single antigen-specific ASCs and a subset of single antigen-specific ASCs was used to assemble the heavy and light chain minigenes. (**) Paired heavy and light chains were obtained from approximately 62% of the antigen-specific ASCs.

Source ID	**Single Antigen-specific ASCs**	**ASCs used for V_H and V_L amplification** (*)	**% of ASCs used for the amplification** (*)	**Paired mini-genes recovery**	**mAbs successfully transfected in Expi 293**
PI-005	6	6	100	3	3
PI-006	17	17	100	11	11
PI-007	1	1	100	0	0
PI-009	28	8	28.6	7	7
PI-010	80	26	32.5	15	15
Total	132	58	44	36 (**)	36

4.A.5. Validation of transient mAb production and binding activity

To confirm the effective production of immunoglobulins and the Spike specificity of our amplification products, the "minigenes", also defined as TAP products, of the heavy and light chain mAbs were transiently co-transfected into Expi293F™ cells. Using the ExpiFectamine™ 293 Transfection Kit (see Materials and Methods), a ratio of 70% and 30%, respectively, between the heavy and light chain encoding chimeric minigenes was used for transfection, adapted to a smaller experiment for 96/2mL deep well plates. The supernatants were harvested 3 days post-transfection and used to validate the Spike-specific binding activity through a single-point assay. We wanted to use both a PCR product as DNA and small volume transfection to increase the speed and feasibility of the process but also to screen our mAbs in a rapid passage. Only the best mAbs were cloned into expression vectors for IgH and Igκ or Igλ as described below and tested in a dilution curve ELISA.

For the single-point qualitative ELISA shown on the left side of **Figure 4.A.5.1**, SpectraPlate-384 High Binding plates were coated with the Spike recombinant fragment, while for the dilution curve shown on the right side of the same figure, eight different concentrations of the protein were used. Both ELISAs included a positive reference, donor serum, and a double negative control, one for transfection and one for immunoenzymatic assay.

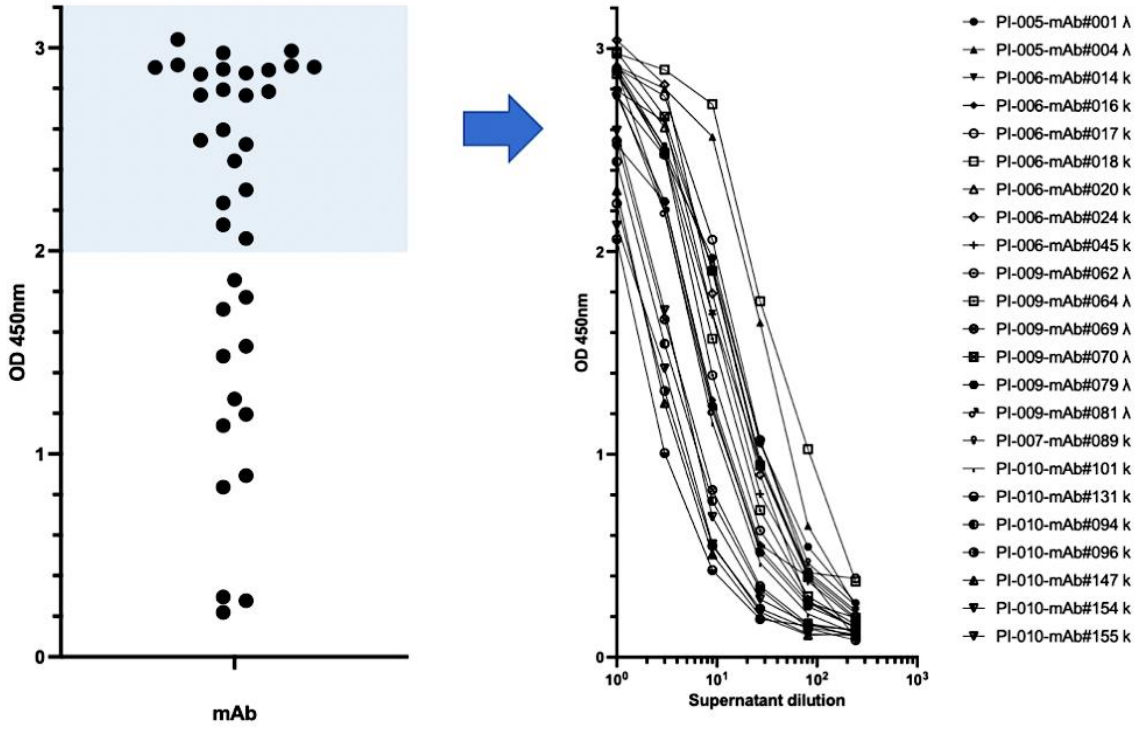

Figure 4.A.5.1. *Single concentration ELISA and dilution curves for mAbs produced by TAP.*

Left side: on the X-axis are shown mAbs as dots tested in single concentration, on the Y-axis the respective O.D. value. On the right: the best supernatants diluted, on the X-axis we can find the dilutions, on the Y-axis the O.D. value, the legend shows all the mAbs tested.

These experiments showed that all the 36 TAP products were positive in the ELISA, ranging from very low O.D. values to higher values. As can be seen in **Figure 4.A.5.1**, due to the exploratory nature of the study, we decided to select only those mAbs that gave an O.D. value greater than 2 and to proceed with them.

4.A.6. V_H and V_L sequences cloning into expression vectors

Once the optimal binding activity of 22 of the 36 mAbs had been assessed, these were selected for the preparation of stable coding plasmids for further functional analysis.

Therefore, the coding sequences of the coupled heavy and light variable regions were recovered and inserted into recombinant plasmids AbVec2.0-IGHG1 and AbVec1.1-IGKC or AbVec1.1-IGλC encoding the constant region of human immunoglobulin heavy chain (IgG1 isotype) and light chain (Kappa or Lambda) (overview of the procedure in **Figure 4.A.6.1**).

The recombinant plasmids AbVec2.0-IGHG1, AbVec1.1-IGKC and AbVec1.1-IGλC were first enzymatically cleaved using the restriction enzymes EcoRI HF and Hind III HF, to open the plasmid backbone. The V_H/V_L TAP products were then amplified using the IgClo-F and

IgClo-R primers, gel purified and then digested using the same restriction enzymes, EcoRI HF and Hind III HF, to obtain the variable linear DNA fragment.

Once the variable regions of interest were obtained from the restriction digestion, they were ligated by enzymatic ligation to the corresponding digested linear vector encoding the constant region of the immunoglobulin, to obtain the recombinant DNA encoding the complete immunoglobulins.

The ligation mixture was then transformed into *Escherichia coli,* as described in the Materials and Methods section.

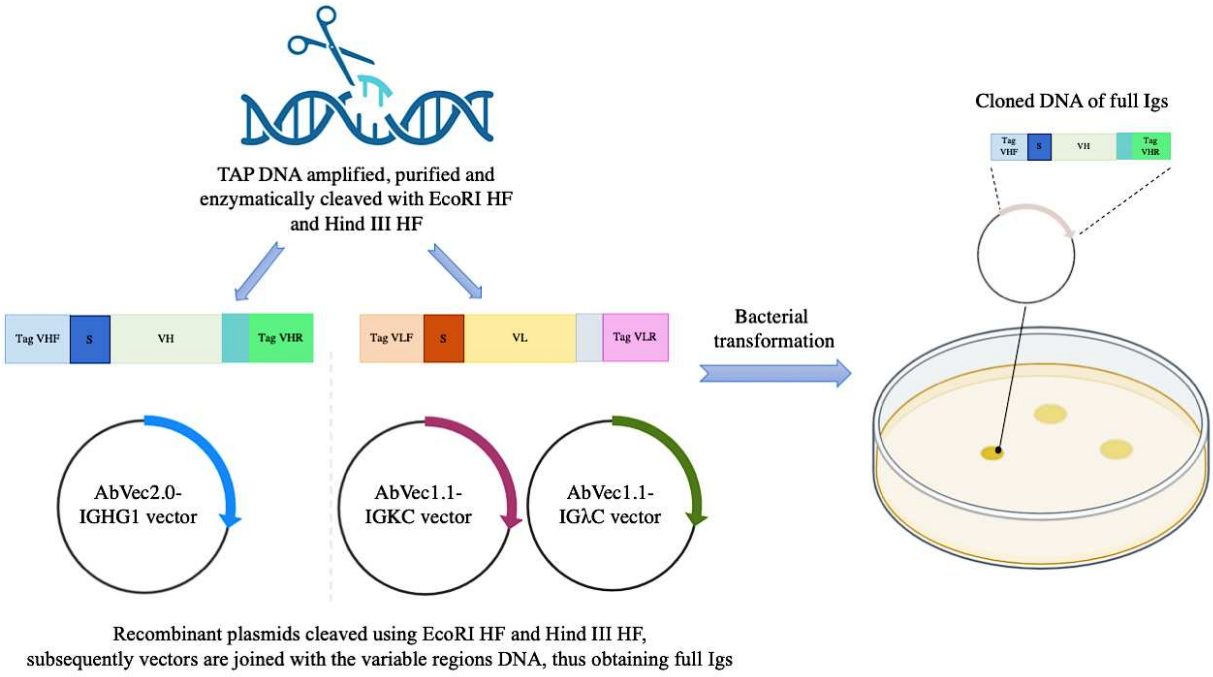

Figure 4.A.6.1. *Cloning procedure.*

Overview of the cloning procedure to obtain plasmids of the heavy and light chains of the mAbs.

To verify the effective cloning of the DNA, some of the bacterial colonies grown on LB-ampicillin plates, due to the resistance cassette of the AbVec2.0-IGHG1, AbVec1.1-IGKC and AbVec1.1-IG λC vectors, were spotted and then screened by colony PCR and then also checked by digestion with the same enzymes used for cloning, EcoRI HF and HindIII HF restriction enzymes, as shown in **Figure 4.A.6.2**.

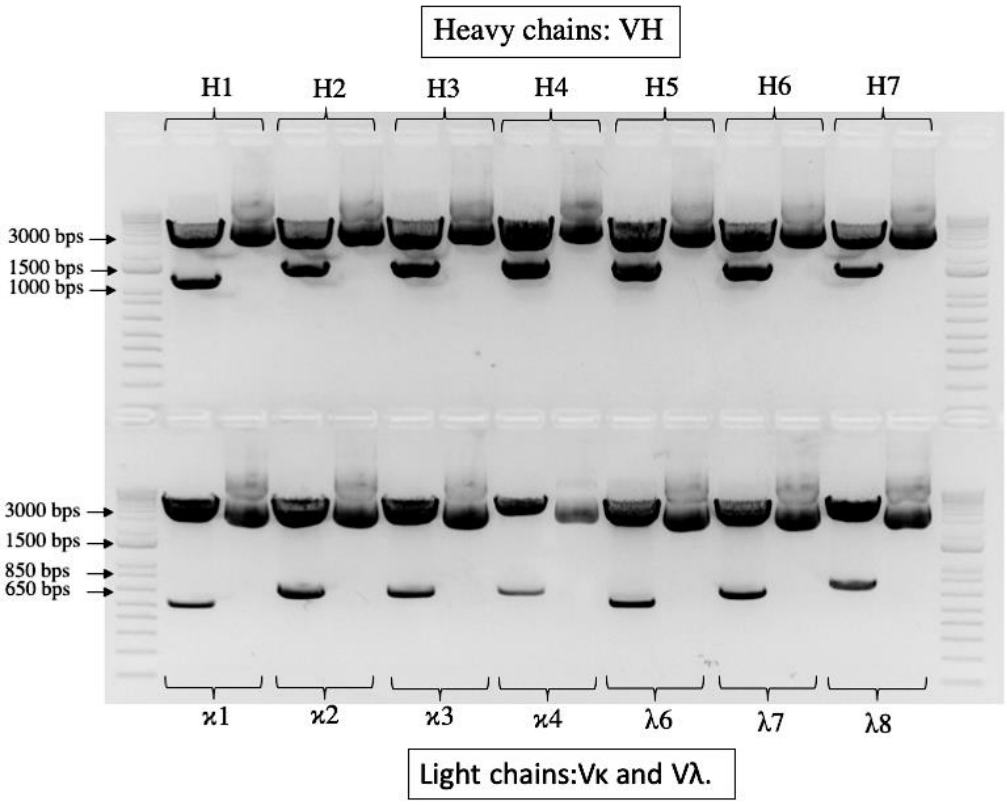

Figure 4.A.6.2. *AbVec2.0-IGHG1, AbVec1.1-IGKC and AbVec1.1-IG λC vectors' enzymatic cleavage (EcoRI HF and HindIII HF).*

In each first well we can observe the DNA cleaved, while in each second well the DNA not cleaved as control. In the upper part are shown heavy chains, and in the lower light chains.

Figure 4.A.6.2 shows the enzymatic cleavage with EcoRI and HindIII (heavy chains in the upper part, light chains in the lower part). Each curly bracket indicates the two wells containing the cleaved and uncleaved plasmid of the heavy and light chains respectively. These control steps, using primers and restriction enzymes, were carried out in order to assess the actual and real presence of V_H and V_L within the recombinant plasmid, thus avoiding the recovery of recircularised vectors without the insert of interest.

Several colonies carrying the recombinant plasmids of the heavy and light chains of 22 Spike-specific mAbs were identified. These positive clones were amplified in a small volume of LB + ampicillin medium and the recombinant plasmid DNA was purified using the Macherey Nagel kit. DNA quantification and purity were determined by measuring absorbance at 260 and 280nm using a NanoVue^{TM} 4282 V1.7 spectrophotometer.

4.A.7. Characterisation of the best mAbs by neutralisation assay

The best performing ELISA Spike-specific mAbs (22) were first cloned and then tested for neutralising activity against three strains of live SARS-CoV-2: Wuhan (Wild Type), Delta, Omicron variants. Recombinant monoclonal antibodies derived from supernatants of transiently transfected Expi-293 cells were first diluted to 10µg/mL and tested for their ability to protect the layer of Vero E6 cells from the cytopathic effect induced by SARS-CoV-2 infection.

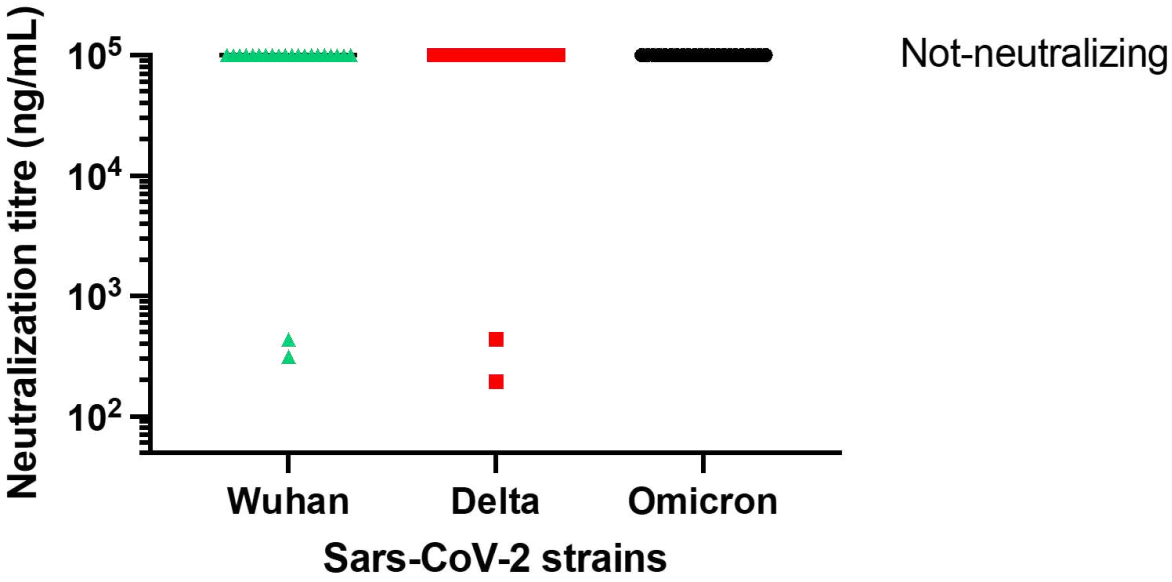

Figure 4.A.7.1. *Neutralization activity of selected mAbs.*

This graph shows on the X-axis the different virus tested: the first Sars-CoV-2 (Wuhan), the Delta and Omicron variants. On the Y-axis are indicated the concentration (ng/mL) of supernatants of these mAbs used for this assay.

Of the 22 monoclonal antibodies evaluated in this study, two (9%) were able to neutralise the authentic Wild type (WT) and Delta viruses and prevent infection of Vero E6 cells, but none was able to neutralise the Omicron BA.1 variant, which emerged 6-9 months after the monoclonal antibodies were isolated from donors, as shown in **Figure 4.A.7.1**.

The best neutralising mAb, called mAbVE-12, was able to neutralise at a concentration of 312.5 and 196ng/mL respectively the WT and Delta variant.

4.A.8. *In silico* design of mAbVE-12 and study on its possible binding interactions with NTD and RBD regions of the Spike glycoprotein

Of the best mAb identified**,** mAbVE-12, we decided to *in silico* investigate the structure and possible binding interactions with the two different regions of the Spike glycoprotein: RBD and NTD, in both the WT and Delta variant, for which the mAb had neutralising activity. The Variable Regions of the monoclonal antibody were modelled using the ABodyBuilder-ML web server (**Figure 4.A.8.1**).

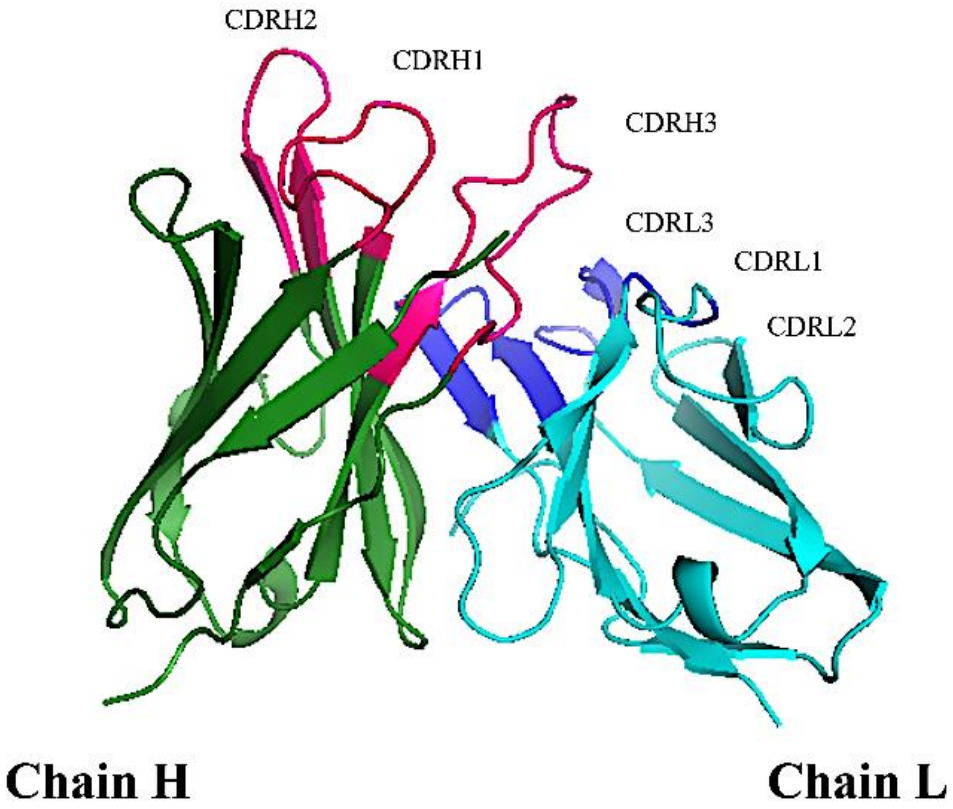

Figure 4.A.8.1. *Protein structure of mAb-VE12.*

The variable heavy chain (Chain H) is shown in green, while its CDRs are in magenta. The variable light chain is coloured in light blue, its CDRs are blue.

After this step, the simulation of molecular docking was performed on the ClusPro web server using the "Antibody Mode" analysis to determine any possible interaction between mAbVE-12 and RBD and mAbVE-12 and NTD. ClusPro ranks docking models based on the size of the cluster conformation, also known as cluster members, and the lowest energy created when a stable complex forms, as a result of docking events.

In **Table 4.A.8.1** below are shown only the best results obtained from the complexes analysed (wtRBD-mAbVE-12 and wtNTD-mAbVE-12). Cluster members involved in the binding between this mAb and wtRBD were notably higher than the ones obtained with the wtNTD, thus being indicative of the preferred hypothetical region of binding. Data shown are relative to the wt RBD/NTD in complex with the mAb, but very similar results have been obtained for the other variant analysed, Delta.

Table 4.A.8.1. *ClusPro results.*

In the first column are shown the protein-protein complex names, in the second column is shown the number of members per cluster and in the third column is shown the lowest energy for each cluster expressed in KJ/mol.

Protein -Protein Complex	**Cluster members**	**The lowest energy (KJ/mol)**
wtRBD_mAbVE-12	239	-315.00
wtNTD_mAbVE-12	95	-285.00

These observations have been corroborated by the PRODIGY web server which calculates the binding energy of the complexes wtRBD -mAbVE-12 and wtNTD -mAbVE-12.
Table 4.A.8.2 shows that the binding energy of the complex wtRBD -mAbVE-12 seems to be higher than the binding energy of the other complex. Similar results have been obtained also for Delta RBD/NTD in complex with mAbVE-12.

Table 4.A.8.2. *PRODIGY prediction of the binding energy in the complexes between wtRBD and wtNTD with mAbVE-12.*

In the first column are shown the protein-protein complex names, in the middle the ΔG (indicated as kcal mol),on the right side the dissociation constant (indicated as M).

Protein-protein complex	ΔG (kcal mol^{-1})	Kd (M) at ℃
wtRBD_mAbVE-12	-15.6	3.9 e^{-12}
wtNTD_mAbVE-12	-13.8	7.1 e^{-11}

The ClusPro results were visualised by the PyMol software (**Figure 4.A.8.2** and **Figure 4.A.8.3**).

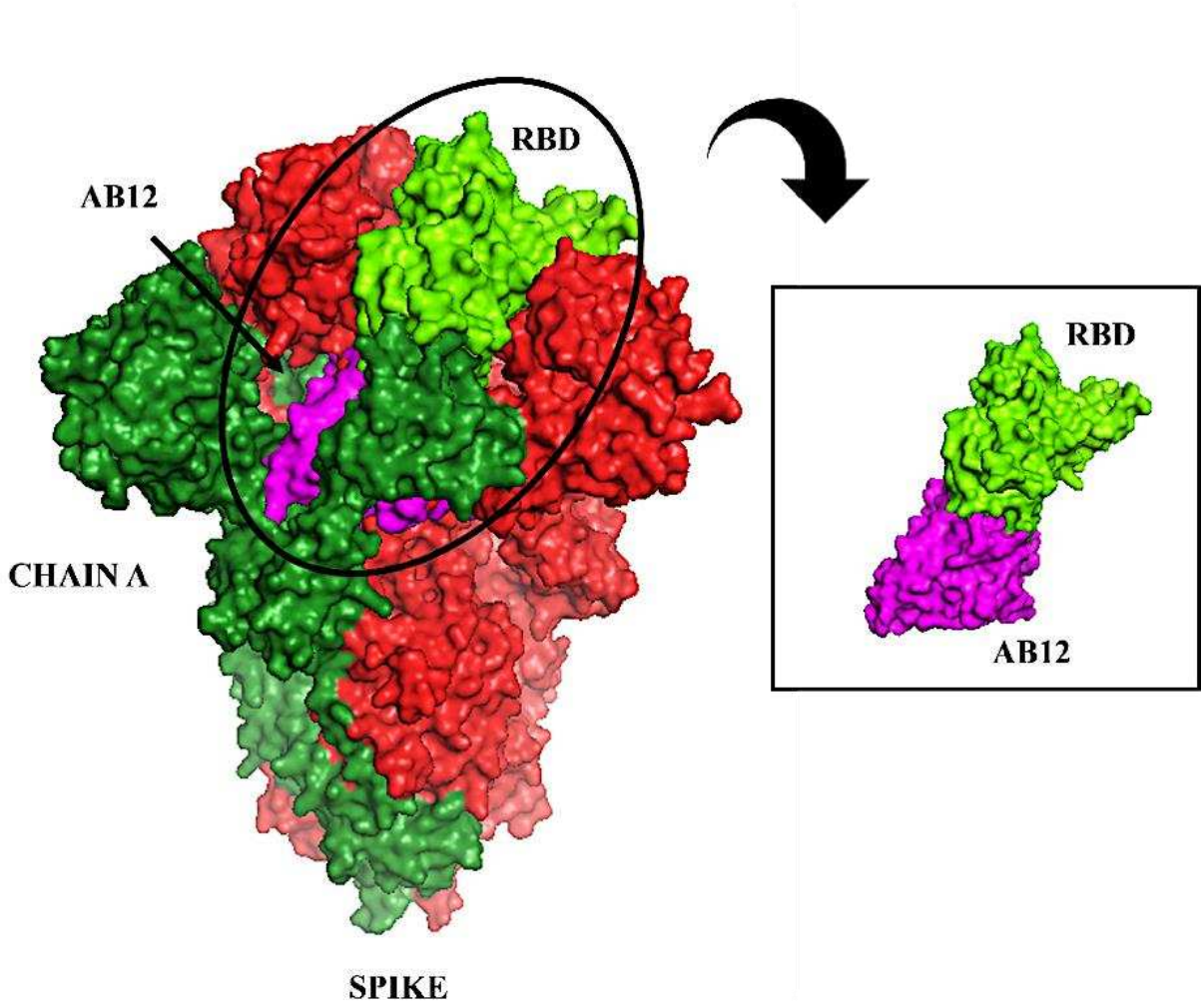

Figure 4.A.8.2. *Protein structure representation of Spike Glycoprotein in complex with mAbVE-12, focus on RBD.*

On the left side is shown the full Spike protein, in red is indicated the chain A. The binding between mAbVE-12 (purple) and WT RBD (lime green) is highlighted in the black box.

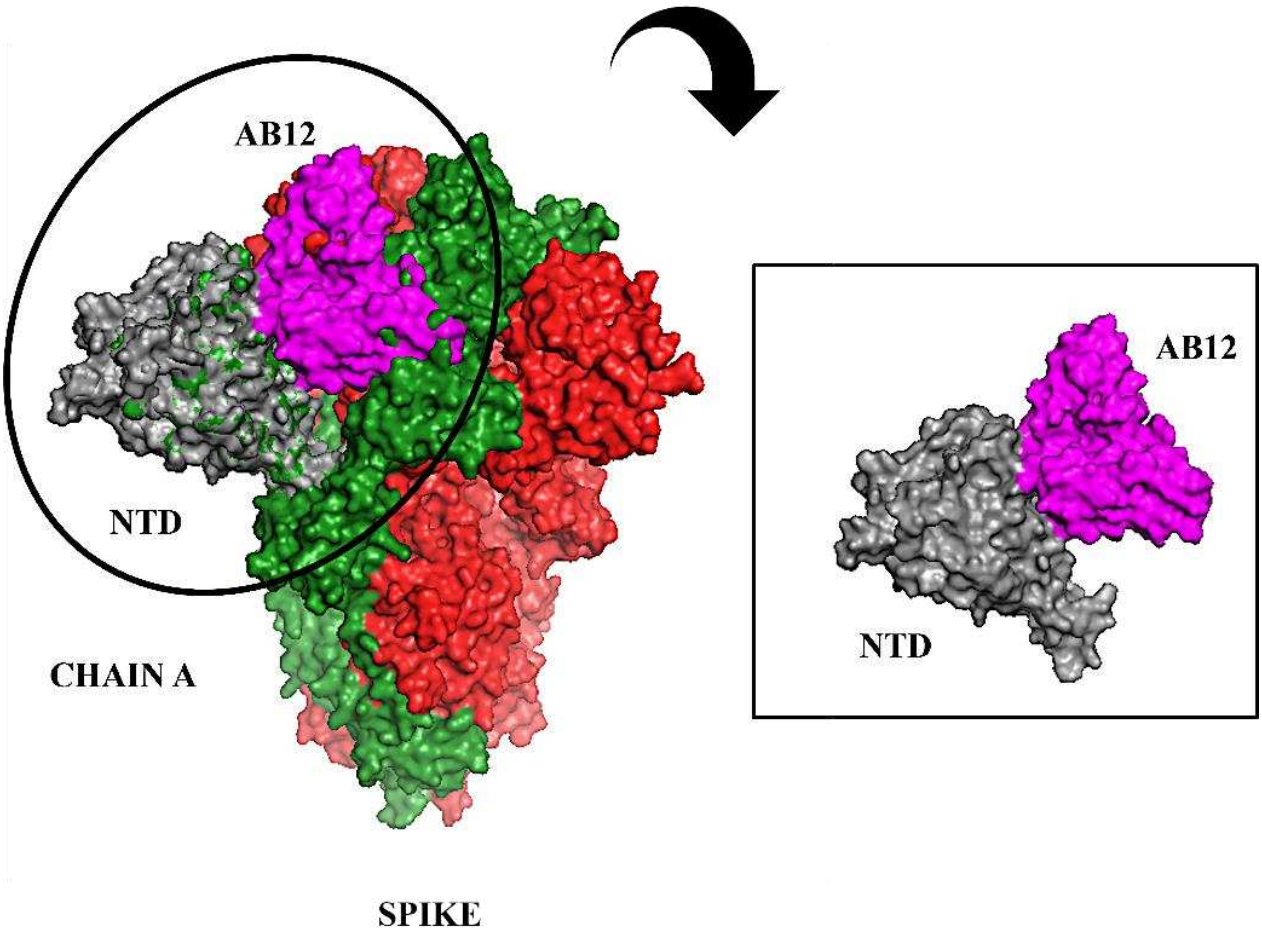

Figure 4.A.8.3. *Protein structure representation of Spike Glycoprotein in complex with mAbVE-12, focus on NTD.*

On the left side is shown the full Spike protein, and in red is indicated the chain A. The binding between mAbVE-12 (purple) and WT NTD (grey) is highlighted in the black box.

Due to the higher affinity of mAbVE-12 with RBD region of Spike glycoprotein, we decided to focus our next predictions only on that region. After docking analysis, we used the RING 2.0 web server to predict potential sites of binding and its interactions with mAbVE-12. The predicted binding of wtRBD-mAbVE-12 was mainly mediated by 14 amino acid residues of wtRBD: H519, L518, A520, D389, K378, Y380, G381, S383, D428, F429, V382, K386, P384, T385.

Among these, 10 amino acid residues, were in common with the Delta RBD: H519, A520, D389, D428, G381, V382, K378, S383, T385, K386.

All residues involved in the binding are shown in the table below (**Table 4.A.8.3**) with a particular focus on the shared ones, which were also recognized as known epitopes from literature [170,171].

Table 4.A.8.3. *Epitopes of the RBD region involved in the binding with mAbVE-12.*

Orange and green dots indicate the predicted epitopes of WT and Delta RBD, respectively, interested in the binding with mAbVE-12. In yellow are highlighted the common epitopes of binding between the two RBDs.

SARS-CoV-2 RBD	Sequence
Wild-Type	333 TNLCPFGEVFNATRFASVYAWNRKRISNCVADYSVLYNSASFSTFKCYGVSPTKLNDLCFTNVYADSFVIRGDEVRQIAPGQTGKADYNYKLPDDFT 430
Delta	----------K---GVS-T-L-D-----------F--
mAbVE-12 epitopes WT	. ******* . ..
mAbVE-12 epitopes Delta	. ••• •• . • •

SARS-CoV-2 RBD	Sequence
Wild-Type	431 GCVIAWNSNNLDSKVGGNYNYLYRLFRKSNLKPFERDISTEIYQAGSTPCNGVEGFNCYFPLQSYGFQPTNGVGYQPYRVVVLSFELLHAP 521
Delta	----------R----------K----------HA-
mAbVE-12 epitopes WT	***
mAbVE-12 epitopes Delta	••• ••

4.A.9. mAbs plasmids sequencing and analysis

The variable regions of the isolated mAbs were Sanger sequenced and analysed for the V_H gene repertoire families and the length of coding region 3 (H-CDR3).

Figure 4.A.9.1.A. shows that the most commonly developed V_Hs were IGHV1-69, IGHV3-33 and IGHV6-1, while the preferred J_H was J_H4.

The length of H-CDR3 ranged from 12 to 24 amino acids (aa) (**Figure 4.A.9.1.B**), with the majority (86%) of antibodies having a length of 15 to 20 aa, which is slightly longer than previously observed.

A.

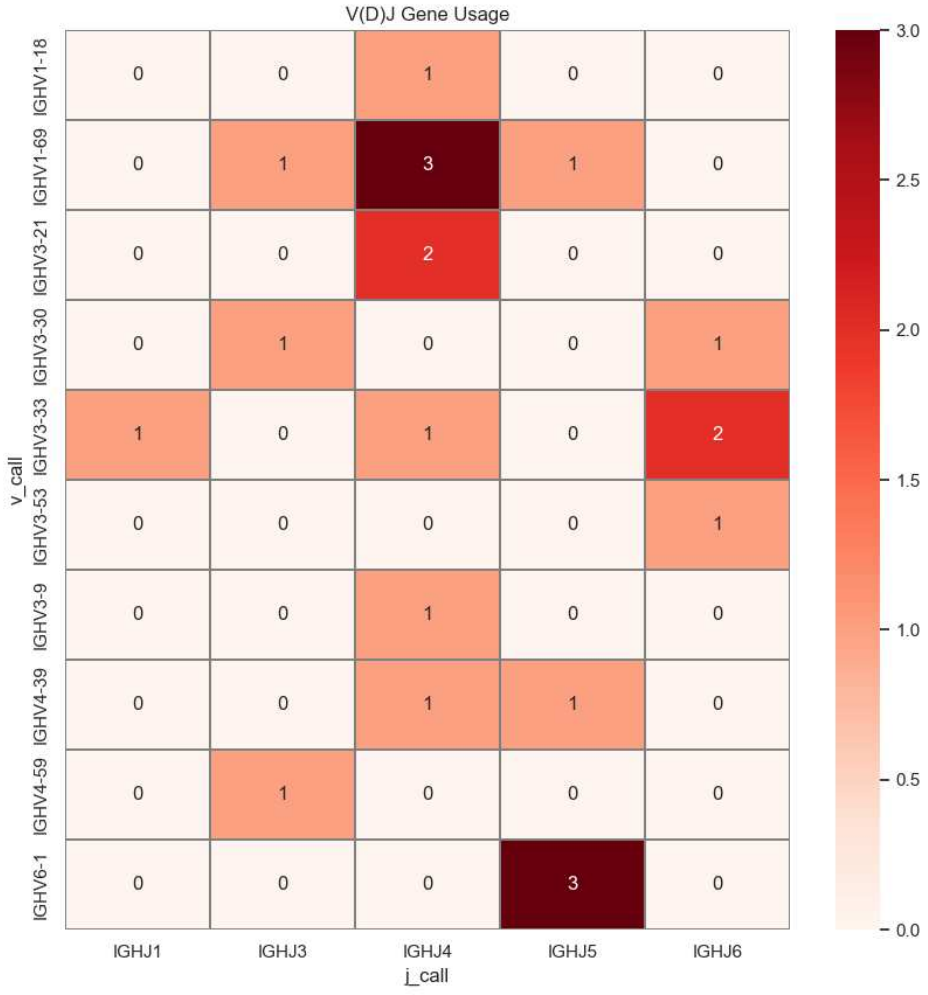

B.

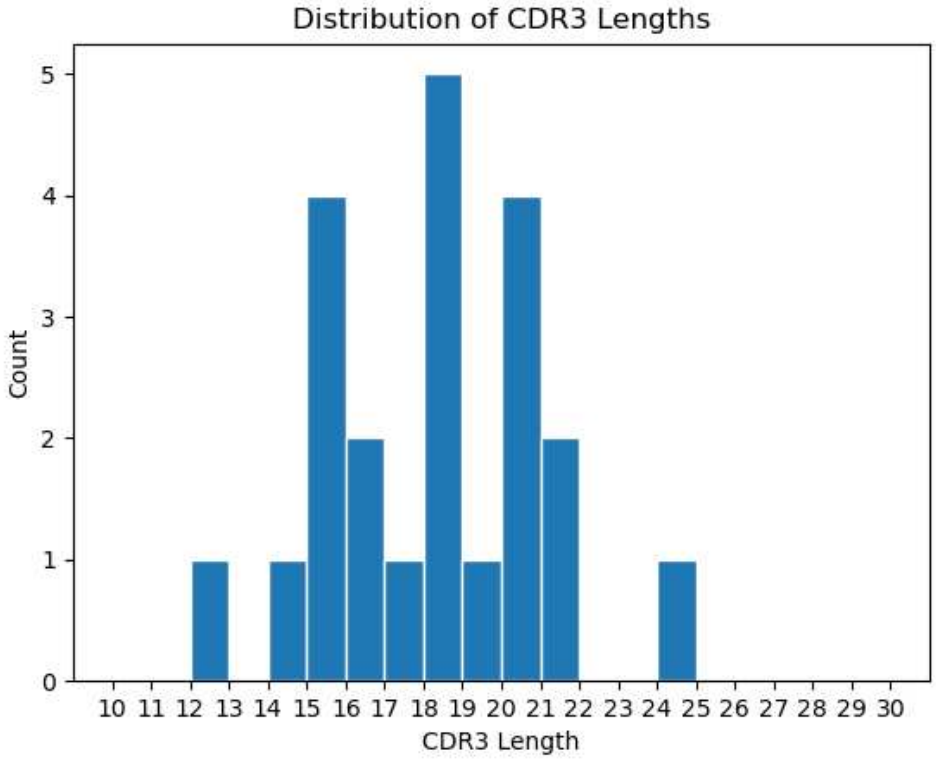

Figure 4.A.9.1. *Analysis of the V_H region in selected monoclonal antibodies.*

A. *IGHV and IGHJ germ line distribution. The first heatmap shows the V_H/J_H usage, with colours ranging from red (high frequency) to light pink (absent) indicating the most frequent V_H/J_H usage. The most frequent IGJ_H families are plotted on the X-axis and the IGV_H families are plotted on the Y-axis.* ***B.*** *CDR3 sequence length variation. This graph shows the number of complementary determining region 3(CDR3) sequences with different lengths of amino acids (aa) among selected mAbs. The Y-axis represents the count, and the X-axis indicates the sequence length.*

5.A. Discussion

In recent years, several technologies that allow the analysis of individual B cells have emerged, facilitating effective sampling of the B cell repertoire. However, despite these advances, the focus of most techniques remains on memory B cells due to the hurdles encountered in screening individual plasma cells and other subsets of Ig-secreting B cells. These difficulties arise from the lack of surface Igs and the complexity of culturing these fully differentiated cells. To gain a more complete understanding of the antibody-mediated immune response in the bloodstream, it's important to look directly at the substances produced by antibody-secreting cells, rather than focusing solely on memory B cells. In fact, antibodies in the bloodstream during an immune response are not produced directly by memory B cells. Instead, they come from antibody-secreting cells. Therefore, studying the repertoire of those cells is crucial to gain real insight into the immune response.

The primary objective of this research was to introduce an innovative, rapid and reliable method for the production of monoclonal antibodies from naturally occurring antigen-specific antibody-secreting cells. These antibodies are particularly valuable in the fight against infectious diseases, as demonstrated by their critical role in combating SARS-CoV-2 infection, helping to neutralise the virus and preventing its spread in the body. The method used a CD138-FF™ enrichment technique coupled with functional screening of the ASCs supernatant to determine antigen specificity.

The results of the study highlighted the success of the CD138-FF™ enrichment method. Analysis showed that 4% of supernatants from single cell cultures within the enriched population had detectable levels of human IgGs after 16 hours, confirming the efficacy of the system in maintaining ASCs functionality.

Using this method, 133 individual SARS-CoV-2 Spike glycoprotein-specific ASCs were identified by ELISA from a pool of 4.4×10^5 CD138-FF™ enriched ASCs, equivalent to approximately 3 antigen-specific plasma cells per 10^4 enriched ASCs, highlighting the potential of the approach. In addition, the study demonstrated the feasibility of generating immunoglobulin variable regions by PCR from individual ASCs and integrating them into linear Ig heavy and light chain gene expression cassettes. This technique allows rapid expression of Ig V_H and V_L minigenes as recombinant antibodies from ASCs, bypassing the time-consuming process of cloning into stable plasmids. Using transient transfection of these immunoglobulins, thirty-six recombinant monoclonal antibodies were successfully obtained from plasma cells derived from five different individuals who had recovered from COVID-19. The best-performing Spike-specific mAbs were tested for their functional activity in a

neutralising assay against SARS-CoV-2. Approximately 10 % of the tested supernatants resulted to be active against the WT and Delta, not against the Omicron. This can be easily explained by the fact that samples were collected before that variant spread. With the best mAb selected, mAbVE-12, we have *in silico* investigated the structure and possible binding interactions, and we have hypothesised that the preference of binding is for the RBD, rather than the NTD region of Spike glycoprotein. Further tests are required to confirm our *in silico* hypothesis, such as an ELISA assay by using the different regions of the Spike protein (RBD and NTD) and a competitive inhibition assay.

Due to the exploratory nature of this study, only a small fraction of the accessible ASCs was used to generate monoclonal antibodies from selected antigen-specific ASCs. However, the ability of this technique to generate thousands of antigen-specific plasma cells from just a few millilitres of blood demonstrates its potential for efficient screening of the adaptive immune response following vaccination or infection. Indeed, it facilitates the high-throughput analysis and characterisation of large numbers of samples, allowing the production and validation of recombinant monoclonal antibodies within ten days of the initial blood collection.

The generation of monoclonal antibodies from ASCs offers several advantages over traditional methods. ASCs are activated cells that actively produce antibodies during an immune response. Selecting and cloning ASCs that produce specific antibodies increases the likelihood of generating functional and potent monoclonal antibodies. In contrast, traditional methods often involve screening large antibody libraries generated by hybridoma or phage display technologies, which may contain non-functional or irrelevant antibodies. The method for generating monoclonal antibodies using ASCs described in this study is unique in that individual ASCs are screened for effector function prior to cloning recombinant antibodies. This screening step is crucial for identifying monoclonal antibodies with desirable properties, particularly in the treatment of viral infections such as COVID-19, where the isolation of functional antibodies capable of neutralising the live virus is essential. Despite the limitations of using ELISA in this proof-of-concept study to identify functional antibodies, the discovery of these antibodies highlights the potential of this approach to generate robust mAbs with potent neutralising capabilities, even in the presence of non-selective ELISA for conformational epitopes. The investigation of the Ig repertoire is proving invaluable in understanding immune responses to specific antigens and in the development of novel vaccines and treatments. This study involves the detection and analysis of individual antibodies produced by the immune system against a specific antigen. Overall, this method can isolate thousands of antigen-specific plasma cells from a small

blood sample, suggesting its potential for high-throughput analysis of ongoing adaptive immune responses following vaccination or infection. This approach could significantly improve researchers' understanding of immune responses to specific antigens and accelerate the development of breakthrough vaccines and treatments, particularly in time-sensitive diseases.

Study B

1.B. Introduction

1.B.1. Malaria

Malaria is a life-threatening disease caused by parasites that are transmitted to people through the bites of infected female *Anopheles* mosquitoes. Malaria has been a human disease of major importance throughout history and it is considered one of the most severe infectious diseases [172–174].

The incidence of this disease decreased by 30% from 2001 to 2015, due to substantial interventions leading to a decline in malaria mortality rate and global incidence. Nevertheless, in 2019, 4 billion people were at risk of disease in over eighty countries, with 229 million cases estimated, killing 409,000 people [175].

The malaria burden is mainly centred in Africa in recent times, whereas in 1975 the WHO declared that malaria had been eradicated in Europe and that all recorded cases were introduced through migration or travellers [176,177]. While China was certified malaria-free by WHO in 2021, sub-Saharan Africa accounted for ~95% of the malaria burden in 2020 [178].

Six species of parasitic protozoan are known to cause malaria in humans: *Plasmodium falciparum, Plasmodium vivax, Plasmodium ovale curtisi, Plasmodium ovale wallikeri, Plasmodium malariae,* and *Plasmodium kwowlesi* [179].

Of these human-infecting *Plasmodium* spp., *P. falciparum* is overwhelmingly responsible for the disease, mainly in Africa; *P. vivax*, is the second most common cause of malaria and the most widely distributed, now makes up ~2% of total global cases [178,180,181].

For most people, malaria symptoms begin 10 days to 4 weeks after the *Pf*-infected mosquito bite and include fever, flu-like illness, myalgia, headache, nausea, vomiting, and diarrhoea. Malaria may also cause anaemia and jaundice due to red blood cell loss. In worst cases, severe malaria can lead to bad outcomes such as kidney failure, pulmonary oedema, cerebral malaria, and coma and if not quickly treated, it can lead, eventually to death [182].

In endemic areas, the most mortality and morbidity from the disease is experienced by pregnant women, infants and children under five years old; among the latter, children are particularly susceptible because they have not yet developed protective immunity but have lost their maternal antibodies [183].

Several strategies were applied to control and prevent malaria over time, historically the main interventions were vector control and small molecule drugs.

The main interventions for controlling the vector, since it is unlikely the possibility of eradication, are Insecticide-Treated bedNets (ITNs) and Indoor Residual Spraying (IRS).

It is estimated that clinical cases associated with *Pf* infection were reduced approximately by 70% since 2,000, thanks to those control intervention contributions [184]. A limited number of insecticides is responsible for these interventions and the emergence of resistance in African Anopheles mosquitoes is a worsening situation that needs urgent action to maintain malaria control. In particular, the trend is the increasing ubiquitous resistance to pyrethroid insecticides, the only class available to treat bed nets [185,186].

Often used in the context of seasonal malaria, as chemoprevention, there are three "gold-standard": daily doxycycline and atovaquone-proguanil and weekly mefloquine [183]. The uncomplicated *P. falciparum* malaria cases are usually treated with Artemisinin-based Combination Therapy (ACT): combinations of two drugs, an artemisin derivative and a quinine derivative [187].

Nevertheless, ACT seems to start to slightly manifest resistance, both *in vitro* and in the clinic. This phenomenon appears to be accompanied by the development of resistance also to piperaquine and mefloquine, thus leading to high rates of treatment failures. Thus there is a good chance that the only use of ACTs will lead to an increase in the difficulty of reducing global eradication of malaria [178,188].

1.B.2. Life cycle of *Plasmodium falciparum*

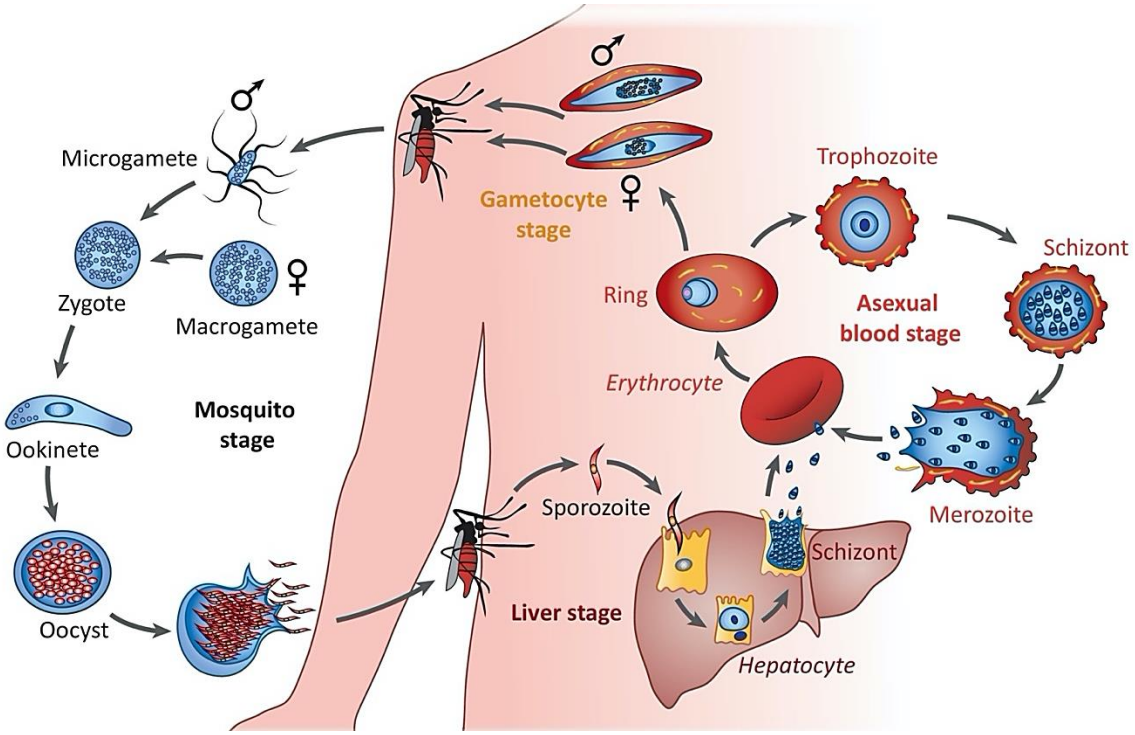

Figure 1.B.2.1. *Plasmodium falciparum life cycle.*

The complete life cycle requires both a mosquito host and a human host. The three main stages of the lifecycle are: pre-erythrocytic, asexual stage and sexual stages. Figure adapted from Plasmodium Falciparum trends in immunology [189].

Plasmodium falciparum has a complex life cycle (**Figure 1.B.2.1.**) divided into two parts, the first in the human host and the second in the insect vector. The life cycle of the *Plasmodium* starts when parasites, also known as sporozoites (SZ), are passed to the vertebrate host through a bite of an infected female mosquito [190] . Those sporozoites pass through the skin to the blood to invade the hepatocytes in the liver where they multiply in a process called "schizogony", over a period of 7-12 days [191–193]. The MeroZoites (MZ), so are now called the parasites, are now released back into the blood and infect the erythrocytes [194].

Now the asexual cycle begins (or asexual blood stage), the merozoites invade Red Blood Cells (RBCs) growing by consuming haemoglobin [195]. It is here that the parasite develops from the early ring stage to late trophozoite to the schizont stage, following mitotic divisions. As soon as schizonts break, merozoites are released and the *Plasmodium* life cycle continues with other RBCs invasions. During the gametocyte stage of the cycle, some merozoites

differentiate in male and female sexual forms, also called erythrocytic gametocytes with a nucleus [196].

Once the gametocytes are taken by a female *Anopheles* mosquito the second part of the cycle starts, inducing gametogenesis. The flagellated microgametes fertilize the macrogametes, the zygotes so generated develop into ookinetes and then become round oocysts. At this point, the oocyst nucleus divides repeatedly, generating a huge number of sporozoites that migrate to the salivary glands of the mosquito once the oocyst bursts. The malaria life cycle continues when those sporozoites are injected again into a new human host [197,198].

1.B.3. Vaccines against malaria

For years innovative and traditional insecticide-based vector control methods such as the use of indoor residual spray, the use of insecticide-treated nets, and the improvement in environmental hygiene conditions have been responsible for interrupting and controlling the malaria transmission cycle [199].

All these measures alone will not solve the malaria burden, to have significant progress in vaccines can be considered one of the most important factors for the eradication of malaria. Different vaccine strategies target distinct stages of the malaria parasite life cycle as shown in **Figure 1.B.3.1**.

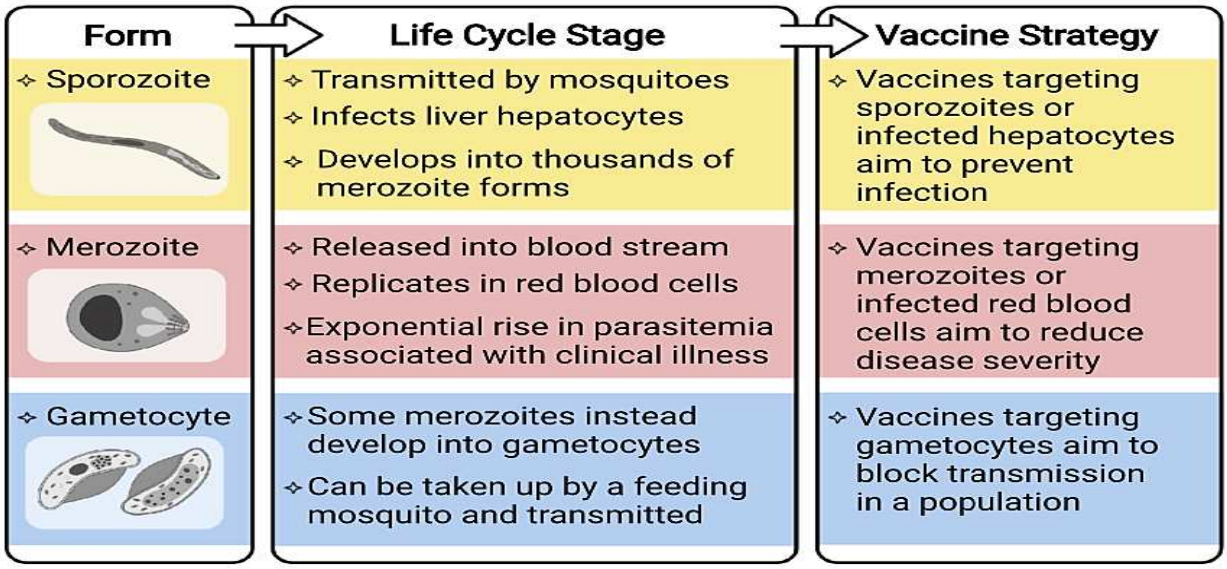

Figure 1.B.3.2. *The different targets of malaria vaccines.*

On the left side are shown the three different forms that can be targeted, in the middle column are shown the respective life cycle stage, and on the right side briefly the vaccine strategy. Figure adapted from Kurtovic L. et al [200].

There are vaccines targeting the pre-erythrocytic (sporozoite and liver-stage) parasites to prevent infection, other vaccines that target the blood-stage merozoite reducing the severity of the disease and others targeting the sexual-stage parasites or mosquito vector reducing transmission, and acting through herd immunity [201].

1.B.4. Pre-Erythrocytic Vaccines (PEV)

Pre-Erythrocytic Vaccines (PEV) target antigens from *Plasmodium* sporozoite and liver stages, blocking the human infection process. In this way, PEV induces mainly two sets of antibodies: on one side antibodies against surface antigens that clear sporozoites from the skin or bloodstream and prevent infection of the liver [202], on the other side T-cell responses that attack infected hepatocytes [203]. The efficacy of these types of vaccines was demonstrated in humans since the 1970s and 1980s when radiation-attenuated whole sporozoite vaccines (WSV) were used [204]. Volunteers were protected against homologous and heterologous *P. falciparum* sporozoites (*Pf*SPZ) but not from challenges with homologous blood-stage parasites [205,206]. Nevertheless, the irradiated sporozoite vaccines had some downsides such as: several exposures were required to develop protective immunity [207], the delivery method for irradiated sporozoites was by mosquito bites or by intravenous injections and the amount of inactivated sporozoites to produce the vaccine was too big to be extended to massive vaccinations. RTS,S/AS01 (also known as Mosquirix™) was the first malaria vaccine approved in October 2021 for children between five and 17 months of age at first vaccination [208]. In collaboration with PATH and other partners, GSK developed Mosquirix™, a subunit vaccine based on a truncated form of the major sporozoite surface antigen, CircumSporozoite Protein (CSP) which is expressed as a virus-like particle and administered with the adjuvant AS01 to increase the immune response to vaccination [200].

According to WHO recommendations the RTS,S/AS01 malaria vaccine has to be used for the prevention of *P. falciparum* malaria in children living in regions with moderate to high transmission as defined by WHO, the majority of which occurs in Sub-Saharan Africa [208].

Another malaria vaccine, R21/Matrix-M™, developed by Oxford University and to be manufactured by Serum Institute of India (SII), is also in an ongoing phase 3 trial. As RTS,S, the R21 malaria vaccine is a virus-like particle with a higher density of the CSP antigen on the particle surface and is formulated with Matrix-M™ adjuvant from Novavax. This vaccine has demonstrated similar efficacy against malaria over 12 months nevertheless, monitoring is required to further investigate this promising candidate [209].

An alternative considered to be protective is Whole-sporozoite vaccines**.** The main issue with this category was mainly the manufacture considered not practical.

Nevertheless, there are several alternatives to attenuate *Pf* sporozoite such as through the use of radiation (*Pf*SPZ vaccine), gene deletions that block the liver-stage development (Genetically Attenuated Parasites or GAP), or chemo attenuation through antimalarial drugs (*Pf*SPZ-CVac for chemoprophylaxis vaccination) [210–212].

*Pf*SPZ vaccine or *Pf*SPZ-CVac has been demonstrated to confer high levels of sterile homologous immunity [213,214] in malaria-naive adults and, at higher doses, durable high-level of sterile heterologous immunity with *Pf*SPZ-CVac using coadministered with antimalarial drugs [215,216]. These types of vaccines stimulate a broad immune response since they express several antigens, but it is not easy to detect and monitor since the hepatic T-cell responses are not accessible through peripheral blood [201].

1.B.5. Transmission Blocking Vaccines (TBV)

Transmission-Blocking Vaccines (TBV) is a class of vaccines that induce antibodies that kill parasites in the mosquito bloodmeal and interrupt parasite transmission through the vector [217,218]. In this way, this system protects populations not by direct immunity but by preventing community transmission of the disease. TBV vaccines target surface antigens of the sexual stages of mosquitoes, creating an antibody response against gametocytes and ookinete antigens. There are four leading candidates (discussed below) that have been grouped as gamete surface proteins: Pfs230 and Pfs48/45, gamete surface proteins first expressed by gametocytes in human blood [219] and Pfs25 and Pfs28, zygote surface proteins expressed only post-fertilization in the mosquito [220,221].

Pfs25 is the major surface protein of zygotes and it was the first TBV candidate antigen to progress to clinical trials. An early trial of Pfs25 with Montanide ISA 51 adjuvant had to be interrupted due to severe reactogenicity [222]. While some trials failed to induce adequate antibody response the situation seemed to get better by conjugating the antigen to a VLP or nanoparticle for example IMX313 [223].

Nevertheless, Pfs25 and Pfs25-IMX313 expressed from ChAd63 and MVA vectors yielded significantly better immune responses than Pfs25 alone [224]. Furthermore, Pfs25-IMX313 went to phase I clinical trials and there was evidence that Pfs25-IMX313 can be combined with RTS,S/AS01 without reduction of immunogenicity for both vaccines [225].

It was also reported that Pfs25-EPA conjugate formulated with Alhydrogel® seemed to be well-tolerated and to induce functional antibodies in humans that block transmission of *P. falciparum* to mosquitoes in membrane-feeding assays as well as with titers [226].

Pfs25 was the first TBV candidate but other antigens of interest have progressed to clinical trials such as the *P. falciparum* 230-kDa sexual stage protein (Pfs230) that forms a complex with Pfs48/45 on the surface of sexual stage parasites. In a comparison between the Pfs25 and Pfs230 Domain 1 (D1) antigens conjugated to ExoProtein (EPA) and formulated in Alhydrogel®, Pfs230 Domain 1 (D1) generated higher transmission-blocking activity than the other antigen in humans and monkeys but not mice [227]. Interestingly Pfs230D1 activity depends on complement and a potent complement-dependent human mAb has identified a large highly conserved neutralizing Pfs230D1 epitope on gametes [228].

One of the new TBV candidates is Pfs48/45, which contains a GPI moiety which anchors the Pfs48/45 - Pfs230 complex to the gametocyte surface [229]. It is exposed when the gametocyte enters the mosquito midgut and the block of its activity precludes the gametocyte fertilization [230,231].

Pfs48/45 is comprised of an N-terminal 6-cysteine domain, a central domain, and a C-terminal 6-cysteine domain, that contains a conformational epitope targeted by potent transmission-blocking mAbs [232]. The cysteine residues have made Pfs45/48 difficult to produce and manufacture as a properly folded protein but recent progress has been made in making a Pfs45/48 fusion with the R0 region of the blood start antigen Glutamate Rich Protein (GLURP) in *Lactococcus lactis* [233,234].

This antigen, called R0.6 C, reacts to conformational and functional monoclonal antibodies and induces transmission-blocking antibodies in animals [235] .

1.B.6. Blood Stage Vaccines (BSV)

Blood Stage Vaccines (BSV) target the asexual blood stage and are protective against clinical disease, reducing morbidity and mortality and indirectly reducing parasite transmission decreasing the number of parasites in the blood. These BSV have been discussed because by targeting the asexual parasites, they clear parasitemia and symptoms but they probably seem to continue the transmission through asymptomatic carriers. Nevertheless, reductions in blood-stage parasitaemia still prevent clinical malaria and deaths, which suggests the importance of developing these vaccine candidates.

The first evidence of the efficacy of this system was observed in 1960s when the passive transfer of African adult IgGs to children affected by malaria reduced the parasite in the blood and symptoms [236,237].

From other studies, it was evident that the immunization of monkeys with preparation enriched in merozoites conferred protection from *P. falciparum* infection [238].

BSV research has been focused mainly on merozoites antigens, before continuing to describe vaccines it is useful to explain the invasion process which is complex and very quick (**Figure 1.B.6.1.**).

It was shown from in vitro studies that merozoites are no more able to invade erythrocytes within 5min, while this invasion process seems to be even quicker *in vivo* due also to the immune system action [239]. Merozoites are polarised cells with the microneme and rhoptry bulb organelles primed with proteins required for entry into a new erythrocyte.

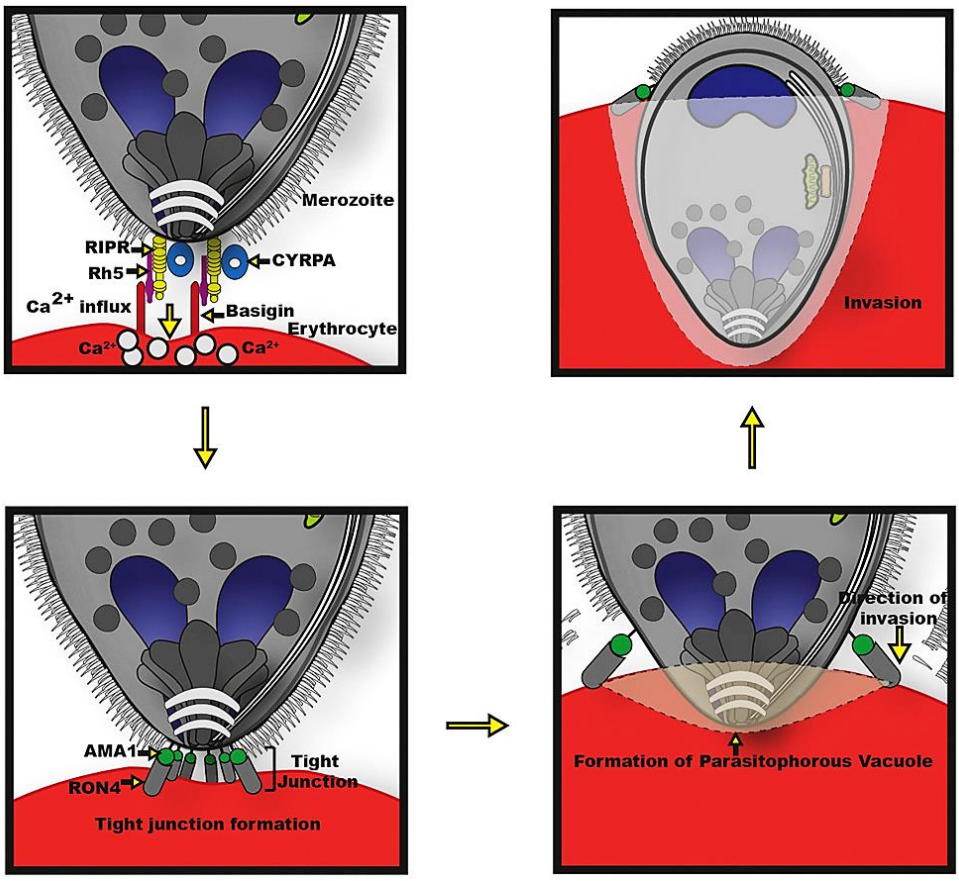

Figure 1.B.6.1. *Plasmodium falciparum Invasion of Erythrocytes.*

RH5, CyRPA, and Ripr are secreted by the MZ and form a trimeric complex at the interface between the MZ apex and the erythrocyte membrane. The binding of RH5 to basigin on the erythrocyte surface triggers intracellular release of calcium within the erythrocyte, a necessary step for the MZ to form a tight junction with the erythrocyte membrane. Figure and legend adapted from Volz et al [240].

At the beginning merozoite seems to bind to the erythrocyte thanks to Merozoite Surface Proteins (MSPs), in particular, MSP1 is the most important of the MSP family which is also composed of MSP3, MSP6, MSP7, MSPDBL1 and MSPDBL2. MSP1 is also required for parasite egress from RBCs [241,242]. Then the invasion process continues through the Erythrocyte-Binding-Like (EBL) proteins and the Reticulocyte-binding-like protein Homolog (RH) proteins.

In particular, *Pf*RH5 is essential for invasion. This protein forms a ~200 kDa 'invasion complex' with Cysteine Rich Protective Antigen (*Pf*CyRPA), *Pf*RH5 Interacting Protein (*Pf*RIPR), and possibly P113 [243–245].

The binding of the EBAs and RH proteins leads to the deformation of the membrane of the erythrocyte, reorientation of the merozoite, and wrapping of the RBC plasma membrane [246]. During this event, the binding of *Pf*RH5 to its receptor basigin is followed by a Ca^{2+} influx into the RBC that is of uncertain function [247]. As soon as this happens a tight junction is

formed by Apical Membrane Antigen 1 (*Pf*AMA1) and Rhoptry Neck Protein 2 (*Pf*RON2) [248]. The formation of this tight junction commits the merozoite to the invasion of the RBC [249]. At this ending point, the merozoite is pulled into the RBC thanks to the 'glidosome', an actomyosin motor, that forms the parasitophorous vacuole whilst shedding the merozoite membrane proteins [250]. One of the challenges for the generation of BSV vaccines indeed is this short window time when merozoites pass between erythrocytes but also the antigenic polymorphism and the large number of parasites to be targeted [235].

The major vaccine targets tested in clinical trials up to 2015 are MSP1 and AMA1 which is essential for invasion as previously explained, but highly polymorphic and so it gives an immune response allele-specific nevertheless, it has been seen poor efficacy in trials up to now [251].

One promising candidate in the pipeline of vaccine is instead the *P. falciparum* Reticulocyte-binding protein Homolog 5 (*Pf*RH5) antigen. This is the only one without a transmembrane region or GPI anchor and the smallest among the Reticulocyte Binding Protein homolog (Rh) family composed also by Rh1, Rh2a, Rh2b and Rh4 [252,253]. *Pf*Rh5 has an essential role in the invasion of erythrocytes since it binds the erythrocyte receptor basigin (BSG), also known as CD147 [254].

The first studies considering *Pf*RH5 as a good antigen for vaccines were done using a viral vector vaccine strategy through a replication-deficient Adenovirus Human serotype 5 (AdHu5) and poxvirus (Modified Vaccinia virus Ankara, MVA) [255].

The strategies for expressing this interesting candidate *Pf*RH5 have been implemented over the years. For instance, the full-length recombinant *Pf*RH5 was expressed in HEK293 cells or in insect cells and a thermostable version that can be produced in *E. coli* has been developed [256–258]. The initial proof of concept that a strain-transcending blood-stage vaccine against *P. falciparum* in Non-Human Primates (NHPs) was possible and gave important correlates of protections against malaria, this was the first clear demonstration of the effectiveness of this candidate [259].

Then the *Pf*RH5 vaccines proceeded to some promising results in a clinical trial, where the replication-deficient ChAd63, and the attenuated MVA, encoding RH5 of *P. falciparum* gave substantial RH5-specific responses for the first time in immunized humans [260].

A second-generation-full-length *Pf*RH5 protein vaccine was designed, producing the protein in a *Drosophila* S2 stable cell line system and C-tag purification technology.

This protein called RH5.1 was used with GSK's $AS01_B$ adjuvant as a vaccine against blood-stage *Plasmodium falciparum* malaria and it was reported to be safe and immunogenic in a phase I/IIa clinical trial (VAC063). It was indeed demonstrated a significantly reduced

blood-stage parasite growth rate in vaccinees following Controlled Human Malaria Infection (CHMI); no other blood-stage *P. falciparum* subunit vaccine candidate has effectively reduced the *in vivo* Parasite Multiplication Rate (PMR) following CHMI in malaria-naive adults [261].

This study has been designed to investigate the monoclonal antibodies derived from volunteers of this VAC063 clinical trial. This chapter of the thesis will be related to this VAC063 clinical trial.

1.B.7. Structure of *P.falciparum* RH5-CyRPA-Ripr and antibodies against the complex

As previously explained the blood stage of *P. falciparum* takes place when the SPZ successfully infects a hepatocyte and multiplies into thousands of MZ that exit the hepatocyte, enter the bloodstream and invade erythrocytes.

It was recently described a pentameric complex, called PCRCR, which is composed of *Pf*RH5-*Pf*CyRPA-*Pf*Ripr (RCR) plus *P. falciparum* Plasmodium Thrombospondin-Related Apical Merozoite Protein (*Pf*PTRAMP) and *P. falciparum* Cysteine-rich Small Secreted protein (*Pf*CSS) [262].

The PCRCR complex was identified as necessary to anchor the contact between merozoite and erythrocyte membranes, increasing the membrane surface contact and bringing them together by strong parasite deformations. This is responsible for an irreversible interaction between the merozoite and erythrocyte and subsequently the activation of the invasion and internalisation steps of the merozoite into the erythrocyte.

To invade the human erythrocytes the parasite requires the ligand *Pf*RH5, which forms a well known trimeric protein complex *Pf*RH5-*Pf*CyRPA-*Pf*Ripr (RCR) (**Figure 1.B.7.1.)** that can bind the erythrocyte surface protein called basigin.

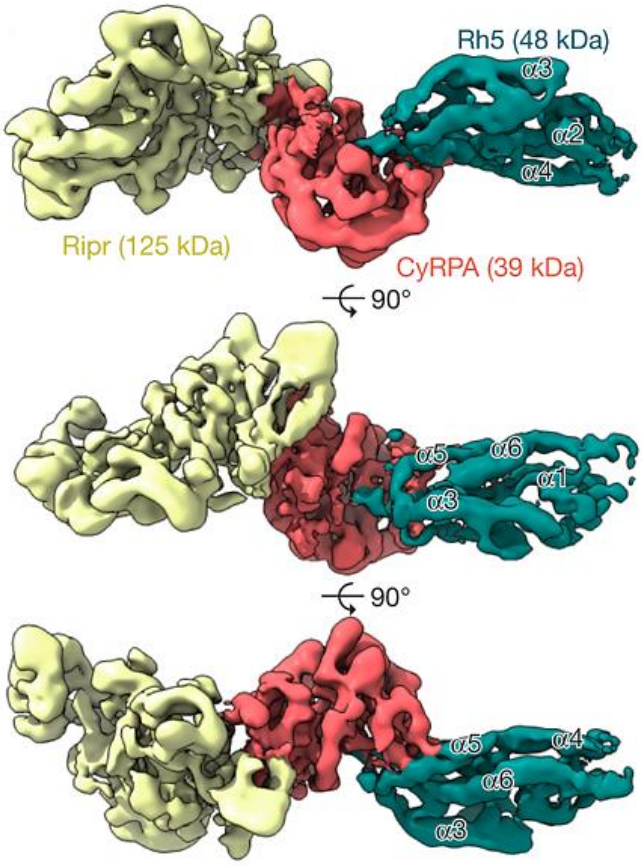

Figure 1.B.7.1. *Structure of the trimeric complex PfRH5-PfCyRPA-PfRipr (RCR).*

3D reconstruction at 7.17 angstrom global resolution obtained by cryogenic electron microscopy. Image taken from Wong et al 2014 [263].

*Pf*RH5 is a 63kDa protein expressed during the mature schizont stages and it is localised to the rhoptries. This kite-like form protein is processed and cleaved to a ~45kDa form that is shed in the parasite culture supernatant [253] .

P. falciparum Reticulocyte-binding protein Homolog 5 has a unique role in the invasion of human erythrocytes since there are no other orthologues in other species of *Plasmodium* that infect humans [252] .

*Pf*CyRPA is a 39kDa protein shaped like a six-bladed β-propeller with five disulfide bonds [264] positioned between *Pf*Rh5 and *Pf*Ripr [263] .

*Pf*RIPR is approximately a 125kDa protein composed of unstructured regions, ten Epidermal Growth Factor-like (EGF) domains, and 87 cysteines. The full-length protein is processed into two fragments, an N-terminal domain (composed of EGF domains 1 and 2) and a C-terminal fragment (including EGF domains 3-10) [244]. These three proteins are highly conserved and in the complex crucial for erythrocyte invasion [265].

Antibodies against *Pf*RH5-*Pf*CyRPA-*Pf*Ripr can neutralise *Plasmodium* strains tested, therefore the RCR complex is considered promising and interesting.

In natural infection history, it was observed in a cohort of children from Papua New Guinea that anti-*Pf*RH5 seropositivity was associated with reduced parasitaemia; similarly, in a study conducted with Malian children, the anti-*Pf*RH5 antibodies were associated with protection from malaria fever [266,267] .

Although a correlation between the naturally acquired response of *Pf*RH5 antibodies and the protection from clinical *P. falciparum* malaria was observed, the immunogenicity resulted to be low compared to other merozoites proteins such as *Pf*AMA, MSP1 and others [255,268] .

There is a simple and reliable *in vitro* assay to assess the neutralization capability of anti-MZ antibodies, that was first reported in 2005 and it is called Growth Inhibition Activity (GIA) assay.

The standardised procedure used by the GIA Reference Center at the National Institutes of Health (NIH) involves culturing erythrocytes infected by synchronised merozoites with antibodies and then the GIA is calculated based on the invasion of parasites when the antibody is present compared to when it is absent [269].

It is reported that this assay strongly correlates with protection mediated by MSP-1, AMA-1, RH5-based vaccines and RH5-specific mAbs in Non-Human Primates (NHPs) challenged with *P. falciparum* or *P. knowlesi* [259,270,271].

There are human *Pf*RH5-specific mAbs, mouse *Pf*RH5 mAbs, mouse *Pf*CyRPA mAbs and mouse *Pf*Ripr mAbs reported so far, of which the one of the most potent human *Pf*RH5 mAb reported was R5.016 with an effective concentration to mediate 50% inhibition (EC50) of 9.6µg/mL in GIA [264,272–275].

Recently it was reported that R5.034, which is the most potent *Pf*RH5 mAb reported to date, has an effective concentration to mediate 50% inhibition (EC50) of 2.5µg/mL in the GIA assay [276]. The most potent neutralising *Pf*RH5 antibodies bind to the tip of the RH5 diamond, making this region a promising candidate for future vaccine studies. Interestingly two of the most potent mAbs (R5.016 and 2AC7) inhibit invasion without blocking the *Pf*RH5-basigin interaction, but binding close to the basigin-binding site [272,274], while other mAbs less potent but still neutralising block directly basigin.

Inhibitory antibodies against *Pf*CyRPA reported seem to bind a conformational epitope between amino acids 26 and 181 [277]. It is thought that protective *Pf*CyRPA mAbs might neutralise invasion or by disrupting the *Pf*CyRPA-RH5 interface, as described for the mouse mAb 8A7, or by steric hindrance of the RCR complex by directly binding the *Pf*CyRPA [273].

*Pf*RIPR is not a target of naturally acquired immunity and against the entirety of the whole RIPR molecule, only two neutralising mAbs have been isolated, both targeting the EGF-7 region. This part appears to be located far from the interface of *Pf*CyRPA-Ripr, towards the

N-terminal half of the protein, thus suggesting that the mechanism of neutralisation of anti-*Pf*RIPR antibodies should not be related to the RCR complex formation [275] .

At present, anti-*Pf*RH5 monoclonal antibodies are the most potent among those targeting the different components of the RCR complex [265].

Nevertheless, in studies in NHPs challenged with *Pf*-infected erythrocytes, it was demonstrated that enormous doses of 100mg/kg were required to provide high titers (600-900µg/mL) to protect from the parasite; a mAb titer order of magnitude higher than those required for analogues studies conducted against bacteria or viruses [278].

Such a high titer required to neutralise the parasite is one of the most challenging points for the development of therapeutic mAbs, therefore to optimise the potency of RCR-specific mAbs or identifying more potent mAbs or trying to combine mAbs targeting different antigens of the complex would be a useful study and prospective for the future progress of this field.

Since we have focused our work on *P. falciparum*, in order to simplify the reading, in the following sections we will refer to *Pf*RH5 simply as RH5.

2.B Outline and aims of STUDY B

This part of the thesis aims to isolate and characterise a repertoire of anti-*Plasmodium falciparum* Reticulocyte-binding protein Homolog 5 (RH5) monoclonal antibodies deriving from peripheral memory B cells of donors vaccinated in the VAC063 study.

The focus of this project was to isolate human mAbs that bind to uncharacterised regions on RH5, potentially identifying new sites of vulnerability on RH5 or "inert" sites that could be excluded from RH5 in next-generation vaccine [279] designs to improve the response.

To frame the study it is important to go back and explain the background. In the first clinical trial of a PfRH5-based vaccine, the VAC057 study, a small panel of monoclonal antibodies were isolated from peripheral blood B cells [272] , among which it was identified that the best neutralizing antibodies bound the RH5 tip. Following on from this observation a second panel of anti-RH5 monoclonal antibodies were isolated[276] from a second clinical trial of a *Pf*-RH5-based vaccine, the VAC063 study. At this point, an RH5-diamond probe was used, which comprised of a truncated version of RH5 that removed the N-terminus and some parts of the C-terminus in order to focus on obtaining mAbs that target the epitopes within RH5 already known to be GIA-positive.

Here is the next step and aim of my project, to develop two new panels of monoclonal antibodies starting from donors of the VAC063 using on one side the full-length RH5 probe and, on the other side, an N-terminus specific probe to pull out a various repertoire of monoclonal antibodies to be analysed and characterised.

Since the biological role of the RH5 N-terminus is unclear thanks to this approach we aim to pull out mAbs to investigate and characterise the N-terminal region.

In the first part of the result section I have described and analysed 100 mAbs isolated from 5 different samples of donors of VAC063 using the RH5 full-length probe, while in the second part, I have described the panel of 51 mAbs isolated from 5 donors of the same clinical trial but using the N-terminus specific probe to address the focus on that specific region.

3.B Material and Methods

3.B.1 Human clinical samples

Memory B-cells (MBCs) were sorted from PBMCs of vaccinated subjects deriving from group 5 of the VAC063 clinical trial conducted at the University of Oxford [261].
VAC063 was an open-label Phase I/IIa dose escalation blood-stage malaria CHMI trial designed to assess the safety, immunogenicity, and efficacy of recombinant *P. falciparum* RH5.1 with the adjuvant $AS01_B$ in healthy, malaria naïve adults aged 18-45 years.

3.B.2 MBCs isolation strategy

3.B.2.1 Probe design and titration

The biotinylated RH5-NT (RH5-Nt Bio) and the RH5.1 FL (RH5-CD4-BAP-Ctag) probes were first tested at four different concentrations on VAC063 clinical trial PBMC samples (RH5-vaccinated Day 63 and an unvaccinated negative control) in order to determine the appropriate concentration of each probe to be used to cell sort antigen-specific memory B cells (MBCs).
Briefly, cryopreserved PBMC were stained for 20min at 4°C in PBS with LIVE/DEAD Fixable Aqua (*Thermo Fisher Scientific*) before addition of the probe. An antibody cocktail for the cell staining was prepared in 1% PBS-FBS. The panel used was as follows: CD3-BV510, CD14-BV510, CD56-BV510, CD27-A488, CD38-APC-Cy7 (*BioLegend*), CD19-ECD (*Beckman Coulter*), IgA-AF647 (*Jackson Immunoresearch*), IgM-PerCP-Cy5.5 (*BD Biosciences*) and IgD-PECy7 (*BD Biosciences*). Finally, the probe was prepared in a stock concentration mixing the biotinylated RH5.1-FL or RH5-NT purified proteins with Streptavidin PE (ratio 4:1) in the buffer of 1% PBS-FBS. These probes were titrated and added to samples at final concentrations of 12.5-2.5-0.5-0.1µg/mL and incubated for 20min at 4°C. Single IgG^+ MBCs were sorted using a BD FACSAria III by gating on: $CD3^-CD14^-$ $CD56^-$ $CD19^+IgD^-IgM^-IgA^-$ cells. Results were then analysed using FlowJo 10.8.1 (*BD, USA*).

3.B.2.2 Isolation of memory B cells antigen-specific

Antigen-specific MBCs were identified by MBCs culture. Briefly, cryopreserved PBMCs were stained for 20min at 4°C in PBS with LIVE/DEAD Fixable Aqua (*Thermo Fisher Scientific*).These cells were then stained for 20min at 4°C in 1% PBS-FBS with an antibody cocktail: CD3-BV510, CD14-BV510, CD56-BV510, CD27-A488, CD38-APC-Cy7 (*BioLegend*), CD19-ECD (*Beckman Coulter*), IgA-AF647 (*Jackson Immunoresearch*), IgM-PerCP-Cy5.5 (*BD Biosciences*), and IgD-PECy7 (*BD Biosciences*) and the specific probe of interest at a concentration (RH5-CD4-BAP-Ctag and RH5-Nt Bio at 0.1µg/mL).

After this incubation IgG^+ MBCs were sorted using a BD FACSAria III by gating on:

$CD3^-CD14^-CD56^-$ $CD19^+IgD^-IgM^-IgA^-$ cells as shown in the following image (**Figure 3.B.2.2.1.**). Thus cells positive for the probe were selected and stored in a sterile filtered lysis buffer composed of Nuclease-free water, 0.1% BSA, and 0.3% IGEPAL.

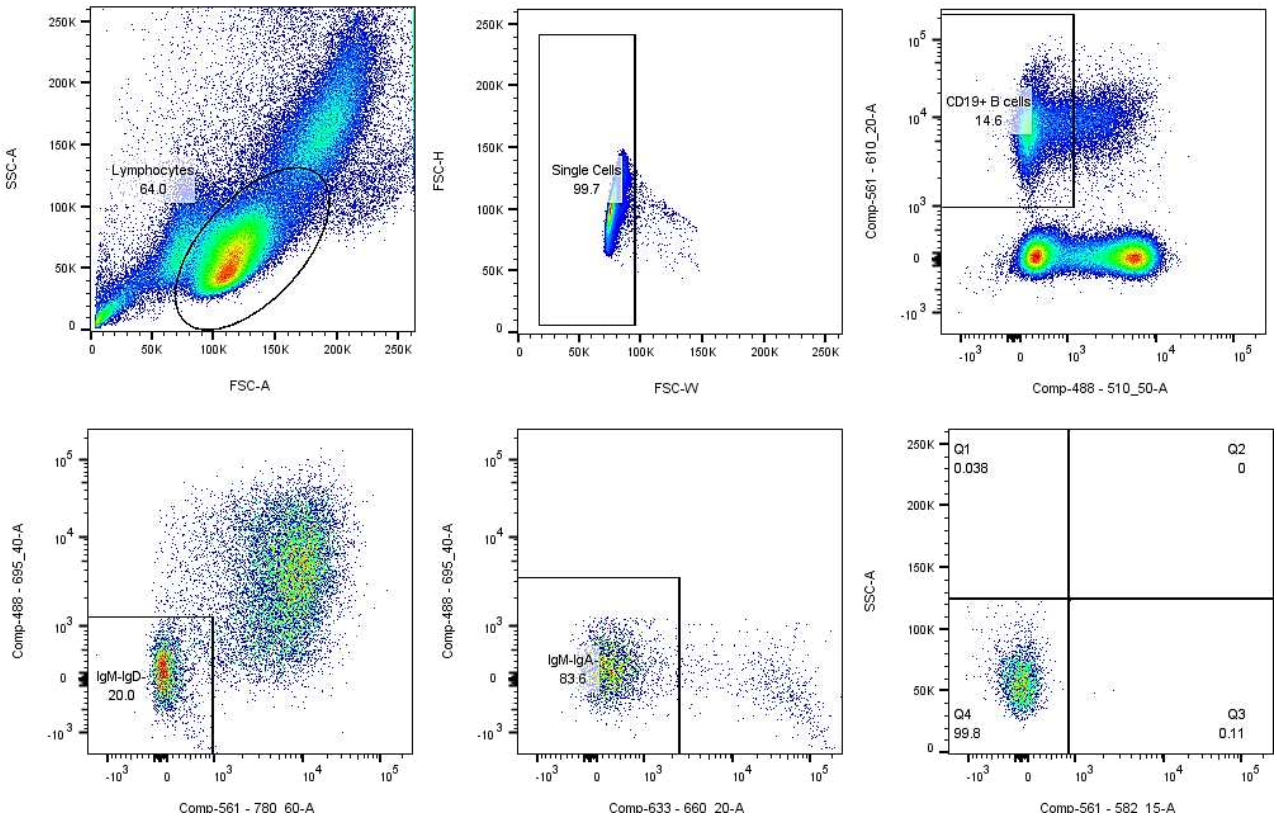

Figure 3.B.2.2.1. *Isolation of MBCs.*

Gating strategy to isolate single, live CD19+,IgM-, IgD-, IgA-MBCs. To sort antigen-specific cells a probe conjugated to PE was used. From the first panel to the last one are indicated the cells sorted:lymphocytes, single cells, B cells CD19+, MBCs IgM- and IgD-, MBCs IgD- and IgA- and in the end MBCs PE positive, therefore antigen-positive.

3.B.3 Cell lines

Expi 293 cells (*Thermo Fisher Scientific*) were used for both the production of the probe, the production of the protein used for the ELISA, and the generation of human recombinant monoclonal antibodies. Cells were cultured at 37°C, with a humidified atmosphere of 8% CO_2 in agitation at 130rpm in a shaker, in Expi293™ Expression Medium (*Gibco*). Expi 293 were cultured in disposable non-flatted Erlenmeyer flasks (*Corning*) and passaged twice weekly at a density of 3.5×10^5 cells/mL in serum-free Gibco Expi 293™medium (*Life Technologies*).

3.B.4 Probe production and RH5 FL, RH5 N-term, RH5ΔNL, RH5.2 recombinant protein

Each probe used (RH5-CD4-BAP-Ctag and RH5-Nt Bio) was expressed as a secreted protein from HEK293F cells using the Expi293™ Expression System (*Thermo Fisher Scientific*). Briefly, HEK293F cells were seeded on day 0 at 1×10^6 cells/mL. On day 1 cells were transfected with a mix of DNA (1µg/mL) ExpiFectamineTM 293 transfection reagent and OptiMEM (*Life Technologies, UK*). DNA and ExpiFectamine™ 293 transfection reagent were mixed and incubated at room temperature for 20min before being added to the cells. After 16 hours, ExpiFectamine™ 293 enhancers 1 and 2 were added according to the manufacturer's instructions. Supernatants were harvested after a further 4-5 days of incubation.

Culture supernatants were harvested by centrifugation at 500g for 5min and then at 3,200g for 15min in a Centrifuge Beckman Coulter Avanti J-15R. The supernatant was then filtered through a 0.22µm SteritopTM (*Merck*).

Proteins were then purified by FPLC on an ÄKTA pure (*GE Lifesciences*) using C-tagXL affinity resin or His-tag purification column followed by size exclusion chromatography (SEC) on a superdex 200 16/600 column (*Cytiva*). Fractions containing the proteins were pooled, quantified on the Nanodrop 8000 (*Thermo Fisher Scientific™*), aliquoted, and stored at -80℃.

The main information about the produced protein is reported in the following table:

Table 3.B.4.1. *Table of recombinant proteins produced.*

In the first column is indicated the plasmid name, in the second column it is shown the amino acid (aa) sequences with light blue aa indicating the signal sequence, while in bold the RH5 sequence, then the third and fourth columns indicate respectively the glycan sites and the purification tag used. RH5-CD4-BAP-Ctag and RH5-Nt Bio are the probes used for sorting (see paragraph 3.B.2.1. Probe design and titration).

Plasmid name	Full sequence	Glycan sites	Purification tag
P2674 RH5-Nt Bio	MEFQTQVLMSLLLCMSGAAAF**ENAIKKTKNQENNLALLPIKSTEEEKD DIKNGKDIKKEIDNDKENIKTNNAKDHSTYIKSYLNTNVNDGLKYLFI PSHNSFIKKYSVFNQINDGMLLNEKNDVKNNEDYKNVDYK**GAPSTSIT AYKSEGESAEFSFPLNLGEESLQGELRWKAEKAPSSQSWITFSLKNQKVS VQKSTSNPKFQLSETLPLTLQIPQVSLQFAGSGNLTLTLDRGILYQEVNLV VMKVTQPDSNTLTCEVMGPTSPKMRLILKQENQEARVSRQEKVIQVQAP EAGVWQCLLSEGEEVKMDSKIQVLSKGLNSGSLHHILDAQKMLWNHRD RNLPPLAPLGPHHHHHH*	T40A	6-His
RH5-CD4-BAP-Ctag (D122)	MEFQTQVLMSLLLCMSGAAAF**ENAIKKTKNQENNLALLPIKSTEEEKD DIKNGKDIKKEIDNDKENIKTNNAKDHSTYIKSYLNTNVNDGLKYLFI PSHNSFIKKYSVFNQINDGMLLNEKNDVKNNEDYKNVDYKNVNFLQ YHFKELSNYNIANSIDILQEKEGHLDFVIIPHYTFLDYYKHLSYNSIYH KSSTYGKCIAVDAFIKKINEAYDKVKSKCNDIKNDLIATIKKLEHPYD INNKNDDSYRYDISEEIDDKSEETDDETEEVEDSIQDTDSNHAPSNKK KNDLMNRAFKKMMDEYNTKKKKLIKCIKNHENDFNKICMDMKNY GTNLFEQLSCYNNNFCNTNGIRYHYDEYIHKLILSVKSKNLNKDLSD MTNILQQSELLLTNLNKKMGSYIYIDTIKFIHKEMKHIFNRIEYHTKII NDKTKIIQDKIKLNIWRTFQKDELLKRILDMSNEYSLFITSDHLRQML YNTFYSKEKHLNNIFHHLIYVLQMKFNDVPIKMEYFQTYKKNKPLT Q**GAPSTSITAYKSEGESAEFSFPLNLGEESLQGELRWKAEKAPSSQSWITF SLKNQKVSVQKSTSNPKFQLSETLPLTLQIPQVSLQFAGSGNLTLTLDRGI LYQEVNLVVMKVTQPDSNTLTCEVMGPTSPKMRLILKQENQEARVSRQ EKVIQVQAPEAGVWQCLLSEGEEVKMDSKIQVLSKGLNSASGLNDIFEA QKIEWHEEPEA	T40A, T216A, T286A, T299A	ctag
RH5deltaNL (SV3)	MKLCILLAVVAFVGLSLG**KNVNFLQYHFKELSNYNIANSIDILQEKEG HLDFVIIPHYTFLDYYKHLSYNSIYHKSSTYGKYIAVDAFIKKINEAYD KVKSKCNDIKNDLIATIKKLEHPYDINNKNRAFKKMMDEYNTKKKK LIKCIKNHENDFNKICMDMKNYGTNLFEQLSCYNNNFCNTNGIRYH YDEYIHKLILSVKSKNLNKDLSDMTNILQQSELLLTNLNKKMGSYIYI DTIKFIHKEMKHIFNRIEYHTKIINDKTKIIQDKIKLNIWRTFQKDELL KRILDMSNEYSLFITSDHLRQMLYNTFYSKEKHLNNIFHHLIYVLQM KFNDVPIKMEYFQTYKKNKPLTQ**EPEA*	T216A	ctag

RH5.1	MKLCILLAVVAFVGLSLGF**ENAIKKTKNQENNLALLPIKSTEEEKDDIK NGKDIKKEIDNDKENIKTNNAKDHSTYIKSYLNTNVNDGLKYLFIPSH NSFIKKYSVFNQINDGMLLNEKNDVKNNEDYKNVDYKNVNFLQYHF KELSNYNIANSIDICQEKEGHLDFVIIPHYTFLDYYKHLSYNSIYHKSS TYGKCIAVDAFIKKINEAYDKVKSKCNDIKNDLIATIKKLCHPYDINN KNDDSYRYDISEEIDDKSEETDDETEEVEDSIQDTDSNHAPSNKKKND LMNRAFKKMMDEYNTKKKKLIKCIKNHENDFNKICMDMKNYGTN LFEQLSCYNNNFCNTNGIRYHYDEYIHKLILSVKSKNLNKDLSDMTNI LQQSELLLTNLNKKMGSYIYIDTIKFIHKEMKHIFNRIEYHTKIINDK TKIIQDKIKLNIWRTFQKDELLKRILDMSNEYSLFITSDHLRQCLYNT FYSKEKCLNNIFHHLIYVLQMKFNDVPIKMEYFQTYKKNKPLT**QEPE A*	T40A, T216A, T286A, T299A	ctag
RH5.2	**Confidential data- not published yet**		

Finally, the proteins RH5ΔNL (SV3), RH5.1 and RH5.2 [279] were previously produced by using an insect cell expression system and C-tag purified.

3.B.5 Production of recombinant immunoglobulins and purification

Following single memory B-cells sorting into lysis buffer (Nuclease-free water + 0.1% BSA + 0.3% IGEPAL), the RNA transcripts were reverse transcribed (RT-PCR) to cDNA using Superscript IV First-Strand Synthesis System (*Thermo Fisher Scientific*).
For this amplification step, Eppendorf™ Dualfilter T.I.P.S™ (*Eppendorf*) PCR clean and sterile were used, and all subsequent mixes were prepared in a DNA/RNA-free hood.
Single antigen-specific memory B cell lysates were thawed on ice for 5min and centrifuged at 400g for 30sec at 4°C. To each sample was then added 10µL of RT-PCR Mix (**Table 3.B.5.1.**):

***Table 3.B.5.1**. RT-PCR Mix.*

RT-PCR Mix I	**1×**
RNase out (*Invitrogen*)	0.5µL
5X FS Buffer (*Life Technologies*)	5µL
DTT (*Life Technologies*)	1.25µL
Random Hexamer (150ng/µL) (*Thermo Fisher Scientific)*	1µL
dNTPs (10 mM) (*Life Technologies*)	2µL
SSIV RT (*Thermo Fisher Scientific*)	0.375µL
Final volume/sample	10µL

Once the RT-PCR Mix was added, plates were centrifugated at 400g for 1min at 4°C and incubated in a Biometra TAdvanced Series (*Analytik Jena*) with the following amplification profile (**Table 3.B.5.2.**):

***Table 3.B.5.2**. Amplification profile of RT-PCR.*

Temperature	**Time**
50°C	5 min
42°C	10min
23°C	10min
50°C	10min
80°C	10min
4°C	∞

At that point, the amplification of the genes encoding the immunoglobulin variable regions of heavy (IgH) and light (kappa and lambda) (Igκ and Ig λ) chains was performed in two rounds of nested PCR using a cocktail of primers listed in **Table 3.B.5.3** [280].

***Table 3.B.5.3**. List of primers.*

Forward primer	Primer name	Sequence 5'-3'
VH1F	v4.Vh1a-ext	ATGGACTGGACCTGGAG
VH1F	v4.Vh1a-ext	ATGGACTGGATTTGGAGG
VH1F	v4.Vh1a-ext	ATGGACTGCACCTGGAG
VH1F	v4.Vh1a-ext	ACATACTTTGTTCCACGCTC
VH1F	v4.Vh1a-ext	GACACACTTTGCTCCACG
VH1F	v4.Vh1a-ext	ATGGACACACTTTGCTACAC
VH1F	v4.Vh1a-ext	ATGGAGTTTGGGCTGAG
VH1F	v4.Vh1a-ext	ATGGAGTTTTGGCTGAGC
VH1F	v4.Vh1a-ext	ATGGAGTTGGGGCTGT
VH1F	v4.Vh1a-ext	ATGGAGTTGGGGCTGA
VH1F	v4.Vh1a-ext	ATGGAGTTGGGACTGAGC
VH1F	v4.Vh1a-ext	ATGGAGTTTGGACTGAGC
VH1F	v4.Vh1a-ext	ATGGAGTTTGGGCTTAGC
VH1F	v4.Vh1a-ext	CGCTGGGTTTTCCTTG
VH1F	v4.Vh1a-ext	GCTGGGTTCTCCTTGTTG
VH1F	v4.Vh1a-ext	ATGGAATTGGGGCTGAG
VH1F	v4.Vh1a-ext	ATGACGGAGTTTGGGCT
VH1F	v4.Vh1a-ext	TGTGGTTCTTCCTCCTCC
VH1F	v4.Vh1a-ext	TGTGGTTCTTTCTCCTCC
VH1F	v4.Vh1a-ext	CTGTGGTTCTTCCTCCTG
VH1F	v4.Vh1a-ext	GTTTTTCCTCCTGCTGGT
VH1F	v4.Vh1a-ext	TGTGGTTCTTCCTTCTCC
VH1F	v4.Vh1a-ext	TGTGGTTCTTCCTGCTC
VH1F	v4.Vh1a-ext	TCAACCGCCATCCTC
VH1F	v4.Vh1a-ext	TAAACCCAGGCTCCCCT
VH1F	v4.Vh1a-ext	ATGTCTGTCTCCTTCCTCATC
Vκ1F	v4.Vk1a-ext	ATGGACATGAGGGTCCC
Vκ1F	v4.Vk1b-ext	ATGGACATGAGGGTGCC
Vκ1F	v4.Vk1c-ext	ATGGACATGATGGTCCCC
Vκ1F	v4.Vk1d-ext	ATGGACATGAGAGTCCTCG
Vκ1F	v4.Vk1e-ext	ATGGACATGAGGGTCCTC

Vκ1F	v4.Vk1f-ext	ATGAGGGTCCCCGCT
Vκ1F	v4.Vk2a-ext	ATGAGGCTCCCTGCTCA
Vκ1F	v4.Vk2b-ext	ATGAGGCTCCTTGCTCAG
Vκ1F	v4.Vk3a-ext	CAGCGCAGCTTCTCTTC
Vκ1F	v4.Vk3b-ext	CCAGCACAGCTTCTTCTTC
Vκ1F	v4.Vk3c-ext	CCAGCTCAGCTTCTCTTC
Vκ1F	v4.Vk4a-ext	ATGGTGTTGCAGACCC
Vκ1F	v4.Vk5a-ext	ATGGGGTCCCAGGTT
Vκ1F	v4.Vk6a-ext	TGCCATCACAACTCATTGG
Vκ1F	v4.Vk6b-ext	CGCCATCACAACTCATTG
Vλ1F	v4.Vl1a-ext	ATGGCCTGGTCTCCTC
Vλ1F	v4.Vl1b-ext	CTCTCCTCCTCACCCTC
Vλ1F	v4.Vl2a-ext	CTCTGCTGCTCCTCACTC
Vλ1F	v4.Vl2b-ext	CTGCTGCTCCTCCTCAC
Vλ1F	v4.Vl3a-ext	CTCTCCTTCTGAGCCTCC
Vλ1F	v4.Vl3b-ext	CTCTCCTCCTCAGCCTC
Vλ1F	v4.Vl3c-ext	TTCTCCTCCTCGGCCT
Vλ1F	v4.Vl3d-ext	CCTCTACTTCTCCCCCTC
Vλ1F	v4.Vl3e-ext	CTCCCCCTCCTCACTTTC
Vλ1F	v4.Vl3f-ext	GATCCCTCTCTTCCTCGG
Vλ1F	v4.Vl3g-ext	ATCCCTCTCCTGCTCC
Vλ1F	v4.Vl3h-ext	TCTCTGGCTCACTCTCCTC
Vλ1F	v4.Vl4a-ext	CTGGGTCTCCTTCTACCTACT
Vλ1F	v4.Vl4b-ext	CCACTCCTCCTCCTCTTC
Vλ1F	v4.Vl4c-ext	TTCCTCACCCTCCTCCT
Vλ1F	v4.Vl5a-ext	ACTCCTCTCCTCCTCCTG
Vλ1F	v4.Vl6a-ext	CTGGGCTCCACTACTTCTC
Vλ1F	v4.Vl7a-ext	CCTGGACTCCTCTCTTTCTG
Vλ1F	v4.Vl8a-ext	CTGGATGATGCTTCTCCTC
Vλ1F	v4.Vl9a-ext	CTGCTCCTCACCCTCCT
Vλ1F	v4.Vl10a-ext	TCCTCCTGACCCTCCTC
Vλ1F	v4.Vl10b-ext	GCTCCTCCTGAAATCCTC
VH2F	v4.Vh1a-int	CTGGAGCATCCTTTTCTTGGTGG
VH2F	v4.Vh1b-int	CCTCTTCTTGGTGGCAGCAGC

VH2F	v4.Vh1c-int	CTGGAGGGTCTTCTGCTTGCTG
VH2F	v4.Vh1d-int	CTCTTTGTGGTGGCAGCAGC
VH2F	v4.Vh1e-int	CCTCTTCTTGGTGGGAGCAGC
VH2F	v4.Vh1f-int	CCTCTTTTTGGTGGCAGCAGC
VH2F	v4.Vh1g-int	CTCCTCTTGGTGGCAGCAGC
VH2F	v4.Vh1h-int	CCTTTTCTTGGTGGCAGCAGC
VH2F	v4.Vh2a-int	CCTGCTGCTGACCATCCCTTC
VH2F	v4.Vh2b-int	CCTGCTACTGACTGTCCCGTC
VH2F	v4.Vh2c-int	ACACTCCTGCTGCTGACCACC
VH2F	v4.Vh3a-int	GTTGGGACTGAGCTGGATTTTCC
VH2F	v4.Vh3b-int	GTTTGGACTGAGCTGGGTTTTCC
VH2F	v4.Vh3c-int	GTTTGGGCTGAGCTGGGTTTTC
VH2F	v4.Vh3d-int	GTTTTGGCTGAGCTGGGTTTTCC
VH2F	v4.Vh3e-int	GGGCTTAGCTGGGTTTTCCTTG
VH2F	v4.Vh3f-int	GGGCTGAGCTGGCTTTTTCTTG
VH2F	v4.Vh3g-int	GGCTGTGCTGGGTTTTCCTTG
VH2F	v4.Vh3h-int	GGCTGAGCTGGGTTTTCCTTG
VH2F	v4.Vh3i-int	GTTTGGGCTGAGCTGGATTTTCC
VH2F	v4.Vh3j-int	GTTGGGGCTGAGGTGGCTTTTTC
VH2F	v4.Vh3k-int	GGCTGAGGTGGGTTTTCCTTG
VH2F	v4.Vh3l-int	GGGCTGAGGTGGATTTTCCTTTTG
VH2F	v4.Vh4a-int	TTCTTCCTCCTCCTGGTGGC
VH2F	v4.Vh4b-int	GGTTCTTTCTCCTCCTGGTGGC
VH2F	v4.Vh4c-int	TTCTTCCTCCTGCTGGTGGC
VH2F	v4.Vh4d-int	GGTTCTTCCTTCTCCTGGTGGC
VH2F	v4.Vh5a-int	TTCTCCAAGGAGTCTGTGCCG
VH2F	v4.Vh5b-int	TCCCCTCCACAGTGAGAGTCTG
VH2F	v4.Vh6a-int	TCTCCTTCCTCATCTTCCTGCC
Vκ2F	v4.Vk1a-int	TGCTGCTCTGGCTCCCA
Vκ2F	v4.Vk1b-int	CTCCTGCTGCTCTGGCTCTC
Vκ2F	v4.Vk1c-int	TCCTGGGGCTCCTGCTACTC
Vκ2F	v4.Vk1d-int	TCCTGCTGCTCTGGTTCCC
Vκ2F	v4.Vk1e-int	TGCAGCTCTGGCTCTCAGGT
Vκ2F	v4.Vk1f-int	CCTGCTGCTCTGTTTCCCAG

Vκ2F	v4.Vk2a-int	CTGGGGCTGCTAATGCTCTG
Vκ2F	v4.Vk2b-int	CTCTTGGGGCTGCTAATGCTC
Vκ2F	v4.Vk3a-int	TCCTGCTACTCTGGCTCCCA
Vκ2F	v4.Vk3d-int	CTCCTGCTACTCTGGCTCACAG
Vκ2F	v4.Vk4a-int	GTTGCTCTGGATCTCTGGTGC
Vκ2F	v4.Vk5a-int	CTTCCTCCTCCTTTGGATCTCTG
Vκ2F	v4.Vk6a-int	GTTTCTGCTGCTCTGGGTTCC
Vλ2F	v4.Vl1a-Int	CACCCTCCTCACTCACTGGTC
Vλ2F	v4.Vl1b-Int	CCTCACTCTCCTCGCTCACTG
Vλ2F	v4.Vl2a-Int	CCTCCTCACTCAGGGCACA
Vλ2F	v4.Vl2b-Int	CACTCTCCTCACTCGGGACAC
Vκ2F	v4.Vl2c-Int	TGCTCCTCACTCTCCTCACTCAG
Vκ2F	v4.Vl3a-Int	CCCTCCTCACTCTCTGCACAG
Vλ2F	v4.Vl3b-Int	CCCTCCTCACTTTCTGCACAG
Vλ2F	v4.Vl3c-Int	GCCTCCTCTCTCACTGCACAG
Vλ2F	v4.Vl3d-Int	AGCCTCCTTGCTCACTTTACAGG
Vλ2F	v4.Vl3e-Int	TCACTCTCCTCACTCTTTGCATAGGT
Vλ2F	v4.Vl3f-Int	CCCCCTCTTCACTCTCTGCA
Vλ2F	v4.Vl3g-Int	TCCCCCTCCTCATTCTCTGC
Vλ2F	v4.Vl3h-Int	CTCGGCGTCCTTGCTTACTG
Vλ2F	v4.Vl3i-Int	CTCAGCCTCCTCGCTCACTG
Vλ2F	v4.Vl4a-Int	CTTCCCTCTCCTCCTCCACTG
Vλ2F	v4.Vl4b-Int	ACTGCCCTTCATTTTCTCCACAG
Vλ2F	v4.Vl5a-Int	TCCTCCTGCTCCTCTCTCACTG
Vλ2F	v4.Vl5b-Int	TCCTCCTGTTCCTCTCTCACTGC
Vλ2F	v4.Vl6a-Int	TTCTCACCCTCCTCGCTCAC
Vλ2F	v4.Vl7a-Int	CTGTTCCTCCTCACTTGCTGC
Vλ2F	v4.Vl8a-Int	CTTCTCCTCGGACTCCTTGCTT
Vλ2F	v4.Vl9a-Int	TCACCCTCCTCAGTCTCCTCAC
Vλ2F	v4.Vl9b-Int	TCCTCCTCCACTGCACAGG
Vλ2F	v4.Vl10a-Int	ACCCTCCTCACTCACTCTGCA

Reverse primer	Primer name	Sequence 5'-3'
VH1R	HuIGHG-revO	GTGTTGCTGGGCTTGTG
Vκ1R	IGKCrev-ext	CCTGCTCTGTGACACTCTC
Vλ1R	IGLCrev-ext	GTCTTCTCCACGGTGCTC
VH2R	HuIGHG-revI	GCTGCTGAGGGAGTAGAGTC
Vκ2R	IGKCrev-int	GGAGGGCGTTATCCACCTTCC
Vλ2R	IGLCrev-int	GCTTCTGTGGGACTTCCACTGCTC

The template for the I PCR was the cDNA, while the template for the II PCR was the DNA resulting from the first PCR. At that point, the PCR products were sent for sequencing (ACTG) and then the sequences were analysed using IMGT.

A fixed amount of unique sequences of matched heavy and light chains were cloned into an IgG1 expression vector. The plasmid of heavy and light chains matched mAbs were co-transfected into 10mL of Expi 293 cells using the ExpiFectamine™ 293 Transfection Kit (*Thermo Fisher Scientific*) and the cultures were incubated at 37°C, 8% CO_2 for 6 days. Supernatants were then harvested and centrifuged for 20min at 3,500g, sterile filtered and purified. This step was done using a HiTrap Fibro™column (*Cytiva*) with the ASX-560 Autosampler connected to an Akta Pure. The mAbs were buffer exchanged in *Pf* ICM (RPMI, 2mM L-glutamine, 0.05g/L hypoxanthine, 5.94g/L HEPES) using 30kDa Amicon Centrifugal Filters (*Millipore*).

The purified mAbs concentrations were determined using a Nanodrop spectrophotometer (*Thermo Fisher Scientific*).

3.B.6 Epitope mapping ELISA

To determine the antigen-specificity to RH5.1 FL, RH5 N-terminus, RH5ΔNL and RH5.2 proteins were used in an epitope mapping ELISA.

The ELISA was carried out by coating the plates with the different proteins at 2µg/mL in 50µL on Maxisorp flat-bottom 96-well plates (*Nunc*) and incubated overnight at 4°C. The following day plates were washed six times with PBS-T (phosphate-buffered saline PBS with 0.05% Tween-20) and blocked with 100µL per well of Blocker™ Casein (*Thermo Fisher Scientific*) for 1 hour at room temperature.

After other six washes with PBS-T, 50µL of purified mAbs to be tested diluted in Blocker™ Casein to a concentration of 2µg/mL were added to each well and the plate was incubated for 2h at RT. The plate was then washed again six times with PBS-T and it was added 50µL

per well of secondary antibody goat Anti-human IgG (γ-chain specific)-alkaline phosphatase conjugate (*Sigma-Aldrich*) diluted to 1:2,000 in Blocker^{TM} Casein.
After 1 hour of incubation at room temperature, the plate was washed six times with PBS-T and then the plate was developed using 4-nitrophenylphosphate substrate at a final concentration of 1mg/mL (*Sigma-Aldrich*) in water and diethanolamine and read on an ELISA reader (ELx808) at 405nm.

3.B.7 Peptide ELISA for determining Rh5 N-terminus-specific peptide epitopes

Nunc flat-bottom 96-well plates were coated with 100µL/well of Streptavidin (*Sigma*) at a concentration of 5µg/mL and incubated overnight at 37°C. The following day plates were washed six times with PBS-T (phosphate-buffered saline PBS with 0.05% Tween-20) and 50µL/well of N-terminus peptides were added at 10µg/mL and incubated for 2 hours at room temperature.
The biotinylated overlapping 20-mer peptides (**Table 3.B.7.1.**) were synthesized for the ELISA by mimotope.

RH5 Nterm sequence:

[1]**ENAIKKTKNQ**[11]**ENNLALLPIK**[21]STEEEKDDIK[31]NGKDIKKEID[41]NDKENIKTNN[51]
AKDHSTYIKS[61]YLNTNVNDGL[71]KYLFIPSHNS[81]FIKKYSVFNQ[91]INDGMLLNEK[101]
NDVK**NNEDYK**[111]**NVDY**

Table 3.B.7.2. *Peptides RH5 Nterm.*

P1 (E28)	1 Amine	**ENAIKKTKNQENQLTLLPIKGSG** Lys(Biotin)
P2 (N36)	2 Biotin	SGSGNQENQLTLLPIKSTEEEKDD
P3 (L42)	3 Biotin	SGSGLPIKSTEEEKDDIKNGKDIK
P4 (E50)	4 Biotin	SGSGEKDDIKNGKDIKKEIDNDKE
P5 (K58)	5 Biotin	SGSGKDIKKEIDNDKENIKTNNAK
P6 (N66)	6 Biotin	SGSGNDKENIKTNNAKDHSTYIKS
P7 (N72)	7 Biotin	SGSGNNAKDHSTYIKSYLNTNVND
P8 (Y90)	8 Biotin	SGSGYIKSYLNTNVNDGLKYLFIP
P9 (N98)	9 Biotin	SGSGNVNDGLKYLFIPSHNSFIKK
P10 (L106)	10 Biotin	SGSGLFIPSHNSFIKKYSVFNQIN
P11 (F114)	11 Biotin	SGSGFIKKYSVFNQINDGMLLNEK
P12 (N122)	12 Biotin	SGSGNQINDGMLLNEKNDVKNNED
P13 (L130)	13 Biotin	SGSGLNEKNDVKNNEDYKNVDYKN
P14 (N138)	14 Biotin	SGSG**NNEDYKNVDY**KNVNFLQYHF
Peptide I	K33-K51-Biotin	KNQENNLTLLPIKSTEEEKSGSGK -Biotin
Peptide II	Biotin-K33-K51	Biotin- SGSGKNQENNLTLLPIKSTEEEK

The plate was washed six times with PBS-T and then it was blocked with 100µL per well of Blocker™ Casein (*Thermo Fisher Scientific*) for 1 hour at room temperature. After the other six were washed with PBS-T 50µL/well of monoclonal antibodies of interest diluted at 2µg/mL were added and incubated for 1 hour at room temperature. The plate was then washed again six times with PBS-T and it was added 50µL per well of secondary antibody goat Anti-human IgG (γ-chain specific)-alkaline phosphatase conjugate (Sigma-Aldrich) diluted to 1:2,000 in Blocker™ Casein. After 1 hour of incubation at room temperature, the plate was washed six times with PBS-T and then developed with the 4-nitrophenylphosphate substrate at a concentration of 1mg/mL (*Sigma-Aldrich*) in water and diethanolamine and read on an ELISA reader (ELx808) at 405nm.

3.B.8 Growth inhibition activity assay GIA

To characterise the ability of the human mAbs to block merozoite entry into RBCs, they were tested for *in vitro* GIA against 3D7 clone *P. falciparum*. Positive monoclonal antibodies were buffer exchanged into incomplete parasite growth media (RPMI, 2mM L-glutamine, 0.05g/L hypoxanthine, 5.94g/L HEPES) before performing a one-cycle GIA, as previously published [269].

To ensure consistency between experiments, in each case the activity of a negative control mAb, EBL04 [281] which binds to the Ebola virus glycoprotein, was used.

Three anti-RH5 mAbs with well-characterised levels of GIA (2AC7, R5.016, BD5/R5.034) were run alongside the test mAbs and used for assay quality control (QC) (Appendix), all were tested in triplicates to known levels of GIA.

Each mAb was assessed by measuring GIA: the test mAb held constant at approximately 0.5mg/mL, if positive (or >40%GIA) the mAb was further tested across a 5-fold eight-step dilution curve beginning at 1mg/mL to determine EC50 (and EC80). Another known mAb (BD5/R5.034) was included as a further benchmark.

3.B.9 Peptide epitope mapping by Surface Plasmon Resonance

High-throughput peptide epitope mapping was performed using the Carterra LSA and a streptavidin coated SAHC30 chip (*Carterra*). The chip was conditioned with 60s injections of 50mM NaOH, 1 M NaCl and 10mM glycine (pH2.0) before an RH5 peptide library (as previously described) was captured as an array on the surface using the LSA 96-channel print head (96PH) mode. In brief, the biotinylated peptide ligands were prepared at two concentrations (5µg/mL and 1µg/mL) in TBST (0.01%Tween) running buffer. Peptides were captured with 2 x 15s injections using the 96PH, followed by a 1 x 5min injection of TBS-T and 2 x 15 s injections of 10 mM glycine (pH2.0) across the whole chip surface using the Single Flow Cell (SFC) mode. The peptide array was then subjected to sequential injections of RH5 antibodies (prepared at 10µg/mL in TBST), in between which the surface was regenerated with 10mM glycine (pH2.0) using 2x30 s regeneration cycles. Data were analysed using the Carterra Epitope software.

4.B Results

4.B.1. Isolation and characterisation of a panel of human RH5 FL mAbs from VAC 063

4.B.1.1. RH5-FL-specific memory B cells isolation

The 5 subjects for the isolation of PBMCs and subsequently mAbs in this study were selected within the VAC063 clinical trial. This was an open-label Phase I/IIa dose escalation blood-stage malaria CHMI trial to assess the safety, immunogenicity, and efficacy of recombinant RH5 with the adjuvant AS01B in healthy, malaria naïve adults aged 18-45 years.

To select the samples, first, the RH5 reactivity of plasma was measured, thus identifying some promising anti-RH5 IgG titers, and then these results were compared with the same plasma used in a GIA assay, to detect the activity.

Of these subjects, five were positive samples, while a sixth was used as negative control.

The time point at which the PBMCs were isolated from the volunteers was day 63, one-week post-third vaccination. As previously reported in the material and method section, RH5-FL specific MBCs were directly sorted in a lysis buffer in a 96-well plate using a BD FACSAria III and selecting $CD3^-$,$CD14^-CD56^-$ $CD19^+IgD^-IgM^-IgA^-$ and RH5-CD4-BAP (D122 probe) positive cells.

As shown in **Table 4.B.1.1.1.**, a total of 805 RH5-FL specific MBCs were sorted in total, with a similar percentage of antigen-specific cell sorting for each subject, around 20% from each donor.

Table 4.B.1.1.1. *Summary table of subjects and RH5-FL specific MBCs sorted.*

Subjects	Cells sorted	% per subject
S1:01-022 (day63)	180	22.4
S2: 01-029 (day63)	158	19.6
S3: 01-036 (day63)	153	19
S4: 01-037 (day63)	167	20.7
S5: 01-051 (day63)	147	18.3
Tot:	805	100

4.B.1.2. Amplification and sequencing of V_H and V_L genes of RH5-FL mAbs

After the single cell sorting of B cells into lysis buffer, all RNA transcripts were reverse transcribed to cDNA. Amplification of the genes encoding the immunoglobulins variable regions heavy chains and kappa or lambda chains was performed by two rounds of nested PCR, using a cocktail of primers (as previously listed in the material and methods section). All the second PCR products were loaded into a 1% agarose gel to evaluate the effective presence of the DNA (**Fig 4.B.1.2.1. and 4B.1.2.2.**), here shown as black bands.

Figure 4.B.1.2.1. *PCR amplification of VH genes from Subject 1.*

Each lane represents a PCR amplicon of the second PCR from a single MBC run on a 1% agarose gel. For the variable heavy amplicons the expected size is ~500bps.

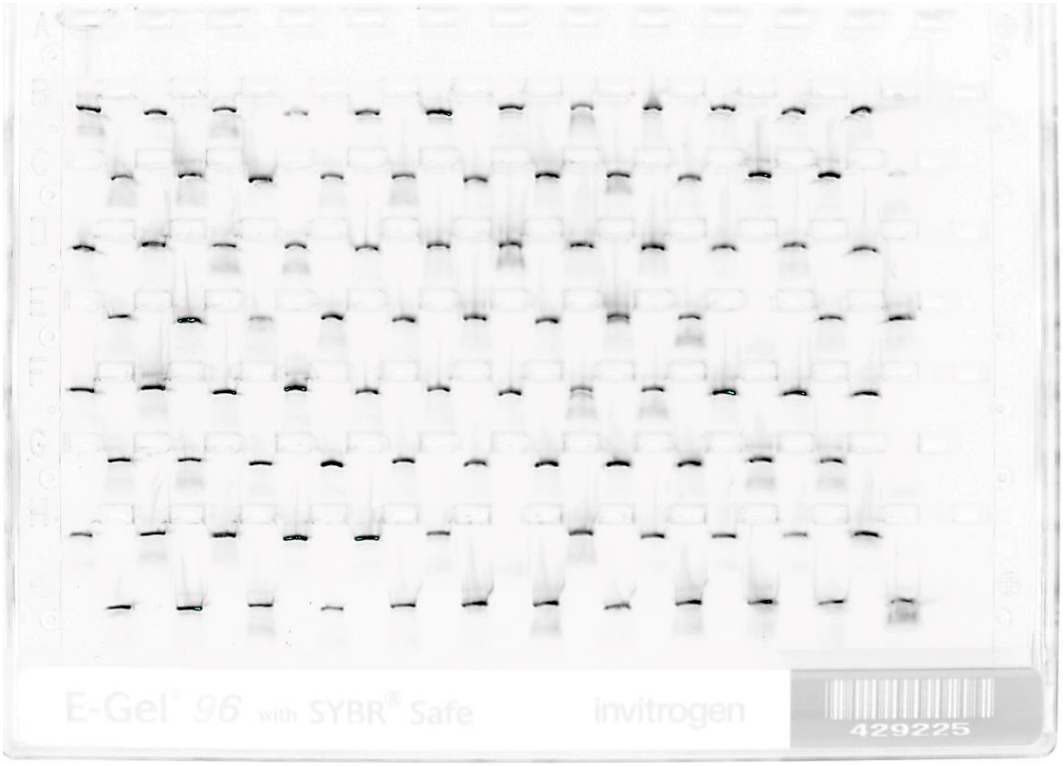

Figure 4.B.1.2.2*. PCR amplification of VL genes from Subject 1.*

Each lane represents a PCR amplicon of the second PCR from a single MBC run on a 1% agarose gel. For the variable heavy amplicons the expected size is ~400bps.

After an evaluation of correspondence between heavy and light chains, samples were diluted and sent for sequencing (ACTG).

As shown in the summary **Table 4.B.1.2.1.**, in total, the amplicons recovered were 614 for V_H and 644 for V_L, out of which a total of 586 were matched (683 of 805 single MBCs were amplified, approximately 85% of the total samples).

It can be assessed that the efficiency of recovery of matched V_H and V_L chains among all the donors is high, ranging between 83.3-90.2%.

Sequences were recovered for 387 matched sequences of V_H and V_L chains, with 384 unique sequences. The efficiency of sequencing with respect to gel amplification was approximately 67.3%, while the overall unique and paired sequences obtained to develop mAbs compared with the starting cell sorted was around 57.6%.

Table 4.B.1.2.1. *Summary table of cell sorted for each subject, gel bands obtained and sequencing considerations.*

On the left side it is shown the subjects and the respective MBCs sorted for the amplifications, numbers in the brackets indicate the total cells isolated but not fully used for the amplifications. The central columns, with the yellow box in the upper part, shows numbers relative to the amplifications for the heavy and light chains, as well as the matched amplicons obtained and the efficiency calculation. The columns of the right instead, with the green box in the upper part, exhibit the sequencing number data of the paired VH and VL , the unique sequences and the efficiencies with respect to the gels and sorted MBCs.

		Gel bands				**Sequencing**			
Subjects	**Cells sorted used**	**HC bands**	**LC bands**	**Matched**	**Efficiency %**	**Paired**	**UNIQUE**	**Efficiency % (vs gel)**	**Overall (%) (vs sorted cells)**
S1	180	160	171	150	83.3	95	95	65.6	53.3
S2	158	147	140	133	84.2	83	81	62.4	52.5
S3	153	141	147	138	90.2	92	91	66.7	60.1
S4	96 (168)	83	91	82	85.4	46	46	56.1	47.9
S5	96 (148)	83	95	83	86.5	71	71	85.5	74.0
Tot:	683	614	644	586	85.9	387	384	67.3	57.6

4.B.1.3. RH5-FL mAbs expression and screening by Epitope mapping ELISA

An equal number of matched V_H/V_L sequences for each subject were sent to Twist for gene synthesis and cloning into human IgG1 plasmid vectors, regardless of original subclasses (IgG1, IgG2, IgG3, or IgG4).

The mAbs received were expressed in Expi 293, a total of 100 mAbs, equally distributed, 20 for each donor (**Fig 4.B.1.3.1.**).

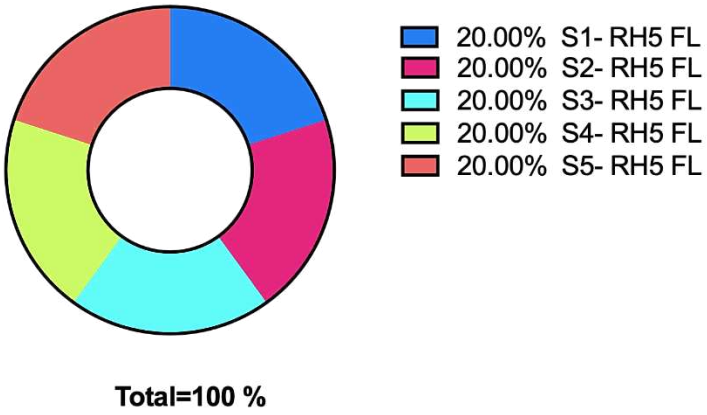

Figure 4.B.1.3.1. *Percentage of plasmids coding for different RH5 FL mAbs from distinct subjects (1-5).*

mAbs are equally distributed, 20% for each subject.

The DNA was then used to transfect cells and obtain 10mL of transfection for each mAb. After 5 days, the supernatants were harvested, purified and then analysed in an ELISA assay. The epitope mapping ELISA was used to test all the purified mAbs, diluted at the same concentration of 2µg/mL, against the full RH5.1, the denatured RH5.1, the N-terminus portion of RH5, the RH5 delta NL and the mutated version of RH5 delta NL, called "RH5.2" [279].

The ELISAs shown are divided per subject, each section has 5 graphs showing the mAbs of that person on the X-axis tested against the protein of interest represented by the OD value on the Y-axis (**Figures 4.B.1.3.2-6.**).

The internal controls used are: R5.016, a conformational mAb that can bind the RH5.1 full-length protein; 4BA7 a chimeric mouse anti-*Pf*RH5 mAb able to bind a linear epitope and 3A11, a mAb able to bind to the N-terminus portion of RH5, to the FL RH5.1 and with less strength also to the denatured version of the same protein.

mAbs obtained from Subject 1:

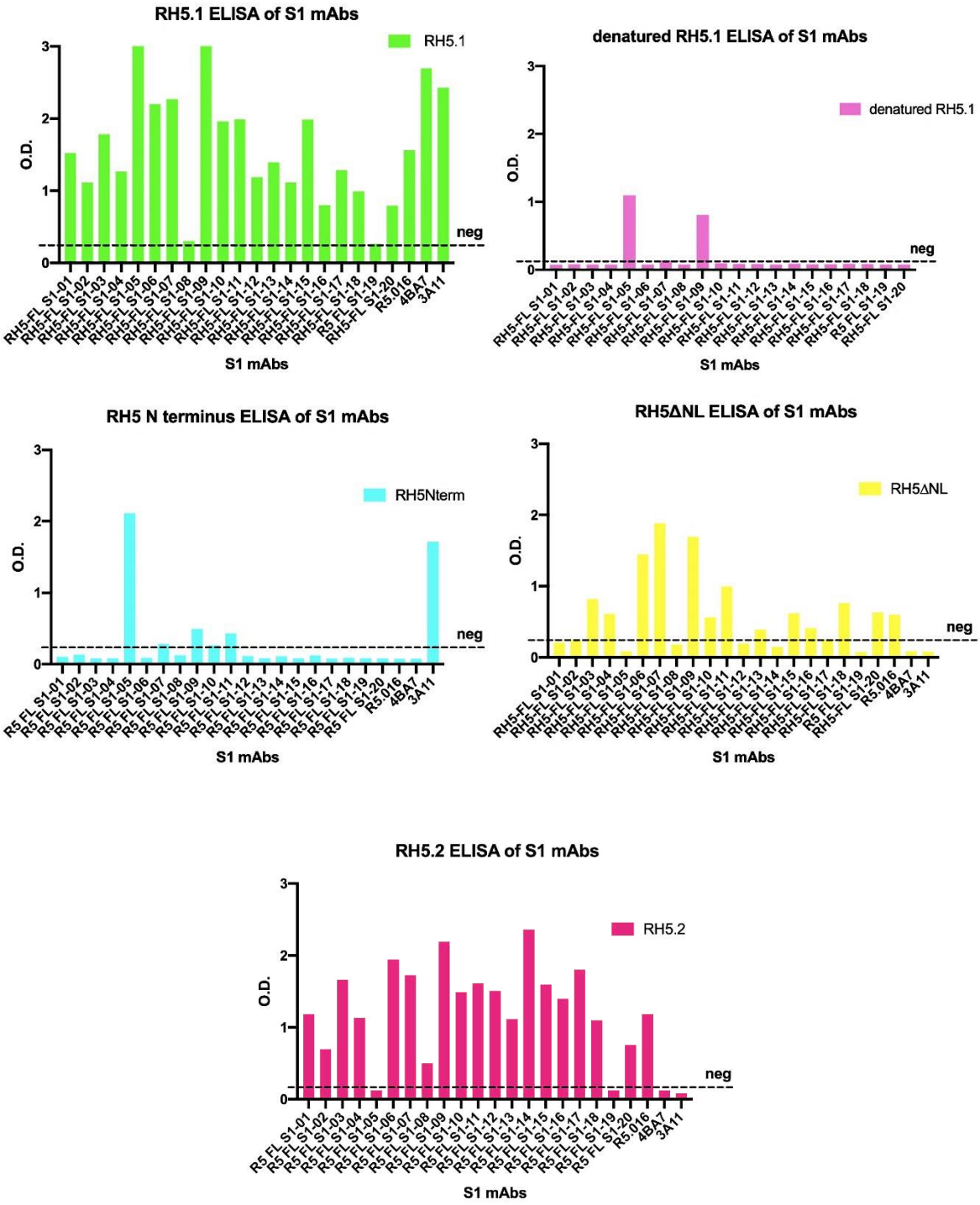

Figure 4.B.1.3.3. *RH5 FL mAbs of Subject 1.*

Here are represented the ELISAs of the 20 S1 mAbs tested against the RH5.1 full-length protein (green), the denatured RH5.1 full-length protein (violet), the N-terminus portion of RH5 (light blue),RH5ΔNL (yellow) and the RH5.2 protein (pink). The X-axis shows all the mAbs and the Y-axis shows the O.D. value in ELISA.

mAbs obtained from Subject 2:

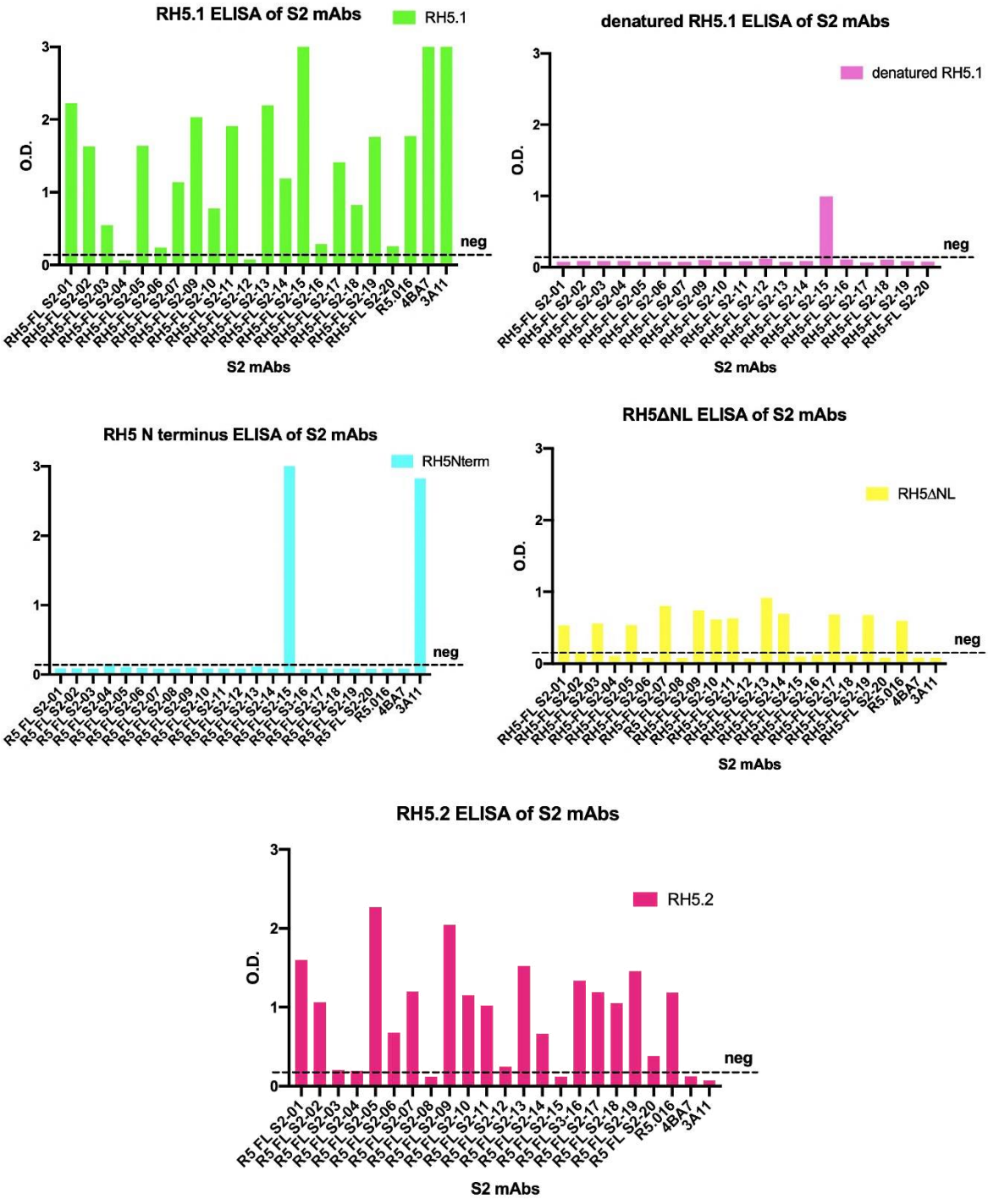

Figure 4.B.1. 3.4. *RH5 FL mAbs of Subject 2.*

Here are represented the ELISAs of the 20 S2 mAbs tested against the RH5.1 full-length protein (green), the denatured RH5.1 full-length protein (violet), the N-terminus portion of RH5 (light blue), RH5ΔNL (yellow) and the RH5.2 protein (pink). The X-axis shows all the mAbs and the Y-axis shows the O.D. value in ELISA.

mAbs obtained from Subject 3:

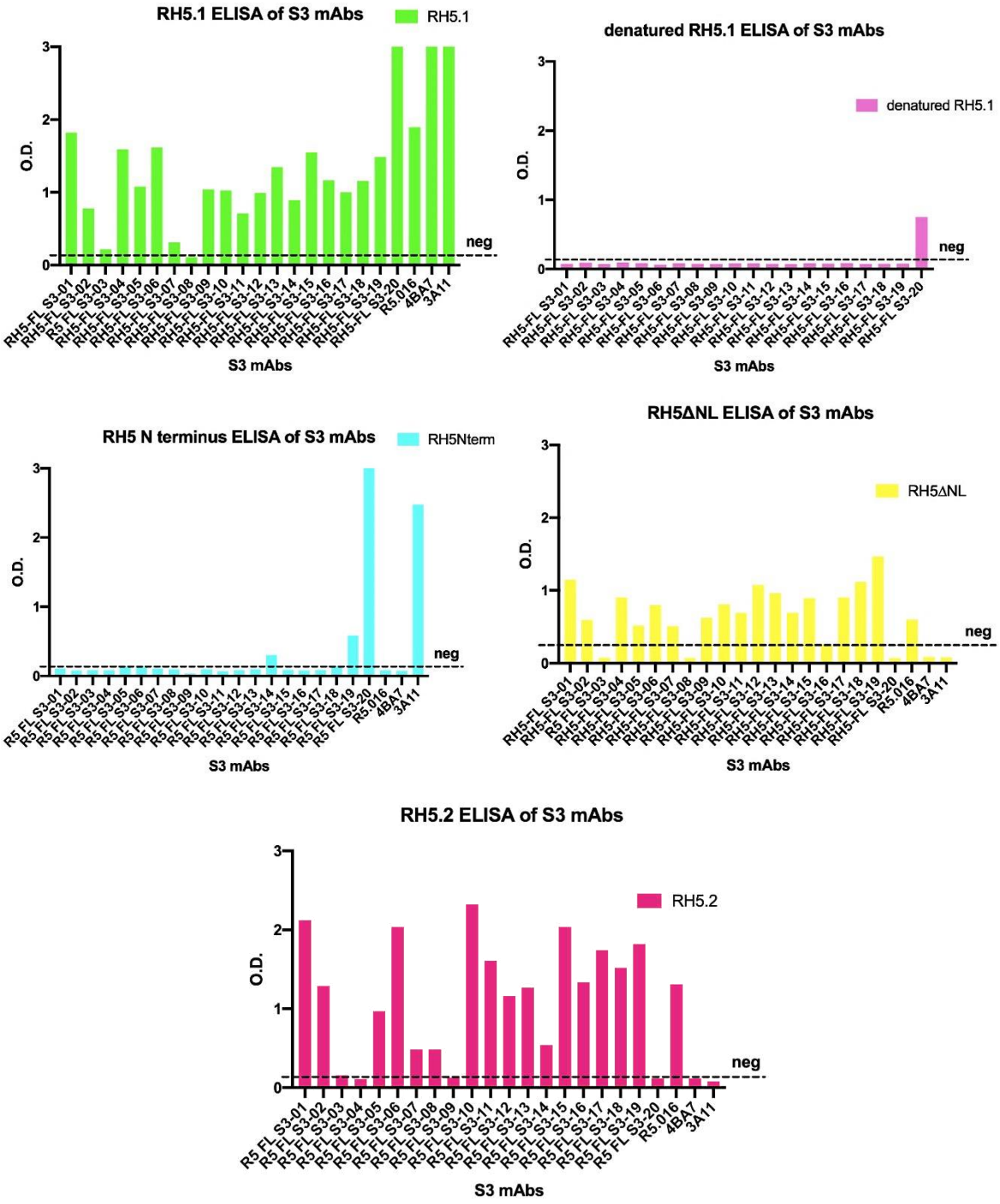

Figure 4.B.1.3.5. *RH5 FL mAbs of Subject 3.*

Here are represented the ELISAs of the 20 S3 mAbs tested against the RH5.1 full-length protein (green), the denatured RH5.1 full-length protein (violet), the N-terminus portion of RH5 (light blue), RH5ΔNL (yellow) and the RH5.2 protein (pink). The X-axis shows all the mAbs and the Y-axis shows the O.D. value in ELISA.

mAbs obtained from Subject 4:

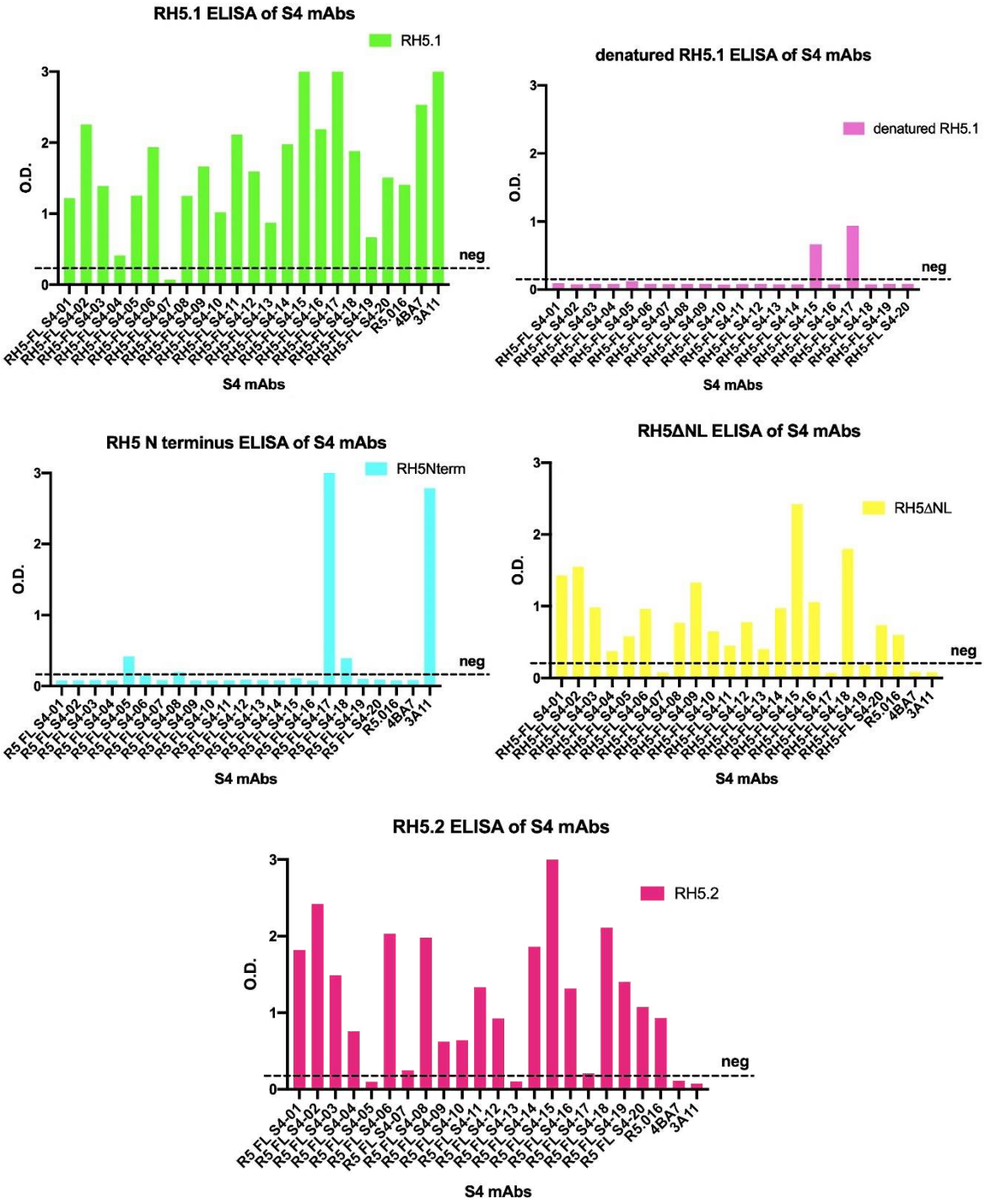

Figure 4.B.1.3.6. *RH5 FL mAbs of Subject 4.*

Here are represented the ELISAs of the 20 S4 mAbs tested against the RH5.1 full-length protein (green), the denatured RH5.1 full-length protein (violet), the N-terminus portion of RH5 (light blue), RH5ΔNL (yellow) and the RH5.2 protein (pink). The X-axis shows all the mAbs and the Y-axis shows the O.D. value in ELISA.

mAbs obtained from Subject 5:

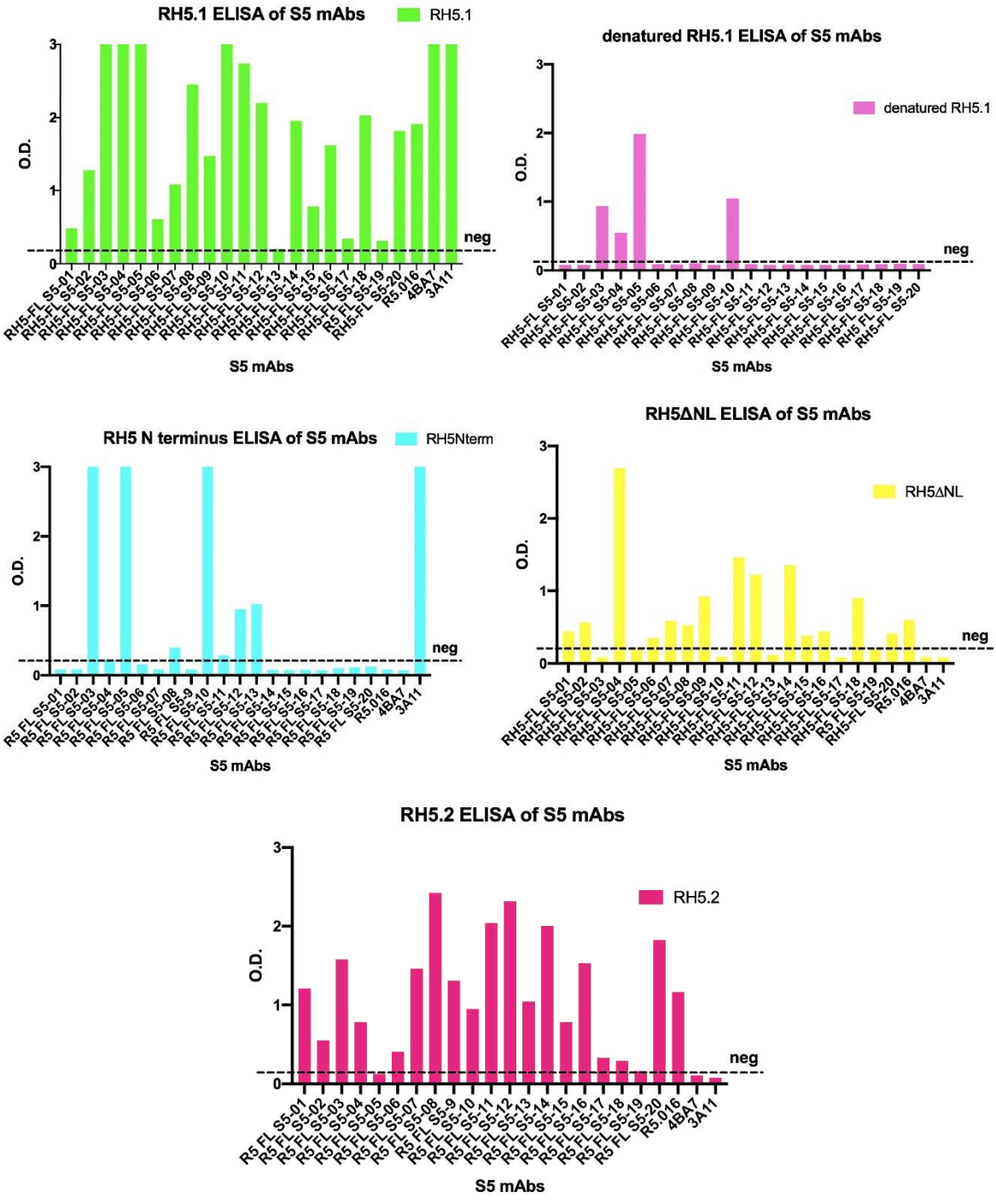

Figure 4.B.1.3.7. *RH5 FL mAbs of Subject 5.*

Here are represented the ELISAs of the 20 S5 mAbs tested against the RH5.1 full-length protein (green), the denatured RH5.1 full-length protein (violet), the N-terminus portion of RH5 (light blue), RH5ΔNL (yellow) and the RH5.2 protein (pink). The X-axis shows all the mAbs and the Y-axis shows the O.D. value in ELISA.

To analyse what we have seen so far in these graphs we can first of all say that of the 100 expressed mAbs, 94% were able to bind the full-length RH5.1 protein for which they were selected. To go further in detail, we have investigated how many mAbs were conformational, thus not able to bind the heat-denatured protein, and then instead how many were linear mAbs and, where it was possible, we have classified the latter.

As we can observe from the pie chart (**Figure 4.B.1.3.8.A.**), 89.4% of the mAbs were conformational (N=84), thus binding RH5.1 as well as the thermostable mutated RH5.2, except in rare cases (N=5) where the binding occurred for RH5.1, RH5ΔNL, but not for RH5.2. The latter is a protein involved in the next-generation vaccine, having improved stability by removing loops and by introducing thermostability mutations. This subclass of mAbs seems to bound conformational epitopes present in the regions where mutations have been introduced.

Nevertheless, this occurred in very rare cases indeed RH5.2 is bound by 86% (N=81) of positive mAbs, a substantial number. The binding to this protein is important because we also wanted to establish if these mAbs were also able to bind to the next-generation vaccine, that is entering trials now and in most cases we can say that the binding effectively exists.

If we focus our attention on the linear RH5 binders (**Figure 4.B.1.3.9.B.**), mAbs that have affinity for the denatured RH5 protein, we can observe that they are 10.6% and of these: the majority, 70%, are N-terminus binders (mAbs S1-05, S2-15, S3-20, S4-17, S5-03, S5-05, S5-10), while 10% are intrinsic loop binders and the remaining 20% are undetermined.

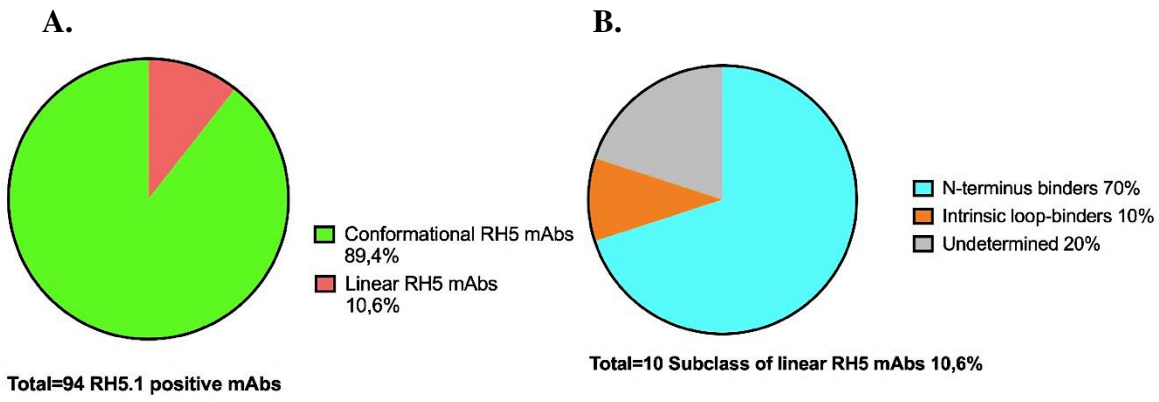

Figure 4.B.1.3.10. *RH5 FL conformational and linear mAbs.*

A. *This graph shows the percentage of positive RH5 FL that bind conformational epitopes or linear epitopes, with the associate percentage.* ***B*** *This graph shows how the subclass of linear RH5 mAbs is divided: N-terminus binders, intrinsic loop binders and undetermined.*

4.B.1.4. Growth inhibition activity of anti-FL RH5 mAbs: single point and eventually dilution curve

To further characterise these mAbs we measured their ability to block 3D7 clone *P. falciparum* parasite invasion *in vitro*. GIA assays were carried out as detailed in section GIA of Material and Methods. All the ELISA-positive RH5 FL mAbs were indeed tested for GIA activity at a single concentration of 0.5mg/mL, always using an internal positive control called BD5/R5.034 and a negative control. This mAb, also known as R5.034 is the most potent RH5 mAb reported to date, which has an effective concentration to mediate 50% inhibition (EC50) of 2.5µg/mL in the GIA assay [276]. GIA to test RH5 FL mAbs were plotted as GIA (%) against RH5 FL mAbs at the same single concentration, as shown in **Figure 4.B.1.4.1.A-E**.

A.

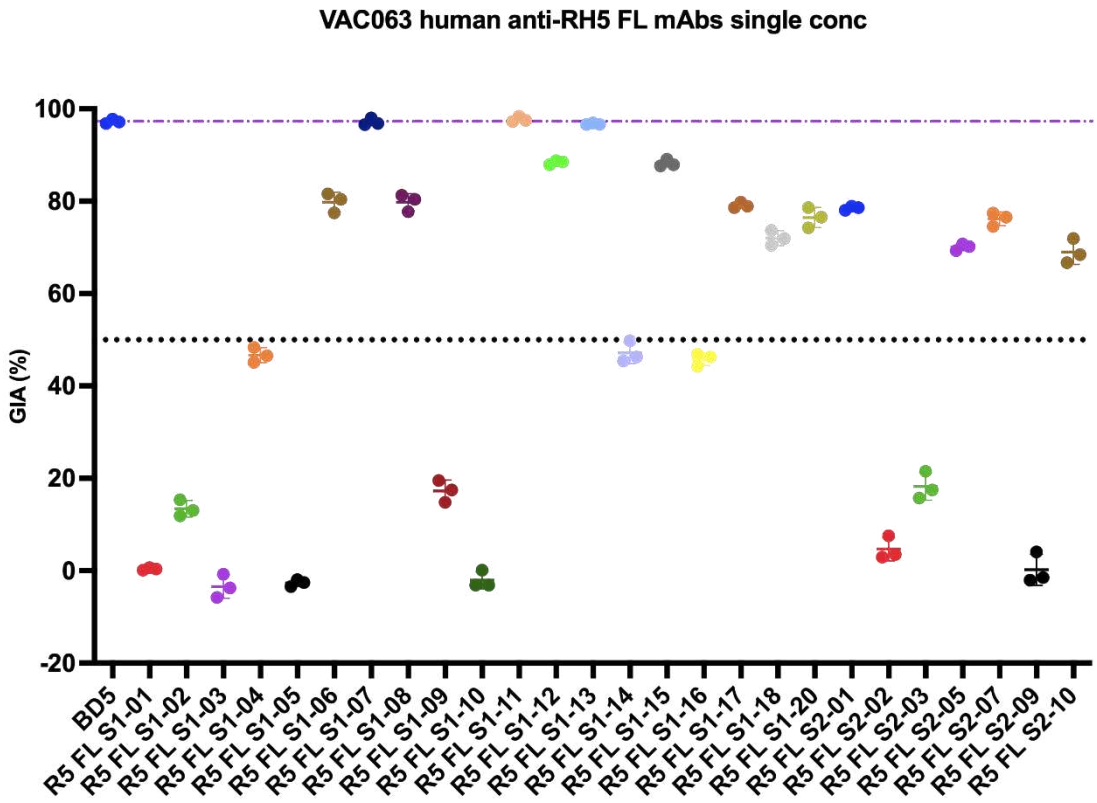

B.

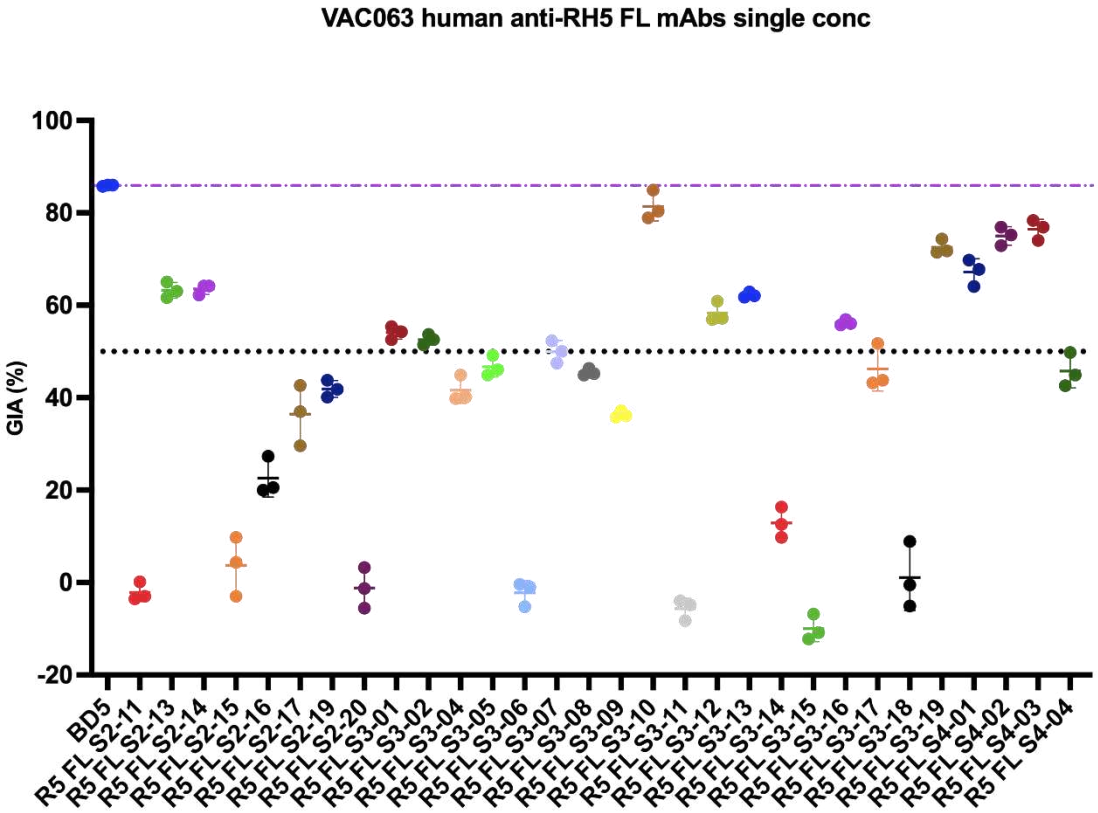
VAC063 human anti-RH5 FL mAbs single conc
GIA (%)
100
80
60
40
20
0
-20
BD5
R5 FL S2-11
R5 FL S2-13
R5 FL S2-14
R5 FL S2-15
R5 FL S2-16
R5 FL S2-17
R5 FL S2-19
R5 FL S2-20
R5 FL S3-01
R5 FL S3-02
R5 FL S3-04
R5 FL S3-05
R5 FL S3-06
R5 FL S3-07
R5 FL S3-08
R5 FL S3-09
R5 FL S3-10
R5 FL S3-11
R5 FL S3-12
R5 FL S3-13
R5 FL S3-14
R5 FL S3-15
R5 FL S3-16
R5 FL S3-17
R5 FL S3-18
R5 FL S3-19
R5 FL S4-01
R5 FL S4-02
R5 FL S4-03
R5 FL S4-04

C.

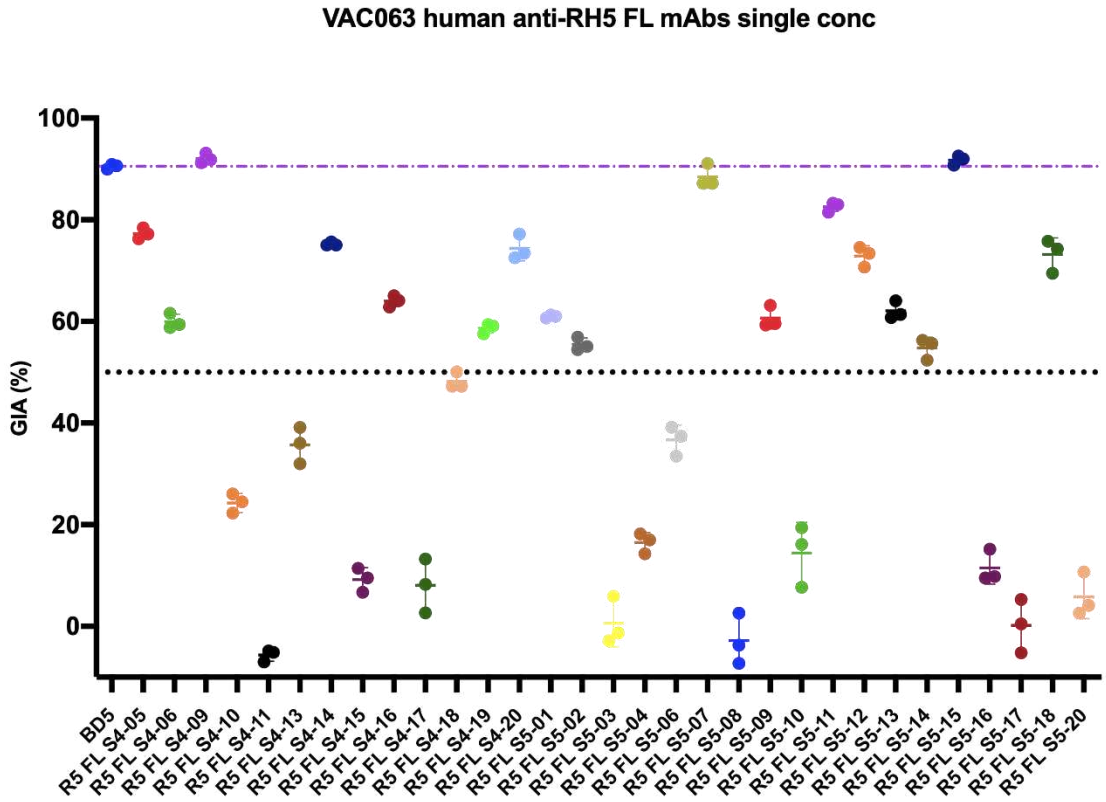
VAC063 human anti-RH5 FL mAbs single conc
GIA (%)
100
80
60
40
20
0
BD5
R5 FL S4-05
R5 FL S4-06
R5 FL S4-09
R5 FL S4-10
R5 FL S4-11
R5 FL S4-13
R5 FL S4-14
R5 FL S4-15
R5 FL S4-16
R5 FL S4-17
R5 FL S4-18
R5 FL S4-19
R5 FL S4-20
R5 FL S5-01
R5 FL S5-02
R5 FL S5-03
R5 FL S5-04
R5 FL S5-06
R5 FL S5-07
R5 FL S5-08
R5 FL S5-09
R5 FL S5-10
R5 FL S5-11
R5 FL S5-12
R5 FL S5-13
R5 FL S5-14
R5 FL S5-15
R5 FL S5-16
R5 FL S5-17
R5 FL S5-18
R5 FL S5-20

D. **E.**

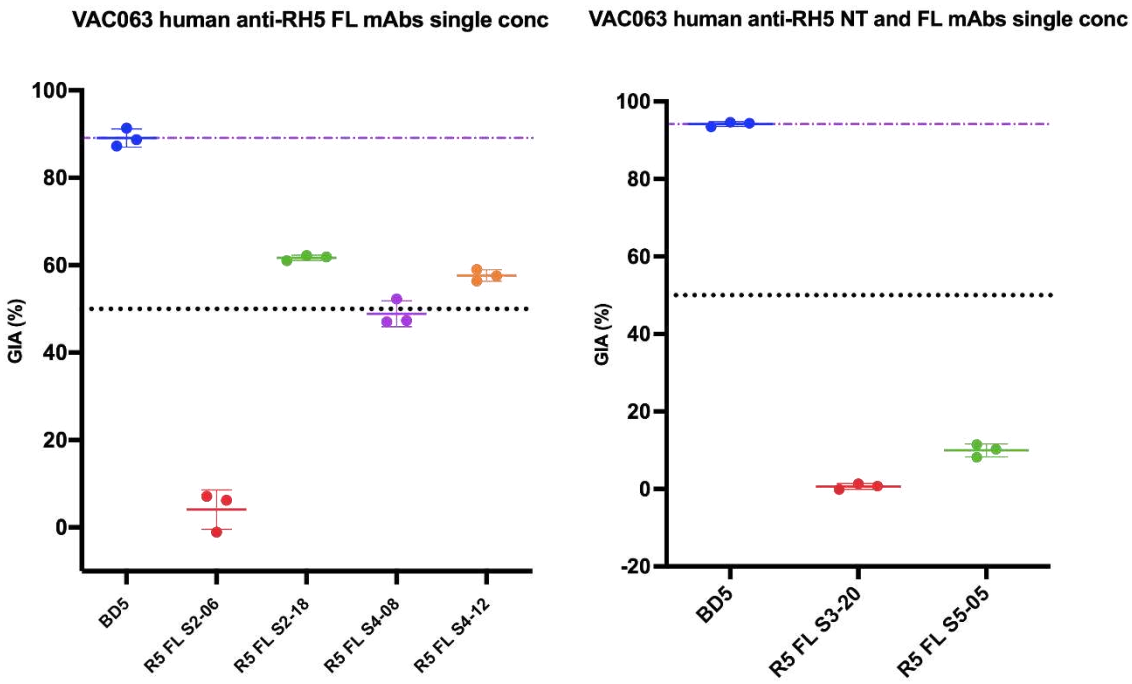

Figure 4.B.1.4.2.A-E. *Single concentration GIA assay against 3D7 clone P. falciparum parasites of RH5 FL mAbs.*

Here are represented five (A-E) GIA assays to test different RH5-FL mAbs. On the X-axis are plotted the names of mAbs, while on the Y axis the GIA (%), is always compared to the internal control BD5. Dots show the mean and error bars the range of N=3 triplicate test wells per test mAb concentration.

Of the 94 RH5 FL mAbs tested 57 had a GIA activity >40%, meaning that 60.1% of the ELISA-positive mAbs has also a growth inhibitory activity more or less strong.

It is possible to underline that some mAbs had an inhibitory activity very similar to the currently most potent RH5 FL mAb.

Indeed, very high GIA activity is seen for Subject 1 mAbs 7, 11, 12 and 13, Subject 3 mAb 10, Subject 4 mAb 9, and Subject 5 mAbs 7 and 15. This is a great result, considering that 20 MBCs were chosen randomly from each donor and a total of 94 ELISA positive mAbs around 8.5% had an important growth inhibitory activity.

To measure relative GIA potency, mAbs were subsequently tested by GIA assay using dilution series (**Figure 4.B.1.4.3.A-F**).

A.

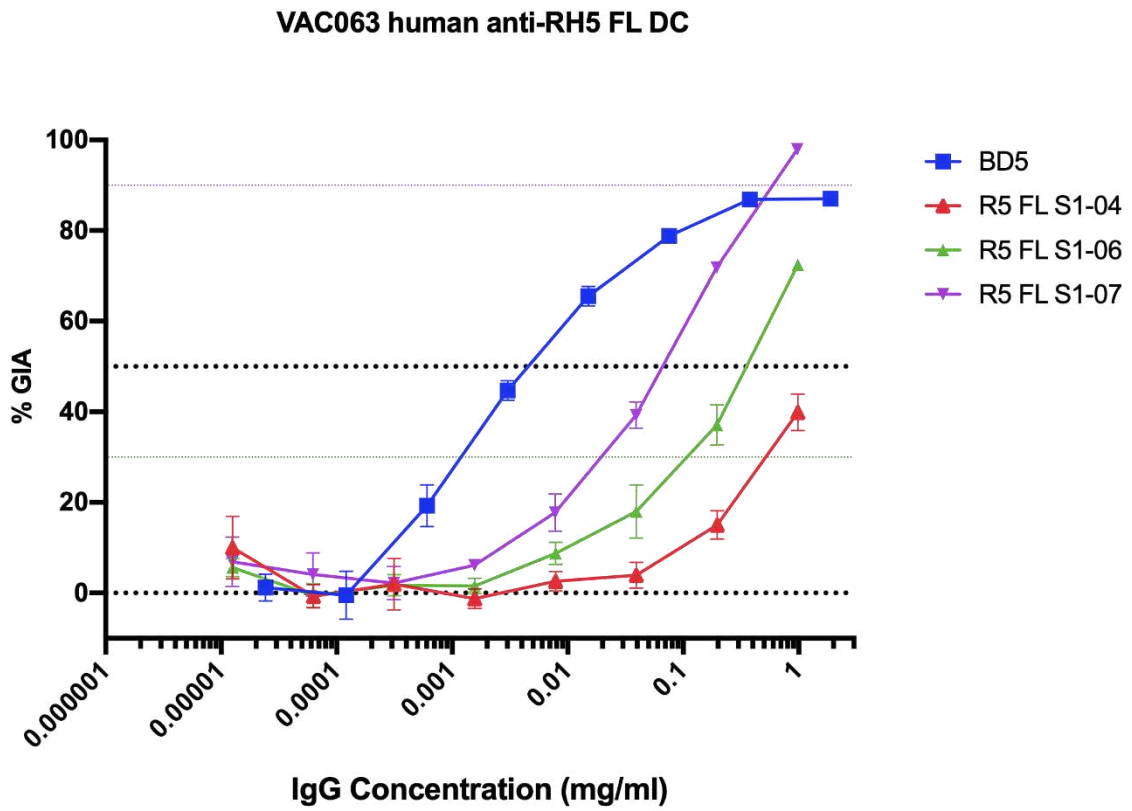
VAC063 human anti-RH5 FL DC
% GIA
100
80
60
40
20
0
0.000001
0.00001
0.0001
0.001
0.01
0.1
1
IgG Concentration (mg/ml)
BD5
R5 FL S1-04
R5 FL S1-06
R5 FL S1-07

B.

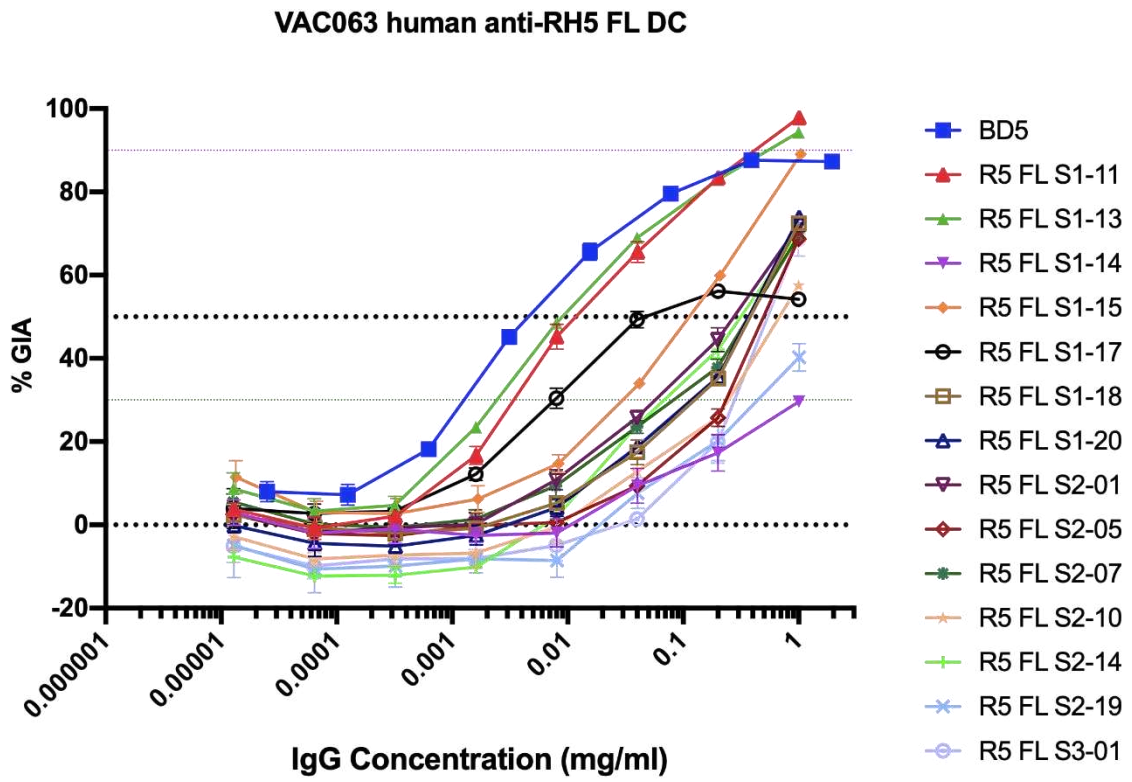
VAC063 human anti-RH5 FL DC
% GIA
100
80
60
40
20
0
-20
0.000001
0.00001
0.0001
0.001
0.01
0.1
1
IgG Concentration (mg/ml)
BD5
R5 FL S1-11
R5 FL S1-13
R5 FL S1-14
R5 FL S1-15
R5 FL S1-17
R5 FL S1-18
R5 FL S1-20
R5 FL S2-01
R5 FL S2-05
R5 FL S2-07
R5 FL S2-10
R5 FL S2-14
R5 FL S2-19
R5 FL S3-01

C.

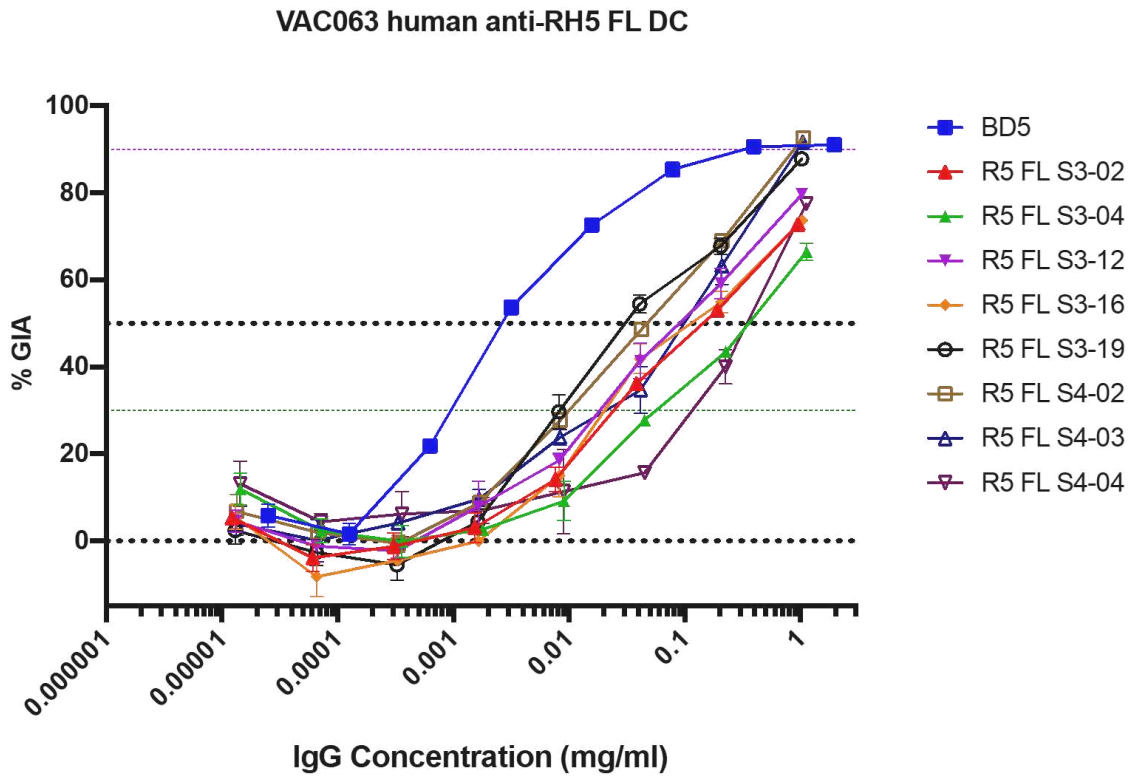
VAC063 human anti-RH5 FL DC
% GIA
100
80
60
40
20
0
0.000001
0.00001
0.0001
0.001
0.01
0.1
1
IgG Concentration (mg/ml)
BD5
R5 FL S3-02
R5 FL S3-04
R5 FL S3-12
R5 FL S3-16
R5 FL S3-19
R5 FL S4-02
R5 FL S4-03
R5 FL S4-04

D.

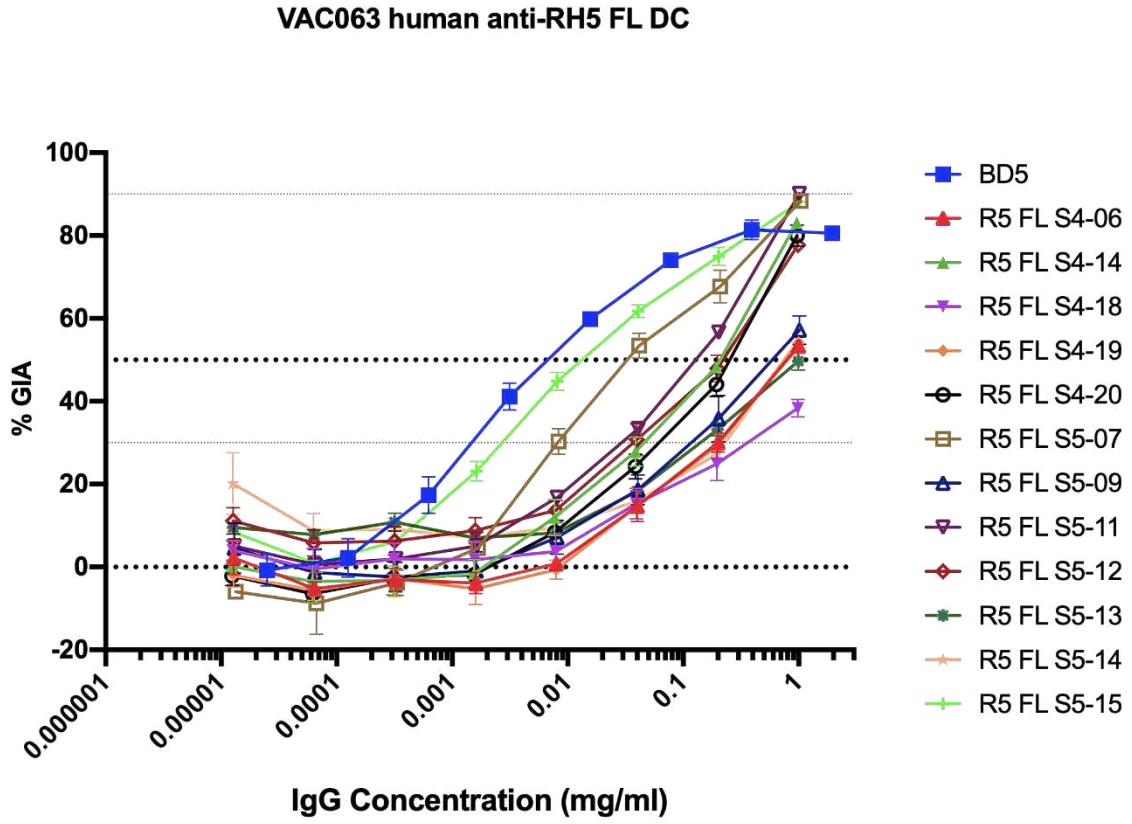
VAC063 human anti-RH5 FL DC
% GIA
100
80
60
40
20
0
-20
0.000001
0.00001
0.0001
0.001
0.01
0.1
1
IgG Concentration (mg/ml)
BD5
R5 FL S4-06
R5 FL S4-14
R5 FL S4-18
R5 FL S4-19
R5 FL S4-20
R5 FL S5-07
R5 FL S5-09
R5 FL S5-11
R5 FL S5-12
R5 FL S5-13
R5 FL S5-14
R5 FL S5-15

E.

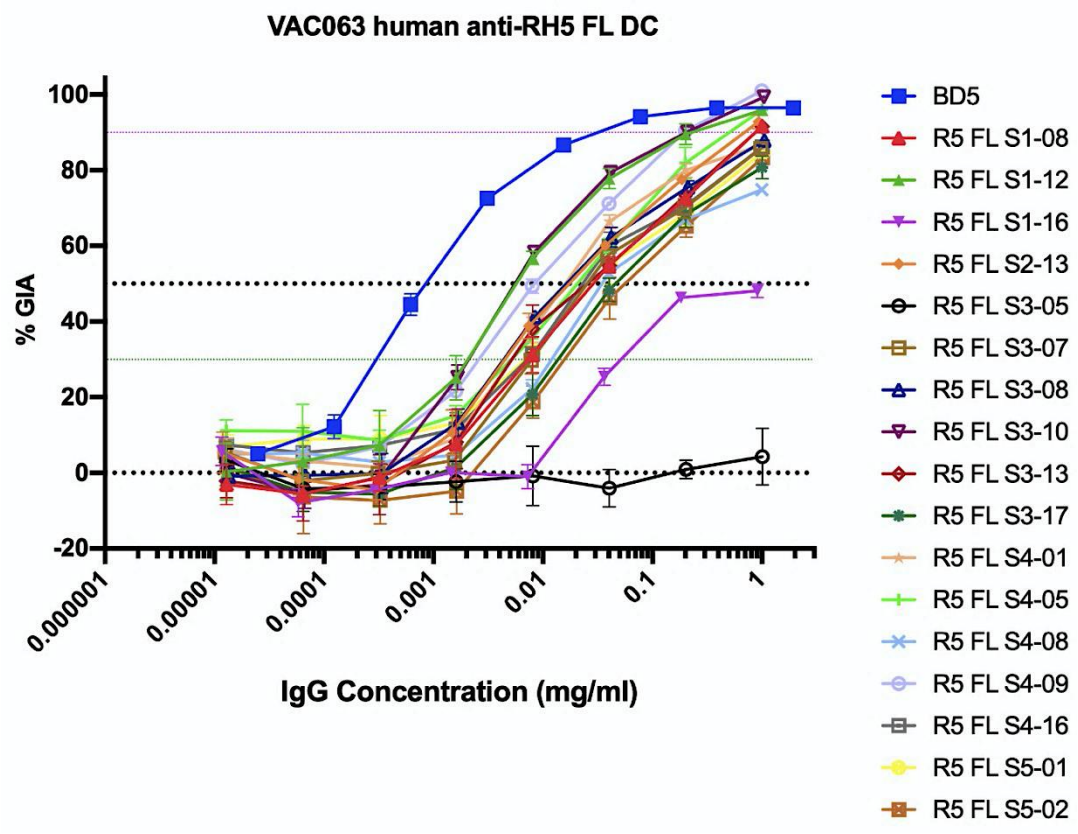

F.

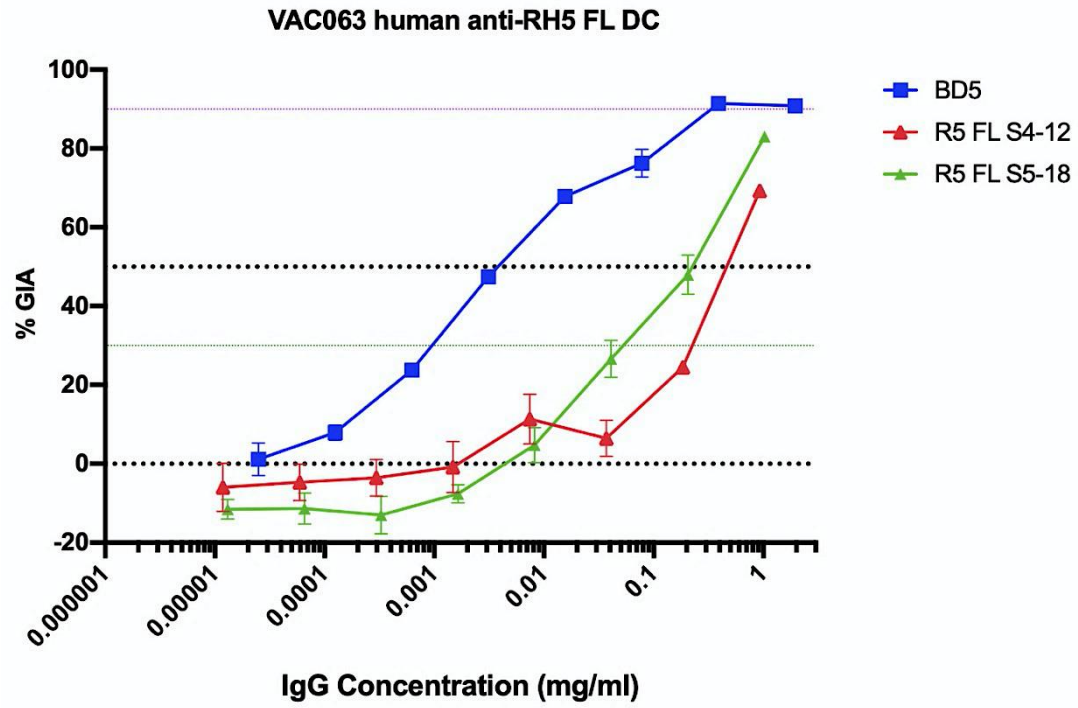

Figure 4.B.1.4.4.A-F. *Titration of the best RH5 FL mAbs in the GIA assay against 3D7 clone P. falciparum parasites.*

*Titration of the 37 best RH5 FL mAbs in different assays of GIA (**A-F**) against 3D7 clone P. falciparum parasites. Dots show the mean and error bars the range of N=3 triplicate test wells per test mAb concentration.On the X axis is represented the concentration of mAbs expressed in mg/ml, while on the Y axis is shown the percentage of GIA.*

To further elaborate the results we have calculated the values in mg/mL of EC50 and EC80, where it was possible, for RH5 FL mAbs tested in the dilution curve (**Figure 4.B.1.4.5.A-F**).

The reference is always BD5, mAbs used for each set of mAbs tested with other internal controls. It can be observed that some mAbs have EC50 and EC80 values close to the one of BD5, as shown in **Table 4.B.1.4.1,** such as: R5 FL S1-11, R5 FL S1-12, R5 FL S1-13, R5 FL S3-10, R5 FL S4-09 and R5 FL S5-15.

The fact there are six mAbs, at least one per subject, except for subject 2, having an EC50 and EC80 value close to the best mAb used as a positive control is a great result, considering that these mAbs were randomly chosen from a pool of antigen-specific MBCs sorted.

Table 4.B.1.4.2. *EC50 and EC80 values of mAbs were tested in dilution curve GIA.*

On the first column, samples are listed, while on the second and third columns, respectively, it can be observed the value of EC50 and EC80 in mg/mL. N/A is written when the value was not applicable. In yellow are highlighted the best values observed.

Sample	EC50 (mg/mL)	EC80 (mg/mL)
BD5 (R5.034)	0.004	1.010
R5 FL S1-04	N/A	N/A
R5 FL S1-06	0.378	N/A
R5 FL S1-07	0.065	1.162
BD5	0.004	1.010
R5 FL S1-11	0.013	1.030
R5 FL S1-13	0.009	1.022
R5 FL S1-14	N/A	N/A
R5 FL S1-15	0.114	1.300
R5 FL S1-17	0.043	1.105
R5 FL S1-18	0.399	2.509
R5 FL S1-20	0.376	2.374
R5 FL S2-01	0.252	N/A
R5 FL S2-05	0.567	N/A
R5 FL S2-07	0.353	N/A
R5 FL S2-10	0.709	N/A
R5 FL S2-14	0.266	1.843
R5 FL S2-19	3.246	N/A
R5 FL S3-01	0.625	N/A
BD5	0.003	1.006
R5 FL S3-02	0.125	N/A
R5 FL S3-04	0.284	1.925
R5 FL S3-12	0.088	1.224
R5 FL S3-16	0.093	1.238
R5 FL S3-19	0.033	1.079
R5 FL S4-02	0.046	1.112
R5 FL S4-03	0.098	1.255
R5 FL S4-04	0.311	N/A
BD5	0.006	1.014
R5 FL S4-06	0.809	N/A
R5 FL S4-14	0.181	1.516
R5 FL S4-18	N/A	N/A

R5 FL S4-19	0.774	N/A
R5 FL S4-20	0.239	1.735
R5 FL S5-07	0.036	1.087
R5 FL S5-09	0.584	3.835
R5 FL S5-11	0.128	1.341
R5 FL S5-12	0.189	N/A
R5 FL S5-13	N/A	N/A
R5 FL S5-14	0.784	N/A
R5 FL S5-15	0.014	1.032
BD5	0.001	1.002
R5 FL S1-08	0.030	1.072
R5 FL S1-12	0.006	1.014
R5 FL S1-16	N/A	N/A
R5 FL S2-13	0.017	1.041
R5 FL S3-05	N/A	N/A
R5 FL S3-07	0.026	1.062
R5 FL S3-08	0.017	1.039
R5 FL S3-10	0.006	1.013
R5 FL S3-13	0.025	1.059
R5 FL S3-17	0.045	1.110
R5 FL S4-01	0.015	1.035
R5 FL S4-05	0.021	1.048
R5 FL S4-08	0.035	N/A
R5 FL S4-09	0.009	1.021
R5 FL S4-16	0.025	1.059
R5 FL S5-01	0.031	1.075
R5 FL S5-02	0.054	1.132
BD5	0.004	1.009
R5 FL S4-12	0.539	N/A
R5 FL S5-18	0.192	1.555

4.B.1.5. Sequence analysis of anti-*Pf*RH5 mAbs

To complement the epitope and functional mapping of anti-*Pf*RH5 antibodies, we next conducted a sequence analysis of all the positive mAbs. Analysis of heavy and light chain gene family usage across the whole anti-RH5 panel revealed a diverse repertoire of heavy chain N=5 and light chain N=10 gene families, although with a prevalence of HV4 (N=28), HV3 (N=32), KV3 (N=23) and LV3 (N=28) gene family usage.

It was then observed (**Figure 4.B.1.5.1.A** and **B**) that N=28 V_H and N=28 $V_{L/K}$ unique sequences were obtained from the full panel of mAbs. We then analysed (**Figure 4.B.1.5.2.C**) the pairing of individual genes, which revealed N=68 possible combinations of pairing V_H plus $V_{L/K}$ from this new panel of RH5-FL mAbs; here the highest frequency gene pairing, HV3-7/LV3-21, included only 5 mAbs.

A.

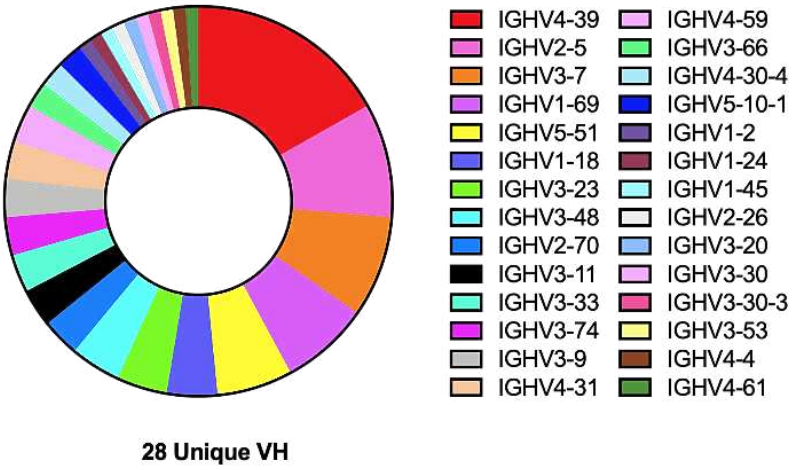

28 Unique VH

B.

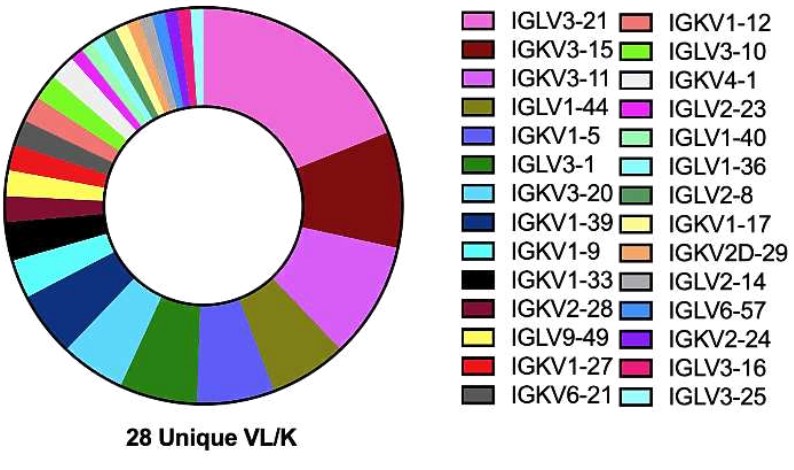

28 Unique VL/K

C.

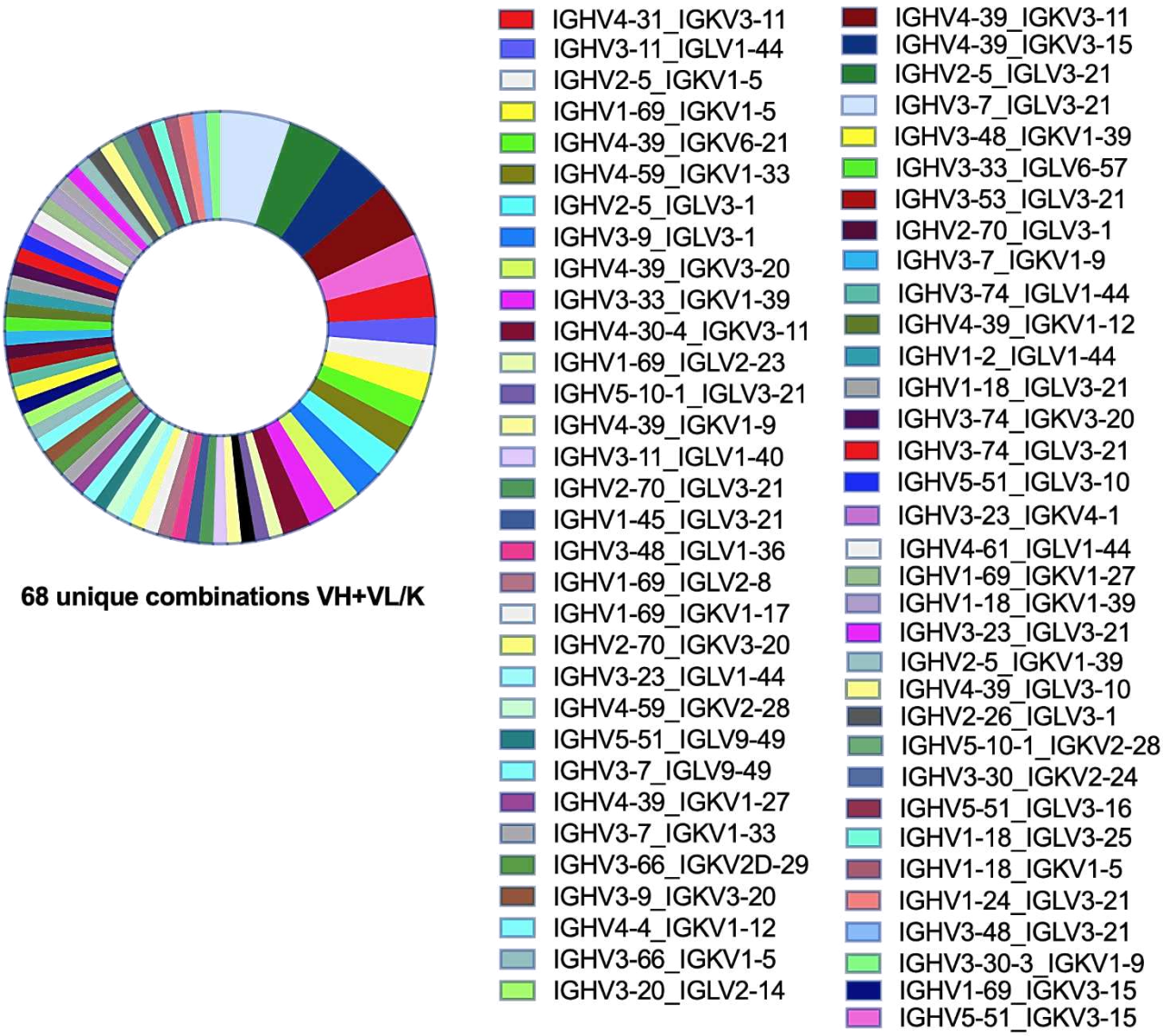

***Figure 4.B.1.5.3.A** and **B.** Unique V_H and $V_{L/K}$. **C.** Unique combinations of VH and VL/K.*

***A** and **B.** represent respectively the frequencies of the unique V_H and $V_{L/K}$ combination obtained from the analysis of the full panel of RH5-FL mAbs. **C.** shows the presence of the 68 unique combinations of V_H plus $V_{L/K}$ coming from the RH5-FL mAbs.*

To assess any eventual association of antibody gene pairing with mAb GIA EC50 potency, we analysed all gene pair combinations present in more than three mAbs (**Figure 4.B.1.5.4.**). We can observe that al mAbs with gene combination IGHV5-51_IGKV3-15 are GIA negative, whereas there didn't appear to be any trend for the others common gene combinations.

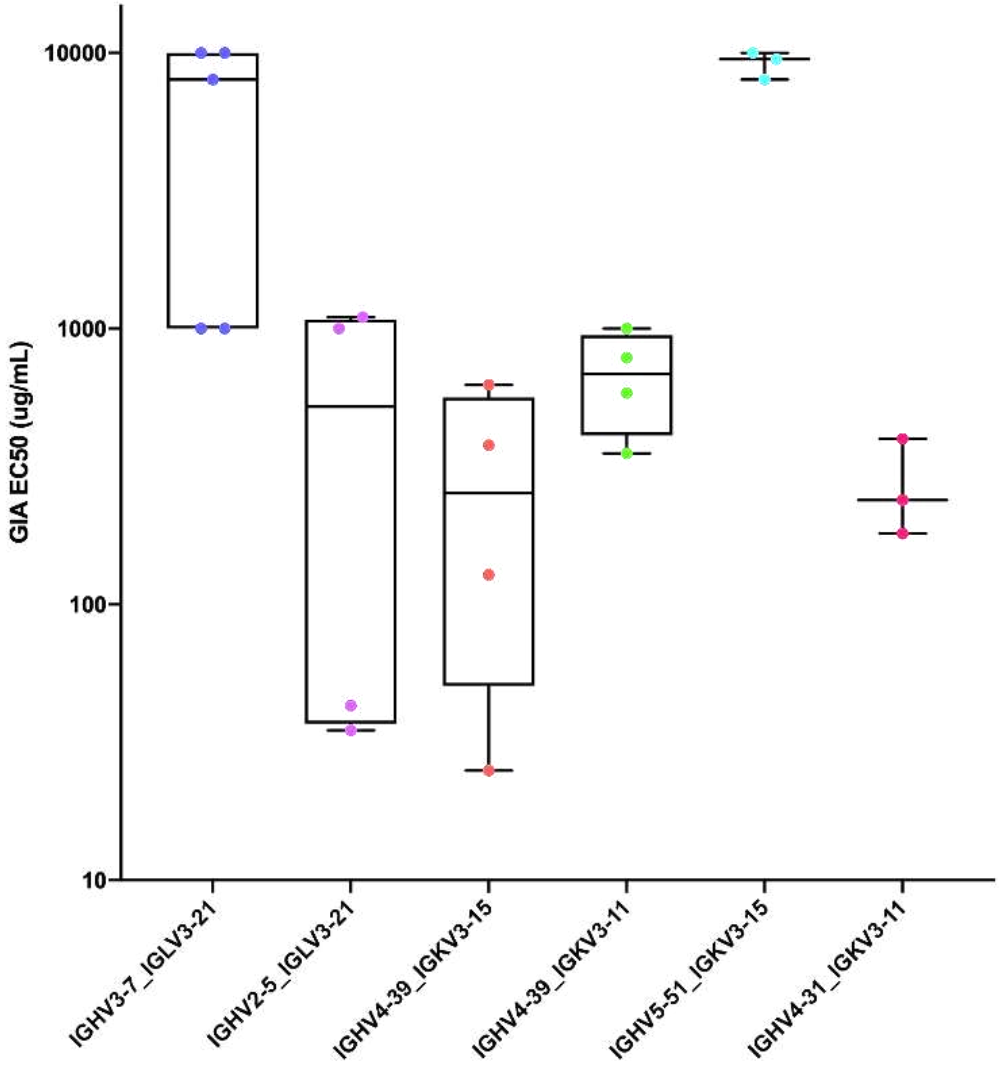

Figure 4.B.1.5.5. *Most frequent antibody gene pairing compared to EC50 values.*

On the X-axis are represented the 6 most common gene combinations (present in more than three mAbs), while on the Y-axis the correspondent EC50 values for that correspondent mAbs.

In a previous study investigating a panel of mAbs deriving from VAC063 [276], it was identified a potent class of anti-*Pf*RH5 antibody deriving from a particular gene combination, IGHV3-7_IGLV1-36. The subset of antibodies identified by this clonotype had a low GIA (EC50 below 5µg/mL). Therefore, we further decided to see if there was a similar correspondence also in our new panel of mAbs. In this case, we do not observe a particular correlation between the most abundant pairing combinations and the best GIA mAbs. Best mAbs have different pairing, except for mAbs S1-11 and S1-12 which instead have the same combination IGHV3-11_IGLV1-44 (**Figure 4.B.1.5.6.**).

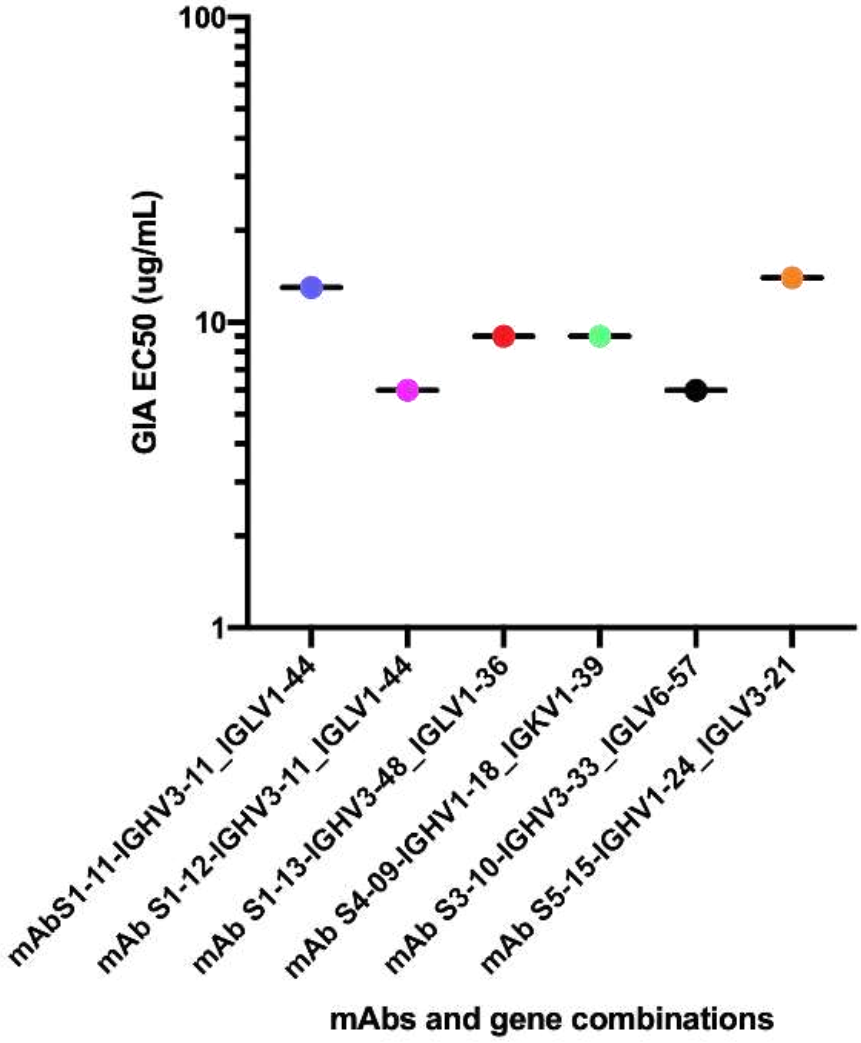

Figure 4.B.1.5.7. *Antibody gene pairing compared to EC50 values of the six best mAbs.*

On the X-axis are represented names and the associated gene combination of the 6 best GIA mAbs, while on the Y-axis the correspondent EC50 values for those mAbs.

4.B.2. Isolation and characterisation of a panel of human RH5 N-terminus mAbs from VAC 063

4.B.2.1. RH5 N-terminus memory B cells isolation

The 5 subjects for the isolation of PBMCs and subsequently mAbs in this study were selected within the VAC063 clinical trial, as well as for the previously shown panel of mAbs.
Once again of the subjects used, five were positive samples, while a sixth was used as negative control. The time point at which the PBMCs were isolated from the volunteers was day 42, two weeks post-second vaccination.
The strategy of sorting was always the same as reported in material and method section, RH5 N-terminus specific MBCs were directly sorted in a lysis buffer in a 96-well plate using a BD FACSAria III and selecting $CD3^-$ $CD14^-$ $CD56^-$ $CD19^+IgD^-$ IgM^- IgA^- and RH5 N-term PE (probe) positive cells.
For this panel a total of 205 RH5 N-terminus specific MBCs were isolated, with different percentage of sorting among the donors ranging between 9.3-32.7% from each one (**Table 4.B.2.1.1.**).

Table 4.B.2.1.1. *Summary table of subjects and RH5 N-terminus specific MBCs sorted.*

On the left side are listed the subjects, in the midle cells sorted for each one and on the right side the correspondent percentage.

Subjects	Cells sorted	% per subject
S1-01-047 (day42)	67	32.7
S2-01-021 (day42)	45	22
S3-06-020 (day42)	21	10.2
S4-06-035 (day42)	53	25.8
S5-02-012 (day42)	19	9.3
Tot:	205	100

The number of cells sorted was lower compared to the full-length RH5 MBCs selection, it can be explained mainly for two reasons. On one side the samples were isolated by using the entire protein rather than a part of this, thus necessarily pulling out more cells, on the other side we can also consider that the day of isolation of PBMCs for this panel was different from the usual. Indeed, in this case, cells were isolated two weeks post-second boost, rather than one-week post-third vaccination, considered instead the optimal time point to recover more antigen-specific MBCs.

4.B.2.2. Amplification and sequencing of V_H and V_L genes of RH5 N-terminus mAbs

Exactly as before explained next to B cell sorting into lysis buffer, all RNA transcripts were reverse transcribed to cDNA and amplified the variable regions of heavy chains and kappa or lambda chains of immunoglobulins by two rounds of nested PCR.
To control the effective presence of the desired amplified products, II PCR products were loaded into a 1% agarose gel, as shown in **Figures 4.B.2.2.1.** and **4.B.2.2.2**.

Figure 4.B.2.2.2. *PCR amplification of VH genes from Subject 2 and 3.*

Each lane represents a PCR amplicon (black band) of the second PCR from a single MBC run on a 1% agarose gel. For the variable heavy amplicons the expected size is ~500bps.

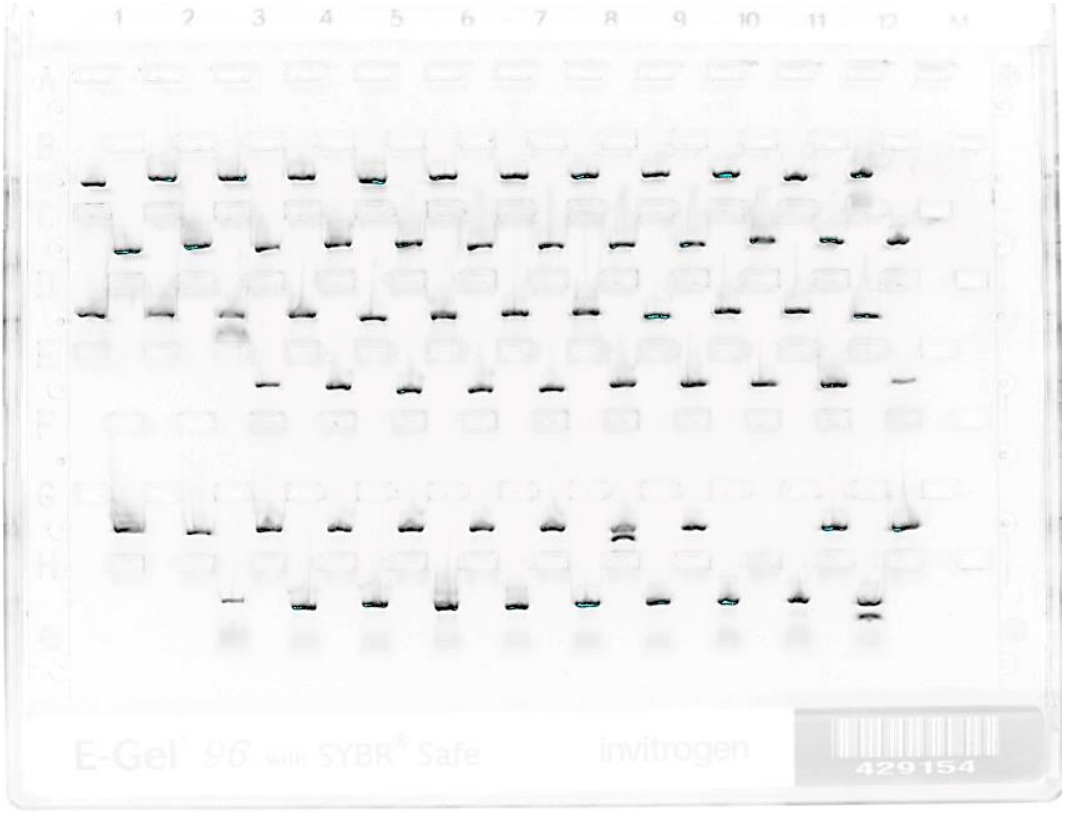

Figure 4.B.2.2.3. *PCR amplification of VL genes from Subject 2 and 3.*

Each lane represents a PCR amplicon (black band) of the second PCR from a single MBC run on a 1% agarose gel. For the variable heavy amplicons the expected size is ~400bps.

The bands were observed and once assessed the correspondence between heavy and light chains, samples were diluted and sent for sequencing (ACTG).

Table 4.B.2.2.1. summarises the gel bands obtained and sequencing from the different subjects.

As shown the amplicons recovered were 152 from the V_H and 194 from the V_L chains, with 149 total matched chains. The efficiency of recovery of matched heavy and light chains is approximately 70% (ranging between 42.1 and 90.6).

Sequences were recovered for 95 matched sequences of V_H and V_L chains, with 81 unique sequences. The sequencing efficiency compared to the gel was of 63.8% instead, the overall unique and paired sequences obtained to develop mAbs compared with the starting cell sorted was of around 45.3%.

Table 4.B.2.2.2. *Summary table of cell sorted for each subject, gel bands obtained and sequencing observations.*

On the left side it is shown the subjects and the respective MBCs sorted for the amplifications.The central columns, with the violet box in the upper part, show numbers relative to the amplifications for the heavy and light chains, as well as the matched amplicons obtained and the efficiency calculation. The columns of the right instead, with the pink box in the upper part, exhibit the sequencing number data of the paired V_H and V_L, the unique sequences, and the efficiencies with respect to the gels and sorted MBCs.

		Gel bands				**Sequencing**			
Subjects	**Cells sorted used**	**HC bands**	**LC bands**	**Matched**	**Efficiency %**	**Paired**	**UNIQUE**	**Efficiency % (vs gel)**	**Overall (%) (vs sorted cells)**
S1	67	43	65	43	64.2	25	24	58.14	37.3
S2	45	34	45	34	75.6	27	15	79.41	60
S3	21	16	20	16	76.2	12	12	75	57.1
S4	53	48	52	48	90.6	27	26	56.25	50.9
S5	19	11	12	8	42.1	4	4	50	21.1
Tot:	205	152	194	149	69.7	95	81	63.8	45.3

4.B.2.3. RH5 N-terminus mAbs expression and screening by Epitope screening ELISA

Matched V_H/V_L sequences for each subject were sent to Twist for gene synthesis and cloning into human IgG1 plasmid vectors, regardless of original subclasses (IgG1, IgG2, IgG3, or IgG4), thus obtaining plasmids for the production of N-terminus RH5 mAbs.
Plasmids were then expressed in 10mL of Expi 293, thus obtaining 51 mAbs in total, coming in different proportions from each donor (**Figure 4.B.2.3.1**.).

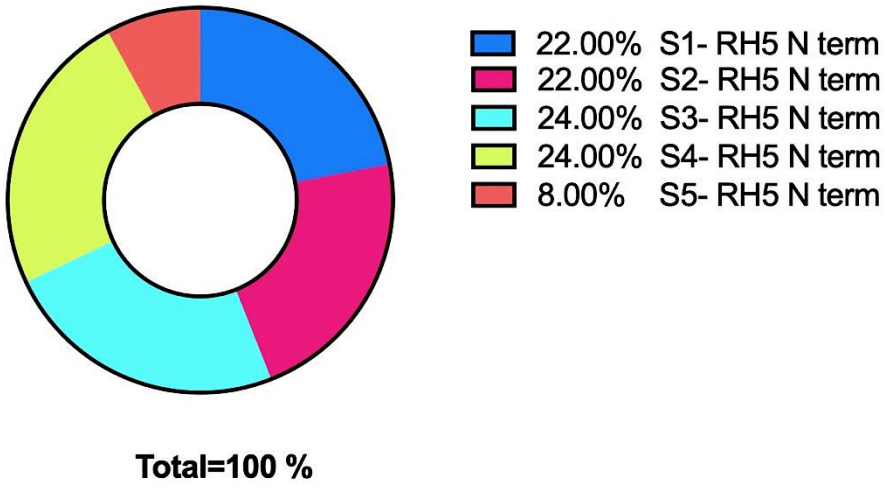

***Figure 4.B.2.3.2**. Percentage of plasmids coding for different RH5 N-terminus mAbs from different subjects (1-5).*

mAbs are equally distributed, approximatively 20% for each subject, except for Subject 5 with 8%

Mabs were expressed in 10mL of Expi 293, and after 5 days of transfection, the supernatants were harvested and purified and then tested in an epitope mapping ELISA assay.
All the mAbs, diluted at the same concentration of 2µg/mL, were tested against the full length of the RH5.1 protein and the N-terminus portion of RH5, for which these mAbs were selected (**Figures 4.B.2.3.3.** and **4.B.2.3.4.**).
The internal control used for each ELISA plate were the same previously used: R5.016, a conformational mAb that is able to bind the RH5.1 full-length protein and 3A11, a mAb able to bind to the N-terminus portion of RH5 and to the FL RH5.1.

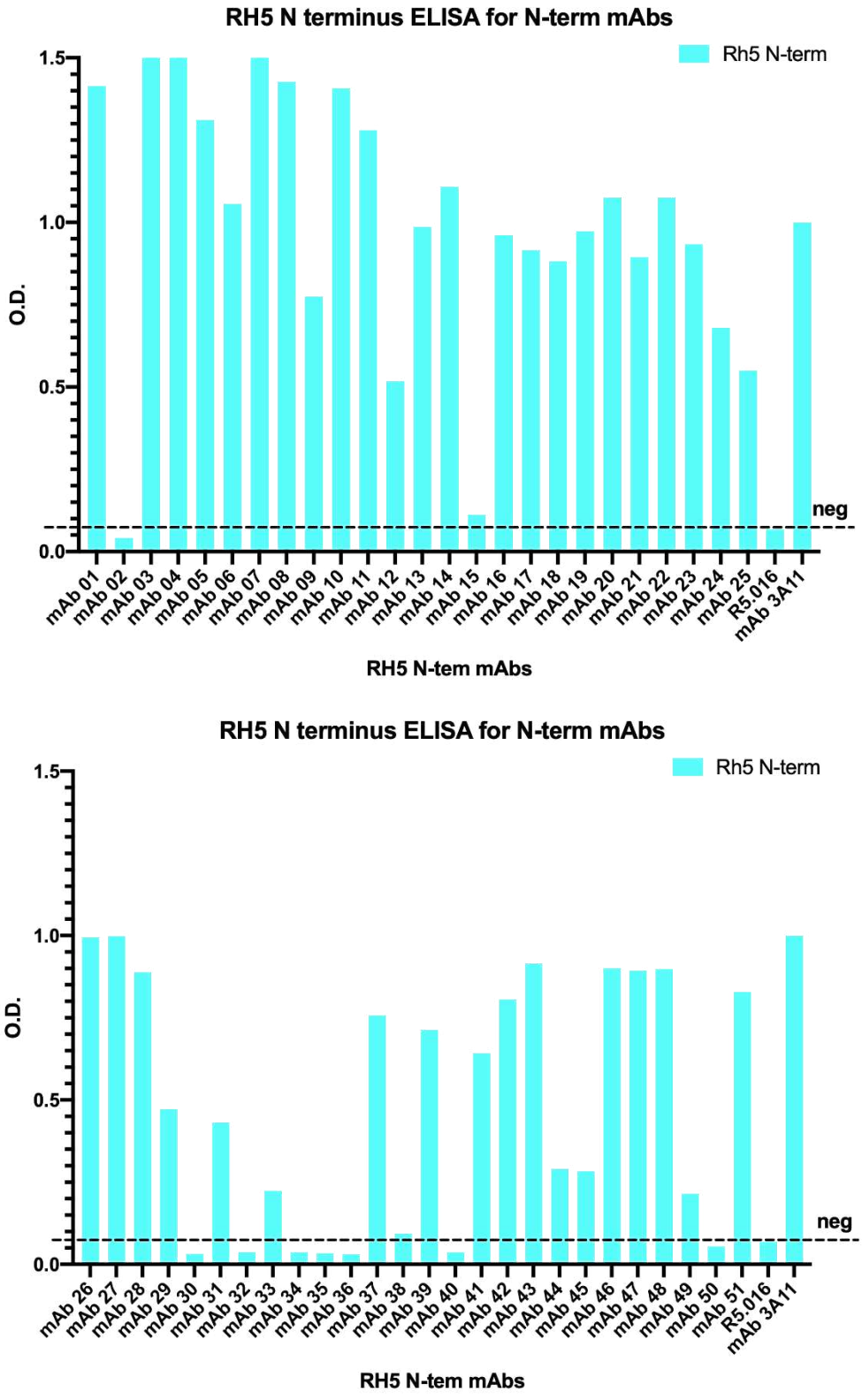

Figure 4.B.2.3.5. *RH5 N-terminus ELISA of RH5 N-terminus mAbs.*

Here are represented the ELISA data of the 51 mAbs (split into 2 graphs) tested against N-terminus portion of RH5 (light blue). The X-axis shows the mAbs and the Y-axis shows the O.D. value in ELISA.

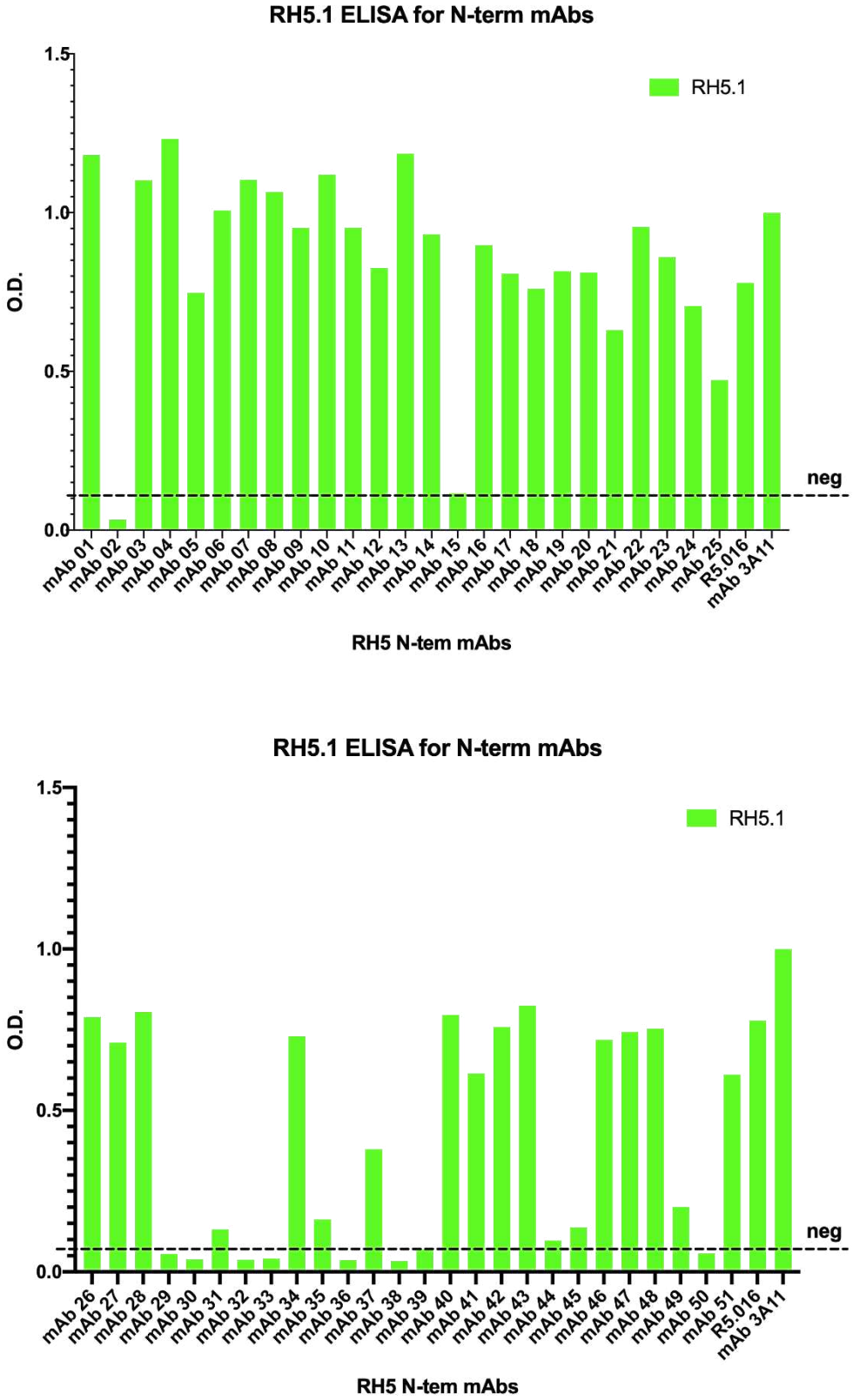

Figure 4.B.2.3.6*.RH5.1 ELISA of RH5 N-terminus mAbs.*

Here are represented the ELISA data of the 51 mAbs (split into 2 graphs) tested against the RH5.1 (green). The X-axis shows the mAbs and the Y-axis shows the O.D. value in ELISA.

As analysed in **Table 4.B.2.3.1**, data shown in **Figures 4.B.2.3.7.** and **4.B.2.3.8.**, 42 mAbs out of 51, approximately the 82%, are able to bind in ELISA N-terminus RH5, in addition the 78.4% of the total mAbs is able to bind the full version of the protein, RH5.1. These numbers allow us to validate the efficiency of this technique for selecting antigen-specific mAbs in the context of memory B cells.

Table 4.B.2.3.1. *Summary table of RH5 N-terminus mAbs.*

Here is shown how many mAbs and the percentage of binding to respectively RH5.1 FL, and the N-terminus portion of RH5 protein.

	N-terminus RH5	**N-terminus RH5 (%)**	**RH5.1 FL**	**RH5.1 FL (%)**
S1+S2+S3+S4+S5	42	82.4	40	78.4

Notably, mAbs RH5-NT-34 and RH5-NT-40 and slightly RH5-NT-35 seemed to be positive for the RH5.1 full protein but negative for the RH5 N-term probe.
All the mAbs of the panel were then used to validate and further investigate the role of the N-terminus portion of the RH5 protein.

4.B.2.4. Peptide-ELISA for *Pf*RH5 N-terminus mAbs

To further resolve the epitopes interested in the binding of the different antibodies, the ELISA-positive RH5 N-terminus mAbs were subjected to a peptide ELISA. This peptide screen was used to try to identify the binding epitopes for each RH5 N-terminus mAb.
The graph that follows (**Figure 4.B.2.4.1.**) shows the mAbs clustered for the binding of different peptides. Some bind only one peptide (7 groups), while other combinations of 2 peptides (5 groups), in some cases others bind a combination of 3 (1 group) or even 4 peptides (3 groups).

mAbs binding Peptide 1:

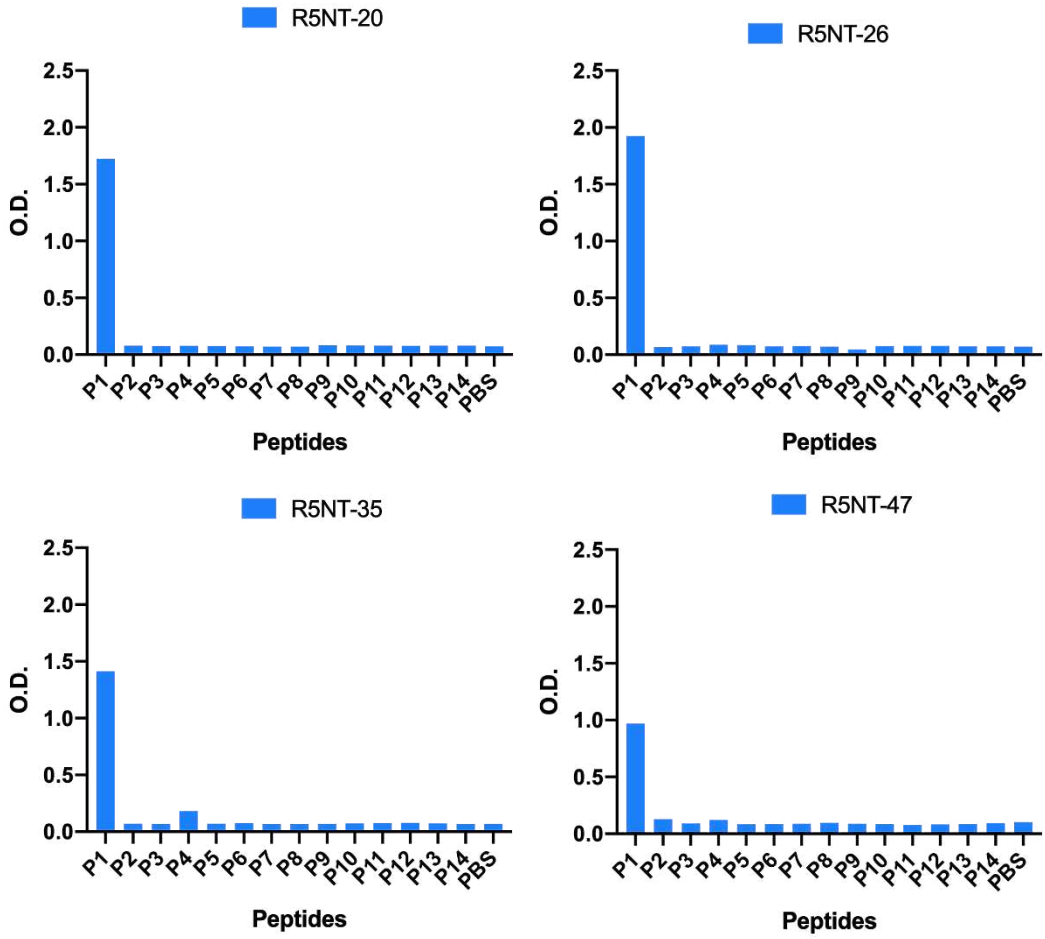

mAbs binding Peptide 2:

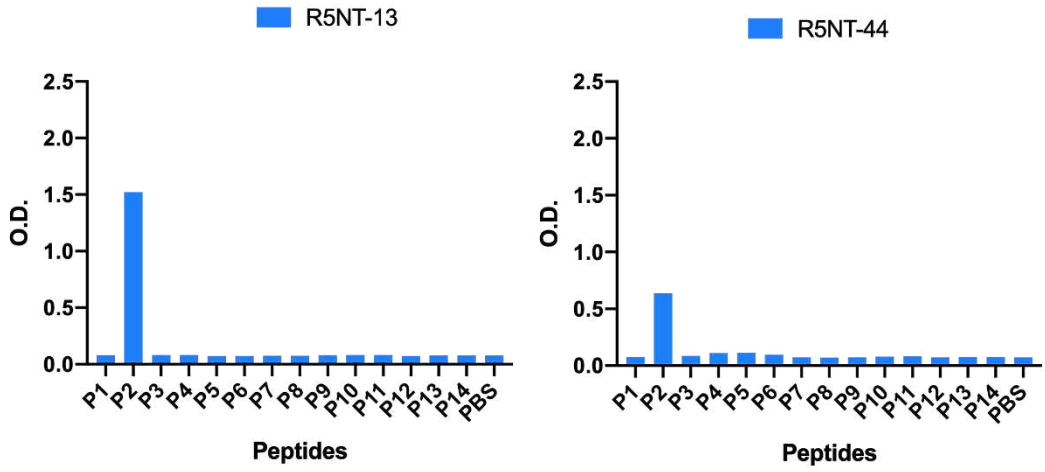

mAb binding Peptide 10:

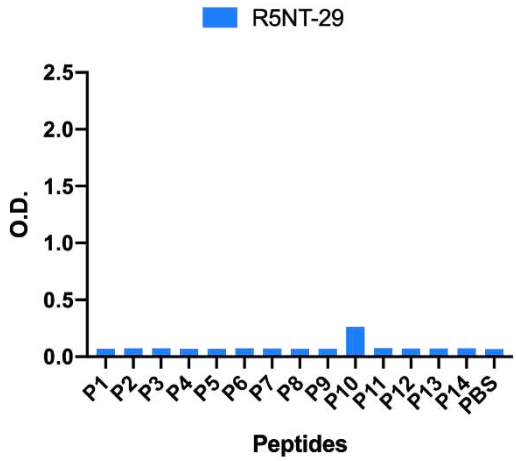

mAbs binding Peptide 7:

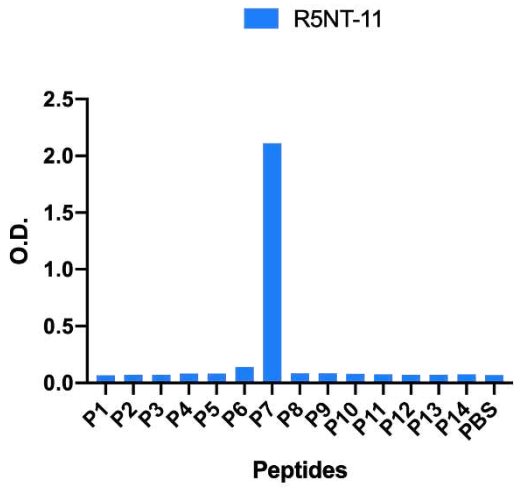

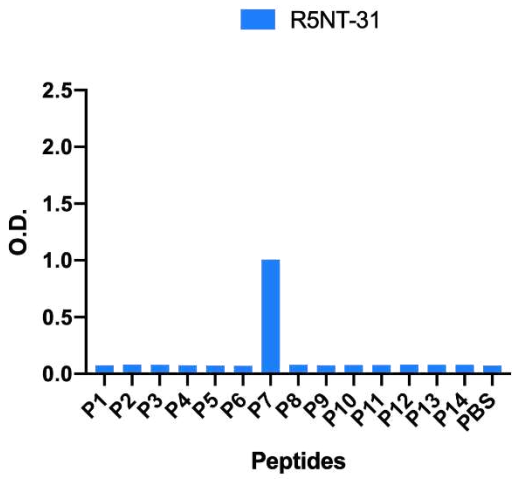

mAbs binding Peptide 9:

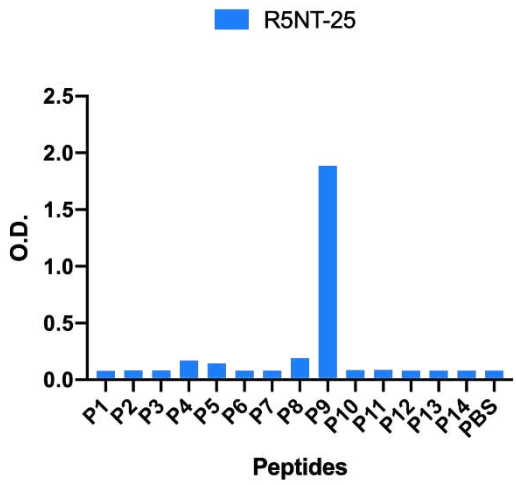

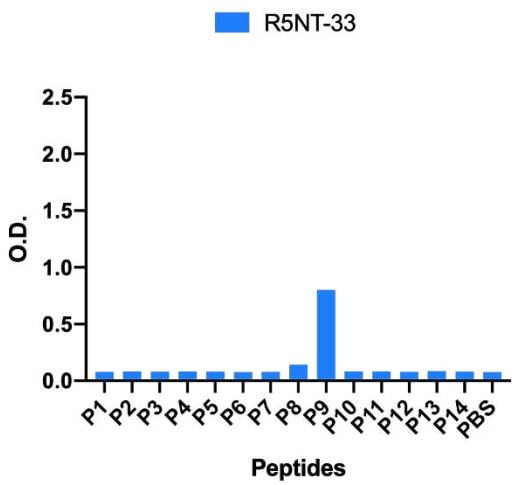

mAbs binding Peptide 11:

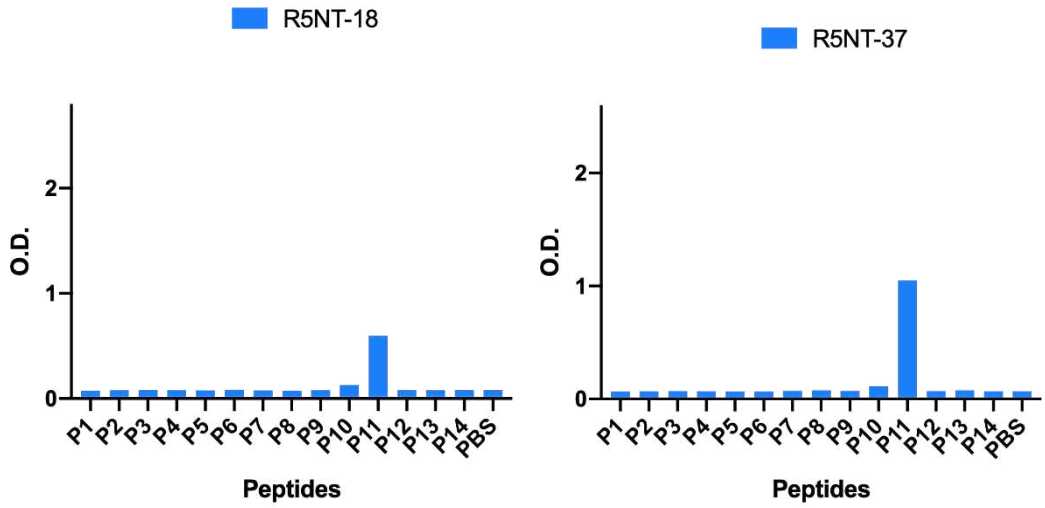

mAbs binding Peptides 8:

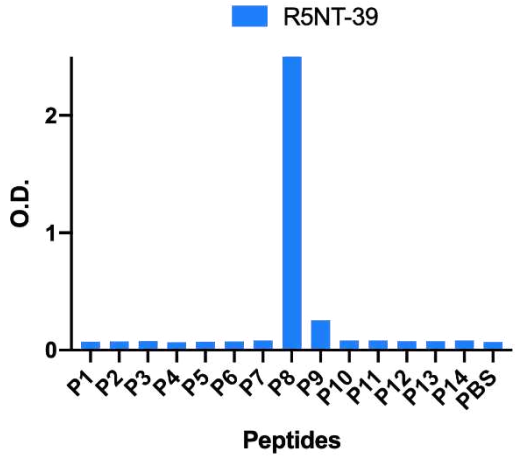

mAbs binding Peptides 2 and 3:

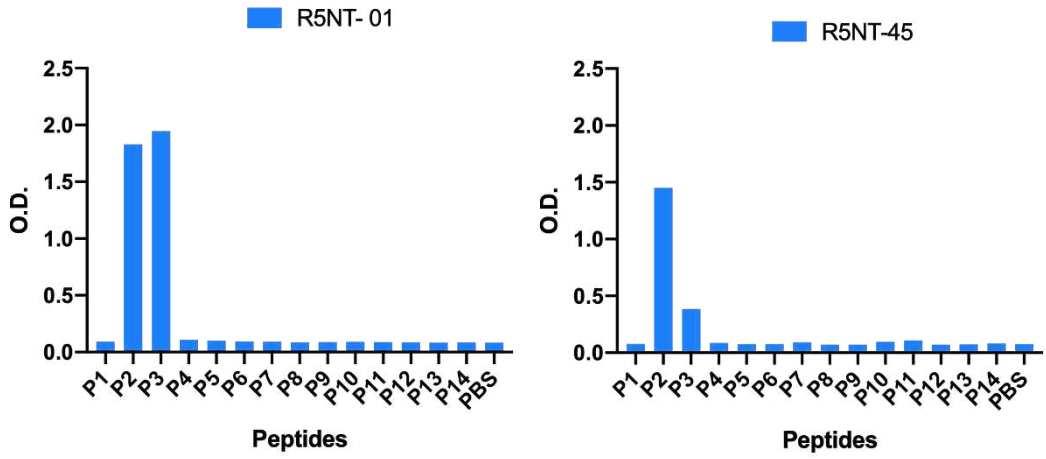

mAbs binding Peptides 4 and 5:

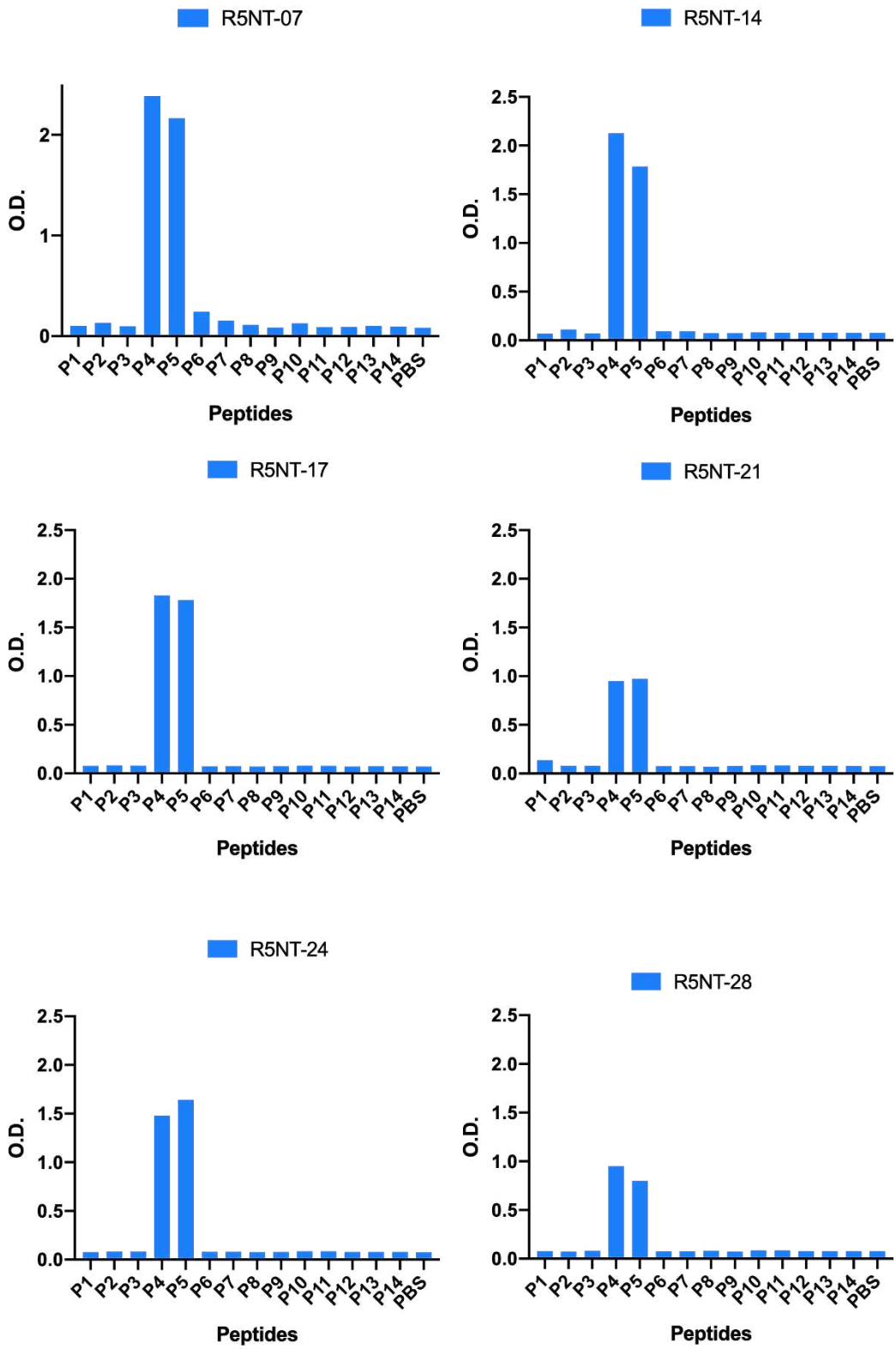

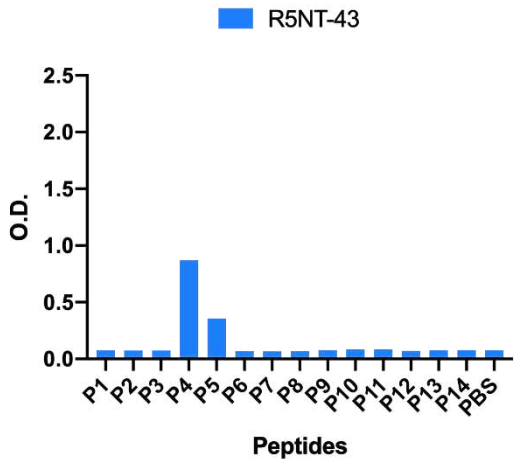

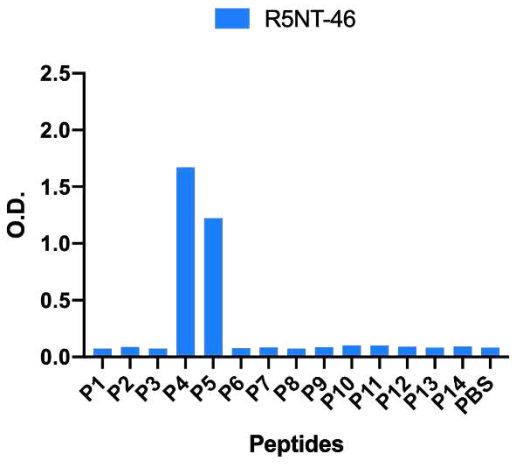

mAbs binding Peptides 6 and 7:

mAbs binding Peptides 7 and 8:

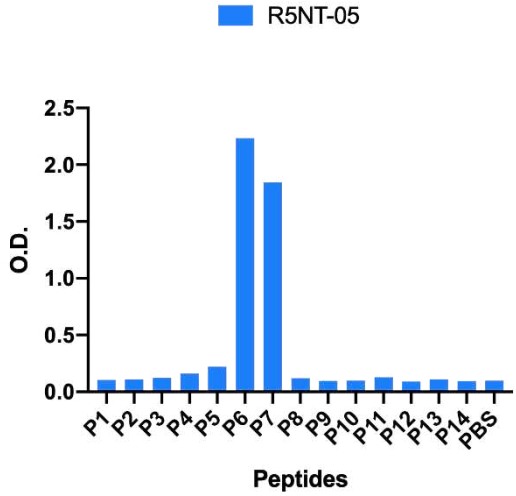

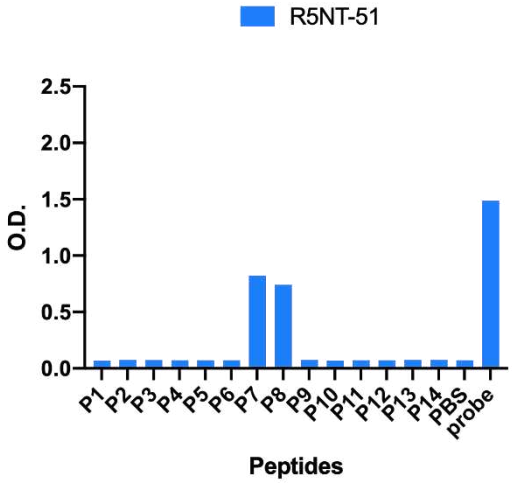

mAbs binding Peptides 10 and 11:

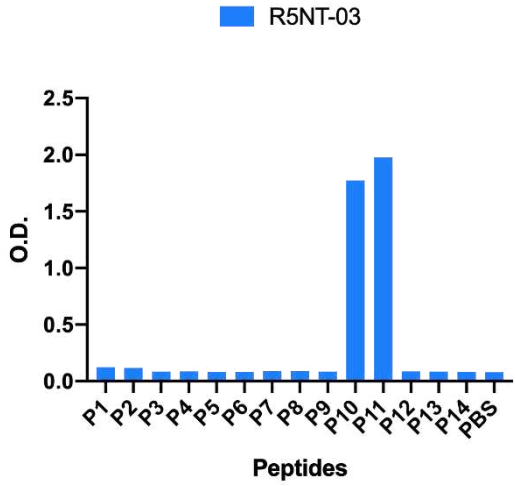

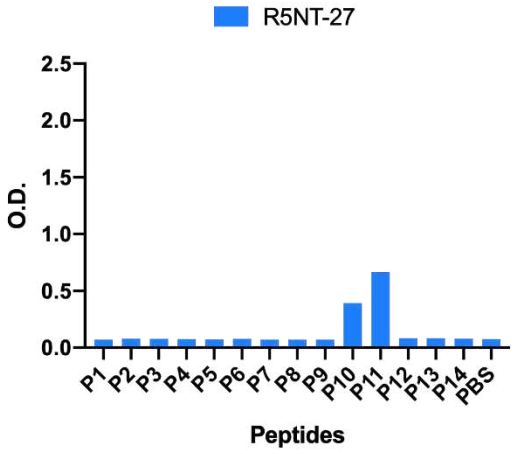

mAbs binding Peptides 4,5 and 6:

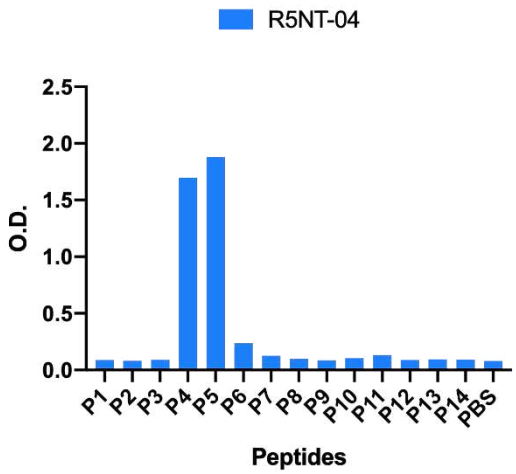

mAbs binding Peptides 3,4,5 and 6:

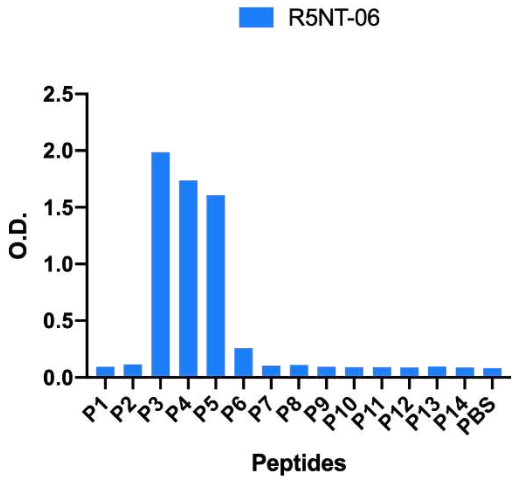

mAbs binding Peptides 3,4,5 and 12:

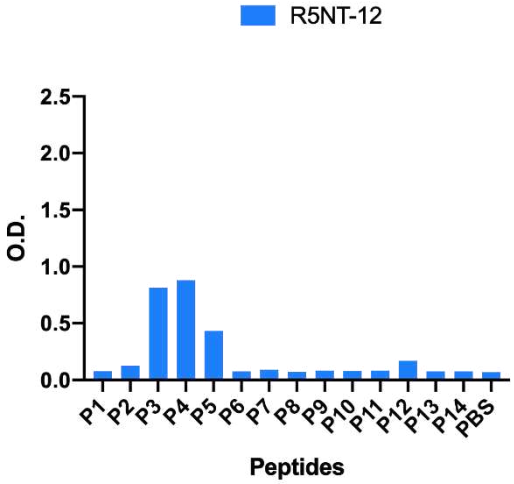

mAbs binding Peptides 3,4,12 and 13:

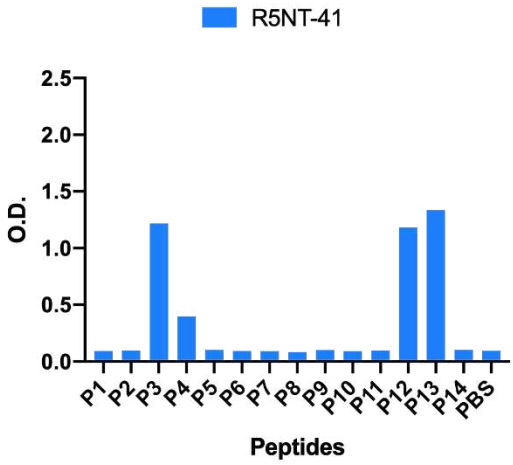

Figure 4.B.2.4.2. *Peptide ELISA for RH5 N-terminus mAbs.*

Here are reported only the graph showing mAbs that bind to different peptides (P1-P14) of the N-terminus region of RH5.1. On the X-axis are listed the peptides (P1-P14), while on the Y-axis it is shown the ELISA O.D. values.

The following heatmap (**Figure 4.B.2.4.3.**) shows an overview of which peptide or sets of peptides are interested in the binding from each mAb tested. Notably, 83% of the RH5 N-term mAbs bound at least one peptide in the panel. Around 20% of the total mAbs, the majority, can bind to peptides 4 and 5, while a 10% is able to bind to peptide 1, the remaining mAbs can bind peptides with a different distribution. Interestingly RH5-NT-12 and RH5-NT-41 seem to bind two different parts of the N-terminus portion, around peptides 3 and 4 and peptides 12 and 13.

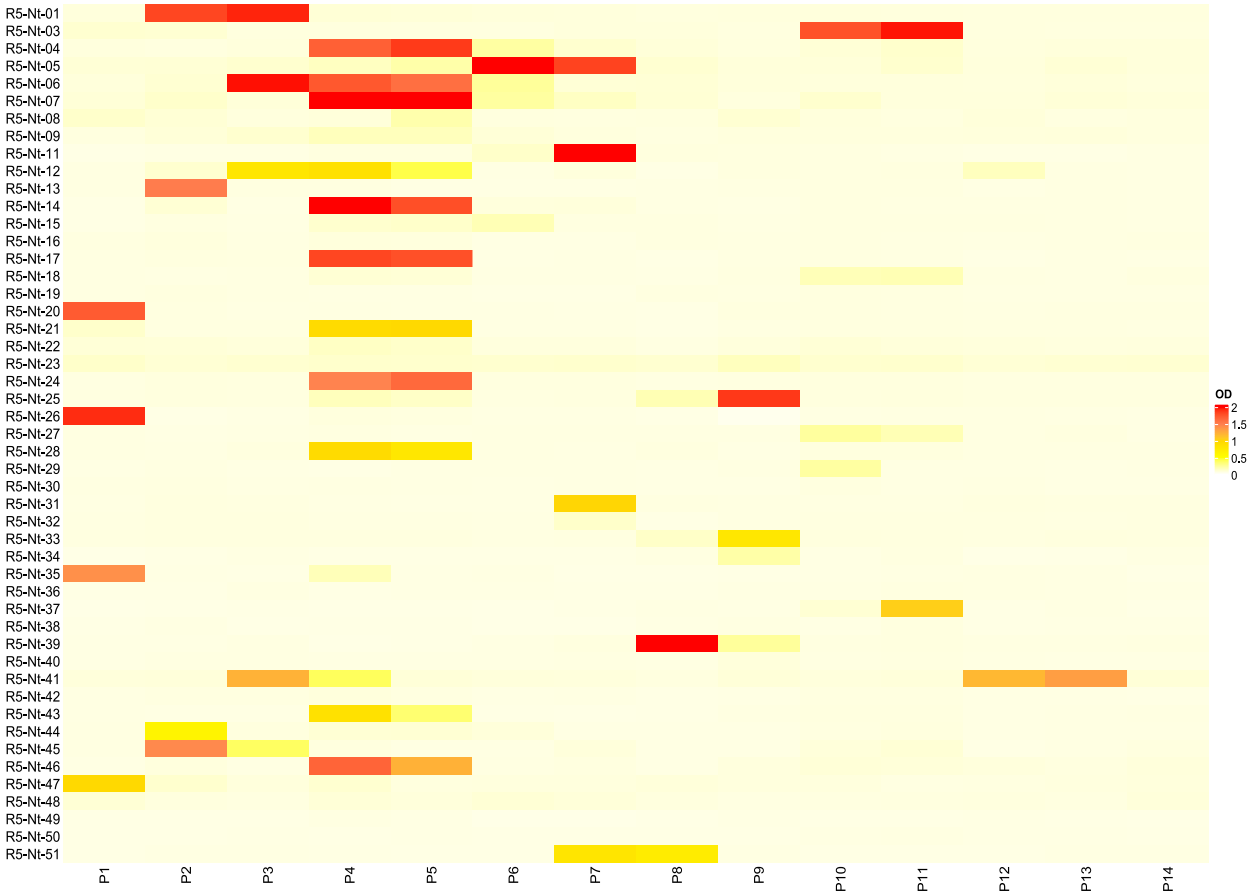

Figure 4.B.2.4.4. *Heatmpat of R5NT mAbs that bind different N-terminus peptides.*

On the horizonal axis are listed the peptides from peptide 1 to 14, on the vertical axis are listed the mAbs tested. The colors represent the intensity of binding, according to ELISA O.D. values, to each peptide. Red represent a high affinity of binding while orange represent no binding.

4.B.2.5. LSA-peptide mapping screening

To confirm or, where it was possible, to implement data, we performed a peptide mapping screening using LSA. **Figure 4.B.2.5.1.** shows the results obtained, indicating on the X-axis the RH5 N-terminus monoclonal antibodies tested, on the Y-axis the percentage of binding and below, as legend, the peptides run in the experiment associated with different colours. What is additional, compared to the ELISA shown in paragraph 4.B.2.4 are Peptides 1 and 2 (here indicated as P1*, P2*) that are peptides overlapping the original probe we have used for sorting, thus having the correct glycan mutations with respect to the P1 and P2 used for the ELISA which instead came from a peptide library, so not completely reflecting the binding sites to which mAbs could address. Furthermore, additional peptides have been added such as P35, site of RH5.1 intrinsic loop, and P57, P61, P62, RH5.1 C-terminus.

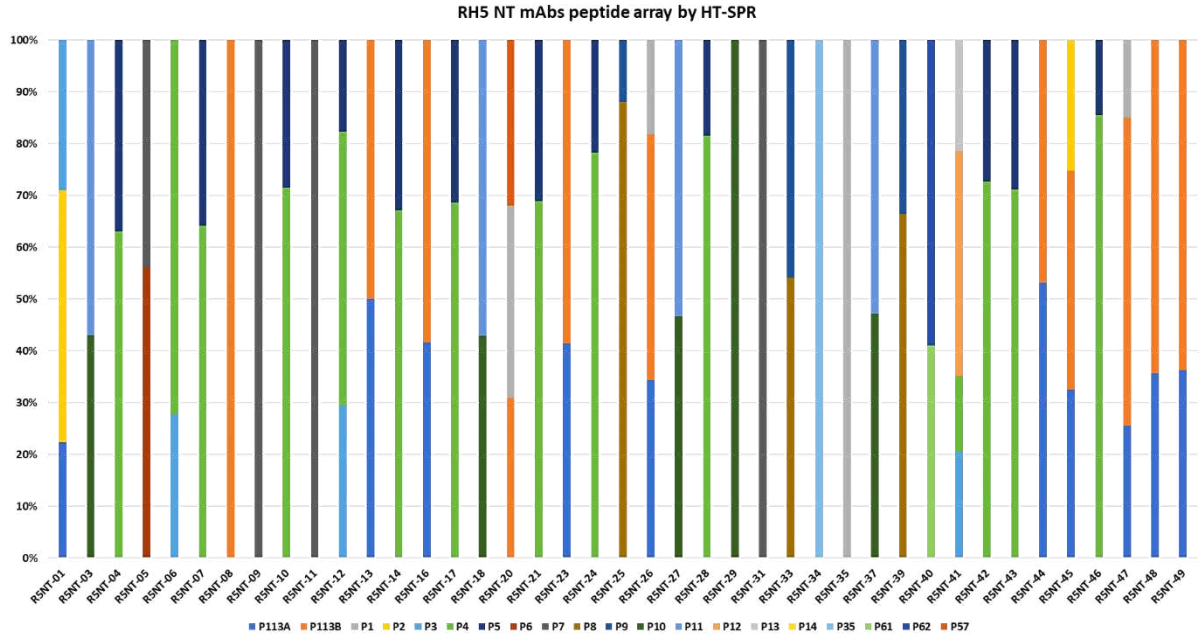

Figure 4.B.2.5.2. *RH5 NT mAbs peptide array by SPR.*

A stacked plot showing the peptides contributing to each mAb analyte's binding specificity, totalling to 100%. The colours for each peptide are denoted in the legend.

Comparing these data with the peptide ELISA, we can see that the results are very similar. In some cases, the difference is that mAbs bound to the already tested version of P1 and P2 but also to P1* and P2*, for instance, RH5-NT-01, RH5-NT-13, RH5-NT-26, RH5-NT-44, RH5-NT-45, RH5-NT-47 and RH5-NT-20 that additionally seems to bind P57.
Some mAbs resulted to have implemented the binding to another close peptide, this is the case of RH5-NT-25, RH5-NT-33 and RH5-NT-37.

If we focus our attention on the RH5-NT mAbs that were negative in the previous peptide ELISA, but positive in the screening, we can notice that the majority of them, instead, had binding with the P1* and P2* (**Table 4.B.2.5.1**).

Table 4.B.2.5.2. *Negative RH5-NT mAbs in ELISA, results in LSA peptide.*

In the first column we can find the RH5 N-terminus mAbs name, in the second column the negative result in ELISA and on the right column to which peptide resulted to bind in LSA peptide array.

mAb number	PEPTIDE ELISA	LSA peptide array
R5NT-08	NEG	P2*
R5NT-09	NEG	P7
R5NT-10	NEG	P4, P5
R5NT-16	NEG	P1*, P2*
R5NT-23	NEG	P1*, P2*
R5NT-34	NEG	P35
R5NT-40	NEG	P61, P62
R5NT-42	NEG	P4, P5
R5NT-48	NEG	P1*, P2*
R5NT-49	NEG	P1*, P2*

We can observe that RH5-NT-09 bound P7, RH5-NT-10 and RH5-NT 42 bound P4, P5. What is surprising is that two mAbs are not binding the N-terminus, RH5-NT-34 bound P35, thus being an RH5 intrinsic loop binder and RH5-NT-40 bound P61, P62, therefore an RH5 C-terminus mAb (**Figure 4.B.2.5.3.A** and **B.**).

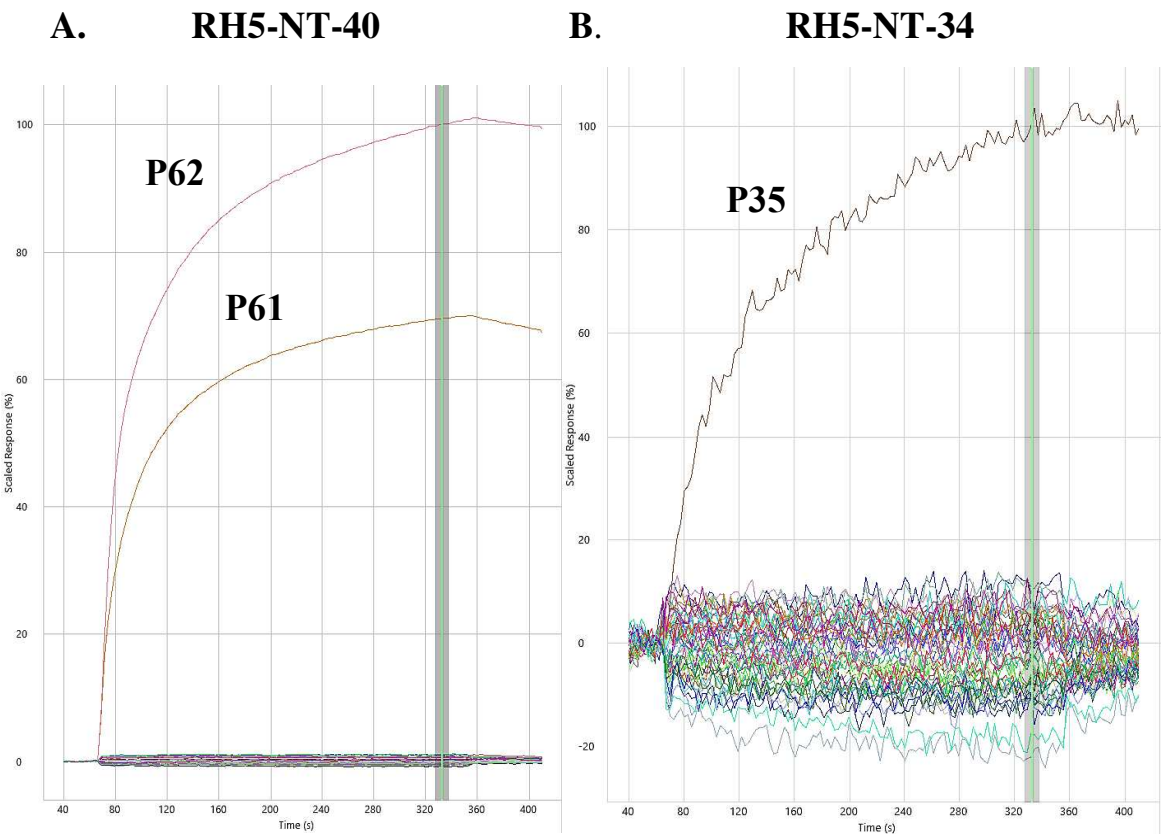

Figure 4.B.2.5.4. *SPR sensorgram plots for RH5-NT-40 and 34 mAbs.*

*Overlay plots of the sensorgrams obtained for single mAb analytes RH5-NT-40 and 34 injected over the entire peptide array are shown. The specific binding of RH5-NT-40 to P61 and P62 (**A**) and the specific binding of RH5-NT-34 to P35 (**B**) are clearly discerned above the baseline or null responses collected for all other peptide-coated spots, allowing these mAbs to be mapped specifically to those peptides.*

4.B.2.6. Growth inhibition activity of anti N-term RH5 mAbs: single point and eventually dilution curve

In order to have a complete characterisation of the RH5 N-terminus mAbs we measured their ability to block 3D7 clone *P. falciparum* parasite invasion *in vitro*. GIA assays were performed to test all the ELISA-positive mAbs, using single concentration of mAbs at 0.5mg/mL, keeping as a positive reference the BD5, known mAb. The GIA data are shown in **Figure 4.B.2.6.1. A,B, C** and **D**. The only mAb that resulted to have a neutralising activity of 50% is mAb RH5 N-terminus 12.

A.

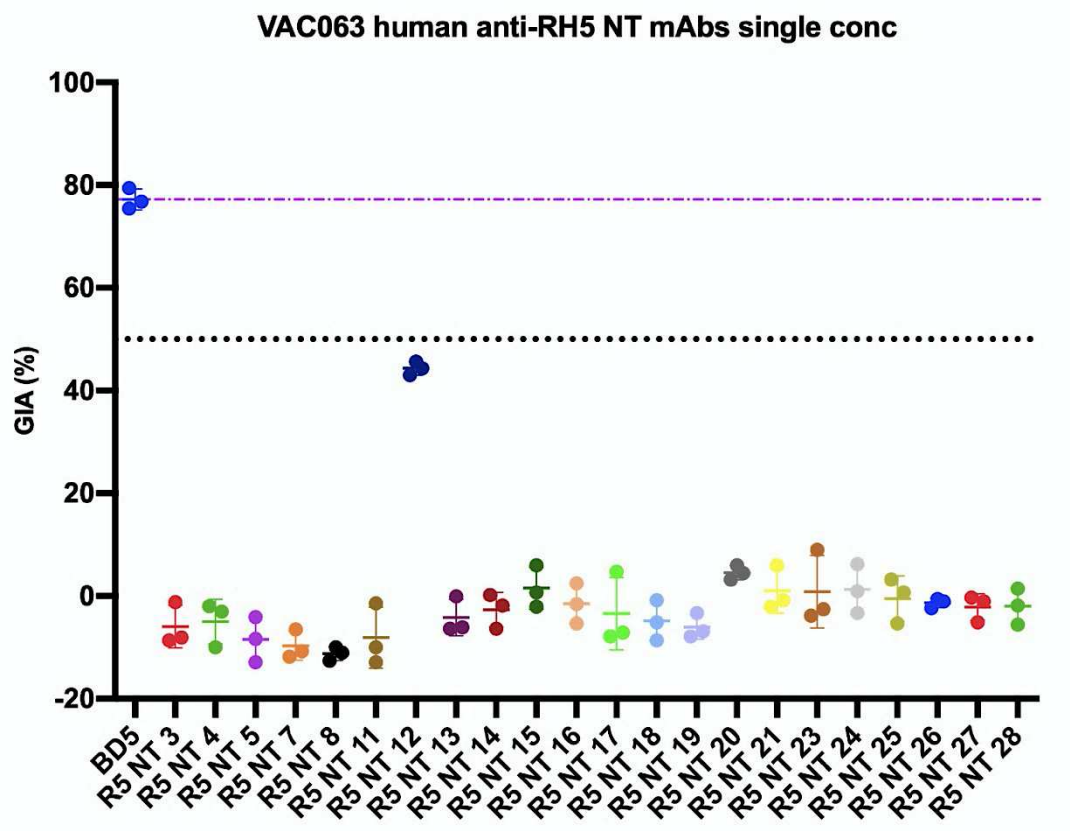

B.

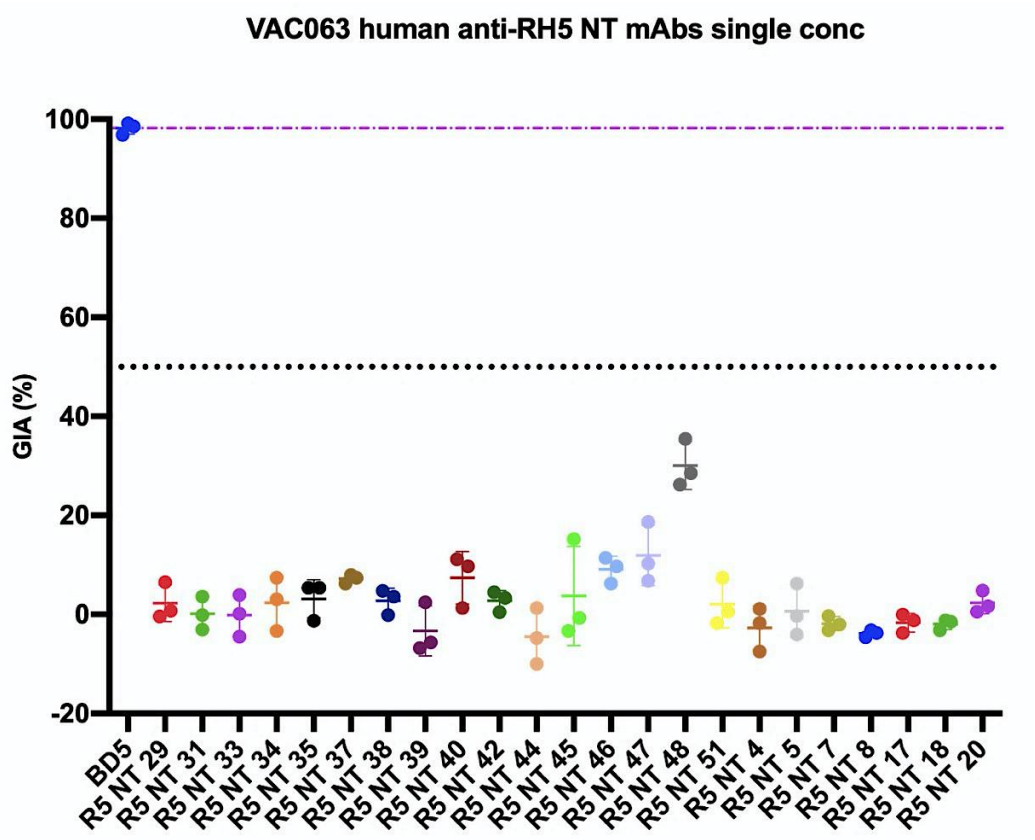

C.

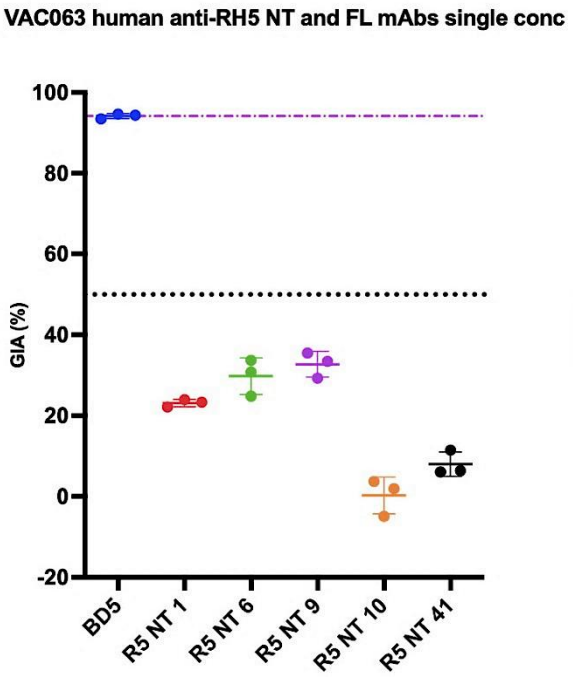

D.

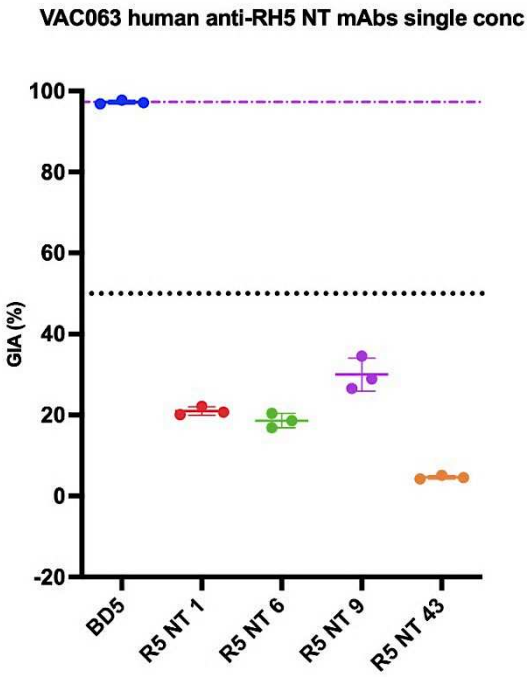

***Figure 4.B.2.6.2. A,B,C** and **D**. Single concentration GIA assay against 3D7 clone P. falciparum parasites of RH5 N-terminus mAbs.*

*Here are represented four (A-D) GIA assays to test different RH5 N-terminus mAbs. On the X-axis are plotted the names of mAbs, while on the Y-axis the GIA (%), always compared to the internal control BD5. Dots show the mean and error bars the range of N=3 triplicate test wells per test mAb concentration. **D.** shows GIA of some mAbs already tested to double check the inhibitory activity, as well as to test another mAb (R5 NT 43).*

To further verify this surprising result, the assay was repeated for RH5 N-terminus mAb 12 and the suspicious mAb 48 as shown in **Figure 4.B.2.6.3**. It was confirmed that R5NT-12 had a growth inhibitory activity against *P. falciparum* parasite invasion *in vitro,* while R5 NT-48 was negative.

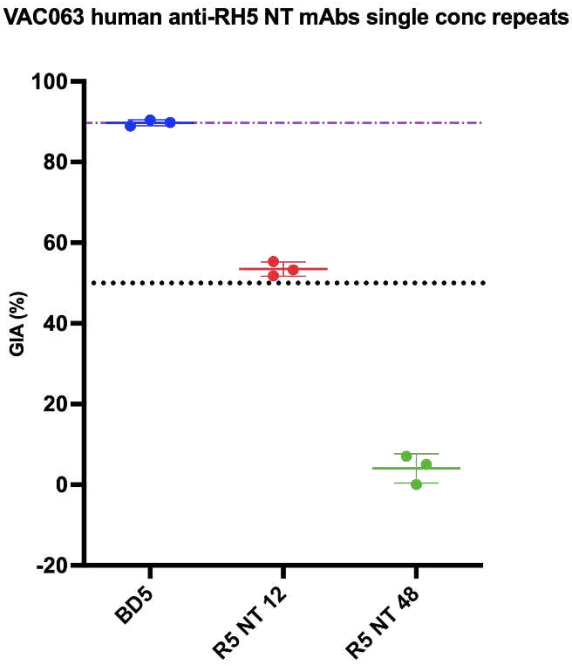

Figure 4.B.2.6.4. *Repeat of Single concentration GIA assay against 3D7 clone P. falciparum parasites of RH5 N-terminus mAbs 12 and 48.*

On the X-axis are plotted the names of mAbs, while on the Y-axis the GIA (%), compared to the internal control BD5.

In addition, RH5 N-terminus mAb 12 was tested in a dilution curve (**Figure 4.B.2.6.5.**) starting from a concentration of 1mg/mL, making a comparison with the control mAb BD5. As it is possible to observe the GIA activity of mAb 12 has a 50% GIA at the higher concentration, but then it decreases slowly, reaching inactivity at 0.1mg/mL.

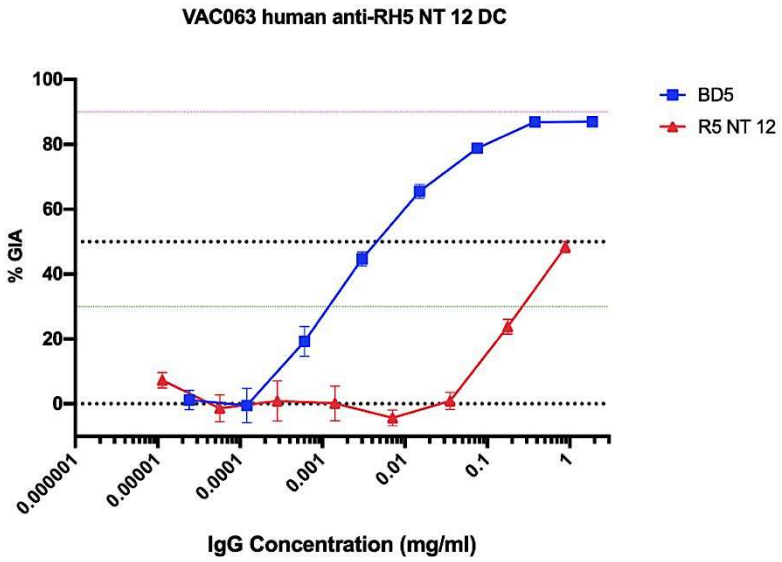

Figure 4.B.2.6.6. *Titration of the RH5 Nterminus mAbs 12 in the GIA assay against 3D7 clone P. falciparum parasites.*

Dots show the mean and error bars the range of N=3 triplicate test wells per test mAb concentration. On the X-axis is shown the concentration of mAbs expressed in mg/ml, while on the Y-axis is shown the percentage of GIA.

Considering the surprising result we decided to further confirm by GIA. The most promising mAbs, R5-NT 1, R5-NT 6, R5-NT 9, R5-NT 12, and R5-NT 41were tested in dilution curve with the R5-NT12 (**Figure 4.B.2.6.7.**). Despite all the mAbs resulted GIA negative in the dilution curve, though this test again confirmed the GIA activity of R5-NT 12.

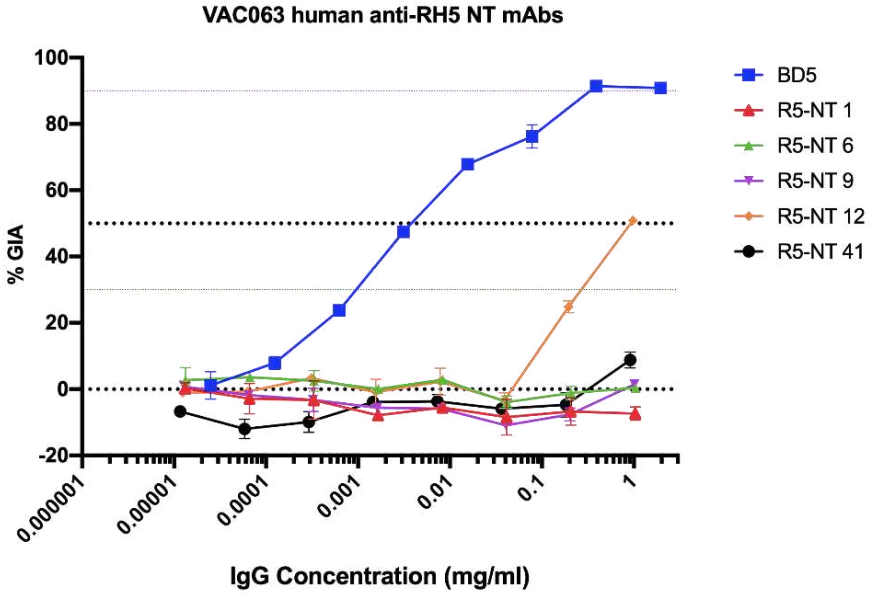

Figure 4.B.2.6.8. *Titration of the RH5 Nterminus mAbs 12, 1, 6, 9,12 and 41 in the GIA assay against 3D7 clone P. falciparum parasites.*

Dots show the mean and error bars the range of N=3 triplicate test wells per test mAb concentration. On the X-axis is shown the concentration of mAbs expressed in mg/ml, while on the Y-axis is shown the percentage of GIA.

4.B.2.7. Characterisation of RH5 N-terminus 12 mAb

To further characterise this unexpected GIA positive mAb we decided to do a more complete ELISA. We tested R5NT-12 in an ELISA against the RH5.1 full length protein, RH5 N-terminus protein as repeat and then also against the heat-denatured RH5.1, the RH5 delta NL and the RH5.2, always adding the three internal control mAbs: R5.016, 4BA7, 3A11 (**Figure 4.B.2.7.1.).**

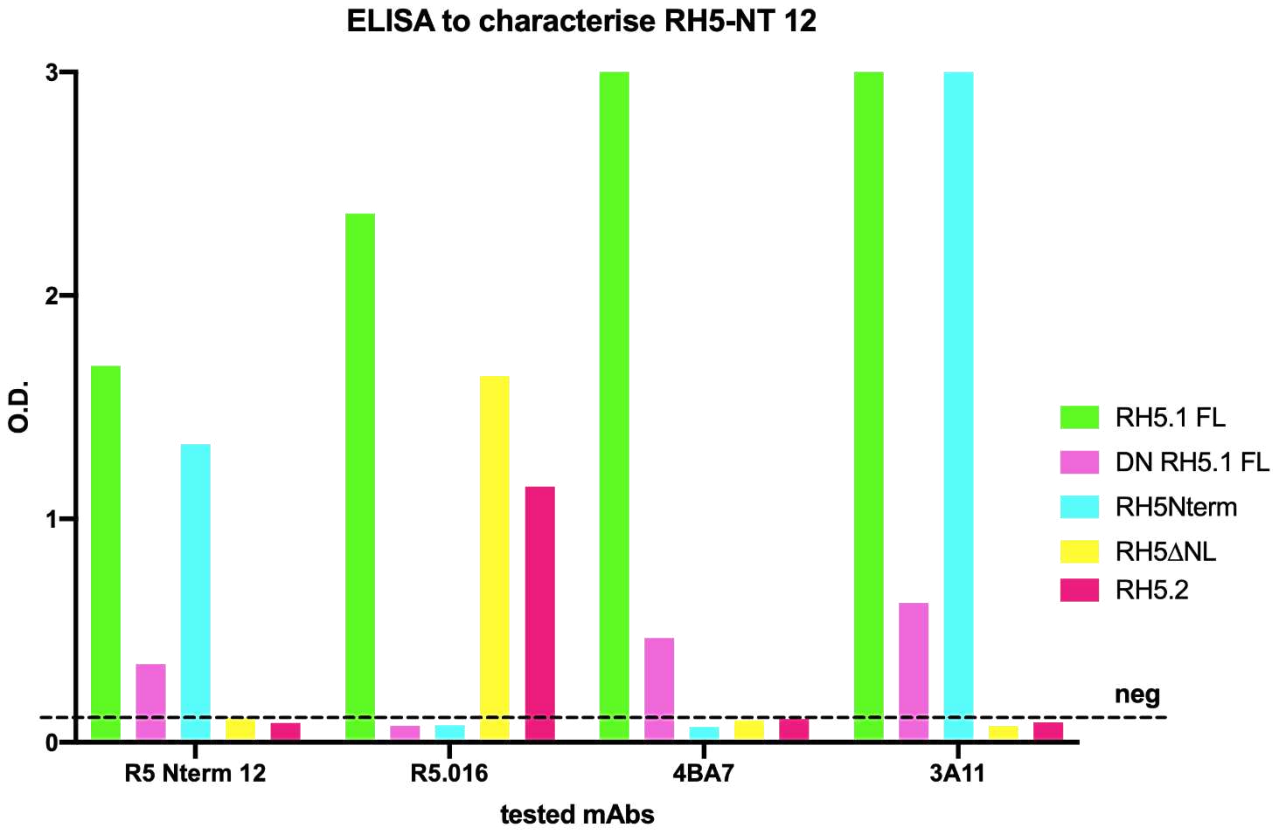

Figure 4.B.2.7.2*. ELISA to characterise RH5-NT-12.*

Here is shown the ELISA of the RH5-NT-12 mAb and the three internal controls R5.016, 4BA7, 3A11 mAbs tested respectively against the RH5.1 full-length protein (green), the denatured RH5.1 full-length protein (violet), the N-terminus portion of RH5 (light blue), RH5ΔNL (yellow) and the RH5.2 protein (pink). The X-axis shows the four mAbs tested and the Y-axis shows the O.D. value in ELISA.

According with what we have observed in this assay we can confirm the fact that RH5-NT-12 is effectively a binder of the N-terminus portion of RH5 protein in ELISA. We can add that it weakly binds the denatured protein, but it definitely doesn't bind the RH5ΔNL, nor the RH5.2 protein.

4.B.2.8. Sequence analysis of anti-PfRH5 N-terminus mAbs

To complement the epitope and functionality mapping of anti-*Pf*RH5 N-terminus antibodies, we conducted a sequence analysis of all the ELISA-positive mAbs. Analysis of heavy and light chain gene family usage across the whole anti-RH5 N-terminus panel revealed a diverse repertoire of heavy chain N=7 and light chain N=8 gene families, although with a prevalence of HV5 (N=19), HV3 (N=10), LV3 (N=31) and KV2 (N=4) gene family usage.

About the uniqueness of sequences instead, we can observe (**Figure 4.B.2.8.1.A and B.**) that there are N=17 V_H and N=13 $V_{L/K}$ unique sequences in this set of mAbs. What is incredibly high in this panel is the frequency of the heavy chain gene IGHV5-51 present is 19 RH5-NT mAbs and the light chain gene IGLV3-25 present in 23 RH5-NT mAbs

While there are N=26 unique possible combinations of pairing of V_H and $V_{L/K}$ from this new panel of RH5-N-terminus mAbs (**Figure 4.B.2.8.2.C.**); the highest gene pairing frequency is for HV5-51/LV3-25, present in 12 mAbs, about 1/3 of the full panel analysed.

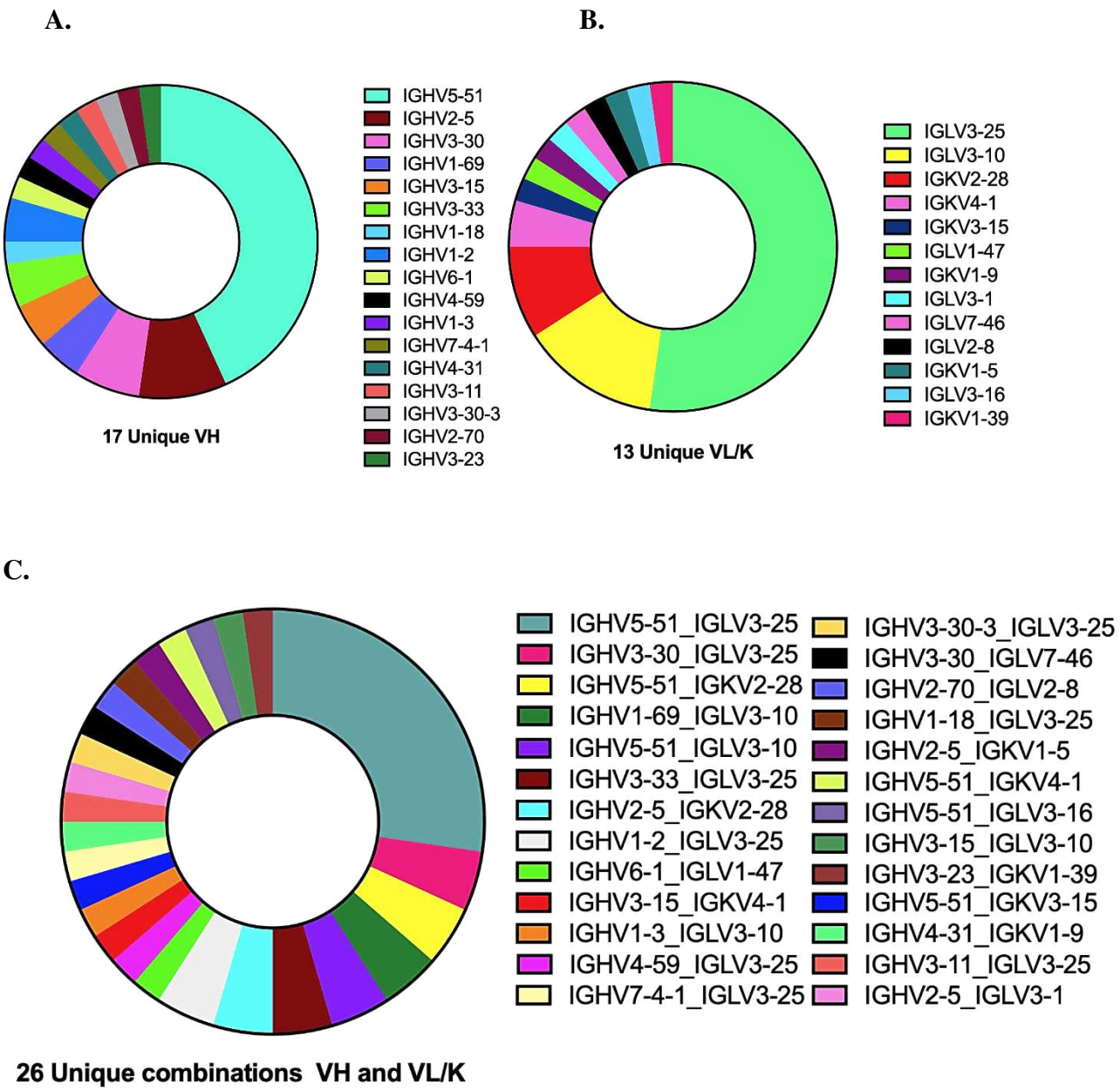

Figure 4.B.2.8.3. ***A*** *and* ***B*** *Unique* V_H *and* $V_{L/K}$. ***C***. *Unique combinations of* V_H *and* $V_{L/K}$.

A. *and* ***B.*** *represent respectively the frequencies of the unique* V_H *and* $V_{L/K}$ *combination obtained from the analysis of the full panel of RH5 N-termius mAbs.* ***C.*** *shows the presence of the 33 unique combinations of* V_H *plus* $V_{L/K}$ *coming from the RH5 N-terminus mAbs.*

To assess any eventual association of antibody gene pairing with mAb GIA EC50 potency, we analysed the gene pair combination of the GIA positive mAb R5-NT 12, which was HV4-59/LV3-25, but it was a unique combination, not even found in the best GIA RH5 FL mAbs described in the previous section.

4.B. Discussion

In this B chapter, we have focused our attention on the isolation and characterisation of a particular repertoire of anti-*Plasmodium falciparum* Reticulocyte-binding protein Homolog 5 (RH5) monoclonal antibodies deriving from peripheral memory B cells of donors vaccinated in the VAC063 study.

As previously explained, in the past, a panel of mAbs, derived from the first clinical trial of a *Pf*RH5-based vaccine, the VAC057 study, identified the best neutralising antibodies bound to the RH5 tip. After this finding, a second panel of mAbs was derived from the second clinical trial of a *Pf*RH5-based vaccine, the VAC063 study, by using an RH5-diamond probe, which was composed of a truncated version of RH5 that removed the N-terminus and some parts of the C-terminus to obtain mAbs that target the epitopes within RH5 already known to be GIA-positive.

Here instead, we provide a wide analysis of two different panels of mAbs deriving from the peripheral blood of UK adults vaccinated with *Pf*RH5 (VAC063 trial) by using different probes to address the full RH5 protein and the N-terminus portion.

In the first part of the results section we described and analysed the 100 mAbs isolated from memory B cells of five different samples of VAC063 using the RH5 full-length probe.

We have pooled out an equal number of mAbs from each donor to have a uniform distribution of mAbs to test. The 94% of selected mAbs resulted were positive for the RH5.1 full-length protein, the majority of them (89.4%) were able to bind conformational epitopes, while the remaining minority bound linear epitopes, mainly the N-terminus portion of RH5. This deserves a reflection, indeed the prevalence of mAbs was oriented to other parts of RH5 rather than to the N-terminus or intrinsic loop linear epitopes. Surprisingly, none of the linear mAbs was identified as a C-terminus, but it may be explained by the fact that the probe has the CD4 and BAP tag directly attached to the C-terminus, thus that sequence could not have been available. A future plan is to design a new probe by introducing a linker or changing the tag position to make the C-terminus more available, or alternatively and complementary to make a probe directly with the C terminus peptide. At this moment we cannot say too much about the absence of mAbs directed against this portion, because it may be that effectively this part is not relevant or that the probe has hidden that C-terminus portion.

Linear or continuous epitopes are composed of a stretch of amino acids in the order of their primary sequence whereas conformational or discontinuous epitopes are formed of amino

acids brought together in a protein's tertiary structure. Up to 90% of B cell epitopes are thought to be conformational [282], this is coherent with our results.

The fact that most mAbs bind conformational epitopes is therefore unsurprising but it does serve to confirm the integrity of the *Pf*RH5 vaccine immunogen associated with $AS01_B$ adjuvant.

If we focus on the *in vitro* growth inhibition, we have identified six conformational mAbs, nearly one for each donor (mAbs S1-11, S1-12, S1-13, R5 FL S3-10, R5 FL S4-09, R5 FL S5-15), having EC50 and EC80 values close to the most potent mAb isolated up to now, BD5. In particular, the two best GIA mAbs discovered were S1-12 and S3-10, which had a great EC50 value of 6µg/mL.

The fact that all the mAbs that bound linear epitopes have no GIA, confirms what was seen in previous studies performed in the Draper Group Lab.

From the sequence analysis of this panel, came to light that the gene pairing is quite unique among the different isolated mAbs, indeed only 5 antibodies had the same gene pairing (HV3-7/LV3-21), giving an idea of the variety of combinations that was present among them. Considering the best GIA mAbs, we couldn't associate them to a particularly overrepresented clonotype, nevertheless, two of the best neutralising mAbs, S1-11 and S1-12, had a repeated gene combination IGHV3-11_IGLV1-44.

All these potent GIA mAbs have unique germline combinations, different from the top BD5 mAb, but approaching his potency, and this could be considered an alternative option, in the future, for the generation of therapeutic mAbs in case of better developability compared to the other mAb already discovered. As next step in this context, an investigation using the Therapeutic Antibody Profiler (TAP) tool can be considered a valuable first-step option.

What is also important to notice is that for the first time, we identified the most potent GIA mAb with a variable K chain, S4-09 (IGHV1-18_IGKV1-39), having an EC50 value of 9µg/mL, better than any previously published best V_K mAb.

Ongoing studies are being performed to determine the epitope binning of this panel of mAbs and future experiments can be planned to investigate any eventual synergy activity with other antibodies.

In the second part of the results section, instead, we have described the panel of 51 mAbs isolated from the memory B cells of five donors of the same clinical trial, but using the N-terminus probe to address the focus on this region that was previously excluded. From the isolated mAbs, approximately 82.4% were detected to be N-terminus-specific. These mAbs were further classified and analysed for the binding to the different peptides of the N-terminus region both with a peptide ELISA and with a peptide mapping LSA. Results were comparable and it was observed that 95% of the RH5 N-terminus mAbs bound at least one peptide in the panel. The main observation we could make is that, thanks to the peptide array done with LSA, we had, on one side, implemented the peptides bound from some mAbs and on the other side found a reason for the RH5-NT mAbs that were negative in peptide ELISA. Mainly this is due to the higher sensitivity of this technique and the fact that we have added P1* and P2*, that were the two having the correct glycan mutations, thus matching the RH5-N-terminus probe used for the sorting.

The majority of these mAbs bound peptides 4 and 5, then several bound peptides 1 or P1* and peptides 2 or P2*, and the remaining mAbs bound peptides with different distributions. There were two mAbs, RH5-NT-12 and RH5-NT-41, that behaved in an alternative way, at least in the ELISA peptide assay, indeed they seemed to bind to two distinct parts the N-terminus region, around peptides 3 and 4 and around peptides 12 and 13.

Thanks to the LSA array we have also explained why the mAbs RH5-NT-34 and RH5-NT-40 were positive for the RH5.1 full-length protein, but negative for the probe. What we have seen is that RH5-NT-34 bound P35, thus being an RH5 intrinsic loop binder and RH5-NT-40 bound P61 and 62, therefore the C-terminus portion of RH5.

An unexpected result here, from this smaller panel we have accidentally identified for the first time, in the Draper Lab group, an RH5 C-terminus mAb: RH5-NT-40. Further ELISA tests are required to confirm this data but, if so, it can be considered an opportunity to explore the C-terminus part, which is thought not to play a relevant role and has been excluded from the latest RH5.2 vaccine design. From the GIA data, this portion seemed effectively to have no activity, but we can further investigate with synergy experiments to really exclude its importance.

From the *in vitro* GIA assay all the mAbs resulted to be negative, except for RH5-NT-12. For unexpected reasons, this mAb resulted four times positive for GIA, even if it had low potency.

Two hypotheses are now possible: on one side we can think that this RH5 N-terminus mAb is effectively binding somehow the N-terminus region of RH5, thus causing GIA activity and inhibiting invasion, on the other side that the mAb predominantly binds the N-terminus

portion but it also can bind elsewhere on RH5 (or even the malaria parasite), in this way inhibiting the invasion by interacting with the main diamond of RH5 or another parasite protein.

Thus, we then decided to start to characterise RH5-NT-12 by testing it in ELISA, to repeat and confirm the binding to the RH5.1 protein and the RH5 N-terminus portion. Furthermore, with the same assay, we have excluded any binding to the RH5ΔNL and to the RH5.2 protein. What resulted evident from this characterisation was that RH5-NT-12 seemed to not cross-react with any other linear part of the RH5 protein, hence being consistent with the fact that we have isolated an N-terminus-specific mAb.

To definitively exclude an eventual binding of RH5-NT-12 to a folded structure of RH5 further follow-up studies are required and Surface Plasmon Resonance (SPR) can be considered a reasonable proposal for future further investigations.

All the GIA-positive mAbs discovered up to now are conformation-dependent antibodies that bind to the diamond region of the RH5, therefore a confirmation of binding to the N-terminus portion by this mAb could open an alternative perspective to what has been observed so far.

As next step for this panel, to see if there is something more that these mAbs can do, not on their own, synergy experiments can be performed, to look at an eventual GIA activity in combination with other monoclonal antibodies or an increase in potency instead for RH5-NT-12.

To make some considerations about the sequence analysis of this panel, we noticed an enrichment in HV5-51 and LV3-25 genes and that the most frequent gene combination was HV5-51/LV3-25, about 30% of the positive mAbs. Consistently with this observation, we can add that even two of the seven N-terminal linear mAbs pooled out from the RH5-FL panel presented the gene IgHV5-51 and one of these seven presented the LV3-25 gene, but none of the other mAbs belonging to this panel presents the relevant combination. Due to the massive prevalence of these two genes (HV5-51 and LV3-25) within the N-terminus subclass, we can easily deduce that there is an association between these and this class of mAbs; thus we can hypothesize that just from the sequences we can predict that there is a more likely chance to obtain N-terminus binder mAbs.

To my knowledge, these two panels of human mAbs, are unique and developed for the first time.

On one side the wider panel of full-length RH5 mAbs allows a comparison with the previous panel, derived from the VAC063 study, that was generated using a truncated RH5-diamond probe. On the other side, we have generated the first set of mAbs addressed against the N-terminus portion of RH5, with the presence of a single neutralising mAb, to be considered as a tool for a future and more advanced investigation of the role of this region of the protein, which is still not clear and controversial, but crucial for the improvement in the development of malaria vaccines and therapeutic interventions.

GENERAL CONCLUSION

Monoclonal antibodies are crucial in biomedical research and have a broad range of applications, including research and therapeutic uses. This thesis focuses on generating monoclonal antibodies for infectious diseases. The text describes two projects with a shared objective of developing monoclonal antibodies from single cells, specifically human monoclonal antibodies from single B cells.

The initial study aimed to develop a cost-effective and efficient method for extracting and producing monoclonal antibodies from donor peripheral blood. Once the technique was developed and any issues were resolved, a rapid process was established to isolate and screen antigen-specific mAbs from $CD138^+$ antibody-secreting cells in peripheral blood within ten days. The generation of recombinant monoclonal antibodies from circulating antibody-secreting cells enables targeted screening during a specific stage of infection and may expedite the development of a monoclonal antibody panel.

The second study aimed to produce and characterise monoclonal antibody panels against the *Plasmodium falciparum* RH5 antigen, the target of blood-stage malaria vaccine, using a well-established antibody discovery pipeline. This study conducted two sub-projects to create monoclonal antibody panels using different probes that targeted the full-length protein and a portion of this. The latter aimed to explore a region that currently lacks a clearly defined function, and the mAbs generated have significant potential as a tool for future research and some interesting observations about gene combinations were made. In addition, the other sub-project produced a set of monoclonal antibodies that, for the majority, resulted to be positive for the growth inhibition assay, including some mAbs that closely resemble the most promising candidate isolate identified so far, and some other interesting candidates were identified.

Both studies yielded valuable and intriguing results, they have accomplished their goals and set the stage for future in-depth research.

Bibliography:

1. Murphy, K. & Weaver, C. *Janewey's Immunobiology 9th Edition*. (2017).
2. Kantha, S. S. A Centennial Review; the 1890 Tetanus Antitoxin Paper of von Behring and Kitasato and the Related Developments. *Keio J. Med.* **40**, 35–39 (1991).
3. Buss, N. A. P. S., Henderson, S. J., McFarlane, M., Shenton, J. M. & De Haan, L. Monoclonal antibody therapeutics: History and future. *Curr. Opin. Pharmacol.* **12**, 615–622 (2012).
4. Moorthy, B. S. et al. Structure of Monoclonal Antibodies. *Biobetters AAPS Adv. Pharm. Sci. Ser.* **19**, 1–378 (2015).
5. Bayer, V. An Overview of Monoclonal Antibodies. *Semin. Oncol. Nurs.* **35**, 150927 (2019).
6. https://www.nobelprize.org/prizes/medicine/1987/tonegawa/facts/.
7. Tonegawa, S. Somatic Generation of Immune Diversity (Nobel Lecture). *Angew. Chemie Int. Ed. English* **27**, (1988).
8. https://bio.libretexts.org/Bookshelves/Microbiology/Microbiology_(Boundless)/11%3A_Immunology/11.07%3A_Antibodies/11.7B%3A_Antibody_Genes_and_Diversity.
9. Tonegawa, S. Somatic generation of antibody diversity. *Nature* **302**, 575–581 (1983).
10. Nishana, M. & Raghavan, S. C. Role of recombination activating genes in the generation of antigen receptor diversity and beyond. *Immunology* **137**, 271–281 (2012).
11. Elhanati, Y. *et al.* Inferring processes underlying B-cell repertoire diversity. *Philos. Trans. R. Soc. B Biol. Sci.* **370**, (2015).
12. Pieper, K., Grimbacher, B. & Eibel, H. B-cell biology and development. *J. Allergy Clin. Immunol.* **131**, 959–971 (2013).
13. Maul, R. W. & Gearhart, P. J. *AID and somatic hypermutation*. *Advances in Immunology* vol. 105 (Elsevier Inc., 2010).
14. Hornbeck, P., Winston, S. E. & Fuller, S. A. Enzyme-Linked Immunosorbent Assays (ELISA) . *Curr. Protoc. Mol. Biol.* **15**, (1991).
15. Klinman, D. ELISPOT Assay to Detect Cytokine-Secreting Murine and Human Cells. *Curr. Protoc. Immunol.* (1994) doi:10.1002/0471142735.im0619s83.

16. Ni, D., Xu, P. & Gallagher, S. Immunoblotting and immunodetection. *Curr. Protoc. Immunol.* **74**, 6.2.1-6.2.37.
17. Bonifacino, J. S., Gershlick, D. C. & Dell'Angelica, E. C. Immunoprecipitation. *Curr. Protoc. Cell Biol.* 7.2.1-7.2.24 (1999) doi:10.1002/cpcb.3.
18. Michaud, G. A. et al. "Analyzing antibody specificity with whole proteome microarrays." *Nat. Biotechnol.* **21,12**, 1509–12. (2003).
19. E. Harlow and D. Lane. "Using Antibodies: A Laboratory Manual". *J. Antimicrob. Chemother.* **45**, 413 (2000).
20. Givan, A. L. *Flow cytometry: first principles. John Wiley & Sons.* (2001).
21. Edwards, P. A. W. Some properties and applications of monoclonal antibodies. *Biochem. J.* **200**, 1–10 (1981).
22. Zola, H. & Roberts-Thomson, P. Monoclonal Antibodies: Diagnostic Uses. in (2001). doi:10.1038/npg.els.0004019.
23. Lonberg, N, and D. H. "Human antibodies from transgenic mice." *Int. Rev. Immunol.* **13,1**, : 65-93. (1995).
24. Kaplon, H., Chenoweth, A., Crescioli, S. & Reichert, J. M. Antibodies to watch in 2022. *MAbs* **14**, 1–45 (2022).
25. Antibody therapeutics approved or in regulatory review in the EU or US-https://www.antibodysociety.org/resources/approved-antibodies/.
26. Ansar, W. & Ghosh, S. Monoclonal Antibodies: A Tool in Clinical Research. *Indian J. Clin. Med.* **4**, IJCM.S11968 (2013).
27. Festing, M. F. W. Inbreeding and its Consequences, and the History of Inbred Strains. *Inbred Strains Biomed. Res.* 3–20 (1979) doi:10.1007/978-1-349-03816-9_1.
28. T. Raybould and M. Takahashi. "Production of stable rabbit-mouse hybridomas that secrete rabbit mAb of defined specificity". *Science (80-.).* **240**, 1788–90.
29. Kishiro, Y., Kagawa, M., Sado, Y. & Naito, I. A Novel Method of Preparing Rat-Monoclonal Antibody-Producing Hybridomas by Using Rat Medial Iliac Lymph Node Cells. *Cell Struct. Funct.* **20**, 151–156 (1995).
30. Shaharir, S. S., Johdi, N. A. & Mohd, R. Monoclonal Antibody. *Encycl. Infect. Immun.* **4**, 741–754 (2022).
31. Yu, X., McGraw, P. A., House, F. S., & Crowe, J. E., J. An optimized electrofusion-based protocol for generating virus-specific human monoclonal antibodies. *J. Immunol. Methods* 142–151 (2008).
32. Gorny, M. K. Human hybridoma technology. *Antib. Technol. J.* **2**, 1–5 (2012).

33. Bradbury, A. R. M. *et al.* When monoclonal antibodies are not monospecific: Hybridomas frequently express additional functional variable regions. *MAbs* **10**, 539–546 (2018).
34. Smith, G. P. Filamentous fusion phage: Novel expression vectors that display cloned antigens on the virion surface. *Science (80-.).* **228**, 1315–1317 (1985).
35. Glanville, J. *et al.* Precise determination of the diversity of a combinatorial antibody library gives insight into the human immunoglobulin repertoire. *Proc. Natl. Acad. Sci. U. S. A.* **106**, 20216–20221 (2009).
36. Frenzel, A., Schirrmann, T. & Hust, M. Phage display-derived human antibodies in clinical development and therapy. *MAbs* **8**, 1177–1194 (2016).
37. Mccafferty, J., Griffiths, A. D., Winter, G. & Chiswellt, D. J. Phage antibodies: filamentous variable domains. *Nature* **348**, 552–554 (1990).
38. Beerli, R. R. & Rader, C. Mining human antibody repertoires. *MAbs* **2**, 365–378 (2010).
39. Barbas, C. F., Kang, A. S., Lerner, R. A. & Benkovic, S. J. Assembly of combinatorial antibody libraries on phage surfaces: The gene III site. *Proc. Natl. Acad. Sci. U. S. A.* **88**, 7978–7982 (1991).
40. Orum, H. et al. Efficient method for construction comprehensive murine fab antibody libraries displayed on phage. *Nucleic Acids Res.* **21**, 4491–4498 (1993).
41. Marks, J. D. *et al.* By-passing immunization. Human antibodies from V-gene libraries displayed on phage. *J. Mol. Biol.* **222**, 581–597 (1991).
42. Ch'ng, A. C. W., Choong, Y. S., & Lim, T. S. Phage display-derived antibodies: application of recombinant antibodies for diagnostics. Proof and concepts in rapid diagnostic tests and technologies. (2016).
43. Hanes, J., Jermutus, L., Weber-Bornhauser, S., Bosshard, H. R. & Plückthun, A. Ribosome display efficiently selects and evolves high-affinity antibodies in vitro from immune libraries. *Proc. Natl. Acad. Sci. U. S. A.* **95**, 14130–14135 (1998).
44. Boder, E. T. & Wittrup, K. D. Yeast surface display for screening combinatorial polypeptide libraries. *Nat. Biotechnol.* **15**, 553–557 (1997).
45. Daugherty, P. S., Olsen, M. J., Iverson, B. L. & Georgiou, G. Development of an optimized expression system for the screening of antibody libraries displayed on the Escherichia coli surface. *Protein Eng. Des. Sel.* **12**, 613–621 (1999).
46. Beerli, R. R. *et al.* Isolation of human monoclonal antibodies by mammalian cell display. *Proc. Natl. Acad. Sci. U. S. A.* **105**, 14336–14341 (2008).
47. Kehoe, J. W. & Kay, B. K. Filamentous phage display in the new millennium.

Chem. Rev. **105**, 4056–4072 (2005).

48. Garufi, G., Minenkova, O., Lo Passo, C., Pernice, I. & Felici, F. Display libraries on bacteriophage lambda capsid. *Biotechnol. Annu. Rev.* **11**, 153—190 (2005).
49. Malys, N., Chang, D. Y., Baumann, R. G., Xie, D. & Black, L. W. A bipartite bacteriophage T4 SOC and HOC randomized peptide display library: Detection and analysis of phage T4 terminase (gp17) and late σ factor (gp55) interaction. *J. Mol. Biol.* **319**, 289–304 (2002).
50. Kalniņa, Z. *et al.* Evaluation of T7 and lambda phage display systems for survey of autoantibody profiles in cancer patients. *J. Immunol. Methods* **334**, 37–50 (2008).
51. O'Connell, D., Becerril, B., Roy-Burman, A., Daws, M. & Marks, J. D. Phage versus phagemid libraries for generation of human monoclonal antibodies. *J. Mol. Biol.* **321**, 49—56 (2002).
52. Chasteen, L., Ayriss, J., Pavlik, P. & Bradbury, A. R. M. Eliminating helper phage from phage display. *Nucleic Acids Res.* **34**, 1–11 (2006).
53. Shi, L. *et al.* De Novo Selection of High-Affinity Antibodies from Synthetic Fab Libraries Displayed on Phage as pIX Fusion Proteins. *J. Mol. Biol.* **397**, 385–396 (2010).
54. Wu, C. H., Liu, I. J., Lu, R. M. & Wu, H. C. Advancement and applications of peptide phage display technology in biomedical science. *J. Biomed. Sci.* **23**, 1–14 (2016).
55. Konthur, Zoltán, Jeannine Wilde, and T. S. L. 'Semi-automated magnetic bead-based antibody selection from phage display libraries.' *Antib. Eng.* : 267-287.
56. Noppe, W. *et al.* Chromato-panning: An efficient new mode of identifying suitable ligands from phage display libraries. *BMC Biotechnol.* **9**, 1–9 (2009).
57. Meijer, P. J. *et al.* Isolation of Human Antibody Repertoires with Preservation of the Natural Heavy and Light Chain Pairing. *J. Mol. Biol.* **358**, 764–772 (2006).
58. Pendley, C. et al. "Immunogenicity of therapeutic monoclonal antibodies." *Curr. Opin. Mol. Ther.* **5,2**, : 172-9.
59. Kuus-Reichel, K. *et al.* Will immunogenicity limit the use, efficacy, and future development of therapeutic monoclonal antibodies? *Clin. Diagn. Lab. Immunol.* **1**, 365–372 (1994).
60. Tomizuka, K. *et al.* Functional expression and germline transmission of a human chromosome fragment in chimaeric mice. *Nat. Genet.* **16**, 133–143 (1997).
61. Lonberg, N. Human monoclonal antibodies from transgenic mice. *Handb. Exp. Pharmacol.* **181**, 69–97 (2008).

62. Mompó, Susana Magadán, and A. G.-F. “Antigen-specific human monoclonal antibodies from transgenic mice.” *Methods Mol. Biol.* **1060**, 245–76. (2014).
63. Brüggemann, M. *et al.* Human Antibody Production in Transgenic Animals. *Arch. Immunol. Ther. Exp. (Warsz).* **63**, 101–108 (2015).
64. Scott, C. T. Mice with a human touch. *Nat. Biotechnol.* **25**, 1075–1077 (2007).
65. Ribatti, D. From the discovery of monoclonal antibodies to their therapeutic application: An historical reappraisal. *Immunol. Lett.* **161**, 96–99 (2014).
66. Borrebaeck, C. A. K., Malmborg, A. C. & Ohlin, M. Does endogenous glycosylation prevent the use of mouse monoclonal antibodies as cancer therapeutics? *Immunol. Today* **14**, 477–479 (1993).
67. Babcook, J. S., Leslie, K. B., Olsen, O. A., Salmon, R. A. & Schrader, J. W. A novel strategy for generating monoclonal antibodies from single, isolated lymphocytes producing antibodies of defined specificities. *Proc. Natl. Acad. Sci. U. S. A.* **93**, 7843–7848 (1996).
68. Obiakor, H. *et al.* A comparison of hydraulic and laser capture microdissection methods for collection of single B cells, PCR, and sequencing of antibody VDJ. *Anal. Biochem.* **306**, 55–62 (2002).
69. Kuppers, R., Zhao, M., Hansmann, M. L. & Rajewsky, K. Tracing B cell development in human germinal centres by molecular analysis of single cells picked from histological sections. *EMBO J.* **12**, 4955–4967 (1993).
70. Lagerkvist, A. C. et al. “Single, antigen-specific B cells used to generate Fab fragments using CD40-mediated amplification or direct PCR cloning.” *Biotechniques* **18,5**, 862–9. (1995).
71. Herzenberg, L. A. *et al.* The history and future of the Fluorescence Activated Cell Sorter and flow cytometry: A view from Stanford. *Clin. Chem.* **48**, 1819–1827 (2002).
72. Scheid, J. F. et al. “A method for identification of HIV gp140 binding memory B cells in human blood.” *J. Immunol. Methods* **343,2**, : 65-7. (2009).
73. https://genovac.com/solutions/single-b-cell-platforms/.
74. Liao, H.-X. *et al.* High-throughput isolation of immunoglobulin genes from single human B cells and expression as monoclonal antibodies. *J. Virol. Methods* **158**, 171—179 (2009).
75. Wilson, P. C. *et al.* Somatic hypermutation introduces insertions and deletions into immunoglobulin V genes. *J. Exp. Med.* **187**, 59–70 (1998).
76. de Wildt RM, van Venrooij WJ, Winter G, Hoet RM, T. I. Somatic insertions and

deletions shape the human antibody repertoire. *J Mol Biol.* **294**, 701–10.

77. Janeway CA Jr, Travers P, Walport M, et al. *Immunobiology: The Immune System in Health and Disease. 5th edition. New York: Garland Science; 2001. Chapter 9, The Humoral Immune Response.*

78. Sethu, S. *et al.* Immunogenicity to biologics: Mechanisms, prediction and reduction. *Arch. Immunol. Ther. Exp. (Warsz).* **60**, 331–344 (2012).

79. https://basicmedicalkey.com/humoral-immune-responses-activation-of-b-lymphocytes-and-production-of-antibodies/.

80. Garside, P. *et al.* Visualization of specific B and T lymphocyte interactions in the lymph node. *Science (80-.).* **281**, 96–99 (1998).

81. Zubler, R. H. Naive and memory B cells in T-cell-dependent and T-independent responses. *Springer Semin. Immunopathol.* **23**, 405–419 (2001).

82. Corti, D. & Lanzavecchia, A. Efficient Methods To Isolate Human Monoclonal Antibodies from Memory B Cells and Plasma Cells. *Microbiol. Spectr.* **2**, (2014).

83. Hibi, T. & Dosch, H. -M. Limiting dilution analysis of the B cell compartment in human bone marrow. *Eur. J. Immunol.* **16**, 139–145 (1986).

84. Nguyen, D. C., Joyner, C. J., Sanz, I. & Lee, F. E. H. Factors Affecting Early Antibody Secreting Cell Maturation Into Long-Lived Plasma Cells. *Front. Immunol.* **10**, 8–10 (2019).

85. Nutt, S. L., Hodgkin, P. D., Tarlinton, D. M. & Corcoran, L. M. The generation of antibody-secreting plasma cells. *Nat. Rev. Immunol.* **15**, 160–171 (2015).

86. Kaminski, D. A., Wei, C., Qian, Y., Rosenberg, A. F. & Sanz, I. Advances in human B cell phenotypic profiling. *Front. Immunol.* **3**, 1–15 (2012).

87. Medina, F., Segundo, C., Campos-Caro, A., González-García, I. & Brieva, J. A. The heterogeneity shown by human plasma cells from tonsil, blood, and bone marrow reveals graded stages of increasing maturity, but local profiles of adhesion molecule expression. *Blood* **99**, 2154–2161 (2002).

88. Wilmore, J. R., Jones, D. D. & Allman, D. Protocol for improved resolution of plasma cell subpopulations by flow cytometry. *Eur. J. Immunol.* **47**, 1386–1388 (2017).

89. O'Connell, F. P., Pinkus, J. L. & Pinkus, G. S. CD138 (Syndecan-1), a Plasma Cell Marker: Immunohistochemical Profile in Hematopoietic and Nonhematopoietic Neoplasms. *Am. J. Clin. Pathol.* **121**, 254–263 (2004).

90. Jacob J, Kassir R, K. G. In Situ Studies of the Primary Immune Response to (4-hydroxy-3-nitrophenyl) acetyl . I . The Architecture and Dynamics of Responding

Cell Populations By Joshy Jacob ," Ramtin Kassir , $ and Garnett Kelsoe ". *J Exp Med.* **173**, (1991).

91. CG., M. I. T. K. C. A. S. K. S. D. Z. E. C. M. V. Extrafollicular Antibody Responses. *Encycl. Immunobiol.* **3**, 208–215 (2016).
92. Radbruch, A. *et al.* Competence and competition: the challenge of becoming a long-lived plasma cell. *Nat. Rev. Immunol.* **6**, 741–750 (2006).
93. Allen, C. D. C., Okada, T., Tang, H. L. & Cyster, J. G. Imaging of germinal center selection events during affinity maturation. *Science (80-.).* **315**, 528–531 (2007).
94. Amanna, I. J. & Slifka, M. K. Mechanisms that determine plasma cell lifespan and the duration of humoral immunity. *Immunol. Rev.* **236**, 125–138 (2010).
95. Smith, K. G. C., Light, A., Nossal, G. J. V. & Tarlinton, D. M. The extent of affinity maturation differs between the memory and antibody-forming cell compartments in the primary immune response. *EMBO J.* **16**, 2996–3006 (1997).
96. Bannard, O. & Cyster, J. G. Germinal centers: programmed for affinity maturation and antibody diversification. *Curr. Opin. Immunol.* **45**, 21–30 (2017).
97. Linterman, M. A. *et al.* IL-21 acts directly on B cells to regulate Bcl-6 expression and germinal center responses. *J. Exp. Med.* **207**, 353–363 (2010).
98. Song, S. & Matthias, P. D. The transcriptional regulation of germinal center formation. *Front. Immunol.* **9**, 1–9 (2018).
99. Cobaleda, C., Schebesta, A., Delogu, A. & Busslinger, M. Pax5: The guardian of B cell identity and function. *Nat. Immunol.* **8**, 463–470 (2007).
100. Nutt, S. L., Taubenheim, N., Hasbold, J., Corcoran, L. M. & Hodgkin, P. D. The genetic network controlling plasma cell differentiation. *Semin. Immunol.* **23**, 341–349 (2011).
101. Kassambara, A. *et al.* GenomicScape: An Easy-to-Use Web Tool for Gene Expression Data Analysis. Application to Investigate the Molecular Events in the Differentiation of B Cells into Plasma Cells. *PLoS Comput. Biol.* **11**, 1–10 (2015).
102. Shi, W. *et al.* Transcriptional profiling of mouse B cell terminal differentiation defines a signature for antibody-secreting plasma cells. *Nat. Immunol.* **16**, 663–673 (2015).
103. Tellier, J. *et al.* Blimp-1 controls plasma cell function through the regulation of immunoglobulin secretion and the unfolded protein response. *Nat. Immunol.* **17**, 323–330 (2016).
104. Todd, D. J. *et al.* XBP1 governs late events in plasma cell differentiation and is not required for antigen-specific memory B cell development. *J. Exp. Med.* **206**, 2151–

2159 (2009).

105. Hu, C.-C. A., Dougan, S. K., McGehee, A. M., Love, J. C. & Ploegh, H. L. XBP-1 regulates signal transduction, transcription factors and bone marrow colonization in B cells. *EMBO J.* **28**, 1624–1636 (2009).
106. Yoshida, T. *et al.* Memory B and memory plasma cells. *Immunol. Rev.* **237**, 117–139 (2010).
107. Pengo, N. *et al.* Plasma cells require autophagy for sustainable immunoglobulin production. *Nat. Immunol.* **14**, 298–305 (2013).
108. Hargreaves, D. C. *et al.* A coordinated change in chemokine responsiveness guides plasma cell movements. *J. Exp. Med.* **194**, 45–56 (2001).
109. Hauser, A. E. *et al.* Chemotactic Responsiveness Toward Ligands for CXCR3 and CXCR4 Is Regulated on Plasma Blasts During the Time Course of a Memory Immune Response. *J. Immunol.* **169**, 1277–1282 (2002).
110. Ellyard, J. I., Avery, D. T., Mackay, C. R. & Tangye, S. G. Contribution of stromal cells to the migration, function and retention of plasma cells in human spleen: Potential roles of CXCL12, IL-6 and CD54. *Eur. J. Immunol.* **35**, 699–708 (2005).
111. Cassese, G. *et al.* Plasma Cell Survival Is Mediated by Synergistic Effects of Cytokines and Adhesion-Dependent Signals. *J. Immunol.* **171**, 1684–1690 (2003).
112. Chu, V. T. *et al.* Eosinophils are required for the maintenance of plasma cells in the bone marrow. *Nat. Immunol.* **12**, 151–159 (2011).
113. Hammarlund, E. *et al.* Plasma cell survival in the absence of B cell memory. *Nat. Commun.* **8**, (2017).
114. Parvez, M. K. & Parveen, S. Evolution and Emergence of Pathogenic Viruses: Past, Present, and Future. *Intervirology* **60**, 1–7 (2017).
115. Jaijyan DK; Liu J; Hai R; et al. Emerging and Reemerging Human Viral Diseases. *Ann. Microbiol. Res.* **2**, 31–44 (2018).
116. Morse, S. S. Factors in the emergence of infectious diseases. *Emerg. Infect. Dis.* **1**, 7–15 (1995).
117. Griffin, D. E. Emergence and re-emergence of viral diseases of the central nervous system. *Prog. Neurobiol.* **91**, 95–101 (2010).
118. A brief guide to emerging infectious diseases and zoonoses - https://iris.who.int/handle/10665/204722.
119. Sastry, A. S. & K, S. B. *Essentials of Medical Microbiology*. (Jaypee Brothers Medical Publishers Pvt. Limited, 2018).
120. Adhikari, S. P. *et al.* Epidemiology, causes, clinical manifestation and diagnosis,

prevention and control of coronavirus disease (COVID-19) during the early outbreak period: A scoping review. *Infect. Dis. Poverty* **9**, 1–12 (2020).

121. Satarker, S. & Nampoothiri, M. Structural Proteins in Severe Acute Respiratory Syndrome Coronavirus-2. *Arch. Med. Res.* **51**, 482–491 (2020).
122. Kampf G, Todt D, Pfaender S, S. E. Persistence of coronaviruses on inanimate surfaces and their inactivation with biocidal agents. *J Hosp Infect.* **104**, :246-251.
123. Yao, H. *et al.* Molecular Architecture of the SARS-CoV-2 Virus. *Cell* **183**, 730-738.e13 (2020).
124. Guo, Y.-R. *et al.* The origin, transmission and clinical therapies on coronavirus disease 2019 (COVID-19) outbreak – an update on the status. *Mil. Med. Res.* **7**, 11 (2020).
125. Han, Y. *et al.* Identification of diverse bat alphacoronaviruses and betacoronaviruses in china provides new insights into the evolution and origin of coronavirus-related diseases. *Front. Microbiol.* **10**, (2019).
126. Chen, Y., Guo, Y., Pan, Y. & Zhao, Z. J. Structure analysis of the receptor binding of 2019-nCoV. *Biochem. Biophys. Res. Commun.* S0006—291X(20)30339—9 (2020) doi:10.1016/j.bbrc.2020.02.071.
127. Neuman, B. W. *et al.* Supramolecular Architecture of Severe Acute Respiratory Syndrome Coronavirus Revealed by Electron Cryomicroscopy. *J. Virol.* **80**, 7918–7928 (2006).
128. Benton, D. J. *et al.* Receptor binding and priming of the spike protein of SARS-CoV-2 for membrane fusion. *Nature* **588**, 327–330 (2020).
129. Xu, C. *et al.* Conformational dynamics of SARS-CoV-2 trimeric spike glycoprotein in complex with receptor ACE2 revealed by cryo-EM. *Sci. Adv.* **7**, 1–13 (2021).
130. V'kovski, P., Gerber, M., Kelly, J., Pfaender, S., Ebert, N., Braga Lagache, S., Simillion, C., Portmann, J., Stalder, H., Gaschen, V., Bruggmann, R., Stoffel, M. H., Heller, M., Dijkman, R., & Thiel, V. Determination of host cell proteins constituting the molecular microenvironment of coronavirus replicase complexes by proximity-labeling. *bioRxiv* 1–30 (2018).
131. Schoeman, D. & Fielding, B. C. Is There a Link Between the Pathogenic Human Coronavirus Envelope Protein and Immunopathology? A Review of the Literature. *Front. Microbiol.* **11**, 1–11 (2020).
132. Fung TS, L. D. Post-translational modifications of coronavirus proteins: roles and function. *Futur. Virol.* **13(6)**, 405–430.
133. Zhang, Z. *et al.* Structure of SARS-CoV-2 membrane protein essential for virus

assembly. *Nat. Commun.* **13**, 1–7 (2022).

134. Transmission of SARS-CoV-2: implications for infection prevention precautions- https://www.who.int/news-room/commentaries/transmission-of-sars-cov-2-implications-for-infection-prevention-precautions.
135. Parasher, A. COVID-19: Current understanding of its Pathophysiology, Clinical presentation and Treatment. *Postgrad. Med. J.* **97**, 312–320 (2021).
136. D'Onofrio, V. *et al.* Studying the clinical, radiological, histological, microbiological, and immunological evolution during the different COVID-19 disease stages using minimal invasive autopsy. *Sci. Rep.* **12**, 1–12 (2022).
137. Symptoms of COVID-19- https://www.cdc.gov/coronavirus/2019-ncov/symptoms-testing/symptoms.html.
138. Cucinotta, D. & Vanelli, M. WHO declares COVID-19 a pandemic. *Acta Biomed.* **91**, 157–160 (2020).
139. Li, Q. *et al.* Cross-species transmission, evolution and zoonotic potential of coronaviruses. *Front. Cell. Infect. Microbiol.* **12**, 1–13 (2023).
140. Mackenzie, J. S. & Smith, D. W. COVID-19—A Novel Zoonotic Disease: A Review of the Disease, the Virus, and Public Health Measures. *Asia-Pacific J. Public Heal.* **32**, 145–153 (2020).
141. Zhou, P. *et al.* A pneumonia outbreak associated with a new coronavirus of probable bat origin. *Nature* **579**, 270–273 (2020).
142. Li Q, Guan X, Wu P, Wang X, Zhou L, Tong Y, Ren R, Leung KSM, Lau EHY, Wong JY, Xing X, Xiang N, Wu Y, Li C, Chen Q, Li D, Liu T, Zhao J, Liu M, Tu W, Chen C, Jin L, Yang R, Wang Q, Zhou S, Wang R, Liu H, Luo Y, Liu Y, Shao G, Li H, Tao Z, Yang Y, Deng Z, F. Z. arly Transmission Dynamics in Wuhan, China, of Novel Coronavirus-Infected Pneumonia. *EN Engl J Med.* **382(13):**, 1199-1207.
143. Peeri, N. C. *et al.* The SARS, MERS and novel coronavirus (COVID-19) epidemics, the newest and biggest global health threats: what lessons have we learned? *Int. J. Epidemiol.* **49**, 717–726 (2021).
144. Morse SS. Global infectious disease surveillance and health intelligence. *Heal. Aff* **26(4):**, 1069–77.
145. Nsubuga, P., Nwanyanwu, O., Nkengasong, J. N., Mukanga, D. & Trostle, M. Strengthening public health surveillance and response using the health systems strengthening agenda in developing countries. *BMC Public Health* **10**, 1–5 (2010).
146. Lindahl, J. F., Grace, D. & Strand, T. The consequences of human actions on risks

for infectious diseases: a review. *Infect. Ecol. Epidemiol.* **5**, 1–11 (2015).

147. Ryu WS. Other Negative-Strand RNA Viruses. (2020).
148. Proserpio, V. & Lönnberg, T. Single-cell technologies are revolutionizing the approach to rare cells. *Immunol. Cell Biol.* **94**, 225–229 (2016).
149. Pantel, K., Brakenhoff, R. H. & Brandt, B. Detection, clinical relevance and specific biological properties of disseminating tumour cells. *Nat. Rev. Cancer* **8**, 329–340 (2008).
150. Challen, G. A., Boles, N., Lin, K. K. Y. & Goodell, M. A. Mouse hematopoietic stem cell identification and analysis. *Cytom. Part A* **75**, 14–24 (2009).
151. Herzenberg, L. A., Bianchi, D. W., Schröder, J., Cann, H. M. & Iverson, G. M. Fetal cells in the blood of pregnant women: Detection and enrichment by fluorescence-activated cell sorting. *Proc. Natl. Acad. Sci. U. S. A.* **76**, 1453–1455 (1979).
152. Lindström, S. & Andersson-Svahn, H. Overview of single-cell analyses: Microdevices and applications. *Lab Chip* **10**, 3363–3372 (2010).
153. Gijs, M. A. M. Magnetic bead handling on-chip: New opportunities for analytical applications. *Microfluid. Nanofluidics* **1**, 22–40 (2004).
154. Weiss, B. *et al.* Circulating Multiple Myeloma Cells (CMMCs): A Novel Method for Detection and Molecular Characterization of Peripheral Blood Plasma Cells in Multiple Myeloma Precursor States. *Blood* **124**, 2031 (2014).
155. Foulk, B. *et al.* Enumeration and characterization of circulating multiple myeloma cells in patients with plasma cell disorders. *Br. J. Haematol.* **180**, 71–81 (2018).
156. Itoua Maïga, R., Lemieux, J., Roy, A., Simard, C. & Néron, S. Flow Cytometry Assessment of In Vitro Generated CD138$^+$ Human Plasma Cells. *Biomed Res. Int.* **2014**, 536482 (2014).
157. Uphoff, Cord C., and H. G. D. *'Detecting Mycoplasma contamination in cell cultures by polymerase chain reaction.' Cancer Cell Culture: Methods and Protocols*. (2004).
158. Tarashansky AJ, Xue Y, Li P, Quake SR, W. B. Self-assembling manifolds in single-cell RNA sequencing data. *Elife.* **8:e48994**,.
159. Bagnoli, J. W. *et al.* Sensitive and powerful single-cell RNA sequencing using mcSCRB-seq. *Nat. Commun.* **9**, 2937 (2018).
160. Tiller, T. *et al.* Efficient generation of monoclonal antibodies from single human B cells by single cell RT-PCR and expression vector cloning. *J. Immunol. Methods* **329**, 112–124 (2008).
161. Tiller, T., Busse, C. E. & Wardemann, H. Cloning and expression of murine Ig

genes from single B cells. *J. Immunol. Methods* **350**, 183–193 (2009).

162. Abanades, B., Georges, G., Bujotzek, A. & Deane, C. M. ABlooper: fast accurate antibody CDR loop structure prediction with accuracy estimation. *Bioinformatics* **38**, 1877–1880 (2022).
163. Lefranc MP, Pommié C, Ruiz M, Giudicelli V, Foulquier E, Truong L, Thouvenin-Contet V, L. G. No TitleIMGT unique numbering for immunoglobulin and T cell receptor variable domains and Ig superfamily V-like domains. *Dev Comp Immunol.* **27(1)**, :55-77.
164. Waterhouse A, Bertoni M, Bienert S, Studer G, Tauriello G, Gumienny R, Heer FT, de Beer TAP, Rempfer C, Bordoli L, Lepore R, S. T. SWISS-MODEL: homology modelling of protein structures and complexes. *Nucleic Acids Res.* ;**46(W1):W2**,.
165. Schrodinger LLC. The AxPyMOL molecular graphics plugin for Microsoft PowerPoint: version 1:8 2015.
166. Kozakov D, Hall DR, Xia B, Porter KA, Padhorny D, Yueh C, Beglov D, V. S. The ClusPro web server for protein-protein docking. *Nat Protoc.*
167. Xue, L. C., Rodrigues, J. P., Kastritis, P. L., Bonvin, A. M. & Vangone, A. PRODIGY: a web server for predicting the binding affinity of protein–protein complexes. *Bioinformatics* **32**, 3676–3678 (2016).
168. Piovesan D, Minervini G, T. S. The RING 2.0 web server for high quality residue interaction networks. *Nucleic Acids Res.* **44(W1):W36**,.
169. Ye, J., Ma, N., Madden, T. L. & Ostell, J. M. IgBLAST: an immunoglobulin variable domain sequence analysis tool. *Nucleic Acids Res.* **41**, W34–W40 (2013).
170. Yuan, M. *et al.* A highly conserved cryptic epitope in the receptor-binding domains of SARS-CoV-2 and SARS-CoV. *bioRxiv* 2020.03.13.991570 (2020) doi:10.1101/2020.03.13.991570.
171. Jette, C. A. *et al.* Broad cross-reactivity across sarbecoviruses exhibited by a subset of COVID-19 donor-derived neutralizing antibodies. *Cell reports* **36**, 109760 (2021).
172. Miller, L. H., Ackerman, H. C., Su, X. & Wellems, T. E. Malaria biology and disease pathogenesis: insights for new treatments. *Nat Med.* **19**, 156–167 (2013).
173. White, N. J. e. al. Malaria. *Lancet* **383**, 723–735 (2014).
174. Cowman, A. F., Healer, J., Marapana, D. & Marsh, K. Malaria: Biology and Disease. *Cell* **167**, 610–624 (2016).
175. GLOBAL TECHINCAL STRATEGY FOR MALARIA 2016-2030.
176. Odolini, S., Gautret, P. & Parola, P. Epidemiology of imported malaria in the

Mediterranean region. *Mediterr. J. Hematol. Infect. Dis.* **4**, (2012).

177. World Health Organization. Fact Sheet-History of Malaria Elimination in the European Region; WHO. (2016).
178. Rosenthal, P. J. Malaria in 2022: Challenges and Progress. *Am. J. Trop. Med. Hyg.* **106**, 1565–1567 (2022).
179. Malaria parasites-Center for disease control and parasite CDC https://www.cdc.gov/malaria/about/biology/#tabs-1-6.
180. Gething, P. W. et al. Mapping Plasmodium falciparum Mortality in Africa between 1990 and 2015. *N.Engl.J.Med.* **375**, 2435–2445 (2016).
181. Miller, L. H., Mason, S. J., Clyde, D. F. & McGinniss, M. H. The Resistance Factor to Plasmodium vivax in Blacks . *N. Engl. J. Med.* **295**, 302–304 (1976).
182. https://www.cdc.gov/malaria/about/biology/parasites.html. (2018).
183. Phillips, M. A. *et al.* Malaria. *Nat. Rev. Dis. Prim.* **3**, 1–24 (2017).
184. Bhatt, S. *et al.* The effect of malaria control on Plasmodium falciparum in Africa between 2000 and 2015. *Nature* **526**, 207–211 (2015).
185. Ranson, H. *et al.* Pyrethroid resistance in African anopheline mosquitoes: What are the implications for malaria control? *Trends Parasitol.* **27**, 91–98 (2011).
186. Ranson, H. & Lissenden, N. Insecticide Resistance in African Anopheles Mosquitoes: A Worsening Situation that Needs Urgent Action to Maintain Malaria Control. *Trends Parasitol.* **32**, 187–196 (2016).
187. World Health Organization. Guidelines for the treatment of malaria, 3rd edn. WHO http://apps.who.int/iris/bitstream/10665/162441/ 1/9789241549127_eng.pdf. (2015).
188. Mukherjee, A. *et al.* Artemisinin resistance without pfkelch13 mutations in Plasmodium falciparum isolates from Cambodia. *Malar. J.* **16**, 1–11 (2017).
189. Plasmodium Antigens-CD Creative Diagnostics. https://www.creative-diagnostics.com/tag-plasmodium-antigens-61.htm.
190. Frischknecht, F. & Matuschewski, K. Plasmodium sporozoite biology. *Cold Spring Harb. Perspect. Med.* **7**, 1–14 (2017).
191. Amino, R. *et al.* Quantitative imaging of Plasmodium transmission from mosquito to mammal. *Nat. Med.* **12**, 220–224 (2006).
192. Prudêncio, M., Rodriguez, A. & Mota, M. M. The silent path to thousands of merozoites: The Plasmodium liver stage. *Nat. Rev. Microbiol.* **4**, 849–856 (2006).
193. T. Ricardo, K. Parisa, A. Katherine, and G. D. Plasmodium life cycle and the pathogenesis of malaria. From innate sensing of malaria parasites. *Nat. Rev. Immunol.* **14**, 744–757 (2014).

194. Sturm, A. *et al.* Manipulation of host hepatocytes by the malaria parasite for delivery into liver sinusoids. *Science (80-.).* **313**, 1287–1290 (2006).
195. Nureye, D. & Assefa, S. Old and Recent Advances in Life Cycle, Pathogenesis, Diagnosis, Prevention, and Treatment of Malaria including Perspectives in Ethiopia. *Sci. World J.* **2020**, (2020).
196. Wipasa, J., Elliott, S., Xu, H. & Good, M. F. Immunity to asexual blood stage malaria and vaccine approaches. *Immunol. Cell Biol.* **80**, 401–414 (2002).
197. Mace, K. E. e. al. 'Malaria Surveillance-United States 2016'. **68**, (2019).
198. *WHO,Training Module on Malaria Control Malaria Entomology and Vector Control.Guide for Partecipants,WHO*. (2013).
199. Cibulskis, R. E. *et al.* Malaria: Global progress 2000 - 2015 and future challenges. *Infect. Dis. Poverty* **5**, 1–8 (2016).
200. Kurtovic, L., Reiling, L., Opi, D. H. & Beeson, J. G. Recent clinical trials inform the future for malaria vaccines. *Commun. Med.* **1**, 1–5 (2021).
201. Duffy, P. E. Current approaches to malaria vaccines. *Curr. Opin. Microbiol.* **70**, (2022).
202. WHO. (World Health Organization, Geneva, Switzerland, 2017).
203. The malERA Consultative Group on Vaccines. A research agenda for malaria eradication: Vaccines. *PLoS Med.* **8**, (2011).
204. Hoffman, S. L. *et al.* Protection of humans against malaria by immunization with radiation-attenuated Plasmodium falciparum sporozoites. *J. Infect. Dis.* **185**, 1155–1164 (2002).
205. Clyde DF,Most H, McCarthy VC, V. J. Immunization of man against sporozoite-iduced falciparum malaria. *Am. J. Med Sci.* **266**, 169–77.
206. Clyde DF. Immunization of man against falciparum and vivax malaria by use of attenuated sporozoites. *Am. J. Trop. Med. Hyg.* **24**, 397–401.
207. Rieckmann, K. H., Beaudoin, R. L., Cassells, J. S. & Sell, K. W. Use of attenuated sporozoites in the immunization of human volunteers against falciparum malaria. *Bull. World Health Organ.* **57**, 261–265 (1979).
208. WHO recommends ground breaking malaria vaccine for children at risk; Historic RTS, S/AS01 recommendation can reinvigorate the fight against malaria. (2021).
209. Datoo, M. S. *et al.* Efficacy of a low-dose candidate malaria vaccine, R21 in adjuvant Matrix-M, with seasonal administration to children in Burkina Faso: a randomised controlled trial. *Lancet* **397**, 1809–1818 (2021).
210. Hoffman, S. L. *et al.* Development of a metabolically active, non-replicating

sporozoite vaccine to prevent Plasmodium falciparum malaria. *Hum. Vaccin.* **6**, (2010).

211. Richie TL, Billingsley PF, Sim BK, James ER, Chakravarty S, Epstein JE, Lyke KE, Mordmüller B, Alonso P, Duffy PE, Doumbo OK, Sauerwein RW, Tanner M, Abdulla S, Kremsner PG, Seder RA, H. S. Progress with Plasmodium falciparum sporozoite (PfSPZ)-based malaria vaccines. *Vaccine* **33**, 7452–61 (2015).
212. Mueller, A. K., Labaied, M., Kappe, S. & Matuschewski, K. Genetically modified Plasmodium parasites as a protective experimental malaria vaccine (Nature (2005) 433, (164-176)). *Nature* **446**, 102 (2007).
213. Mordmüller, B. *et al.* Sterile protection against human malaria by chemoattenuated PfSPZ vaccine. *Nature* **542**, 445–449 (2017).
214. Seder, R. A. *et al.* Protection against malaria by intravenous immunization with a nonreplicating sporozoite vaccine. *Science (80-.).* **341**, 1359–1365 (2013).
215. Murphy, S. C. *et al.* PfSPZ-CVac efficacy against malaria increases from 0% to 75% when administered in the absence of erythrocyte stage parasitemia: A randomized, placebo-controlled trial with controlled human malaria infection. *PLoS Pathog.* **17**, 1–23 (2021).
216. Mwakingwe-Omari, A. *et al.* Two chemoattenuated PfSPZ malaria vaccines induce sterile hepatic immunity. *Nature* **595**, 289–294 (2021).
217. Carter, R. & Chen, D. H. Malaria transmission blocked by immunisation with gametes of the malaria parasite. *Nature* **263**, 57–60 (1976).
218. RW., G. Malaria: Successful immunization against the sexual stages of Plasmodium gallinaceum. **193**, 1150–1151.
219. Kaushal DC, C. R. Characterization of antigens on mosquito midgut stages of Plasmodium gallinaceum. II. Comparison of surface antigens of male and female gametes and zygotes. *Mol Biochem Parasitol.* **11**, 145–156 (1984).
220. Duffy, B. P. E., Pimenta, S. P. & Kaslow, D. C. Pgs 28 Be longs to a Family o f Epide rmal Growth Factor-like Antige ns That Are Targe ts o f Malaria Trans mis s ion-blocking Antibodie s. **177**, 505–510 (1993).
221. Grotendorst, C. A., Kumar, N., Carter, R. & Kaushal, D. C. A surface protein expressed during the transformation of Zygotes of Plasmodium gallinaceum is a target of transmission-blocking antibodies. *Infect. Immun.* **45**, 775–777 (1984).
222. Wu, Y. *et al.* Phase 1 trial of malaria transmission blocking vaccine candidates Pfs25 and Pvs 25 formulated with montanide ISA 51. *PLoS One* **3**, (2008).
223. Ogun, S. A., Dumon-Seignovert, L., Marchand, J. B., Holder, A. A. & Hill, F. The

oligomerization domain of C4-binding protein (C4bp) acts as an adjuvant, and the fusion protein comprised of the 19-kilodalton merozoite surface protein 1 fused with the murine C4bp domain protects mice against malaria. *Infect. Immun.* **76**, 3817–3823 (2008).

224. Li, Y. *et al.* Enhancing immunogenicity and transmission-blocking activity of malaria vaccines by fusing Pfs25 to IMX313 multimerization technology. *Sci. Rep.* **6**, 1–13 (2016).
225. Brod, F. *et al.* Combination of RTS,S and Pfs25-IMX313 Induces a Functional Antibody Response Against Malaria Infection and Transmission in Mice. *Front. Immunol.* **9**, 1–13 (2018).
226. Talaat, K. R. *et al.* Safety and immunogenicityof Pfs25-EPA/ alhydrogel1, a transmission blocking vaccine against Plasmodium falciparum: An open label study in malaria naïve adults. *PLoS One* **11**, 1–17 (2016).
227. Healy, S. A. *et al.* Pfs230 yields higher malaria transmission-blocking vaccine activity than Pfs25 in humans but not mice. *J. Clin. Invest.* **131**, 1–10 (2021).
228. Coelho, C. H. *et al.* A human monoclonal antibody blocks malaria transmission and defines a highly conserved neutralizing epitope on gametes. *Nat. Commun.* **12**, 1–12 (2021).
229. N., K. Target antigens of malaria transmission blocking immunity. *J. Commun. Dis.* **9**, 321–35 (1987).
230. Vermeulen AN, Ponnudurai T, Beckers PJ, Verhave JP, Smits MA, M. J. EXPRESSION OF ANTIGENS ON SEXUAL that the immunogens were present on the surface of both male and female. **162**, 1460–1476 (1985).
231. Van Dijk, M. R. *et al.* A central role for P48/45 in malaria parasite male gamete fertility. *Cell* **104**, 153–164 (2001).
232. Roeffen, W. *et al.* Plasmodium falciparum: Production and characterization of rat monoclonal antibodies specific for the sexual-stage Pfs48/45 antigen. *Exp. Parasitol.* **97**, 45–49 (2001).
233. Theisen, M. *et al.* A multi-stage malaria vaccine candidate targeting both transmission and asexual parasite life-cycle stages. *Vaccine* **32**, 2623–2630 (2014).
234. Singh, S. K. *et al.* Construct design, production, and characterization of Plasmodium falciparum 48/45 R0.6C subunit protein produced in Lactococcus lactis as candidate vaccine. *Microb. Cell Fact.* **16**, 1–11 (2017).
235. Duffy, P. E. & Patrick Gorres, J. Malaria vaccines since 2000: progress, priorities, products. *npj Vaccines* **5**, 1–9 (2020).

236. COHEN S, McGREGOR IA, C. S. Gamma-globulin and acquired immunity to human malaria. *Nature* **192**, 733–737 (1961).
237. Edozien, J. C., Gilles, H. M. & Udeozo, I. O. K. Adult and cord-blood gamma-globulin and immunity to malaria in Nigerians. *Lancet* **280**, 951–955 (1962).
238. Siddiqui, W. A. An effective immunization of experimental monkeys against a human malaria parasite, Plasmodium falciparum. *Science (80-.).* **197**, 388–389 (1977).
239. Boyle, M. J. *et al.* Isolation of viable Plasmodium falciparum merozoites to define erythrocyte invasion events and advance vaccine and drug development. *Proc. Natl. Acad. Sci. U. S. A.* **107**, 14378–14383 (2010).
240. Volz, J. C. *et al.* Essential Role of the PfRh5/PfRipr/CyRPA Complex during Plasmodium falciparum Invasion of Erythrocytes. *Cell Host Microbe* **20**, 60–71 (2016).
241. Das, S. *et al.* Processing of Plasmodium falciparum Merozoite Surface Protein MSP1 Activates a Spectrin-Binding Function Enabling Parasite Egress from RBCs. *Cell Host Microbe* **18**, 433–444 (2015).
242. Lin, C. S. *et al.* Multiple plasmodium falciparum merozoite surface protein 1 complexes mediate merozoite binding to human erythrocytes. *J. Biol. Chem.* **291**, 7703–7715 (2016).
243. Reddy, K. S. *et al.* Multiprotein complex between the GPI-anchored CyRPA with PfRH5 and PfRipr is crucial for Plasmodium falciparum erythrocyte invasion. *Proc. Natl. Acad. Sci. U. S. A.* **112**, 1179–1184 (2015).
244. Chen, L. *et al.* An EGF-like Protein Forms a Complex with PfRh5 and Is Required for Invasion of Human Erythrocytes by Plasmodium falciparum. **7**, (2011).
245. Galaway, F. *et al.* P113 is a merozoite surface protein that binds the N terminus of Plasmodium falciparum RH5. *Nat. Commun.* **8**, 1–11 (2017).
246. Dasgupta, S. *et al.* Membrane-Wrapping Contributions to Malaria Parasite Invasion of the Human Erythrocyte. *Biophysj* **107**, 43–54 (2014).
247. Volz, J. C. *et al.* Essential Role of the PfRh5/PfRipr/CyRPA Complex during Plasmodium falciparum Invasion of Erythrocytes. *Cell Host Microbe* **20**, 60–71 (2016).
248. Cao, J. *et al.* Rhoptry neck protein RON2 forms a complex with microneme protein AMA1 in Plasmodium falciparum merozoites. *Parasitol. Int.* **58**, 29–35 (2009).
249. Srinivasan, P. *et al.* Binding of Plasmodium merozoite proteins RON2 and AMA1 triggers commitment to invasion. *Proc. Natl. Acad. Sci. U. S. A.* **108**, 13275–13280

(2011).

250. Baum, J. *et al.* A conserved molecular motor drives cell invasion and gliding motility across malaria life cycle stages and other apicomplexan parasites. *J. Biol. Chem.* **281**, 5197–5208 (2006).
251. Sagara, I. *et al.* A randomized controlled phase 2 trial of the blood stage AMA1-C1/Alhydrogel malaria vaccine in children in Mali. *Vaccine* **27**, 3090–3098 (2009).
252. Hayton, K. *et al.* Erythrocyte Binding Protein PfRH5 Polymorphisms Determine Species-Specific Pathways of Plasmodium falciparum Invasion. *Cell Host Microbe* **4**, 40–51 (2008).
253. Baum, J. *et al.* Reticulocyte-binding protein homologue 5 - An essential adhesin involved in invasion of human erythrocytes by Plasmodium falciparum. *Int. J. Parasitol.* **39**, 371–380 (2009).
254. Crosnier, C. *et al.* Basigin is a receptor essential for erythrocyte invasion by Plasmodium falciparum. *Nature* **480**, 534–537 (2011).
255. Douglas, A. D. *et al.* The blood-stage malaria antigen PfRH5 is susceptible to vaccine-inducible cross-strain neutralizing antibody. *Nat. Commun.* **2**, (2011).
256. Bustamante, L. Y. *et al.* A full-length recombinant Plasmodium falciparum PfRH5 protein induces inhibitory antibodies that are effective across common PfRH5 genetic variants. *Vaccine* **31**, 373–379 (2013).
257. Hjerrild, K. A. *et al.* Production of full-length soluble Plasmodium falciparum RH5 protein vaccine using a Drosophila melanogaster Schneider 2 stable cell line system. *Sci. Rep.* **6**, 1–15 (2016).
258. Campeotto, I. *et al.* One-step design of a stable variant of the malaria invasion protein RH5 for use as a vaccine immunogen. *Proc. Natl. Acad. Sci. U. S. A.* **114**, 998–1002 (2017).
259. Douglas, A. D. *et al.* A PfRH5-based vaccine is efficacious against heterologous strain blood-stage plasmodium falciparum infection in Aotus monkeys. *Cell Host Microbe* **17**, 130–139 (2015).
260. Payne, R. O. *et al.* Human vaccination against RH5 induces neutralizing antimalarial antibodies that inhibit RH5 invasion complex interactions. *JCI Insight* **2**, 1–19 (2017).
261. Minassian, A. M. *et al.* Reduced blood-stage malaria growth and immune correlates in humans following RH5 vaccination. *Med* **2**, 701-719.e19 (2021).
262. Scally, S. W. *et al.* PCRCR complex is essential for invasion of human erythrocytes by Plasmodium falciparum. *Nat. Microbiol.* **7**, 2039–2053 (2022).

263. Wong, W. *et al.* Structure of Plasmodium falciparum Rh5-CyRPA-Ripr invasion complex. *Nature* **565**, 118–121 (2019).
264. Favuzza, P. *et al.* Structure of the malaria vaccine candidate antigen CyRPA and its complex with a parasite invasion inhibitory antibody. *Elife* **6**, 1–21 (2017).
265. Ragotte, R. J., Higgins, M. K. & Draper, S. J. The RH5-CyRPA-Ripr Complex as a Malaria Vaccine Target. *Trends Parasitol.* **36**, 545–559 (2020).
266. Tran, T. M. *et al.* Naturally acquired antibodies specific for plasmodium falciparum reticulocyte-binding protein homologue 5 inhibit parasite growth and predict protection from malaria. *J. Infect. Dis.* **209**, 789–798 (2014).
267. Chiu, C. Y. H. *et al.* Association of antibodies to Plasmodium falciparum reticulocyte binding protein homolog 5 with protection from clinical malaria. *Front. Microbiol.* **5**, 1–8 (2014).
268. Richards, J. S. *et al.* Identification and Prioritization of Merozoite Antigens as Targets of Protective Human Immunity to Plasmodium falciparum Malaria for Vaccine and Biomarker Development . *J. Immunol.* **191**, 795–809 (2013).
269. Malkin, E. M. *et al.* Phase 1 Clinical Trial of Apical Membrane Antigen 1: an Asexual Blood-Stage Vaccine for. *Society* **73**, 3677–3685 (2005).
270. Stephens, R. *et al.* Malaria-specific transgenic CD4+ T cells protect immunodeficient mice from lethal infection and demonstrate requirement for a protective threshold of antibody production for parasite clearance. *Blood* **106**, 1676–1684 (2005).
271. Mahdi Abdel Hamid, M. *et al.* Vaccination with Plasmodium knowlesi AMA1 formulated in the novel adjuvant co-vaccine HT™ protects against blood-stage challenge in rhesus macaques. *PLoS One* **6**, (2011).
272. Alanine, D. G. W. *et al.* Human Antibodies that Slow Erythrocyte Invasion Potentiate Malaria-Neutralizing Antibodies. *Cell* **178**, 216-228.e21 (2019).
273. Chen, L. *et al.* Structural basis for inhibition of erythrocyte invasion by antibodies to plasmodium falciparum protein CyRPA. *Elife* **6**, 1–15 (2017).
274. Douglas, A. D. *et al.* Neutralization of Plasmodium falciparum Merozoites by Antibodies against PfRH5 . *J. Immunol.* **192**, 245–258 (2014).
275. Healer, J. *et al.* Neutralising antibodies block the function of Rh5/Ripr/CyRPA complex during invasion of Plasmodium falciparum into human erythrocytes. *Cell. Microbiol.* **21**, 1–15 (2019).
276. Barrett, J. R. *et al.* Analysis of the Diverse Antigenic Landscape of the Malaria Invasion Protein RH5 Identifies a Potent Vaccine-Induced Human Public Antibody

Clonotype. *bioRxiv* 2023.10.04.560576 (2023) doi:10.1101/2023.10.04.560576.

277. Dreyer, A. M. *et al.* Passive Immunoprotection of Plasmodium falciparum -Infected Mice Designates the CyRPA as Candidate Malaria Vaccine Antigen . *J. Immunol.* **188**, 6225–6237 (2012).

278. Douglas, A. D. *et al.* A defined mechanistic correlate of protection against Plasmodium falciparum malaria in non-human primates. *Nat. Commun.* **10**, 1–8 (2019).

279. King, L. D. W. *et al.* Preclinical Development of a Stabilized RH5 Virus-Like Particle Vaccine that Induces Improved Anti-Malarial Antibodies. *bioRxiv* (2024) doi:10.1101/2024.01.04.574181.

280. Wang LT, Pereira LS, Flores-Garcia Y, O'Connor J, Flynn BJ, Schön A, Hurlburt NK, Dillon M, Yang ASP, Fabra-García A, Idris AH, Mayer BT, Gerber MW, Gottardo R, Mason RD, Cavett N, Ballard RB, Kisalu NK, Molina-Cruz A, Nelson J, Vistein R, Barillas-Mury C, S. R. A Potent Anti-Malarial Human Monoclonal Antibody Targets Circumsporozoite Protein Minor Repeats and Neutralizes Sporozoites in the Liver. *Immunity.* **53(4):733**-,.

281. Rijal, P. *et al.* Therapeutic Monoclonal Antibodies for Ebola Virus Infection Derived from Vaccinated Humans. *Cell Rep.* **27**, 172—186.e7 (2019).

282. Andersen, P. H., Nielsen, M. & Lund, O. Prediction of residues in discontinuous B-cell epitopes using protein 3D structures. *Protein Sci.* **15**, (2006).

Appendix

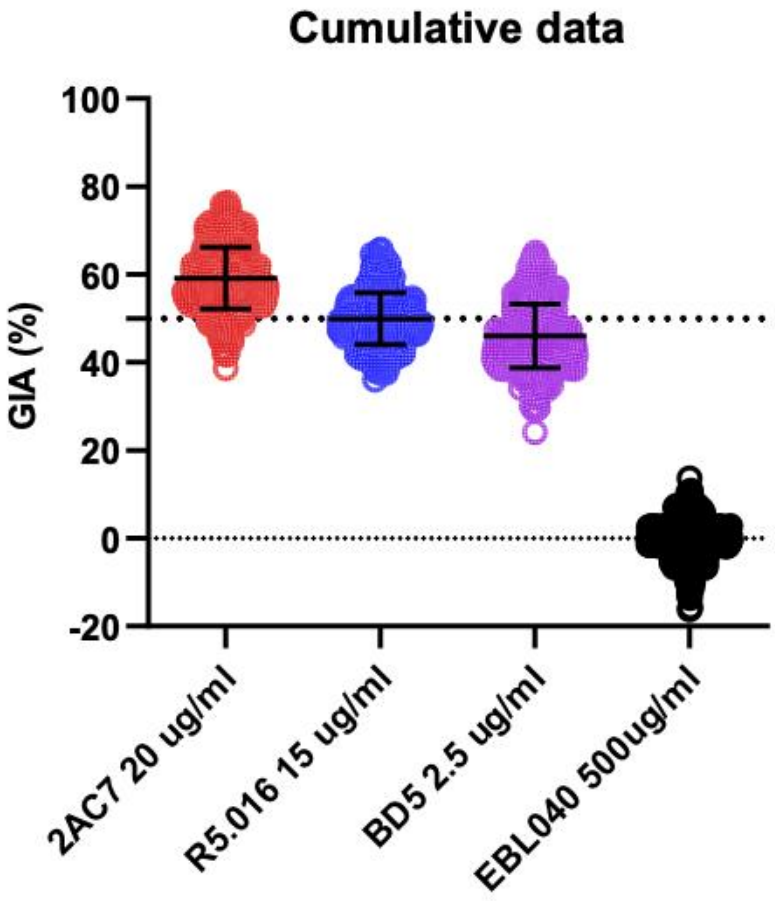

Figure A. 1.*GIA internal controls.*

On the X-axis are shown respectively Three anti-RH5 mAbs with well-characterised levels of GIA (2AC7, R5.016, BD5/R5.034) and a negative control mAb, EBL04.
On the y-axis it is represented the GIA activity, expressed in percentage.